

NONLINEAR MODELING AND FLIGHT CONTROL SYSTEM DESIGN OF AN
UNMANNED AERIAL VEHICLE

A THESIS SUBMITTED TO
THE GRADUATE SCHOOL OF NATURAL AND APPLIED SCIENCES
OF
MIDDLE EAST TECHNICAL UNIVERSITY

BY

DENİZ KARAKAŞ

IN PARTIAL FULFILLMENT OF THE REQUIREMENTS
FOR
THE DEGREE OF MASTER OF SCIENCE
IN
MECHANICAL ENGINEERING

SEPTEMBER 2007

Approval of the thesis:

**NONLINEAR MODELING AND FLIGHT CONTROL SYSTEM DESIGN OF
AN UNMANNED AERIAL VEHICLE**

submitted by **DENİZ KARAKAŞ** in partial fulfillment of the requirements for the
degree of **Master of Science** in **Mechanical Engineering Department, Middle
East Technical University** by,

Prof. Dr. Canan Özgen
Dean, Graduate School of **Natural and Applied Sciences**

Prof. Dr. S. Kemal İder
Head of Department, **Mechanical Engineering**

Prof. Dr. R. Tuna Balkan
Supervisor, **Mechanical Engineering Dept., METU**

Prof. Dr. E. Bülent Platin
Co-Supervisor, **Mechanical Engineering Dept., METU**

Examining Committee Members:

Prof. Dr. M. Kemal Özgören
Mechanical Engineering Dept., METU

Prof. Dr. R. Tuna Balkan
Mechanical Engineering Dept., METU

Prof. Dr. E. Bülent Platin
Mechanical Engineering Dept., METU

Prof. Dr. Y. Samim Ünlüsoy
Mechanical Engineering Dept., METU

Dr. Volkan Nalbantoğlu
Principal Controls Engineer, ASELSAN

Date:

07.09.2007

I hereby declare that all information in this document has been obtained and presented in accordance with academic rules and ethical conduct. I also declare that, as required by these rules and conduct, I have fully cited and referenced all material and results that are not original to this work.

Name, Last name : Deniz KARAKAŞ

Signature :

ABSTRACT

NONLINEAR MODELING AND FLIGHT CONTROL SYSTEM DESIGN OF AN UNMANNED AERIAL VEHICLE

Karakaş, Deniz

M.Sc., Department of Mechanical Engineering

Supervisor : Prof. Dr. R. Tuna Balkan

Co-Supervisor : Prof. Dr. E. Bülent Platin

September 2007, 225 pages

The nonlinear simulation model of an unmanned aerial vehicle (UAV) in MATLAB[®]/Simulink[®] environment is developed by taking into consideration all the possible major system components such as actuators, gravity, engine, atmosphere, wind-turbulence models, as well as the aerodynamics components in the 6 DOF equations of motion. Trim and linearization of the developed nonlinear model are accomplished and various related analyses are carried out. The model is validated by comparing with a similar UAV data in terms of open loop dynamic stability characteristics. Using two main approaches; namely, classical and optimal, linear controllers are designed. For the classical approach, Simulink Response Optimization (SRO) tool of MATLAB[®]/Simulink[®] is utilized, whereas for the optimal controller approach, linear quadratic (LQ) controller design method is implemented, again by the help of the tools put forth by MATLAB[®]. The controllers are designed for control of roll, heading, coordinated turn, flight path, pitch, altitude, and airspeed, i.e., for the achievement of all low-level control functions. These linear controllers are integrated into the nonlinear model, by carrying out gain scheduling with respect to airspeed and altitude, controller input linearization regarding the perturbed states and control

inputs, and anti integral wind-up scheme regarding the possible wind-up of the integrators in the controller structures. The responses of the nonlinear model controlled with the two controllers are compared based on the military flight control requirements. The advantages and disadvantages of these two frequently used controllers in industry are investigated and discussed. These results are to be evaluated by the designers themselves based on the design criteria of a project that is worked on.

Keywords: UAV, Nonlinear Modeling, Trim, Linearization, Dynamic Stability, Linear Control, Classical Flight Control, Optimal Flight Control, Simulink Response Optimization (SRO), Linear Quadratic (LQ) Controller, Total Energy Control System (TECS), Target Zeros, Gain Scheduling

ÖZ

BİR İNSANSIZ HAVA ARACININ DOĞRUSAL OLMAYAN MODELLEMESİ VE UÇUŞ KONTROL SİSTEMİ TASARIMI

Karakaş, Deniz

Yüksek Lisans, Makine Mühendisliği Bölümü

Tez Yöneticisi : Prof. Dr. R. Tuna Balkan

Ortak Tez Yöneticisi: Prof. Dr. E. Bülent Platin

Eylül 2007, 225 sayfa

Doğrusal olmayan bir insansız hava aracı (İHA) benzetim modeli, eyleyiciler, yer çekimi, atmosfer, rüzgar-türbülans modelleri gibi sistem bileşenlerinin yanısıra, 6 serbestlik dereceli hareket denklemlerindeki aerodinamik bileşenler de göz önüne alınarak MATLAB®/Simulink® ortamında geliştirilmiştir. Geliştirilen doğrusal olmayan modelin trim ve doğrusallaştırılması işlemleri gerçekleştirilmiş ve ilgili analizler yapılmıştır. Model, açık döngü dinamik kararlılık karakteristikleri açısından benzer bir İHA verisiyle karşılaştırılarak doğrulanmıştır. Klasik ve optimal olmak üzere başlıca iki yaklaşım kullanılarak, doğrusal kontrolcüler tasarlanmıştır. Klasik yaklaşım için, MATLAB®/Simulink® – Simulink Tepki Eniyilemesi aracı kullanılırken, optimal yaklaşım için yine MATLAB® tarafından ortaya konulan araçların yardımıyla doğrusal-kuadratik tasarım metodu kullanılmıştır. Kontrolcüler, yatış, baş, koordineli dönüş, uçuş yolu açısı, yunuslama, yükseklik, ve hız kontrolü gibi bütün düşük seviye kontrol fonksiyonlarının yerine getirilebilmesi amaçlı tasarlanmıştır. Bu doğrusal kontrolcüler, yükseklik ve hıza göre kazanç seçimi, sarsım durum değişkenleri ve kontrol girdileriyle bağlantılı olarak kontrolcü girdi doğrusallaştırması ve kontrolcü yapılarında yer alan integrallerin ilgili kontrol

girdisinin sınırlarına ulaşması sonucu integrasyona devam etmesini önleme amaçlı uygulamalar ile doğrusal olmayan modele entegre edilmişlerdir. İki ayrı kontrolcü ile kontrol edilen doğrusal olmayan model benzetim tepkileri askeri uçuş kontrol gereksinimleri temel alınarak karşılaştırılmıştır. Endüstride sıkça kullanılan bu iki kontrolcünün avantaj ve dezavantajları incelenmiş ve tartışılmıştır. Bu sonuçlar tasarımcının kendisi tarafından üzerinde çalışılan projenin tasarım kriterlerine göre değerlendirilecektir.

Anahtar Kelimeler: İHA, Doğrusal Olmayan Modelleme, Trim, Doğrusallaştırma, Dinamik Kararlılık, Doğrusal Kontrol, Klasik Uçuş Kontrolü, Optimal Uçuş Kontrolü, Simulink Tepki Eniyilemesi, Doğrusal Kuadratik Kontrolcü (DKK), Toplam Enerji Kontrol Sistemi, Hedef Sınırlar, Kazanç Seçimi

To My Family

ACKNOWLEDGMENTS

The author wishes to express her deepest gratitude to her supervisor Prof. Dr. Tuna Balkan and co-supervisor Prof. Dr. Bülent Platin for their constant guidance, advice, criticism, encouragements and insight throughout the research.

The author would like to express her special thanks to her former chief and current manager in TAI, Mr. Remzi Barlas for his support on the thesis subject, motivation, technical assistance, and suggestions.

The author would like to thank her other former chief in TAI, Mr. Bülent Korkem for his support on technical and administrative issues.

The author would also like to thank her colleagues and friends, Senem Atalayer Kırçalı, Alp Marangoz, Derya Gürak, Umut Susuz, Ömer Onur, and Kerem Adıgüzel for their enjoyable friendship, support and advices.

The author would like to express her special thanks to her parents and her sister for their endless love, patience, and support.

TABLE OF CONTENTS

ABSTRACT	<i>iv</i>
ÖZ	<i>vi</i>
ACKNOWLEDGMENTS	<i>ix</i>
TABLE OF CONTENTS	<i>x</i>
LIST OF TABLES	<i>xiii</i>
LIST OF FIGURES	<i>xv</i>
LIST OF SYMBOLS & ABBREVIATIONS	<i>xix</i>
CHAPTERS	
1. INTRODUCTION	1
1.1 Background and Motivation	1
1.2 Literature Survey	5
1.3 Research Objectives	13
1.4 Thesis Outline	14
2. DEVELOPMENT OF NONLINEAR SIMULATION MODEL	17
2.1 Introduction	17
2.2 The UAV – Properties	17
2.3 Assumptions	20
2.4 Reference Coordinate Frames	21
2.5 Body-fixed axes Components and Sign Conventions	23
2.6 Equations of Motion	25
2.6.1 Forces and Moments	27
2.6.1.1 Aerodynamic Forces and Moments	28
2.6.1.2 Propulsive Forces and Moments – Engine Model	31
2.6.1.3 Gravitational Forces and Moments – Gravity Model	35
2.7 Actuators Model	36
2.8 Atmosphere and Wind-Turbulence Model	37
2.8.1 Atmosphere Model	37
2.8.2 Wind-Turbulence Model	38
2.8.2.1 Background Wind Model	39
2.8.2.2 Turbulence Model	39
2.8.2.3 Wind Shear Model	39
2.9 Flight Parameters Calculation	40
2.10 MATLAB®/Simulink® Correlation	41

3. TRIM - LINEARIZATION.....	42
3.1 Introduction	42
3.2 Trim	43
3.2.1 Trim Method	44
3.2.2 Trim Results	46
3.3 Linearization	46
3.3.1 Linearization Methods	47
3.3.2 Modal Matrix and Linearization Results.....	49
3.3.3 Linearization Methods Verification	54
4. UAV MODEL VERIFICATION	64
4.1 Introduction	64
4.2 Pole-Zero Maps.....	64
4.3 Dynamic Stability Requirements and Analyses Results.....	68
4.3.1 Longitudinal Dynamic Stability Requirements and Analyses Results	70
4.3.2 Lateral-Directional Dynamic Stability Requirements and Analyses Results.....	77
4.3.3 Validation of the Results	82
5. FLIGHT CONTROL SYSTEM DESIGN.....	88
5.1 Introduction	88
5.2 Assumptions	89
5.3 Flight Control Requirements.....	90
5.3.1 Attitude (Pitch & Roll) Control Requirements	90
5.3.1.1 Attitude Hold.....	90
5.3.1.1.1 Pitch Transient Response	90
5.3.1.1.2 Roll Transient Response	90
5.3.2 Heading Control Requirements	91
5.3.2.1 Heading Hold	91
5.3.2.2 Heading Select.....	91
5.3.2.2.1 Transient Heading Response.....	91
5.3.2.2.2 Altitude Coordinated Turns	91
5.3.3 Altitude Control Requirements.....	92
5.3.4 Airspeed Control Requirements	92
5.4 Classical Controller Design.....	92
5.4.1 Controller Loops Generation	92
5.4.1.1 Building Heading Controller.....	93
5.4.1.2 Building Altitude Controller	98
5.4.1.3 Building Airspeed Controller.....	100
5.4.1.4 Simulink Response Optimization (SRO) Application	101
5.4.1.4.1 Roll Attitude Response Characteristics	102
5.4.1.4.2 Turn Coordination Response Characteristics	104
5.4.1.4.3 Heading Response Characteristics.....	107
5.4.1.4.4 Pitch Attitude Response Characteristics.....	108
5.4.1.4.5 Altitude Response Characteristics	110
5.4.1.4.6 Airspeed Response Characteristics	112
5.4.1.5 Closed Loop Poles.....	113
5.4.1.5.1 Lateral-Directional Controller – Closed Loop Poles.....	113
5.4.1.5.2 Longitudinal Controller – Closed Loop Poles.....	114

5.4.2	Complete Controller – Implementing in Nonlinear Model.....	116
5.4.2.1	Gain Scheduling	116
5.4.2.2	Controller Input Linearization	119
5.4.2.3	Anti Integral Wind-up Scheme	120
5.5	Optimal Controller Design	127
5.5.1	Linear Quadratic (LQ) Controller Approach	128
5.5.2	Building Longitudinal Controller (TECS)	132
5.5.2.1	Building up Inner Loop TECS.....	136
5.5.2.1.1	Synthesis Model	136
5.5.2.1.2	Weighting Matrices Selection – Obtaining K_{lqr}	138
5.5.2.2	Building up Outer Loop TECS	142
5.5.3	Building Lateral-Directional Controller	144
5.5.3.1	Building up Inner Loop Lateral-Directional Controller	145
5.5.3.1.1	Synthesis Model	145
5.5.3.1.2	Weighting Matrices Selection – Obtaining K_{lqr}	149
5.5.3.2	Building up Outer Loop Lateral-Directional Controller	152
5.5.4	Closed Loop Poles	154
5.5.4.1	Longitudinal Controller – Closed Loop Poles.....	154
5.5.4.2	Lateral-Directional Controller – Closed Loop Poles.....	155
5.5.5	Complete Controller – Implementing in Nonlinear Model.....	157
5.5.5.1	Gain Scheduling	157
5.5.5.2	Controller Input Linearization	163
5.5.5.3	Anti Integral Wind-up Scheme	164
6.	CASE STUDIES – CLOSED LOOP NONLINEAR MODEL SIMULATIONS & COMPARISON	171
6.1	Introduction	171
6.2	Comparison Results – Flight Control Requirements	171
7.	SUMMARY, CONCLUSIONS AND RECOMMENDATIONS.....	191
7.1	Summary	191
7.2	Conclusions	193
7.3	Recommendations for Future Work.....	196
	REFERENCES	197
	APPENDICES	
A.	DERIVATION OF 6 DOF EQUATIONS OF MOTION	202
B.	DERIVATION OF THE FLIGHT PARAMETERS; $\dot{V}, \dot{\alpha}, \dot{\beta}$	209
C.	NONLINEAR MODELING BLOCKS – MATLAB®/SIMULINK®	213
D.	TRIM-LINEARIZATION SCRIPT – “trimUAV.m”	218

LIST OF TABLES

TABLES

<i>Table 2.1 Basic Geometrical Data.....</i>	<i>19</i>
<i>Table 2.2 Positive Sign Conventions for Angles.....</i>	<i>24</i>
<i>Table 2.3 Coefficients in the nonlinear engine model of the “DHC-2 Beaver” aircraft....</i>	<i>34</i>
<i>Table 3.1 Eigenvalues of the nominal linear model-linmod2.....</i>	<i>50</i>
<i>Table 3.2 Eigenvalues of the nominal linear model-linmod.....</i>	<i>50</i>
<i>Table 4.1 Short period mode damping ratio, ζ_{sp} requirements – Category B Flight Phases</i> <i>.....</i>	<i>75</i>
<i>Table 4.2 Dutch roll mode damping ratio, ζ_{dr}, natural frequency, ω_{ndr} requirements –</i> <i>Category B Flight Phases / Class II.....</i>	<i>78</i>
<i>Table 5.1 Minimum Acceptable Control Accuracy.....</i>	<i>92</i>
<i>Table 5.2 Roll attitude desired response characteristics.....</i>	<i>103</i>
<i>Table 5.3 Turn coordination desired response characteristics.....</i>	<i>104</i>
<i>Table 5.4 Heading desired response characteristics.....</i>	<i>107</i>
<i>Table 5.5 Pitch attitude desired response characteristics.....</i>	<i>109</i>
<i>Table 5.6 Altitude desired response characteristics.....</i>	<i>111</i>
<i>Table 5.7 Airspeed desired response characteristics.....</i>	<i>112</i>
<i>Table 5.8 Eigenvalues of the nominal open loop and closed loop linear models in lateral-</i> <i>directional axis.....</i>	<i>114</i>
<i>Table 5.9 Eigenvalues of the nominal open loop and closed loop linear models in</i> <i>longitudinal axis.....</i>	<i>115</i>
<i>Table 5.10 Gain scheduling breakpoint values of airspeed and altitude.....</i>	<i>118</i>
<i>Table 5.11 Dependency condition of the controller gains and values of constant ones...</i>	<i>118</i>
<i>Table 5.12 Transmission zeros of lateral-directional synthesis model.....</i>	<i>147</i>
<i>Table 5.13 Eigenvalues of the nominal open loop and two closed loop linear models in</i> <i>longitudinal axis.....</i>	<i>155</i>

<i>Table 5.14 Eigenvalues of the nominal open loop and two closed loop linear models in lateral-directional axis</i>	<i>156</i>
<i>Table 5.15 Breakpoint values of airspeed and altitude.....</i>	<i>158</i>
 <i>Table C.1 List of parameter definitions and symbols used in main level Simulink® diagram input-outputs</i>	 <i>216</i>

LIST OF FIGURES

FIGURES

<i>Figure 1.1 General Atomics Predator B UAV [6].....</i>	<i>3</i>
<i>Figure 1.2 SRC view [10].....</i>	<i>10</i>
<i>Figure 1.3 Inner loop-outer loop Beaver autopilot [11-12].....</i>	<i>12</i>
<i>Figure 2.1 The UAV view</i>	<i>18</i>
<i>Figure 2.2 Earth-Fixed and Body-Fixed Coordinate Systems.....</i>	<i>22</i>
<i>Figure 2.3 Relationships between body-fixed, stability-axes, and wind-axes reference frames</i>	<i>23</i>
<i>Figure 2.4 Positive directions for body-fixed axes components and angles</i>	<i>25</i>
<i>Figure 3.1 Doublet column input.....</i>	<i>55</i>
<i>Figure 3.2 Linear and nonlinear responses to doublet column input</i>	<i>56</i>
<i>Figure 3.3 Pulse throttle input</i>	<i>57</i>
<i>Figure 3.4 Linear and nonlinear responses to pulse throttle input</i>	<i>58</i>
<i>Figure 3.5 Doublet wheel input.....</i>	<i>58</i>
<i>Figure 3.6 Linear and nonlinear responses to doublet wheel input</i>	<i>60</i>
<i>Figure 3.7 Doublet pedal input.....</i>	<i>60</i>
<i>Figure 3.8 Linear and nonlinear responses to doublet pedal input.....</i>	<i>61</i>
<i>Figure 4.1 Longitudinal axis poles.....</i>	<i>65</i>
<i>Figure 4.2 Blown up longitudinal axis poles around phugoid and altitude modes.....</i>	<i>66</i>
<i>Figure 4.3 Lateral-directional axis poles</i>	<i>67</i>
<i>Figure 4.4 Blown up lateral-directional axis poles around Dutch roll, spiral, and heading modes.....</i>	<i>68</i>
<i>Figure 4.5 Short period mode undamped natural frequency, ω_{nsp} requirements – Category B Flight Phases [4, 30-32]</i>	<i>72</i>
<i>Figure 4.6 Short period mode undamped natural frequency, ω_{nsp}</i>	<i>73</i>
<i>Figure 4.7 Short period mode damping ratio, ζ_{sp}</i>	<i>74</i>
<i>Figure 4.8 Phugoid mode damping ratio, ζ_{ph}</i>	<i>77</i>

<i>Figure 4.9 Dutch roll mode damping ratio, ζ_{dr} and natural frequency, ω_{ndr}</i>	<i>79</i>
<i>Figure 4.10 Roll mode time constant, τ_r.....</i>	<i>80</i>
<i>Figure 4.11 Spiral mode 1/Time to Double, $1/T_{2s}$.....</i>	<i>81</i>
<i>Figure 4.12 Three plan view of Predator RQ [28].....</i>	<i>83</i>
<i>Figure 4.13 Results of dynamic stability comparisons between the subject UAV and Predator RQ-1 [28].....</i>	<i>86</i>
<i>Figure 5.1 Inner roll attitude and roll rate control loops.....</i>	<i>94</i>
<i>Figure 5.2 Inner yaw rate control loop with washout filter and coordinated turn control loop</i>	<i>96</i>
<i>Figure 5.3 Heading controller structure.....</i>	<i>97</i>
<i>Figure 5.4 Inner pitch attitude and pitch rate control loops.....</i>	<i>99</i>
<i>Figure 5.5 Altitude controller structure.....</i>	<i>100</i>
<i>Figure 5.6 Airspeed controller structure.....</i>	<i>101</i>
<i>Figure 5.7 Roll attitude final response to 60° step input</i>	<i>103</i>
<i>Figure 5.8 Sideslip velocity final response.....</i>	<i>105</i>
<i>Figure 5.9 Linear model responses to $+30^\circ$ reference ϕ command with and without washout filter.....</i>	<i>107</i>
<i>Figure 5.10 Heading final response to 90° step input</i>	<i>108</i>
<i>Figure 5.11 Pitch angle final response to 10° step input.....</i>	<i>110</i>
<i>Figure 5.12 Altitude final response to 1 m step input.....</i>	<i>111</i>
<i>Figure 5.13 Airspeed final response to 1 m/s step input.....</i>	<i>113</i>
<i>Figure 5.14 Graphs of the varying controller gains with respect to the dependent parameter(s)</i>	<i>119</i>
<i>Figure 5.15 Implementation of perturbation controller into nonlinear model</i>	<i>120</i>
<i>Figure 5.16 Actuator saturation function.....</i>	<i>121</i>
<i>Figure 5.17 Integrator clamping ($e \cdot d > 0$)</i>	<i>122</i>
<i>Figure 5.18 Lower and upper θ limits throughout the operational flight envelope.....</i>	<i>123</i>
<i>Figure 5.19 Responses to 100 m reference altitude increase command with and without anti-integral wind up.....</i>	<i>125</i>
<i>Figure 5.20 Responses to 10 knots reference KEAS increase command with and without anti-integral wind up.....</i>	<i>126</i>
<i>Figure 5.21 LQ controller design flowchart</i>	<i>131</i>

<i>Figure 5.22 General Inner loop TECS structure – γ and \dot{V} controller.....</i>	<i>135</i>
<i>Figure 5.23 Outer loop TECS structure – h and V controller.....</i>	<i>136</i>
<i>Figure 5.24 Longitudinal synthesis model.....</i>	<i>137</i>
<i>Figure 5.25 Inner loop TECS – Linear model time simulation responses to simultaneous +4° FPA and 0.1 m/s² acceleration reference commands.....</i>	<i>141</i>
<i>Figure 5.26 Altitude final response to 1 m step input.....</i>	<i>142</i>
<i>Figure 5.27 Airspeed final response to 1 m/s step input.....</i>	<i>143</i>
<i>Figure 5.28 Inner loop lateral-directional LQ controller structure – β and ϕ controller</i>	<i>144</i>
<i>Figure 5.29 Outer loop lateral-directional controller structure – ψ controller.....</i>	<i>145</i>
<i>Figure 5.30 Lateral-directional synthesis model</i>	<i>147</i>
<i>Figure 5.31 Inner loop lateral-directional controller – Linear model time simulation responses to +60° bank angle command</i>	<i>151</i>
<i>Figure 5.32 Lateral-directional linear model with heading controller simulation responses to +180° bank angle command</i>	<i>153</i>
<i>Figure 5.33 Graphs of the longitudinal LQ controller gains with respect to the dependent parameters</i>	<i>161</i>
<i>Figure 5.34 Graphs of the lateral-directional LQ controller gains with respect to the dependent parameters</i>	<i>163</i>
<i>Figure 5.35 Implementation of perturbation controller into nonlinear model</i>	<i>164</i>
<i>Figure 5.36 Actuator saturation function.....</i>	<i>164</i>
<i>Figure 5.37 Integrator clamping ($e \cdot d > 0$)</i>	<i>165</i>
<i>Figure 5.38 Lower and upper γ limits throughout the operational flight envelope.....</i>	<i>166</i>
<i>Figure 5.39 Responses to 4,000 m reference altitude increase command with and without anti-integral wind up.....</i>	<i>168</i>
<i>Figure 5.40 Responses to 35 knots reference KEAS increase command with and without anti-integral wind up.....</i>	<i>170</i>
 <i>Figure 6.1 Classical controlled nonlinear model responses to +3° θ increase reference step command</i>	 <i>172</i>
<i>Figure 6.2 LQ controlled nonlinear model responses to +3.35° γ increase reference step command</i>	<i>174</i>

<i>Figure 6.3 Classical controlled nonlinear model responses to continuous column input generating $+6.56^\circ$ change in pitch attitude.....</i>	<i>176</i>
<i>Figure 6.4 LQ controlled nonlinear model responses to column pulse input generating $+7.2^\circ$ change in FPA</i>	<i>178</i>
<i>Figure 6.5 Classical and LQ controlled nonlinear model responses to $+45^\circ \phi$ increase reference step command.....</i>	<i>180</i>
<i>Figure 6.6 Classical and LQ controlled nonlinear model responses to negative continuous wheel inputs.....</i>	<i>183</i>
<i>Figure 6.7 Classical and LQ controlled nonlinear model responses to $+180^\circ \psi$ increase reference step command</i>	<i>185</i>
<i>Figure 6.8 Classical and LQ controlled nonlinear model responses to $+3,000 \text{ m h}$ increase reference step command.....</i>	<i>188</i>
<i>Figure 6.9 Classical and LQ controlled nonlinear model responses to $+10 \text{ KEAS}$ increase reference step command.....</i>	<i>190</i>
 <i>Figure A.1 Earth-Fixed and Body-Fixed Coordinate Systems [14-15]</i>	 <i>202</i>
 <i>Figure C.1 Main level nonlinear model MATLAB[®]/Simulink[®] display.....</i>	 <i>213</i>
<i>Figure C.2 Major nonlinear model build up blocks of the UAV subsystem.....</i>	<i>214</i>
<i>Figure C.3 FORCES AND MOMENTS subsystem.....</i>	<i>215</i>

LIST OF SYMBOLS & ABBREVIATIONS

Symbols (LATIN)	Definition and Description
a	Speed of sound
a_0	Speed of sound in mean sea level
a, b	Engine model parameters
A	Aspect ratio
\mathbf{A}	System matrix
\mathbf{A}'	Augmented system matrix
b	Wing span
\mathbf{B}	Control input matrix
\mathbf{B}'	Augmented control input matrix
\bar{c}	Mean Aerodynamic Chord (MAC)
c_r	Root chord
c_t	Tip chord
c_t/c_r	Taper ratio
\mathbf{C}	Output matrix
\mathbf{C}'	Augmented output matrix
C_{aileron}	Static nondimensional aerodynamic coefficients originated from aileron deflection
C_D	Nondimensional drag coefficient
C_L	Nondimensional lift coefficient
CL_α	Air vehicle lift-curve slope
$CL_{\dot{\alpha}}$	Variation of lift coefficient with nondimensional rate of change of angle of attack
CL_q	Variation of lift coefficient with nondimensional pitch rate
C_M	Nondimensional pitching moment coefficient
$CM_{\dot{\alpha}}$	Variation of pitching moment coefficient with nondimensional rate of change of angle of attack
CM_q	Variation of pitching moment coefficient with nondimensional pitch rate
C_N	Nondimensional yawing moment coefficient
CN_p	Variation of yawing moment coefficient with nondimensional roll rate
CN_r	Variation of yawing moment coefficient with nondimensional yaw rate
CR	Nondimensional rolling moment coefficient

CR_p	Variation of rolling moment coefficient with nondimensional roll rate
CR_r	Variation of rolling moment coefficient with nondimensional yaw rate
$C_{ruddervator}$	Static nondimensional aerodynamic coefficients originated from ruddervator deflection
C_{total}	Total nondimensional aerodynamic force and moment coefficients (static and dynamic)
$C_{wing-body-tail}$	Static nondimensional aerodynamic coefficients originated from wing-body-tail
CX	Nondimensional body-fixed drag force coefficient
CY	Nondimensional side force coefficient
CY_p	Variation of side force coefficient with nondimensional roll rate
CY_r	Variation of side force coefficient with nondimensional yaw rate
CZ	Nondimensional body-fixed lift force coefficient
d	Demanded plant input by the controller
dm	Airplane mass element
ds	Airplane surface area element
dv	Airplane volume element
$\frac{dv_w}{dt}, \frac{dw_w}{dt}$	Body-fixed y-, and z-axes accelerations due to background wind plus turbulence
D	Matrix representing the relationship between control inputs and outputs
e	Input to the compensator, error
E	Total energy of the air vehicle
\dot{E}	Total energy rate of the air vehicle
f	Nonlinear system function
\bar{F}	Body-fixed total force
\bar{F}	Force per unit area (aerodynamic and/or thrust)
\bar{g}	Gravitational acceleration
h	Geopotential height
h	Nonlinear output function
$\dot{h}, hdot$	Rate of climb
$h_{troposphere}$	Troposphere height
$\vec{i}, \vec{j}, \vec{k}$	Unit vectors along body-fixed axes
i_t	Tail incidence angle
i_w	Wing incidence angle
I_{xx}, I_{yy}, I_{zz}	Moment of inertias about x-, y-, z- axes
I_{xy}, I_{xz}, I_{yz}	xy, xz, yz products of inertia

J	Performance index/Quadratic cost function
K	Classical controller feedback gain
K_{CP}, K_{CI}	TECS inner loop proportional-integral column gains
K_h, K_v	TECS outer loop proportional altitude, airspeed gains
K_{lqr}	Optimal gain matrix
K_p, K_i, K_d	Proportional-integral-derivative gains
K_ψ	LQ lateral-directional controller outer loop proportional heading gain
K_{TP}, K_{TI}	TECS inner loop proportional-integral throttle gains
L	Lapse rate
m	Air vehicle mass
\vec{M}	Body-fixed total moment
M_α	Pitch angular acceleration per unit angle of attack
$M_{\dot{\alpha}}$	Pitch angular acceleration per unit change of angle of attack
M_q	Pitch angular acceleration per unit pitch rate
n	Engine speed
n	Normal load factor
n/α	Acceleration sensitivity of the air vehicle
N_β	Yaw angular acceleration per unit sideslip angle
N_r	Yaw angular acceleration per unit yaw rate
p, q, r	Body-fixed roll, pitch, yaw rates
p_w, q_w, r_w	Wind roll, pitch, yaw rates in body-fixed axes
p_z	Manifold pressure nonlinearly related to engine speed
P	Air pressure
P	Engine power
P_0	Ambient pressure at mean sea level
\bar{q}	Dynamic pressure
Q	States weighting matrix
\vec{r}	Body-fixed position vector
\vec{r}	Vector which connects the c.m. with a mass element
\vec{r}'	Vector which connects the origin of $X_E Y_E Z_E$ with an airplane mass element
\vec{r}_p'	Vector which connects the origin of $X_E Y_E Z_E$ with airplane c.m.
R	Control inputs weighting matrix
R	Specific gas constant
R, M, N	Body-fixed roll, pitch, yaw moments
s	Pole

S	Wing planform area
T	Ambient temperature
T_0	Ambient temperature at mean sea level
T_2	Time-to-double
$\text{Thrust}_{\text{REQ}}$	Thrust required to maneuver
\mathbf{u}	p-dimensional time varying control input vector
$\tilde{\mathbf{u}}$	Small control input perturbations vector
$\mathbf{u}_{\text{max}}, \mathbf{u}_{\text{min}}$	Maximum and minimum allowable control effort limits
\mathbf{u}_n	Nominal or trimmed control settings
u, v, w	Body-fixed velocities in x-, y-, z-axes
u_w, v_w, w_w	Wind velocities in body-fixed x-, y-, z-axes
v	Velocity in body y-axis/Sideslip velocity
\vec{V}, \vec{V}_p	Body-fixed total air vehicle velocity
$\dot{V}, \dot{\vec{V}}_p, \dot{V}_{\text{dot}}$	Air vehicle acceleration
w	Velocity in body z-axis
\vec{W}	Earth-fixed gravitational force vector
\mathbf{x}	n-dimensional state vector
$\tilde{\mathbf{x}}$	Small state perturbations vector
x_E, y_E, z_E	Air vehicle coordinates
\mathbf{x}_n	Nominal or trimmed states vector
X, Y, Z	Body-fixed drag, sideforce, lift forces
$X_B Y_B Z_B$	Body-fixed axes reference frame
$X_E Y_E Z_E$	Earth-fixed axes reference frame
$X_S Y_S Z_S$	Stability-axes reference frame
X_u	Forward acceleration per unit change in speed
$X_W Y_W Z_W$	Wind-axes reference frame
\mathbf{y}	Output vector
$\tilde{\mathbf{y}}$	Small output perturbations vector
\mathbf{y}_n	Nominal or trimmed outputs vector
Y_β	Lateral acceleration per unit sideslip angle
Y_r	Lateral acceleration per unit yaw rate
\mathbf{Z}	Synthesis model criterion outputs
Z_α	Vertical acceleration per unit angle of attack
Z_u	Vertical acceleration per unit change in speed
(GREEK)	
α	Angle of attack

β	Sideslip angle
δ	Relative pressure ratio at the flight altitude
δ_{aileron}	Aileron deflection
δ_{column}	Column deflection/Symmetric ruddervator deflection
δ_{flap}	Flap deflection
δ_{pedal}	Pedal deflection/Asymmetric ruddervator deflection
$\delta_{\text{ruddervator}}$	Ruddervator deflection
δ_{throttle}	Throttle position change
$\delta_{\text{ThrottleDemand}}$	Demanded throttle input
δ_{wheel}	Wheel deflection/Aileron deflection
Δp_t	Difference between the total pressure in front of the propeller and the total pressure behind the propeller
ϕ	Bank angle
γ	Adiabatic index
γ	Flight path angle (FPA)
Γ	Dihedral angle
$-\lambda$	Real target zero location
$\vec{\omega}$	Body-fixed total angular rate
ω_a	Natural frequency of the actuator dynamics
ω_n	Natural frequency
ρ	Air density
ρ_0	Air density at mean sea level
ψ	Yaw angle/Heading angle
τ	Time constant
θ	Pitch angle
ζ	Damping ratio
ζ_a	Damping ratio of the actuator dynamics
Λ	Sweep angle at 25% chord

Subscripts

airspeed	Denotes airspeed
altitude	Denotes altitude
A	Denotes aerodynamics
β	Denotes sideslip angle
c	Denotes command
dynamic	Denotes dynamic coefficients
dr	Denotes Dutch roll mode
e	Denotes error

ϕ	Denotes bank angle
heading	Denotes heading
lat-dir.	Denotes lateral-directional axis
long.	Denotes longitudinal axis
ph	Denotes phugoid mode
pitch	Denotes pitch attitude
pitch rate	Denotes pitch rate
roll rate	Denotes roll rate
sp	Denotes short period mode
G	Denotes gravity
r, roll	Denotes roll mode
s, spiral	Denotes spiral mode
sideslip velocity	Denotes sideslip velocity
static	Denotes static coefficients
T	Denotes thrust
wo	Denotes washout filter
yaw rate	Denotes yaw rate

Abbreviations

AFCS	Automatic Flight Control System
CFD	Computational Fluid Dynamics
c.m.	Center of Mass
DATCOM	Data Compendium
DCM	Direction Cosine Matrix
DLR	German Aerospace Center
DOF	Degree of Freedom
EAS	Equivalent Airspeed
EGT	Exhaust Gas Temperature
FBW	Fly-by-Wire
FMS	Flight Management System
FPA	Flight Path Angle
ISA	International Standard Atmosphere
JSF	Joint Strike Fighter
KEAS	Knots-Equivalent Airspeed
LQ	Linear Quadratic
LQG	Linear Quadratic Gaussian
LQR	Linear Quadratic Regulator
LRU	Line Replaceable Unit

MALE	Medium Altitude-Long Endurance
MIMO	Multi Input-Multi Output
NED	North-East-Down
NDI	Nonlinear Dynamic Inversion
PI	Proportional-Integral
PID	Proportional-Integral-Derivative
REAL	Robust and Efficient Autoland Control Law
RF	Radio Frequency
RPM	Revolution per Minute
RPV	Remotely Piloted Vehicles
S&C	Stability and Control
SISO	Single Input-Single Output
SQP	Sequential Quadratic Programming
SRC	SIMICon Rotor-craft
SRO	Simulink Response Optimization
TAI	TUSAŞ Aerospace Industries
TAS	True Airspeed
TECS	Total Energy Control System
TSRV	Transport System Research Vehicle
UAV	Unmanned Aerial Vehicle
USAF	United States Air Force
WGS	World Geodetic System
WO	Washout Filter

CHAPTER 1

INTRODUCTION

1.1 Background and Motivation

An unmanned aerial vehicle (UAV) is defined as “a powered, aerial vehicle that does not carry a human operator, uses aerodynamic forces to provide vehicle lift, can fly autonomously or piloted remotely, can be expendable or recoverable, and can carry a lethal or non-lethal payload.” in Joint Publication 1-02, the Department of Defense Dictionary [1]. According to this reference, ballistic or semi-ballistic vehicles, cruise missiles, and artillery projectiles are not considered as unmanned aerial vehicles.” UAVs are clearly delimited with this definition by being distinguished from missiles or unpowered air vehicles like gliders.

In recent years, both in civilian and military environments, it is accepted that UAVs have many advantages over manned air vehicles. These advantages arise from important characteristics like human risk avoidance, cost efficiency, portability, longer operational endurance, etc. The resultant increase of UAV project investments is causing rapid development in unmanned technologies.

The potential civil applications of UAVs can be categorized [2, 3] as

- Dangerous missions including operations at poisonous environment, radiation disaster hazard, extreme high altitudes, and severe weather conditions,
- Scientific missions including environmental monitoring, weather forecasting, atmospheric data collection, oceanographic data collection, agricultural hyper-spectral imaging, and magnetic, radiological, gravimetric mapping,
- Commercial missions including border surveillance, city automobile traffic monitoring, airborne cellular antenna, wildland monitoring and fire-fighting, pipelines and power line monitoring, and satellite relay.

The major military missions UAVs are given to accomplish depending on their maneuverability levels and masses (sizes) are [4] as follows

- Surveillance and reconnaissance,
- Electronic warfare (early warning/electronic counter measures),
- Harassment,
- Relay command/control/communications,
- Terrain following/avoidance,
- Antisubmarine search,
- Surface attack,
- Formation flying,
- Weapon delivery,
- Air-to-air combat,
- Target acquisition,
- Interceptor, etc.

The maneuverability level and mass (size) together are also used for the UAV classification. UAVs that sustain maximum load factors of 4g are thought to be of low-maneuverable type. Besides this, if they are heavier than 300 lbs (136 kg) as an additional feature, they belong to Class II [4].

In general, a medium altitude-long endurance (MALE) type UAV has an endurance more than 20 hours and an operational flight altitude more than 20,000 ft (~6,100 m) [3, 5]. General Atomics “Predator B” UAV is a typical example of MALE type UAVs with its long wing span, high aspect ratio, V-tail and pusher propeller configuration. Figure 1.1 displays a picture of Predator B.

The subject of the present study is a MALE type UAV belonging to Class II for which the main appointed mission is surveillance and reconnaissance. The configurations are very alike with Predator B given in Figure 1.1. While one could

say that the pilotless aircraft discipline started quite some time ago, the long-range reconnaissance mission is what is currently making a further dent into the pilots' private hunting grounds.



Figure 1.1 General Atomics Predator B UAV [6]

The flight control is the key design issue of unmanned systems. The fly-by-wire (FBW) system, high reliability and safety, high level of autonomy, automatic takeoff and landing and more electric aircraft constitute the baseline of UAV flight control technologies. A large number of design methods were applied to flight control ranging from proportional-integral-derivative (PID) control to model predictive control. From an industrial perspective, it can be said that today's standard to design automatic flight control laws use some multivariable techniques blended with classical tools. For example, linear quadratic (LQ) control and nonlinear dynamic inversion (NDI) are two of the most successful multivariable methods. Following examples of various flight control laws and control applications utilized in respective

aircraft projects of industry mentioned in [7] may also give an insight about the control applications selections in real life:

- France, Airbus – A320: Classical proportional-integral (PI) control / flight envelope protection / first FBW control system,
- France, Airbus – A340: Reproduced architecture and principles for A320 / addition of structural mode control to reduce structural mode vibration caused from the increased size and flexibility,
- US/Germany program – X-31A Post stall experimental aircraft: Optimal LQ digital regulator scheduled with angle of attack, Mach number and altitude / nonlinear feedforward blocks,
- Germany, DLR – Robust and Efficient Autoland Control Law (REAL) program: Stability and command augmentation, tracking, and guidance applications where inner loops designed using NDI and PI control used in lateral tracking / total energy control system (TECS) application,
- Italy, Alenia – Eurofighter: Classical control tools such as Nichols/Bode plots, linear time responses / large amplitude nonlinear closed loop simulations / modified control structure with nonlinear elements,
- Israel – Lavi: Classical technique with optimal control methods used in preliminary design process,
- Russia – Sukhoi 37: Adaptive controller to eliminate small amplitude self-induced oscillations due to actuator nonlinearities / longitudinal controller synthesized with classical control methods,
- USA, Boeing: Linear quadratic regulator (LQR)-linear quadratic gaussian (LQG) based multivariable control / integrator attachment and target zeros setting,
- USA, Honeywell Research Center: Proportional or PI control at outer loops and dynamic inversion control at inner-loops,
- USA, Lockheed Martin – JSF: NDI control / direct mapping of flying qualities to control laws,

- Brazil, Embraer – ERJ170: Standard classical flight control selection because of cost constraints and accelerated time schedule / improved flying qualities / digital FBW system.

In the present research, the control approaches chosen are classical and optimal control. A multivariable technique – LQ control is to be developed in the scope of optimal flight control. This selection gives the chance of examining the advantages and disadvantages of two industrial based control methods that have been frequently applied till today. The motivation for this study is arisen from the research and development activities currently continuing in TAI (TUSAŞ Aerospace Industries, INC.).

1.2 Literature Survey

A literature survey given here mainly covers the areas of aircraft modeling and simulation, classical flight control and optimal flight control. The studies done in these areas are in a wide range in terms of quantity and focused topics, so only the ones that cover at least two main subjects of the present research are selected in order to summarize the key points:

M.Sc. thesis “*Design and Rapid Prototyping of Flight Control and Navigation System for an Unmanned Aerial Vehicle*” conducted in the Aeronautical Engineering of Naval Postgraduate School, CA, USA [8]:

This study specifically sought to design and implement an onboard flight control and navigation system for a UAV called as “FROG”, to be used as the autonomous airborne vehicle for the research, using the xPC Target Rapid Prototyping System from The Mathworks, Inc. The scope of work included the process to create a simple 6 DOF model for the UAV, design of two autopilots with classical and modern control approaches utilizing MATLAB[®]/Simulink[®], exploring suitable trajectory

planning navigation algorithms, and assembling an onboard computer to perform data fusion, flight control and guidance commands computation.

The first autopilot was designed based on the classical inner-outer loop control approach using the linearized model of the developed 6 DOF FROG UAV model and adjusted for nonlinearity via gain scheduling with respect to dynamic pressure parameter. The classical control design procedure consisted of evaluating the stability of the feedback loop using root locus techniques, adding poles or zeros to shape the system behavior in the compensator where needed, adjusting loop gains to achieve desired gain and phase margins and verifying the response in each loop with step commands of reasonable magnitude. General requirements were to attain more than 6 dB gain margin, at least 45° phase margin, and at least one decade bandwidth separation between inner and outer loops. Altitude and heading control channels were examples of the classical inner-outer loop control approach mentioned in this thesis, as for altitude control, pitch angle hold constitute the inner loop whereas for heading control, bank angle hold was the inner loop. It should be noted at this point that, another use of inner loop-outer loop concept which might create confusion with the case in here is the autopilot hold functions at inner loop and guidance functions at outer loop. In addition to the altitude and heading controls, yaw damper and airspeed control channels were designed. The turn coordination was imposed in the yaw damper. A PI controller was used in the yaw damper, airspeed control, and inner-outer loops of heading control with a roll rate feedback. PID controller was used in inner-outer loops of altitude control.

The second autopilot was designed for the control variables airspeed, sideslip, heading, and altitude. The design used an integral LQR (LQ controller) structure. The design requirements adopted were a zero steady state error to a constant command in airspeed, sideslip, heading, and altitude, an overshoot less than 10% to step commands in the altitude and airspeed, a rise time around 10 s in response to step altitude commands and step airspeed commands, at least 6 dB gain margin in control loops, at least 45° phase margin, around 10 rad/s aileron, elevator and rudder

loop bandwidths, maximum 5 rad/s thrust loop bandwidth. To ensure zero steady state errors, the integral control is used in conjunction with the LQR technique. To design the LQ controller, the following steps were applied respectively;

- Constructing the synthesis model for the plant,
- Inserting transmission zeros to the synthesis model (the “target” poles location for the state feedback plant),
- Linearizing the synthesis model,
- Adjusting the weighting matrices **Q** and **R** to vary the cost of states and control inputs (starting with identity),
- Obtaining the optimal gain **K** using MATLAB[®] `lqr (A, B, Q, R, N)` function,
- Inserting the optimal gain **K** for the plant’s states and error states feedback,
- Repeating the last two steps until adjusting **Q** and **R** that give the desired control bandwidths, gain and phase margins.

Comments on the clarity level: Since the UAV modeling and flight control design were not the only topics that were focused on in the reviewed study, there were some important details that were not clear including aerodynamic coefficients establishment (how they were obtained and implemented, reliability of the methods used), trimming and linearization steps, an important part of the nonlinear implementation – gain scheduling application and results where only responses to small amplitude step inputs were plotted. Also the conclusions did not include the comments on whether or not the control system requirements were met except for the ones determining gain and phase margin limits.

A study “Rapid Development Of UAV Autopilot Using MATLAB[®]/Simulink[®]” done in BAE Systems Controls [9]:

This research was summarized in a published paper, including UAV modeling, design analysis, code generation, testing of autopilot, and engine monitoring algorithms using MATLAB[®]/Simulink[®].

MATLAB[®]/Simulink[®] was used to model the UAV system with high fidelity to reduce the rework cost. The nonlinear model included the following components:

- 6 DOF nonlinear dynamic model of the UAV,
- Atmosphere model and turbulence model,
- Landing gear model and steering wheel model,
- Control surface models,
- Actuator models,
- Sensor models,
- Engine RPM and EGT model, and propeller thrust model,
- Radio frequency (RF) data link model,
- Autopilot model including flight phase and mode logic, longitudinal, lateral and directional control, throttle and fuel mixture controls, braking and ground steering controls, guidance and navigation data computation, and engine status monitoring.

Some intricate details of the UAV system were included in the overall model that permitted complete flight mission verification by simulation. “Stateflow”, which is a part of Simulink[®] environment, was used in designing the system mode transition logic and flight phase logic.

The UAV autopilot was based on an existing UAV design by another BAE Systems Controls division. Commands `trim` and `linmod` were used for obtaining linear time invariant models from the 6 DOF nonlinear aircraft model. The trim points were determined based on the flight envelope of the UAV in terms of speed and altitude, mass configurations, center of mass locations, flap settings, and flight path angles. Commands `sisotool` and `ltiview` were invoked for linear analysis and the objectives were to ensure that under all flying conditions bandwidth requirements, stability margins and robustness requirements, dynamic performance (rise time, overshoot, settling time and steady state error) requirements, and turbulence response

requirements were met. Some inner loop control gains were scheduled based on the computed dynamic pressure. All the control loop parameters were fed into the autopilot and engine monitoring algorithm design model.

The study showed that MATLAB[®]/Simulink[®] could play a major role in embedded system and flight-critical system development and great savings could be achieved.

Comments on the clarity level: Since the reviewed study was in the form of a published paper, some important details of the applications were not given because of the restricted space.

M.Sc. thesis “Modeling and Control of the SimiCon UAV” conducted in the Department of Electric and Electronics of Glasgow University [10]:

This study covers the modeling and control of a novel, disc-shaped hybrid UAV called “SIMICon Rotor-craft (SRC)”. Figure 1.2 displays a view of the subject UAV.

The analysis can be divided into three parts: the use of easily available computer tools to evaluate the aerodynamic properties of the air vehicle, the construction of a simulation environment, and the design and simulation of a control system.

The software used to model the aircraft was the USAF Digital DATCOM[®], augmented by various other programs. This gathered data was formed into a large set of lookup tables. The modeling was carried out using MATLAB[®]/Simulink[®]. In the simulation environment, atmosphere, wind-turbulence, gravity, engine, and actuator models were included.

The controller was of LQR structure. After various maneuvers are carried out, including steady level flight, altitude changes, and turns the controller was decided to be improved further by augmenting it with integral action. The LQ controller was

developed using full state feedback, without any observer design. In order to derive \mathbf{Q} and \mathbf{R} weighting matrices, Bryson inverse square method was used.

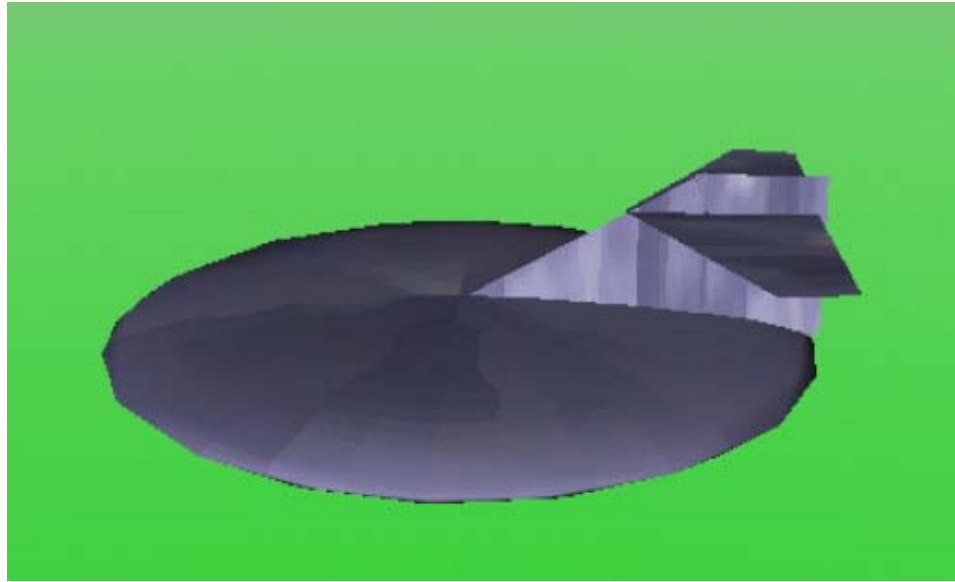


Figure 1.2 SRC view [10]

Comments on the clarity level: The nonlinear model development part was explained in a detailed way, displaying most of the modeling blocks utilized in MATLAB[®]/Simulink[®]. In the LQ controller development part, the build up phase of the flight controller was not very clear causing questions to arise while reading. Besides, only a few graphs of controlled model simulation results were displayed. Concrete measures for the acceptability of controller performance i.e. the flight control requirements were not stated.

M.Sc. thesis “A SIMULINK® Environment for Flight Dynamics and Control Analysis – application to the DHC-2 Beaver” conducted in the Faculty of Aerospace Engineering of Delft University of Technology [11-12]:

This study was composed of two parts. In the first part, an environment for the analysis of aircraft dynamics and control was developed for the “DHC-2 Beaver” aircraft using MATLAB®/Simulink®. In second part, this model was used for the analysis of the Beaver autopilot. Aircraft trim and linearization tools were included, in order to carry out a whole linear and nonlinear control system design and analysis from within the same MATLAB®/Simulink® environment. In the package, blocks to simulate the influence of atmospheric disturbances upon the motions of the aircraft and to generate radio-navigation signals for the assessment of navigation and approach control laws were also included. The tools from this study were worked out for the Beaver aircraft.

The Beaver autopilot, which was based upon classical linear control theory, served as an example for a similar baseline autopilot, to be developed for the new “Cessna Citation II” laboratory aircraft. The longitudinal autopilot modes developed were composed of pitch attitude hold mode, altitude hold mode, altitude select mode, longitudinal part of the approach mode – glideslope, and longitudinal part of the go-around mode, whereas the lateral autopilot modes were roll attitude hold mode with turn coordinator, heading hold/heading select modes, lateral part of the approach mode – localizer, navigation mode, and lateral part of the go-around mode. In short, the autopilot consists of basic control (hold/select modes) at the inner loops and guidance (glideslope, localizer, and go-around) at the outer loops. Figure 1.3 displays a representation of this inner loop-outer loop relationship of basic control modes and guidance modes.

Nonlinear simulations were used for fine tuning the limiters in the model. It was shown that the influence of the propeller-slipstream caused large sideslip angles if

the velocity or engine power was changed. In turns, the sideslip angle was suppressed effectively by means of a turn coordinator which worked well, even for the fast turns that were allowed for the Beaver autopilot.

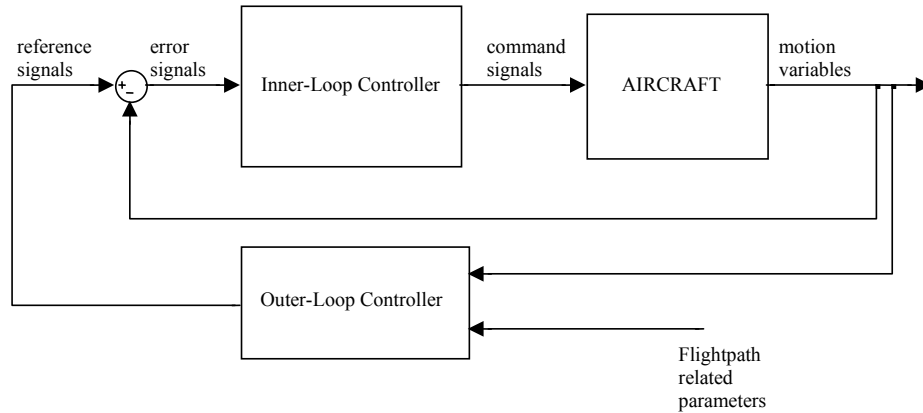


Figure 1.3 Inner loop-outer loop Beaver autopilot [11-12]

Comments on the clarity level: The main purpose of this study (the autopilot design constituting Part II is developed as the case study of Part I) was to obtain a MATLAB®/Simulink® model library, therefore the descriptions were given in a very detailed and systematic way throughout the whole work. In the development part of the classical controller, the selection method and justification of gains were not described in detail, or controller requirements were not stated clearly, either.

It is possible to supply a nonlinear aircraft model from internet such as the library obtained with the baseline model of Beaver aircraft or from software demos such as Aerospace Toolbox demo of MATLAB®/Simulink®, etc. These models may be flexible or not in terms of difficulty of adapting a different aircraft configuration into it. However, in either case, spending a considerable time and effort is unavoidable

since it is required to examine and understand in detail the nonlinear model draft someone else has developed. Therefore, in order to obtain a nonlinear Simulink® model of a new configuration that one has complete control on and in the meantime learns a lot while developing the model, the best way is to start from an empty “.mdl” file and building up the nonlinear model. The Aerospace Toolbox provides a good means of aircraft nonlinear model build up if Simulink® is the tool intended to be used. This makes the model troubleshooting faster if a problem arises and also makes the trim/linearization applications and autopilot implementations easier. However, the existing models can be used as guides while developing a new model.

1.3 Research Objectives

The objectives of this work can be divided into two parts:

Part I: The first objective is to develop a nonlinear simulation model of the subject UAV using MATLAB®/Simulink® environment. This part includes building up the Simulink® blocks in a modular form that will be a close representation of the dynamics thus of the real behavior of the UAV together with its major parts like actuators and engine. The atmospheric effects and major flight parameter calculations are also to be included in order to have the complete base for the UAV motion analyses and controller design. To have the nonlinear simulation model in hand gives an opportunity of obtaining trim points and thereby the linear models. Trimming followed by a linearization is a required transition step into the linear control applications. The validation studies are also to be carried out including the validation of linearization method by comparing linear and nonlinear model responses and the validation of nonlinear model by comparing the dynamic stability analyses results with the results of an existing UAV, which has a similar configuration.

Part II: The second objective is to develop two different flight controllers by using classical and optimal control approaches. SRO tool of MATLAB®/Simulink® is to be utilized in the classical flight controller design to obtain the gains in the desired time

domain specification ranges, whereas an LQ controller is to be utilized to obtain gains for the application of full state feedback in an optimal manner. In the longitudinal LQ controller, an innovative design approach total energy control system (TECS) is to be applied in order to achieve an improved performance of an integrated autothrottle/autopilot concept. For both classical and optimal control approaches, the methodology to be applied is first to design linear model controllers at several equilibrium points in the operational flight envelope and then to implement these controllers into the nonlinear simulation model of the UAV developed in Part I.

The nonlinear implementation includes gain scheduling, control input linearization, and dealing with nonlinearities such as saturations. If the linear analysis yields satisfying control laws, detailed simulations of the system must be made, to make sure that the control system behaves well over the part of the flight envelope for which it is designed. This often demands analyses over a wide range of flight speeds, altitudes, or air vehicle configurations, and hence, nonlinear simulations. Finally, it is intended to compare the simulation results of the nonlinear model controlled with two different autopilots.

1.4 Thesis Outline

The present study is composed of seven chapters, each is summarized as follows:

Chapter 1 is an introductory part, which puts forward the motivation and aim of this study, supplies the definition and properties of UAVs in general stressing on the UAV type specific to this study, and briefly gives some flight control applications used in industry. The published studies in literature including the aircraft modeling and control subjects are reviewed and discussed, and finally the research objectives of this study are given.

Chapter 2 covers the development of nonlinear simulation model of the subject UAV including aerodynamic forces and moments, engine, actuators, 6 DOF equations of motion, atmosphere and wind-turbulence, and flight parameters calculation model

blocks using MATLAB[®]/Simulink[®]. Furthermore, system parameters related to the geometry, mass, center of mass, and inertia of the UAV are given, assumptions are listed, and 6 DOF equations of motion of the air vehicle, reference axes systems, and sign conventions are presented.

Chapter 3 defines the trim and linearization processes in general, gives the approaches specific to this study, and presents the related results at a nominal flight condition. The modal matrix is demonstrated and evaluated in order to verify decoupling in longitudinal and lateral-directional axes. Next to this, to verify the linearization methods applied, the linear and nonlinear model responses to the same doublet control inputs in both axes are compared.

Chapter 4 covers the studies related to the nonlinear model validation by presenting the eigenvalues of the linearized models, and the results of dynamic stability analyses at trim points throughout the operational flight envelope. Discussions and illustrations aiming the comparison with an existing UAV data regarding the dynamic stability analyses are also given.

Chapter 5 gives the flight control requirements in military standards and the flight control design of the UAV under enlightenment of these requirements by two control approaches; namely, classical and optimal. The classical flight control design includes the development of roll, heading, pitch, altitude, and airspeed controllers. The optimal control design includes the development of longitudinal and lateral flight controllers. Implementation phases of these controllers into nonlinear UAV model are also covered.

Chapter 6 presents and discusses the results of controlled nonlinear model simulations and performance comparisons of two autopilots.

Chapter 7 summarizes the whole performed study, and gives concluding remarks and recommendations for future work.

CHAPTER 2

DEVELOPMENT OF NONLINEAR SIMULATION MODEL

2.1 Introduction

It is well known that for the analysis of an aircraft dynamics and linear controller applications on this dynamics, linear models are needed. By the development of a nonlinear model on which a linearization procedure is carried out, linear models can be obtained. In addition, a detailed simulation environment generated by the nonlinear model itself helps visualizing and analyzing various flights including maneuvers thereby determining the limitations for the UAV throughout the operational flight envelope. MATLAB®/Simulink® provides effective means of modeling, simulation, and controller development to the designer.

Following a brief definition of geometrical properties of the subject UAV, this chapter gives a survey of the mathematical models forming the nonlinear modeling blocks in Simulink®. The overall model includes 6 DOF aircraft equations of motions, aerodynamics, engine and gravity generated forces and moments, actuators, atmosphere and wind-turbulence models, and flight parameters calculations. The equations of motion are very general, but the forces and moments which act upon the UAV depend on the characteristics of the air vehicle itself.

2.2 The UAV – Properties

The subject air vehicle of this study is a medium altitude-long endurance (MALE) type UAV. Therefore, the configuration selection studies conducted in TAI (TUSAŞ Aerospace Industries, INC.) are based on this fact. The major determinants of the selected configuration are the V-tail, high wing aspect ratio, and a single engine with pusher propeller. The high aspect ratio wing is essential to reduce the induced drag, which should be taken into consideration based on long endurance demand. With

fewer surfaces than a conventional tail, the V-tail is lighter and also produces less drag in addition to high aspect ratio wing advantage. A V-tail also tends to reflect radar at an angle that reduces the return signal, making the aircraft harder to detect which is an advantage for military aircrafts. Its major disadvantage is to increase the complexity of the control system by combining the pitch and yaw controls. A pusher propeller configuration is a natural choice for reconnaissance-surveillance type UAVs, not to limit the seeing capabilities of the front-body sensors. Pusher propeller driven aircrafts tend to exhibit a slight stabilizing tendency in pitch and yaw in comparison to a tractor configuration. The pusher configuration also has an aerodynamic advantage that it can reduce skin friction drag because the part of the aircraft in front of the propeller flies in undisturbed air.

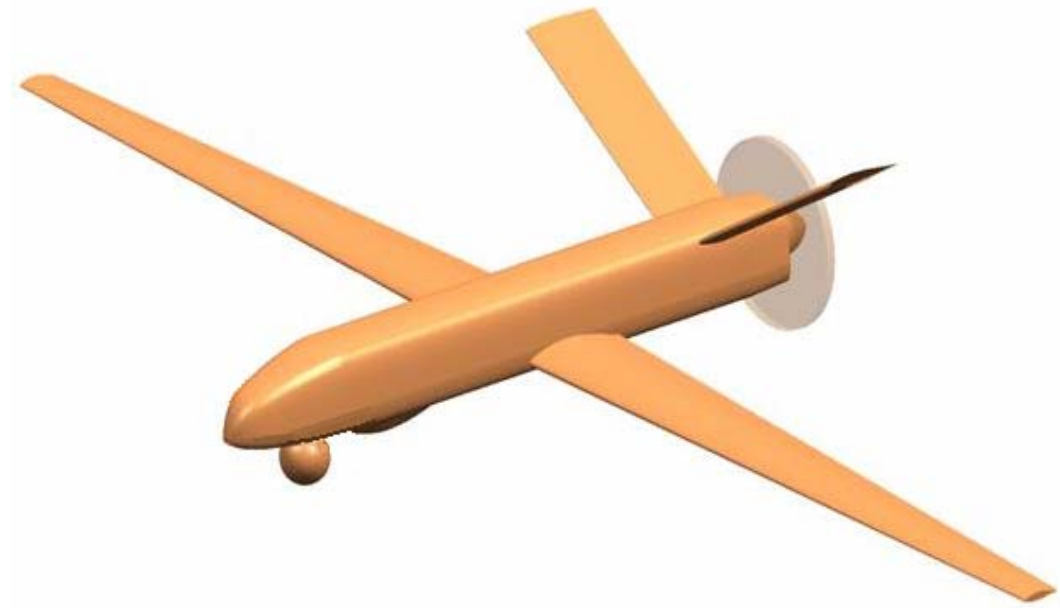


Figure 2.1 The UAV view

A view of the subject UAV is displayed by Figure 2.1, based on the features of the defined configuration. The basic geometrical data of the UAV that is referred to during the computation of aerodynamic coefficients and nonlinear model development phase is given in Table 2.1.

Table 2.1 Basic Geometrical Data

Mass/Center of Mass/Inertial Moments	Values
Mass, m [kg]	1,280
Center of mass, c.m. (% MAC)	23.8
Moment of inertia about x-axis, I_{xx} [kg.m ²]	1,673.35
Moment of inertia about y-axis, I_{yy} [kg.m ²]	3,677.14
Moment of inertia about z-axis, I_{zz} [kg.m ²]	5,154.30
xz product of inertia, I_{xz} [kg.m ²]	276.13
xy product of inertia, I_{xy} [kg.m ²]	0
yz product of inertia, I_{yz} [kg.m ²]	0
Fuselage	Values
Length [m]	7
Maximum height [m]	0.83
Maximum width [m]	0.85
Wing	Values
Surface area, S [m ²]	13.63
Span, b [m]	17.31
Aspect ratio, A	22
Sweep angle at 25% chord, Λ [°]	0
Tip chord, c_t [m]	0.45

Table 2.1 Basic Geometrical Data (continued)

Root chord, c_r [m]	1.124
Taper ratio, c_t/c_r	0.4
Dihedral angle, Γ [$^\circ$]	1.5
Twist angle [$^\circ$]	-1
Incidence angle, i_w [$^\circ$]	5.66
Mean Aerodynamic Chord (MAC) , \bar{c} [m]	0.834
V-tail	Values
Surface area [m ²]	4.244
Span [m]	4.607
Aspect Ratio	5
Sweep angle at 25% chord [$^\circ$]	0
Tip chord [m]	0.761
Root chord [m]	0.761
Taper ratio	1
Dihedral angle [$^\circ$]	34.3
Twist angle [$^\circ$]	0
Incidence angle, i_t [$^\circ$]	0
Mean Aerodynamic Chord (MAC)	0.761

2.3 Assumptions

The air vehicle is modeled as a standard 6 DOF system with the following main assumptions:

1. The aerodynamic database composed of static and dynamic aerodynamic coefficients does not include any nonlinearities at low speeds.

2. Only the aerodynamic coefficients for the flaps-up configuration are included, i.e., takeoff and landing flight phases are not to be taken into account during analyses or flight control system design.
3. Rigid body assumption is done, i.e. aeroelastic effects are not included.
4. Ground effect is not included.
5. Landing gear model is not included.
6. Hinge moments effects are not included.
7. Airframe has a fixed centre of mass (c.m.) position.
8. Vehicle mass and moments of inertia are fixed time invariant quantities.
9. Vehicle has a centered longitudinal plane of symmetry that passes through the c.m.
10. Gravitational acceleration, \vec{g} is constant over the air vehicle body.
11. Earth is flat and fixed in space, and atmosphere is fixed with respect to Earth.

2.4 Reference Coordinate Frames

The Earth-fixed frame denoted by $X_E Y_E Z_E$ and the body-fixed frame denoted by $X_B Y_B Z_B$ are the two reference coordinate frames most frequently used to describe the motion of an air vehicle, as shown in Figure 2.2.

In the Earth-fixed (non-rotating) frame, it is assumed that the Z_E -axis points downwards, parallel to the local direction of the gravitation, whereas the X_E -axis is directed north and the Y_E -axis east. This frame is considered to be fixed in space and is useful for describing the position and orientation of the air vehicle.

In the body-fixed (rotating) frame, the origin is at the air vehicle center of mass. The X_B -axis is directed towards the nose of the air vehicle, the Y_B -axis points to the right wing (starboard), and the Z_B -axis towards the bottom of the air vehicle. In this frame, the inertia matrix of the air vehicle is fixed which makes this frame suitable for describing angular motions.

In addition to these two reference frames, the two other reference frames; namely, the stability-axes and wind-axes reference coordinate frames, are also used for convenience in expressing certain aspects of air vehicle kinematics and dynamics, as shown in Figure 2.3.

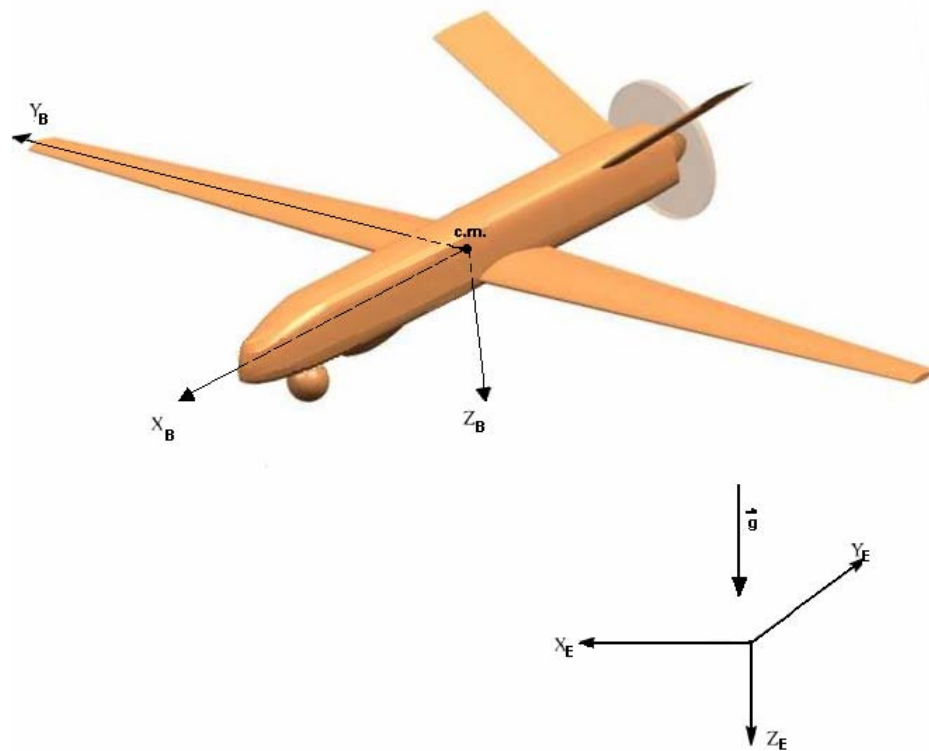


Figure 2.2 Earth-Fixed and Body-Fixed Coordinate Systems

The stability-axes reference frame denoted by $X_S Y_S Z_S$ has its origin at the air vehicle c.m., is a special body-fixed frame, used in the study of small deviations from a nominal flight condition. The orientation of this frame relative to the body-fixed

frame is determined by the angle of attack, α . The X_S -axis is chosen parallel to the projection of the absolute velocity \vec{V} of the air vehicle c.m. on the $X_B Z_B$ -plane (if the air vehicle is symmetric, this is the plane of symmetry), or parallel to \vec{V} itself in case of a symmetrical nominal flight condition.

In the wind-axes reference frame denoted by $X_W Y_W Z_W$, the origin is at the air vehicle c.m. and the x-axis is directed along the velocity vector of the air vehicle, \vec{V} . The orientation of this frame relative to the stability-axes reference frame is determined by the sideslip angle, β .

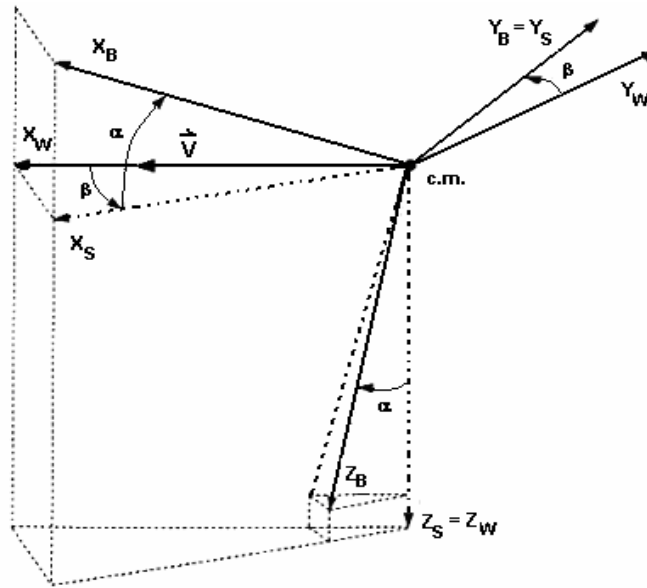


Figure 2.3 Relationships between body-fixed, stability-axes, and wind-axes reference frames

2.5 Body-fixed axes Components and Sign Conventions

Body-fixed axes components are given as

$$\text{Position components: } \vec{r} = x_E \vec{i} + y_E \vec{j} + z_E \vec{k} \quad (2.1)$$

$$\text{Velocity components: } \vec{V} = u \vec{i} + v \vec{j} + w \vec{k} \quad (2.2)$$

$$\text{Angular rate components: } \vec{\omega} = p \vec{i} + q \vec{j} + r \vec{k} \quad (2.3)$$

$$\text{Force components: } \vec{F} = X \vec{i} + Y \vec{j} + Z \vec{k} \quad (2.4)$$

$$\text{Moment components: } \vec{M} = R \vec{i} + M \vec{j} + N \vec{k} \quad (2.5)$$

where $\vec{i}, \vec{j}, \vec{k}$ are the unit vectors along the $X_B Y_B Z_B$ denoted body-fixed axes. In Table 2.2, the positive directions for aerodynamic angles α, β , and Euler angles ϕ, θ, ψ are defined, whereas in Figure 2.4 the positive directions for these angles and body-fixed axes components are illustrated on a representative air vehicle.

Table 2.2 Positive Sign Conventions for Angles

Parameter	Symbol	Positive direction
Angle of attack	α	Nose up with respect to freestream
Angle of sideslip	β	Nose left, looking forward
Bank angle	ϕ	Right wing down, looking forward
Pitch angle	θ	Nose up
Yaw angle	ψ	Nose right, looking forward

The positive sign conventions of the control surface deflections and the resultant moments should also be defined. The control surfaces of the subject UAV are composed of ruddervators and ailerons (flaps are thought as configuration components). The necessity for use of ruddervators, which give the effect of both elevators and rudder, comes from the V-tail configuration. A symmetric downwards

(positive) deflection of ruddervators causes a negative pitching moment whereas a symmetric upwards (negative) deflection causes a positive pitching moment. An asymmetric deflection causes yawing of the UAV. If the resultant asymmetric deflection is oriented towards left, this corresponds to a positive rudder deflection causing a negative yawing moment and vice versa. For both right and left ailerons, a downward deflection is the positive direction and the resultant aileron deflection is given by the relation $\delta_{\text{aileron}} = (\delta_{\text{ail_right}} - \delta_{\text{ail_left}})/2$. A positive δ_{aileron} causes a negative rolling moment and vice versa. The deflections of the right and left ailerons are always asymmetric and equal in magnitude.

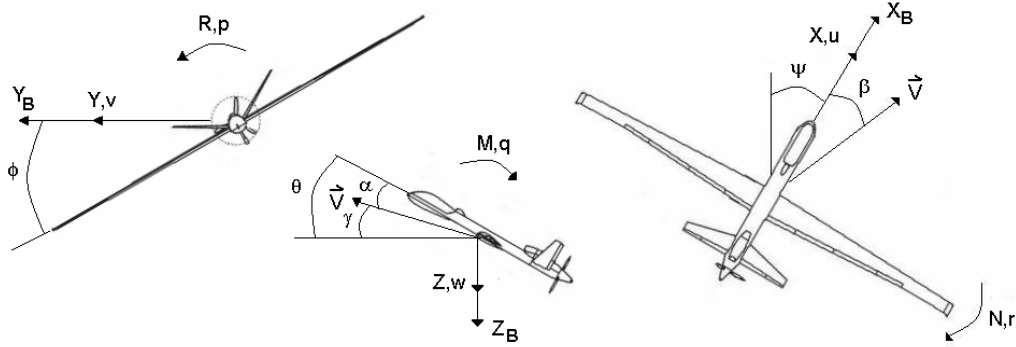


Figure 2.4 Positive directions for body-fixed axes components and angles

2.6 Equations of Motion

Air vehicle equations of motion are derived from Newton's second law of motion. They basically describe the dynamic behavior of the air vehicle as a rigid body moving through the atmosphere. The detailed derivation of these equations is given in many text books and other studies such as [13-15]. The procedure of such detailed derivation is also given in Appendix A.

The nonlinear flight dynamics of an airplane is represented by translational and rotational equations of motion. In this section, the translational and rotational (angular) equations of motion, kinematical relations in body-fixed axes and equations for air vehicle coordinates are given. In the equations, the “A” subscript stands for “aerodynamic” and “T” subscript stands for “thrust”, and “G” subscript stands for “gravity” in forces and moments.

Translational equations of motion:

$$\text{Drag Equation: } m(\dot{u} - vr + wq) = X_A + X_T + X_G \quad (2.6a)$$

$$\text{Sideforce Equation: } m(\dot{v} + ur - wp) = Y_A + Y_T + Y_G \quad (2.6b)$$

$$\text{Lift Equation: } m(\dot{w} - uq + vp) = Z_A + Z_T + Z_G \quad (2.6c)$$

Rotational equations of motion:

$$\text{Roll Moment Equation: } I_{xx}\dot{p} - I_{xz}\dot{r} - I_{xz}pq + (I_{zz} - I_{yy})rq = R_A + R_T \quad (2.7a)$$

$$\text{Pitch Moment Equation: } I_{yy}\dot{q} + (I_{xx} - I_{zz})pr + I_{xz}(p^2 - r^2) = M_A + M_T \quad (2.7b)$$

$$\text{Yaw Moment Equation: } I_{zz}\dot{r} - I_{xz}\dot{p} + (I_{yy} - I_{xx})pq + I_{xz}qr = N_A + N_T \quad (2.7c)$$

Euler angles are one of the standard specifications used for expressing the orientation of the body-fixed frame relative to the Earth-fixed frame. The alternative of such specifications are the direction cosine matrix (DCM) and Quaternion. Given any representation, it is possible to drive the other two. In this study, Euler angles are used to represent the propagation of the airframe attitude in time. Kinematical relationship between Euler angles and body-fixed angular rates are given as

$$\begin{bmatrix} \dot{\phi} \\ \dot{\theta} \\ \dot{\psi} \end{bmatrix} = \begin{bmatrix} 1 & \sin \phi \tan \theta & \cos \phi \tan \theta \\ 0 & \cos \phi & -\sin \phi \\ 0 & \sin \phi \sec \theta & \cos \phi \sec \theta \end{bmatrix} \begin{bmatrix} p \\ q \\ r \end{bmatrix} \quad (2.8)$$

It should be noted that Equations (2.8) are not defined at $\theta = 90^\circ$, where there is a singularity.

Another important set of equations, the navigation equations which relate translational velocity components in body-fixed axes to Earth-fixed axes components, in other words the equations for air vehicle coordinates are given as

$$\dot{x}_E = u \cos \psi \cos \theta + v(\cos \psi \sin \theta \sin \phi - \sin \psi \cos \phi) + w(\cos \psi \sin \theta \cos \phi + \sin \psi \sin \phi) \quad (2.9a)$$

$$\dot{y}_E = u \sin \psi \cos \theta + v(\sin \psi \sin \theta \sin \phi + \cos \psi \cos \phi) + w(\sin \psi \sin \theta \cos \phi - \cos \psi \sin \phi) \quad (2.9b)$$

$$\dot{z}_E = -u \sin \theta + v \cos \theta \sin \phi + w \cos \theta \cos \phi \quad (2.9c)$$

2.6.1 Forces and Moments

The contributions to forces acting on the air vehicle are from aerodynamics, thrust, and gravity, whereas contributions to moments are from aerodynamics and thrust. Each contributing term form the resultant of the corresponding right hand side components of the translational and rotational equations of motion given by Equations 2.6 and 2.7, respectively.

$$\vec{F} = \vec{F}_A + \vec{F}_T + \vec{F}_G \quad (2.10a)$$

$$\vec{M} = \vec{M}_A + \vec{M}_T \quad (2.10b)$$

2.6.1.1 Aerodynamic Forces and Moments

Stability and control derivatives should be available for an efficient system design. These values have some uncertainties and their determination is too expensive especially when some wind tunnel and flight tests are carried out in order to obtain their values accurately. For an industrial based air vehicle design, these tests are inevitable, but in the scope of this study it is acceptable to use their values obtained by employing some computational and empirical methods. The aerodynamic coefficients are computed in TAI using the panel solver “xPAN” as the CFD (Computational Fluid Dynamics) method to obtain static coefficients and using the empirical method USAF Digital DATCOM[®] to obtain the dynamic derivatives. The coefficients are found on the mean aerodynamic center (%25 MAC).

The majority of aerodynamic database is constructed from nondimensional static force and moment coefficients of wing-body-tail with and without control surface deflections. The summation terms determined in order to give the whole static coefficients in a compact form are

- coefficients of wing-body-tail without control surface deflections which are computed at predetermined α , β values, and flap configurations,
- coefficients of additional effects of aileron deflections which are computed at predetermined α , β , δ_{aileron} values and flap configurations, and
- coefficients of additional effects of ruddervator deflections which are computed at predetermined α , β , $\delta_{\text{ruddervator}}$ values and flap configurations.

Only flaps-up ($\delta_{\text{flap}} = 0^\circ$) configuration is included in the nonlinear model in this study. The rest of the aerodynamic database is constructed from dynamic force and moment derivatives obtained at predetermined angle of attack values which are to be transformed into nondimensional coefficients form in the model.

Since DATCOM[®] provides angle of attack dependent dynamic force and moment derivatives, in order to obtain the nondimensional dynamic coefficients; the following relations hold for the nonlinear model [16]:

$$CD_{\text{dynamic}} = 0 \quad (2.11a)$$

$$CY_{\text{dynamic}} = \frac{b}{2V}[(p - p_w)CY_p + (r - r_w)CY_r] \quad (2.11b)$$

$$CL_{\text{dynamic}} = \frac{\bar{c}}{2V}[(q - q_w)CL_q + \dot{\alpha}CL_{\dot{\alpha}}] \quad (2.11c)$$

$$CR_{\text{dynamic}} = \frac{b}{2V}[(p - p_w)CR_p + (r - r_w)CR_r] \quad (2.11d)$$

$$CM_{\text{dynamic}} = \frac{\bar{c}}{2V}[(q - q_w)CM_q + \dot{\alpha}CM_{\dot{\alpha}}] \quad (2.11e)$$

$$CN_{\text{dynamic}} = \frac{b}{2V}[(p - p_w)CN_p + (r - r_w)CN_r] \quad (2.11f)$$

where, CD: drag coefficient

CY: side force coefficient

CL: lift coefficient

CR: rolling moment coefficient

CM: pitching moment coefficient

CN: yawing moment coefficient

p_w, q_w, r_w : wind angular rates in [rad/s] (equal to zero for no wind condition)

The axis systems at which the coefficients obtained are not the same. The nondimensional static coefficients CD_{static} , and CL_{static} obtained by xPAN panel

solver are at the wind-axes reference frame, therefore, need to be converted into the body-fixed axes, whereas the remaining ones, CY_{static} , CR_{static} , CM_{static} , and CN_{static} are already obtained at the body-fixed axes reference frame. The dynamic coefficients obtained from DATCOM[®] are at stability-axes reference frame; hence, they too need to be converted into body-fixed axes.

The summing up procedure is summarized by the relations

$$C_{total} = C_{static} + C_{dynamic} \quad (2.12a)$$

$$C_{total} = (C_{wing-body-tail} + C_{aileron} + C_{ruddervator}) + C_{dynamic} \quad (2.12b)$$

where C_{total} represents the total nondimensional force and moment coefficients of the UAV in body-fixed axes reference frame.

The way to implement these coefficients into nonlinear model is not unique in this study. $C_{wing-body-tail}$ and $C_{aileron}$ tables are converted into nonlinear parameterized functions depending on α , β and α , β , $\delta_{aileron}$ respectively. The remaining terms $C_{ruddervator}$ and $C_{dynamic}$ are stored as look up tables and the intermediate values are computed by interpolation.

In order to obtain the aerodynamic force and coefficients, the body-fixed axes nondimensional aerodynamic coefficients (CX , CY , CZ , CR , CM , CN) are dimensionalized as follows.

$$X_A = CX \frac{1}{2} \rho V^2 S \quad (2.13a)$$

$$Y_A = CY \frac{1}{2} \rho V^2 S \quad (2.13b)$$

$$Z_A = CZ \frac{1}{2} \rho V^2 S \quad (2.13c)$$

$$R_A = CR \frac{1}{2} \rho V^2 S b \quad (2.13d)$$

$$M_A = CM \frac{1}{2} \rho V^2 S \bar{c} \quad (2.13e)$$

$$N_A = CN \frac{1}{2} \rho V^2 S b \quad (2.13f)$$

where ρ : the air density in $[\text{kg/m}^3]$.

It should be denoted that, in this study, the mean aerodynamic center position where the aerodynamic coefficients are obtained at, is same as the position of the center of mass. Therefore, no additional moments occurred about c.m. due to forces.

2.6.1.2 Propulsive Forces and Moments – Engine Model

The engine model used is from the “DeHavilland Beaver” model demo of MATLAB[®]/Simulink[®]. The model is originated from DHC-2 Beaver engine, for which the force and moment coefficients were determined specifically for the Beaver aircraft valid within 35-55 m/s TAS range. It is a part of the work created by Marc Rauw for Delft University of Technology [11]. Although, this engine model does not totally fit to a different air vehicle and a pusher propeller configuration, the approach in this study is to have a trimmable nonlinear UAV model that includes an engine with a reasonable behavior, and can experience steady state flight in the predetermined operational velocity and altitude ranges. These conditions are satisfied with this engine implemented in the nonlinear model.

The contributions from the engine to the external forces and moments, and the influence of changes in airspeed, are expressed in terms of changes of $dpt = \frac{\Delta p_t}{\frac{1}{2}\rho V^2}$, where Δp_t is the difference between the total pressure in front of the propeller and the total pressure behind the propeller. The relation between dpt , the airspeed V , and the engine power P is given in Equation (2.14).

$$\frac{\Delta p_t}{\frac{1}{2}\rho V^2} = a + b \left(\frac{P}{\frac{1}{2}\rho V^3} \right) \quad (2.14)$$

where $\frac{P}{\frac{1}{2}\rho V^3}$ is in $\left[\frac{\text{kW}}{\text{Pa} \cdot \text{m}^3/\text{s}} \right]$ and engine model parameters; $a = 0.08696$ and $b = 191.18$.

The engine power in [W] is calculated using the following relation

$$P = 0.7355 \left[-326.5 + (0.00412(p_z + 7.4)(n + 2010) + (408 - 0.0965n) \left(1 - \frac{\rho}{\rho_0} \right) \right] \quad (2.15)$$

where n : the engine speed in [rpm] related to throttle input nonlinearly,

p_z : the manifold pressure in [”Hg] related to the engine speed nonlinearly,

ρ_0 : air density at mean sea level, $\rho_0 = 1.225 \text{ kg/m}^3$.

The nondimensional engine force and moments coefficients along the body-fixed axes are expressed in terms of dpt as

$$CX_T = CX_{\Delta p_t} \left(\frac{\Delta p_t}{\frac{1}{2} \rho V^2} \right) + CX_{\alpha \Delta p_t^2} \alpha \left(\frac{\Delta p_t}{\frac{1}{2} \rho V^2} \right)^2 \quad (2.16a)$$

$$CY_T = 0 \quad (2.16b)$$

$$CZ_T = CZ_{\Delta p_t} \left(\frac{\Delta p_t}{\frac{1}{2} \rho V^2} \right) \quad (2.16c)$$

$$CR_T = CR_{\alpha^2 \Delta p_t} \alpha^2 \left(\frac{\Delta p_t}{\frac{1}{2} \rho V^2} \right) \quad (2.16d)$$

$$CM_T = CM_{\Delta p_t} \left(\frac{\Delta p_t}{\frac{1}{2} \rho V^2} \right) \quad (2.16e)$$

$$CN_T = CN_{\Delta p_t^3} \left(\frac{\Delta p_t}{\frac{1}{2} \rho V^2} \right)^3 \quad (2.16f)$$

where the values for parameters in Equations (2.16) for the original DHC-2 Beaver engine are given in Table 2.3. It should be noted that the dynamics of the powerplant itself is absent within these equations.

These coefficients include slipstream effects, which are quite large for the Beaver aircraft, as well as the gyroscopic effect of the propeller. In this study, since a pusher

propeller configuration is foreseen, the slipstream effects are not needed to be taken into account, therefore different from the original engine model, CN_T is taken as 0.

Table 2.3 Coefficients in the nonlinear engine model of the “DHC-2 Beaver” aircraft

Engine Coefficient	Parameter	Value
CX_T	$CX_{\Delta p_t}$	0.1161
	$CX_{\alpha \Delta p_t^2}$	0.1453
CY_T	-	-
CZ_T	$CZ_{\Delta p_t}$	-0.1563
CR_T	$CR_{\alpha^2 \Delta p_t}$	-0.01406
CM_T	$CM_{\Delta p_t}$	-0.07895
CN_T	$CN_{\Delta p_t^3}$	-0.003026

Similar to the of aerodynamic forces and moments, it is required to express the nondimensional body-fixed axes engine coefficients in dimensional forms as follows in order to obtain the actual values of the engine forces and moments.

$$X_T = CX_T \frac{1}{2} \rho V^2 S \quad (2.17a)$$

$$Y_T = CY_T \frac{1}{2} \rho V^2 S \quad (2.17b)$$

$$Z_T = CZ_T \frac{1}{2} \rho V^2 S \quad (2.17c)$$

$$R_T = CR_T \frac{1}{2} \rho V^2 S b \quad (2.17d)$$

$$M_T = CM_T \frac{1}{2} \rho V^2 S \bar{c} \quad (2.17e)$$

$$N_T = CN_T \frac{1}{2} \rho V^2 S b \quad (2.17f)$$

These coefficients are obtained at the c.m. of the aircraft, so no additional moments occurred about c.m. due to forces.

2.6.1.3 Gravitational Forces and Moments – Gravity Model

By matrix multiplying Earth-fixed gravitational force vector, $\vec{W} = [0 \quad 0 \quad mg]_E$, with DCM, the gravitational force components in body-fixed axes are obtained as

$$\begin{bmatrix} X_G \\ Y_G \\ Z_G \end{bmatrix} = \begin{bmatrix} 1 & 0 & 0 \\ 0 & \cos \phi & \sin \phi \\ 0 & -\sin \phi & \cos \phi \end{bmatrix} \begin{bmatrix} \cos \theta & 0 & -\sin \theta \\ 0 & 1 & 0 \\ \sin \theta & 0 & \cos \theta \end{bmatrix} \begin{bmatrix} \cos \psi & \sin \psi & 0 \\ -\sin \psi & \cos \psi & 0 \\ 0 & 0 & 1 \end{bmatrix} \begin{bmatrix} 0 \\ 0 \\ mg \end{bmatrix} \quad (2.18)$$

$$\text{where, the gravitational force along x-axis: } X_G = -mg \sin \theta \quad (2.18a)$$

$$\text{the gravitational force along y-axis: } Y_G = mg \sin \phi \cos \theta \quad (2.18b)$$

$$\text{the gravitational force along z-axis: } Z_G = mg \cos \phi \cos \theta \quad (2.18c)$$

World Geodetic System “WGS84” is used as the gravity model in order to compute the Earth’s gravity at a specific location using Taylor series. With this model, the mathematical representation of the geocentric equipotential ellipsoid of the WGS84 is implemented. Since the gravity potential is assumed to be the same everywhere on the ellipsoid, there must be a specific theoretical gravity potential that can be uniquely determined from the four independent constants defining the ellipsoid. It should be denoted that use of the WGS84 Taylor Series model should be limited to

low geodetic heights, i.e. to a geodetic height of 20,000 m. Hence, it is sufficient near the surface of the Earth [17].

2.7 Actuators Model

The UAV model has four control surfaces:

Two ailerons: right (starboard) and left (port) ailerons; always deflect asymmetrically in the same magnitudes, i.e. they do not move independently and a single actuator is used.

Two ruddervators: right (starboard) and left (port) ruddervators; a symmetric deflection gives the effect of an elevator whereas an asymmetric deflection gives the effect of a rudder requiring independent movements and actuators.

Since the subject UAV has a V-tail configuration, without a stand alone rudder, the control coordination between the longitudinal and directional motions is provided by the inputs expressed by “column” for pitch and “pedal” for yaw demands. This coordination is defined as,

$$\delta_{\text{column}} + \delta_{\text{pedal}} \rightarrow \text{port ruddervator command}$$

$$\delta_{\text{column}} - \delta_{\text{pedal}} \rightarrow \text{starboard ruddervator command}$$

Signs of the column and pedal inputs are the same as the signs of the pitching and yawing motion corresponding ruddervator deflections. This is a determinant for the above relation in terms of port and starboard matches. Besides column and pedal, the remaining input expressions are “wheel” and “throttle” with direct effects to ailerons and engine, respectively.

All actuators used in this model are assumed to be identical. An ideal second order actuator dynamics is used as the model with the transfer function as follows.

$$\frac{\delta}{\delta_c} = \frac{\omega_a^2}{s^2 + 2 \cdot \zeta_a \cdot \omega_a \cdot s + \omega_a^2} \quad (2.19)$$

where, ω_a and ζ_a are the natural frequency and damping ratio of the actuator dynamics. In this study, the actuator parameters are selected as $\omega_a = 40\pi$ rad/s (20 Hz) and $\zeta_a = 0.7$ in order to have ideal actuator motion characteristics.

2.8 Atmosphere and Wind-Turbulence Model

2.8.1 Atmosphere Model

The International Standard Atmosphere (ISA) model is used for atmospheric calculations. With this model, the mathematical representation of the international standard atmosphere values for ambient temperature, pressure, density, and speed of sound for the input geo-potential altitude is implemented. Below the geo-potential altitude of 0 km and above the geo-potential altitude of 20 km, temperature and pressure values are held. The air density and speed of sound are calculated using a perfect gas relationship [17].

The calculation procedure for the ISA model outputs are given in Equations (2.20) to (2.23).

$$\text{Ambient temperature [K]: } T = T_0 - Lh \quad (2.20)$$

where T_0 : ambient temperature at mean sea level, $T_0 = 288.15$ K,

L : Lapse rate, $L = 0.0065$ K/m,

h : geopotential height [m].

Equation (2.20) indicates that, the air temperature in the troposphere decreases linearly as the altitude increases.

$$\text{Speed of sound [m/s]: } a = \sqrt{\gamma \cdot R \cdot T} \quad (2.21)$$

where γ : adiabatic index, $\gamma = 1.4$ for air,

R : specific gas constant, $R = 287.0531 \text{ J/K}\cdot\text{kg}$ for dry air.

$$\text{Air pressure [Pa]: } P = \left[\left(\frac{T}{T_0} \right)^{\frac{g}{L \cdot R}} \cdot P_0 \right] \cdot e^{\left[\left(h_{\text{troposphere}} - h \right) \frac{g}{R} \right] / T} \quad (2.22)$$

where P_0 : ambient pressure at mean sea level, $P_0 = 101,325 \text{ Pa}$,

g : acceleration due to gravity, $g = 9.80665 \text{ m/s}^2$

$h_{\text{troposphere}}$: troposphere height, $h_{\text{troposphere}} = 11,000 \text{ m}$,

$e^{\left[\left(h_{\text{troposphere}} - h \right) \frac{g}{R} \right] / T}$: Stratosphere model.

$$\text{Air density [kg/m}^3\text{]: } \rho = \left[\frac{\left(\frac{T}{T_0} \right)^{\frac{g}{L \cdot R}}}{\left(\frac{T}{T_0} \right)} \cdot \rho_0 \right] \cdot e^{\left[\left(h_{\text{troposphere}} - h \right) \frac{g}{R} \right] / T} \quad (2.23)$$

2.8.2 Wind-Turbulence Model

For the evaluation of the performance of the air vehicle control systems, it is necessary to include wind and atmospheric turbulence to simulations of the air vehicle. In this section, the utilized wind-turbulence model components are described.

2.8.2.1 Background Wind Model

This model computes the background wind velocity and acceleration components in the body-fixed axes. The wind velocity vector in the Earth-fixed frame (North-East-Down) is multiplied with the rotation matrix DCM, for its components to be transformed into wind velocities in body-fixed axes. Wind accelerations in the body-fixed axes are also obtained, by taking the numerical time derivative of the wind velocity vector in the Earth-fixed frame and matrix multiplying with DCM in a similar manner. This captures the effect of time-varying background wind which can be encountered in some weather conditions (wind shear, thermals, and cyclones) [21].

2.8.2.2 Turbulence Model

The Von Kármán turbulence model that computes turbulence velocities and accelerations in the body-fixed axes is used. The computation is performed by implementing the Von Kármán spectral representation to add turbulence to the nonlinear model by passing a band-limited white noise through appropriate longitudinal, lateral and vertical turbulence shaping filters. The filter parameters depend on background wind magnitude and current air vehicle altitude [21]. One can refer to [4, 17, 30] for the detailed mathematical representation of the Von Kármán turbulence model.

2.8.2.3 Wind Shear Model

The wind shear model computes the body-fixed angular rate effects caused by the variation in time/space of the background wind and turbulence velocities. The wind shear effects considered are the angular velocities and accelerations for pitch and yaw where roll wind shear effect is zero. The wind angular accelerations are computed by taking numerical time derivatives of the following angular rates due to wind [21].

$$\text{Roll rate due to wind [rad/s]: } p_w = 0 \quad (2.24a)$$

$$\text{Pitch rate due to wind [rad/s]: } q_w = \frac{1}{u} \cdot \frac{dw_w}{dt} \quad (2.24b)$$

$$\text{Yaw rate due to wind [rad/s]: } r_w = \frac{1}{u} \cdot \frac{dv_w}{dt} \quad (2.24c)$$

where $\frac{dv_w}{dt}$ and $\frac{dw_w}{dt}$ stand for the body-fixed y- and z-axes accelerations respectively due to background wind plus turbulence which is totally expressed as “wind”.

A distinguishing definition between the wind and atmospheric turbulence was given in [11] as: “Wind is the mean or steady-state velocity of the atmosphere with respect to the Earth at a given position. Usually, the mean wind is measured over a certain time interval of several minutes. The remaining fluctuating part of the wind velocity is then defined as atmospheric turbulence.”

2.9 Flight Parameters Calculation

The results of the calculations included in the flight parameters part of the nonlinear model are composed of angle of attack, α , airspeed, V , sideslip angle, β , and their derivatives – wind-axes translational acceleration parameters derived in Appendix B referring to [18], dynamic pressure, \bar{q} , and equivalent airspeed, EAS. The calculation procedures applied are given below.

$$\text{Airspeed [m/s]: } V = \sqrt{(u - u_w)^2 + (v - v_w)^2 + (w - w_w)^2} \quad (2.25a)$$

$$\text{Angle of attack [rad]: } \alpha = a \tan \left(\frac{w - w_w}{u - u_w} \right) \quad (2.25b)$$

$$\text{Sideslip angle [rad]: } \beta = a \sin \left(\frac{v - v_w}{V_a} \right) \quad (2.25c)$$

where u_w, v_w, w_w : wind velocities [m/s] (equal to zero for no wind condition)

Derivative of V [m/s^2]:

$$\dot{V} = \frac{X \cdot \cos \alpha \cdot \cos \beta + Y \cdot \sin \beta + Z \cdot \sin \alpha \cdot \cos \beta}{m} \quad (2.26a)$$

Derivative of α [rad/s]:

$$\dot{\alpha} = \frac{-X \cdot \sin \alpha + Z \cdot \cos \alpha}{m \cdot V \cdot \cos \beta} - \tan \beta \cdot (p \cdot \cos \alpha + r \cdot \sin \alpha) + q \quad (2.26b)$$

Derivative of β [rad/s]:

$$\dot{\beta} = \frac{-X \cdot \cos \alpha \cdot \sin \beta + Y \cdot \cos \beta + Z \cdot \sin \alpha \cdot \sin \beta}{m \cdot V} + p \cdot \sin \alpha - r \cdot \cos \alpha \quad (2.26c)$$

$$\text{Dynamic pressure [Pa]: } \bar{q} = \frac{1}{2} \cdot \rho \cdot V^2 \quad (2.27)$$

$$\text{Equivalent airspeed [m/s]: } EAS = \frac{TAS \cdot a_0 \cdot \sqrt{\delta}}{a} \quad (2.28)$$

where TAS: true airspeed, that is V [m/s],

a_0 : speed of sound in mean sea level, $a_0 = 340.294$ m/s

δ : relative pressure ratio at the flight altitude.

2.10 MATLAB[®]/Simulink[®] Correlation

Since MATLAB[®]/Simulink[®] environment is utilized for the nonlinear modeling of the UAV that is been explained so far, the modeling correlation with this environment is to be demonstrated in Appendix C, starting with main level modeling blocks and their subsystems.

CHAPTER 3

TRIM - LINEARIZATION

3.1 Introduction

During normal flight, the motion of an air vehicle as a rigid body can be described by a set of nonlinear state equations represented as

$$\dot{\mathbf{x}} = \mathbf{f}(\mathbf{x}, \mathbf{u}) \quad (3.1)$$

where \mathbf{x} is the n-dimensional state vector, $\dot{\mathbf{x}}$ is the derivative of \mathbf{x} vector with respect to time, \mathbf{u} is the p-dimensional time varying control input vector, and \mathbf{f} is an n-dimensional nonlinear function. Outputs of the vehicle state can be represented as

$$\mathbf{y} = \mathbf{h}(\mathbf{x}, \mathbf{u}) \quad (3.2)$$

where, \mathbf{y} is a q-dimensional output vector, and \mathbf{h} is a q-dimensional nonlinear function expressing the relationship for the outputs in terms of air vehicle states and control inputs. The 12 state variables used in the representation of 6 DOF rigid body equations of the air vehicle motions, and four inputs used to control these motions are given in Equations (3.3) respectively, with their corresponding definitions.

The classical approach to a stability and control analysis of a nonlinear dynamical system is to start with the complete equations of motion and make assumptions that would help to linearize these equations about a specific local equilibrium point found by a process called as “trimming”. During the initial flight control system design phase, the linear system theory can be applied to these linear mathematical models of the air vehicle dynamics. Consequently, the trim and linearization of the nonlinear

model are the major steps to be carried out on the way to linear control theory applications.

$$\mathbf{x} = \begin{bmatrix} x_E \\ y_E \\ z_E \\ \phi \\ \theta \\ \psi \\ u \\ v \\ w \\ p \\ q \\ r \end{bmatrix} = \begin{bmatrix} \text{position in x-direction [m]} \\ \text{position in y-direction [m]} \\ \text{--altitude [m]} \\ \text{bank angle [rad]} \\ \text{pitch angle [rad]} \\ \text{heading angle [rad]} \\ \text{velocity in x-axis [m/s]} \\ \text{velocity in y-axis [m/s]} \\ \text{velocity in z-axis [m/s]} \\ \text{roll rate [rad/s]} \\ \text{pitch rate [rad/s]} \\ \text{yaw rate [rad/s]} \end{bmatrix}, \mathbf{u} = \begin{bmatrix} \delta_{\text{column}} \\ \delta_{\text{throttle}} \\ \delta_{\text{wheel}} \\ \delta_{\text{pedal}} \end{bmatrix} = \begin{bmatrix} \text{symmetric ruddervator deflection [}^\circ\text{]} \\ \text{throttle position change [\%]} \\ \text{aileron deflection [}^\circ\text{]} \\ \text{asymmetric ruddervator deflection [}^\circ\text{]} \end{bmatrix} \quad (3.3)$$

This chapter covers the trim and linearization definitions, types and methods implemented for both, and the results shown in order to verify the applied methods.

3.2 Trim

The term “trim” relates to a condition of static equilibrium corresponding to a set of constant controls. Under a trimmed condition, there should be no net moments or forces acting on the center of mass of the air vehicle, resulting in no changes in the motion variables in time; that is, they all should be zero or constant. The orientation of the air vehicle is said to be trimmed at a set of nominal values (\mathbf{x}_n , \mathbf{u}_n) when the nonlinear state equations, Equation (3.1), become

$$\mathbf{f}(\mathbf{x}_n, \mathbf{u}_n) = 0 \quad (3.4)$$

and correspondingly the nonlinear output equations, Equation (3.2), can now be expressed as

$$\mathbf{y}_n = \mathbf{h}(\mathbf{x}_n, \mathbf{u}_n) \quad (3.5)$$

During a straight and level flight, the nominal control settings \mathbf{u}_n are determined which maintain steady state flight ($\dot{\mathbf{x}} = 0$) with wings level at constant altitude, airspeed, and heading.

A steady flight or trimmed flight is defined as one of the generalized expressions in Equations (3.6) [15, 19].

$$\text{Steady wings-level flight: } \phi = \dot{\phi} = \dot{\theta} = \dot{\psi} = 0 \quad (3.6a)$$

$$\text{Steady turning flight: } \dot{\phi} = \dot{\theta} = 0, \dot{\psi} = \text{turn rate} \quad (3.6b)$$

$$\text{Steady pull-up: } \phi = \dot{\phi} = \dot{\psi} = 0, \dot{\theta} = \text{pull-up rate} \quad (3.6c)$$

where, $\dot{p} = \dot{q} = \dot{r} = \dot{u} = \dot{v} = \dot{w} = 0$ and all control surface inputs are constant or zero.

The tool utilized for trim determines the equilibrium (or trim) points of the nonlinear model based on the specified altitude, airspeed, mass, center of mass, flight path angle, etc.

3.2.1 Trim Method

MATLAB[®] function `trim` is used on the nonlinear model of the UAV to obtain the steady state flight trim with wings level at constant altitude, airspeed, and zero sideslip in this study. In order to utilize the generalized `trim` function as specific to a steady wings-level flight trim condition and produce a feasible solution for the implementation, some initial guesses are needed for the air vehicle state variables (elements of \mathbf{x}), control inputs (elements of \mathbf{u}), and outputs (elements of \mathbf{y}), and some proper constraints on the magnitudes of the individual states, control inputs, and outputs are needed based on Equations (3.6a). The `trim` function starts from an initial point and searches for values of the state and input vectors for which $\dot{\mathbf{x}}$ is

sufficiently small, using a sequential quadratic programming (SQP) algorithm, until it finds the nearest trim point. The SQP algorithm is a solution to the constrained optimization problem as described in detail in [20].

In order to speed up the MATLAB[®] trimming routine, through the optimal state and control input vector values search, a preprocess providing better initial guesses is applied in this study [21]. Including this preprocess, the trimming part of the developed algorithm “trimUAV.m” carries out the following steps:

1. The default optional simulation parameters structure of the Simulink[®] model to be trimmed is obtained. Initial parameters are set, including the Simulink[®] model name, and values for air vehicle control inputs, states, and outputs regarding the flight condition at which the air vehicle is to be trimmed.
2. Initial guesses set at Step 1 are improved. Since the flight condition is completely defined, the Simulink[®] model is run for a limited amount of time, in an iterative process. Each time the user defined error values for airspeed, altitude, and bank angle variables are overshoot, the air vehicle control inputs are adjusted by proportional feedback from selected model outputs (e.g. column feedback is provided by airspeed error, throttle feedback by altitude error, and wheel feedback by bank angle error). The feedback gains are specific to the subject UAV and selected by a fast trial and error process. The method provides a better initial guess of control inputs and states for the optimization step.
3. Before the optimization step, the states, state derivatives, outputs, and control inputs to be fixed at the corresponding initial guesses are indicated specific to the steady wings-level flight trim condition with constant altitude, airspeed and heading. The ones that are not indicated as fixed are to be floating.
4. The trim is performed. The program runs the optimization which accurately trims the air vehicle nonlinear model for the selected flight trim condition, where the MATLAB[®] function `trim` is used for this procedure.

3.2.2 Trim Results

In order to show the flight trimming and linearization results, a nominal flight condition of 100 KEAS (knots-equivalent airspeed) and 15,000 ft (4,572 m) altitude is selected as a representative example of the operational flight envelope. The values of the state, state derivatives, and control input vectors obtained from the steady wings-level flight trim, at the mentioned airspeed, altitude, and zero sideslip conditions are given in Equations (3.7).

$$\mathbf{x} = \begin{bmatrix} x_E \\ y_E \\ z_E \\ \phi \\ \theta \\ \psi \\ u \\ v \\ w \\ p \\ q \\ r \end{bmatrix} = \begin{bmatrix} 0.0 \text{ [m]} \\ 0.0 \text{ [m]} \\ -4,572 \text{ [m]} \\ -5.35 \cdot 10^{-5} \text{ [rad]} \\ -0.0377 \text{ [rad]} \\ -4.5 \cdot 10^{-5} \text{ [rad]} \\ 64.805 \text{ [m/s]} \\ 0.00306 \text{ [m/s]} \\ -2.4431 \text{ [m/s]} \\ 0.0 \text{ [rad/s]} \\ 0.0 \text{ [rad/s]} \\ 0.0 \text{ [rad/s]} \end{bmatrix}, \dot{\mathbf{x}} = \begin{bmatrix} \dot{x}_E \\ \dot{y}_E \\ \dot{z}_E \\ \dot{\phi} \\ \dot{\theta} \\ \dot{\psi} \\ \dot{u} \\ \dot{v} \\ \dot{w} \\ \dot{p} \\ \dot{q} \\ \dot{r} \end{bmatrix} = \begin{bmatrix} 64.85 \text{ [m/s]} \\ 0.0 \text{ [m/s]} \\ 0.0 \text{ [m/s]} \\ 0.0 \text{ [rad/s]} \\ 0.0 \text{ [rad/s]} \\ 0.0 \text{ [rad/s]} \\ 0.0 \text{ [m/s}^2\text{]} \\ 0.0 \text{ [m/s}^2\text{]} \\ 0.0 \text{ [m/s}^2\text{]} \\ 0.0 \text{ [rad/s}^2\text{]} \\ 0.0 \text{ [rad/s}^2\text{]} \\ 0.0 \text{ [rad/s}^2\text{]} \end{bmatrix}, \mathbf{u} = \begin{bmatrix} \delta_{\text{column}} \\ \delta_{\text{throttle}} \\ \delta_{\text{wheel}} \\ \delta_{\text{pedal}} \end{bmatrix} = \begin{bmatrix} 4.6284 \text{ [}^\circ\text{]} \\ 55.09 \text{ [\%]} \\ 0.0013 \text{ [}^\circ\text{]} \\ 0.0042 \text{ [}^\circ\text{]} \end{bmatrix} \quad (3.7)$$

It can be concluded from the values of the trimmed state derivatives, $\dot{\mathbf{x}}$, that the trim quality is very well, satisfying the condition of trim given by Equation (3.4) originated from Equation (3.1).

3.3 Linearization

The short term local behavior of the air vehicle at a given flight condition can be approximated by the linearization of its nonlinear model about the equilibrium points obtained by trimming. The standard linear state equations or the state space representation for a linear differential system has the form,

$$\dot{\mathbf{x}} = \mathbf{Ax} + \mathbf{Bu} \quad (3.8)$$

$$\mathbf{y} = \mathbf{C}\mathbf{x} + \mathbf{D}\mathbf{u} \quad (3.9)$$

where \mathbf{A} , \mathbf{B} , \mathbf{C} , and \mathbf{D} are the constant matrices. \mathbf{A} is the $(n \times n)$ system matrix, \mathbf{B} is the $(n \times p)$ control matrix representing the relationship between the control inputs and states, \mathbf{C} is the $(q \times n)$ output matrix representing the relationship between states and outputs, and \mathbf{D} is a $(q \times p)$ matrix representing the relationship between control inputs and outputs.

3.3.1 Linearization Methods

In order to compare and select the better one, two linearization methods are used to linearize the nonlinear UAV model about a flight trim condition; a numerical perturbation method introduced by MATLAB[®] function `linmod2`, and a block-by-block analytic linearization introduced by MATLAB[®] function `linmod`. The nonlinear Simulink[®] trim model, trim states, and trim control inputs are to be given to these functions as the inputs. A linear model is extracted as the result of the each function at a user specified operating point of the flight envelope with the state variables \mathbf{x} and the control inputs \mathbf{u} set to zero.

In the block perturbation algorithm `linmod2`, introducing a small perturbation to the nonlinear model and measuring the response to this perturbation is involved. Both the perturbation and the response are used to create the matrices in the linear state-space model of this block. The value of the perturbation may be defined by the user or be retained as default for every individual state or control input variable. In this study, 0.015 is chosen as the small perturbation value, which is the smallest value for which the obtained linear model matrices do not include any elements with NaN (Not-a-Number) representation of MATLAB[®]. The function outputs the constant \mathbf{A} , \mathbf{B} , \mathbf{C} , and \mathbf{D} matrices of the state space model, represented by,

$$\dot{\tilde{\mathbf{x}}} = \mathbf{A}\tilde{\mathbf{x}} + \mathbf{B}\tilde{\mathbf{u}} \quad (3.10)$$

$$\tilde{\mathbf{y}} = \mathbf{C}\tilde{\mathbf{x}} + \mathbf{D}\tilde{\mathbf{u}} \quad (3.11)$$

where $\tilde{\mathbf{x}} = \mathbf{x} - \mathbf{x}_n$, $\tilde{\mathbf{u}} = \mathbf{u} - \mathbf{u}_n$, and $\tilde{\mathbf{y}} = \mathbf{y} - \mathbf{y}_n$ are the small state, control input, and output perturbations obtained by subtracting the known trim states, \mathbf{x}_n , trim control inputs, \mathbf{u}_n , and trim outputs, \mathbf{y}_n respectively from the states, inputs, and outputs. The states and control inputs are perturbed around the flight trim points in order to find the rate of change of \mathbf{x} and \mathbf{u} (Jacobians). The coefficients \mathbf{A} , \mathbf{B} , \mathbf{C} , and \mathbf{D} are the Jacobian matrices of the model evaluated on this nominal solution as,

$$\mathbf{A} = \left. \frac{\partial \mathbf{f}}{\partial \mathbf{x}} \right|_n, \mathbf{B} = \left. \frac{\partial \mathbf{f}}{\partial \mathbf{u}} \right|_n, \mathbf{C} = \left. \frac{\partial \mathbf{h}}{\partial \mathbf{x}} \right|_n, \mathbf{D} = \left. \frac{\partial \mathbf{h}}{\partial \mathbf{u}} \right|_n \quad (3.12)$$

where for a vector of functions expressed as

$$\mathbf{g}(\mathbf{t}) = \begin{bmatrix} g_1(t_1, t_2, \dots, t_n) \\ g_2(t_1, t_2, \dots, t_n) \\ \vdots \\ g_m(t_1, t_2, \dots, t_n) \end{bmatrix} \quad (3.13)$$

the Jacobian $\partial \mathbf{g} / \partial \mathbf{t}$ in variables t_1, t_2, \dots, t_n is as

$$\frac{\partial \mathbf{g}}{\partial \mathbf{t}} = \begin{bmatrix} \frac{\partial g_1}{\partial t_1} & \frac{\partial g_1}{\partial t_2} & \dots & \frac{\partial g_1}{\partial t_n} \\ \frac{\partial g_2}{\partial t_1} & \frac{\partial g_2}{\partial t_2} & \dots & \frac{\partial g_2}{\partial t_n} \\ \vdots & \vdots & \vdots & \vdots \\ \frac{\partial g_m}{\partial t_1} & \frac{\partial g_m}{\partial t_2} & \dots & \frac{\partial g_m}{\partial t_n} \end{bmatrix} \quad (3.14)$$

In a similar manner the `linmod2` function attempts to find a linearized state space approximation to the nonlinear vector of functions \mathbf{f} and \mathbf{h} expressed by Equations (3.1) and (3.2) [18, 22-23].

By the function `linmod`, preprogrammed analytic block Jacobians are used for most Simulink[®] blocks which contain analytic Jacobians for an exact linearization. A complete list of these blocks is given in [23]. When a preprogrammed block linearization can not be used, `linmod` computes the block linearization by numerically perturbing the states and inputs of the block about the operating point of the block. As opposed to the numerical-perturbation linearization method, applied by function `linmod2`, this perturbation is local and its propagation through the rest of the model is restricted. The output is again the constant \mathbf{A} , \mathbf{B} , \mathbf{C} , and \mathbf{D} matrices of the state space model represented by the Equations (3.10) and (3.11).

The extraction of the linear model is carried out by the linearization step of the developed algorithm `trimUAV.m`, where the application of the two mentioned linearization methods is provided. The nonlinear air vehicle model is linearized about the trim condition obtained at the previous step of the algorithm. The detailed application procedure, related to the mentioned algorithm is explained in Appendix D.

3.3.2 Modal Matrix and Linearization Results

The steady wings-level flight trim condition given by Equation (3.6a), leads to decoupling of the flat-Earth equations of motion [24]. Hence, the respective linear models can be decoupled into longitudinal (including motions of pitching and translation in x-z plane) and lateral-directional (including motions of rolling, sideslipping, and yawing) axes. In order to verify and demonstrate this weakly coupled condition, the eigenvalues and the respective modal matrices are obtained at 100 KEAS and 15,000 ft (4,572 m) altitude by using MATLAB[®] linearization

function `linmod2` and `linmod`, respectively, followed by the use of function `eig`. The linear model system matrix **A** is the input to the function `eig`.

Table 3.1 Eigenvalues of the nominal linear model-`linmod2`

	Flight Mode	Eigenvalues	Damping Ratio, ζ	Natural Frequency, ω_n [rad/s]
Longitudinal axis	Altitude	0.000188	-	-
	Phugoid	$-0.00154 + 0.207i$	0.00744	0.207
		$-0.00154 - 0.207i$		
	Short period	$-1.31 + 2.11i$	0.529	2.48
		$-1.31 - 2.11i$		
Lateral axis	Spiral	0.0103	-	-
	Heading	0.0	-	-
	Dutch roll	$-0.167 + 2.03i$	0.0821	2.04
		$-0.167 - 2.03i$		
	Roll	-17.3	-	-

Table 3.2 Eigenvalues of the nominal linear model-`linmod`

	Flight Mode	Eigenvalues	Damping Ratio, ζ	Natural Frequency, ω_n [rad/s]
Longitudinal axis	Altitude	0.000408	-	-
	Phugoid	$-0.00188 + 0.21i$	0.00894	0.21
		$-0.00188 - 0.21i$		
	Short period	$-1.31 + 2.11i$	0.529	2.48
		$-1.31 - 2.11i$		
Lateral axis	Spiral	0.0103	-	-
	Heading	0.0	-	-
	Dutch roll	$-0.167 + 2.03i$	0.0821	2.04
		$-0.167 - 2.03i$		
	Roll	-17.3	-	-


The eigenvalues obtained by the two methods are given in Tables 3.1 and 3.2. The respective flight modes are determined from the definitions of general characteristics


and possible locations in complex plane, which are involved in many references such as [13-14, 24]. It is observed from the tables that small differences occur between the resultant eigenvalues of the two methods, in longitudinal phugoid and altitude modes.


The elements of the obtained modal matrices are transformed into non-dimensional elements in order to compare and determine the dominant states accurately, since their units are not the same. The finalized modal matrices obtained based on the two methods introduced by `linmod2` and `linmod` are given in Equations (3.15) and (3.16), respectively, where columns are the non-dimensional eigenvectors for the states $u, w, \theta, q, z, v, \phi, p, r, \psi$, and the corresponding special flight modes are also shown. It should be noted that at each eigenvector, the velocity terms, u, v , and w are normalized by the trim V in [m/s], and the altitude term, z_E is normalized by the trim altitude, h in [m]. Thus, they are scaled so that all of them can be physically interpreted as angles in [rad] and angular rates in [rad/s] [25-26].


It can be investigated from the modal matrices of the two methods that, some differences in eigenvectors occur. The effect of these unsimilarities is to be better examined with comparisons of the simulation results of the two linear models and the nonlinear model.

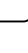
$$\begin{bmatrix}
 0.0 & 0.0 & -0.0042 & -0.0324 & 0.0008 & 0.0003 & -0.0552 & 0.7192 & -0.2648 & -0.0003 \\
 0.0 & 0.0002 & 0.107 & -0.4412 & 0.0064 & 0.0027 & 0.0089 & -0.0295 & 0.0148 & 0.0 \\
 0.0 & 0.0002 & -0.2131 & -0.3419 & 0.0082 & -0.0031 & 1.0 & 0.0 & -0.0084 & 0.0001 \\
 0.0 & -0.0031 & 1.0 & 0.0 & 0.0049 & 0.0173 & -0.0015 & 0.207 & 0.0 & 0.0 \\
 0.0 & 0.0 & -0.0015 & -0.0012 & 0.0 & 0.0 & 0.0003 & 0.0681 & 1.0 & -0.0001 \\
 \hline
 0.0 & 0.0072 & 0.0001 & 0.0001 & 0.0175 & 0.5131 & 0.0 & 0.0 & 0.0 & 0.0009 \\
 0.0 & -0.0576 & 0.0003 & -0.0002 & -0.2951 & -0.0137 & 0.0005 & 0.0001 & 0.0005 & 0.0690 \\
 0.0 & 1.0 & 0.0002 & 0.0009 & 0.1150 & -0.5980 & 0.0 & 0.0001 & 0.0 & 0.0011 \\
 0.0 & 0.0744 & 0.0002 & -0.0001 & 1.0 & 0.0 & 0.0001 & 0.0 & 0.0001 & 0.0102 \\
 1.0 & -0.0043 & -0.0001 & 0.0 & -0.0402 & -0.4886 & 0.0 & -0.0004 & 0.3535 & 1.0
 \end{bmatrix} \quad (3.15)$$



 heading / roll


 / short period


 / Dutch roll


 / phugoid


 / altitude


 / spiral

$$\begin{bmatrix}
0.0 & 0.0 & -0.0041 & -0.0324 & 0.0007 & 0.0003 & -0.0546 & 0.7084 & -0.5927 & -0.0001 \\
0.0 & 0.0002 & 0.1069 & -0.4412 & 0.0062 & 0.0029 & 0.0093 & -0.0287 & 0.0331 & 0.0 \\
0.0 & 0.0002 & -0.2131 & -0.3419 & 0.0082 & -0.0029 & 1.0 & 0.0 & -0.0179 & 0.0 \\
0.0 & -0.0032 & 1.0 & 0.0 & 0.0045 & 0.0171 & -0.0019 & 0.2101 & 0.0 & 0.0 \\
0.0 & 0.0 & -0.0015 & -0.0012 & 0.0 & 0.0 & 0.0005 & 0.067 & 1.0 & 0.0 \\
\hline
0.0 & 0.0072 & 0.0001 & 0.0001 & 0.0175 & 0.5131 & 0.0 & 0.0 & 0.0 & 0.0009 \\
0.0 & -0.0576 & 0.0003 & 0.0002 & -0.2951 & -0.0137 & 0.0005 & 0.0001 & 0.001 & 0.0690 \\
0.0 & 1.0 & 0.0002 & 0.0009 & 0.1150 & -0.5980 & 0.0 & 0.0001 & 0.0 & 0.0011 \\
0.0 & 0.0744 & 0.0002 & 0.0 & 1.0 & 0.0 & 0.0001 & 0.0 & 0.0001 & 0.0102 \\
1.0 & -0.0043 & -0.0001 & -0.0001 & -0.0402 & -0.4886 & 0.0 & -0.0004 & 0.3615 & 1.0
\end{bmatrix} \quad (3.16)$$

heading / roll

/ short period

/ Dutch roll

/ phugoid

/ altitude

/ spiral

In both modal matrices, it is observed that the matrix elements with higher magnitudes located in the columns of basic longitudinal modes (short period and phugoid) correspond to longitudinal state vectors above the dashed lines, whereas the matrix elements with higher magnitudes located in columns of the basic lateral-directional modes (Dutch roll, spiral and roll) correspond to lateral-directional state vectors below the dashed line, i.e., indicating that no important cross-coupling effects occur between longitudinal and lateral-directional axes. This situation leads to design the controllers separately for two axes as if they are ideally decoupled, thereby simplifying the control design problem. Consequently, the resulting linear models obtained by both methods, are decoupled into longitudinal and lateral-directional plants at the end of the trimUAV.m algorithm. The longitudinal and lateral-directional states which cover the complete motion of the air vehicle together and the control input vectors are given by Equations (3.17) and (3.18) respectively with their corresponding definitions.

The system matrices **A**, and control matrices **B** obtained by the two linearization methods about the flight trim condition of 100 KEAS and 15,000 ft (4,572 m) altitude are given in Equations (3.19) through (3.22) which are decoupled into

longitudinal and lateral-directional axes with the corresponding states and control inputs of Equations (3.17) and (3.18).

$$\mathbf{x}_{\text{long.}} = \begin{bmatrix} u \\ w \\ \theta \\ q \\ z_E \end{bmatrix} = \begin{bmatrix} \text{velocity in x-axis [m/s]} \\ \text{velocity in z-axis [m/s]} \\ \text{pitch angle [rad]} \\ \text{pitch rate [rad/s]} \\ \text{-altitude [m]} \end{bmatrix}, \mathbf{u}_{\text{long.}} = \begin{bmatrix} \delta_{\text{column}} \\ \delta_{\text{throttle}} \end{bmatrix} = \begin{bmatrix} \text{symmetric ruddervator deflection [}^\circ\text{]} \\ \text{throttle position change [\%]} \end{bmatrix} \quad (3.17)$$

$$\mathbf{x}_{\text{lat-dir.}} = \begin{bmatrix} v \\ \phi \\ p \\ r \\ \psi \end{bmatrix} = \begin{bmatrix} \text{velocity in y-axis [m/s]} \\ \text{bank angle [rad]} \\ \text{roll rate [rad/s]} \\ \text{yaw rate [rad/s]} \\ \text{heading angle [rad]} \end{bmatrix}, \mathbf{u}_{\text{lat-dir.}} = \begin{bmatrix} \delta_{\text{wheel}} \\ \delta_{\text{pedal}} \end{bmatrix} = \begin{bmatrix} \text{aileron deflection [}^\circ\text{]} \\ \text{asymmetric ruddervator deflection [}^\circ\text{]} \end{bmatrix} \quad (3.18)$$

Results of the function `linmod2` are

$$\mathbf{A}_{\text{long.}} = \begin{bmatrix} -0.0255 & 0.0421 & -9.7613 & 2.3992 & -0.0001 \\ -0.3475 & -1.8019 & 0.2947 & 63.6411 & -0.0009 \\ 0.0 & 0.0 & 0.0 & 1.0 & 0.0 \\ 0.0004 & -0.0736 & 0.0 & -0.802 & 0.0 \\ 0.0377 & 0.9993 & -64.8501 & 0.0 & 0.0 \end{bmatrix}, \mathbf{B}_{\text{long.}} = \begin{bmatrix} -0.0047 & 0.0338 \\ -0.1153 & -0.0467 \\ 0.0 & 0.0 \\ -0.0948 & -0.0069 \\ 0.0 & 0.0 \end{bmatrix} \quad (3.19)$$

$$\mathbf{A}_{\text{lat-dir.}} = \begin{bmatrix} -0.1425 & 9.7591 & -2.6881 & -64.5518 & 0.0 \\ 0.0 & 0.0 & 1.0 & -0.0377 & 0.0 \\ -0.3033 & 0.0 & -17.4441 & 3.5477 & 0.0 \\ 0.0377 & 0.0 & -1.3019 & -0.0604 & 0.0 \\ 0.0 & 0.0 & 0.0 & 1.0007 & 0.0 \end{bmatrix}, \mathbf{B}_{\text{lat-dir.}} = \begin{bmatrix} -0.008 & 0.0659 \\ 0.0 & 0.0 \\ -1.8496 & 0.1347 \\ -0.0605 & -0.0361 \\ 0.0 & 0.0 \end{bmatrix} \quad (3.20)$$

Results of the function `linmod` are

$$\mathbf{A}_{\text{long.}} = \begin{bmatrix} -0.0255 & 0.0418 & -9.7593 & 2.3992 & -0.0003 \\ -0.3474 & -1.802 & 0.3679 & 63.6411 & -0.0021 \\ 0.0 & 0.0 & 0.0 & 1.0 & 0.0 \\ 0.0004 & -0.0736 & 0.0 & -0.802 & 0.0 \\ 0.0377 & 0.9993 & -64.8512 & 0.0 & 0.0 \end{bmatrix}, \mathbf{B}_{\text{long.}} = \begin{bmatrix} -0.0047 & 0.0338 \\ -0.1153 & -0.0467 \\ 0.0 & 0.0 \\ -0.0948 & -0.0069 \\ 0.0 & 0.0 \end{bmatrix} \quad (3.21)$$

$$\mathbf{A}_{\text{lat-dir.}} = \begin{bmatrix} -0.1425 & 9.7593 & -2.6881 & -64.5518 & 0.0 \\ 0.0 & 0.0 & 1.0 & -0.0377 & 0.0 \\ -0.3033 & 0.0 & -17.4441 & 3.5477 & 0.0 \\ 0.0377 & 0.0 & -1.3019 & -0.0604 & 0.0 \\ 0.0 & 0.0 & 0.0 & 1.0007 & 0.0 \end{bmatrix}, \mathbf{B}_{\text{lat-dir.}} = \begin{bmatrix} -0.008 & 0.0659 \\ 0.0 & 0.0 \\ -1.8496 & 0.1347 \\ -0.0605 & -0.0361 \\ 0.0 & 0.0 \end{bmatrix} \quad (3.22)$$

3.3.3 Linearization Methods Verification

It is very crucial to validate the degree of matching of linear and nonlinear models, in order to assure that the linearization results are satisfying and the obtained linear model is a well representative of the nonlinear model at that condition. To perform this validation, the linear and nonlinear time simulation responses to the same doublet control inputs are to be compared. Since the linearization model is extracted at a user specified operating point of the flight envelope with the state variables, \mathbf{x} and the control inputs, \mathbf{u} set to zero, all the output variables of the time simulation results are accommodated around zero. Therefore, the simulated linear model outputs should be added up with the constant trim output values of the corresponding variables, in order to have realistic linear model time simulation results, and compare with nonlinear simulation results.

The graphs of Figures 3.1 through 3.8 show the superimposed linear and nonlinear responses to inputs given to the controls column, throttle, wheel, and pedal respectively, which are also demonstrated. The right hand columns in the figures are the plots of differences between the linear responses and nonlinear responses shown

on the left hand columns. The doublet inputs are of size $+0.15^\circ$ at 5 seconds and -0.15° at 10 seconds with durations of 5 seconds each, except for throttle inputs. Amplitude of value 0.15 is the 0.3% of the total possible control input range varying between -25° and $+25^\circ$ all for column, wheel and pedal controls. The throttle inputs are given in pulse form again with amplitude of 0.3% at 5 seconds and 0% at 10 seconds, where the possible throttle input values range between 0% and 100%. The amplitudes of doublet and pulse inputs applied are small enough, in order to compensate with the small-perturbation linear models, at the considered trim condition.

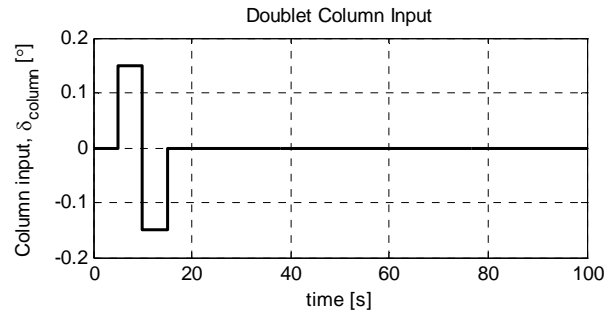
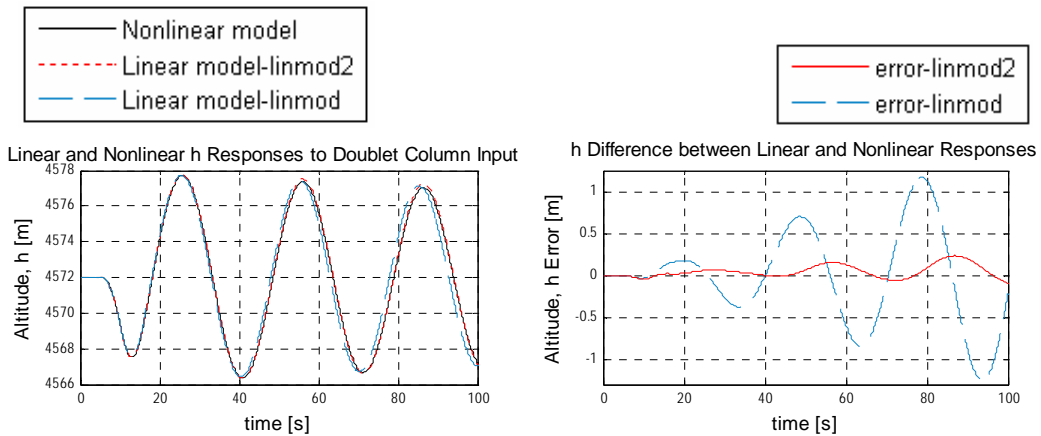


Figure 3.1 Doublet column input



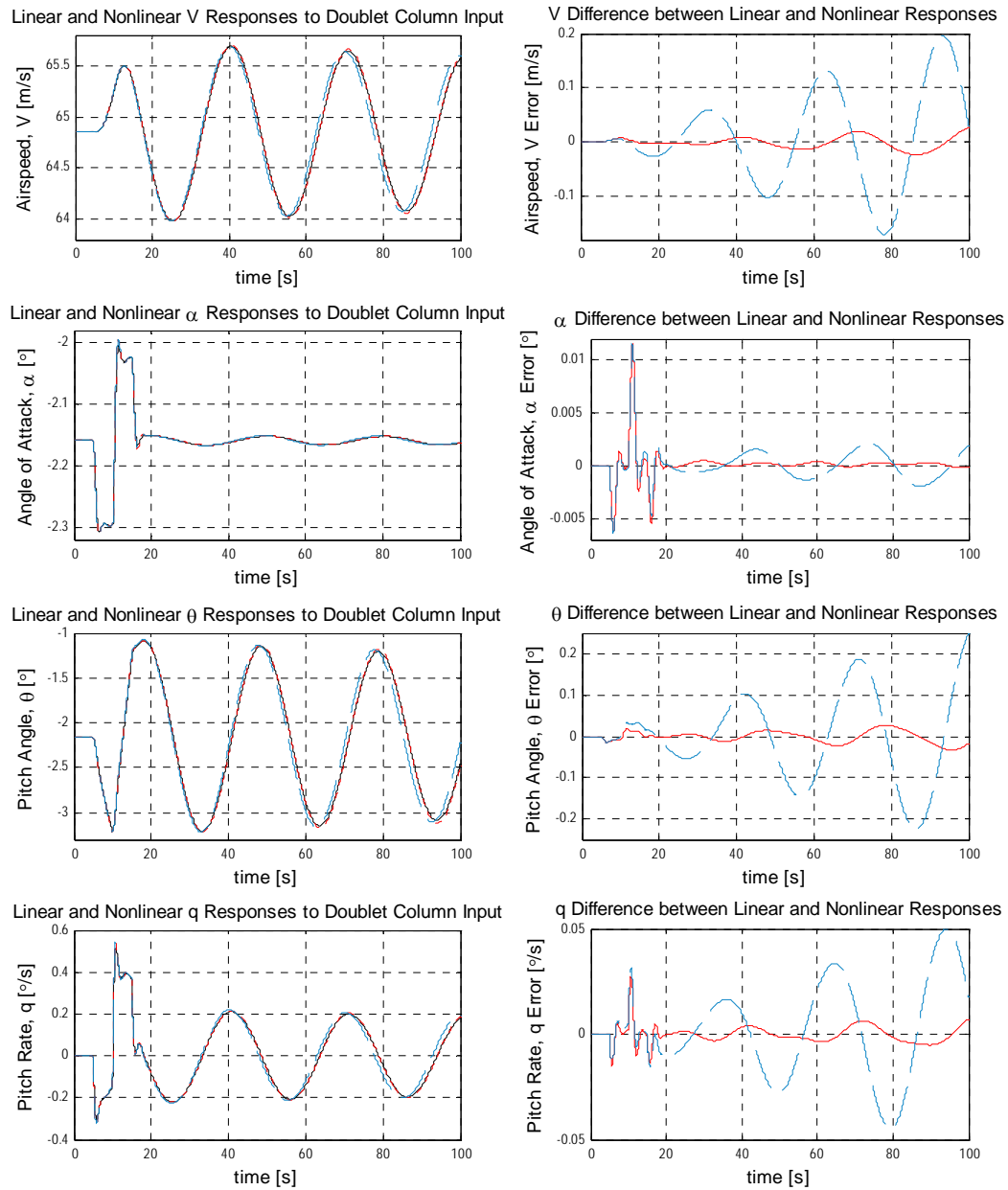


Figure 3.2 Linear and nonlinear responses to doublet column input

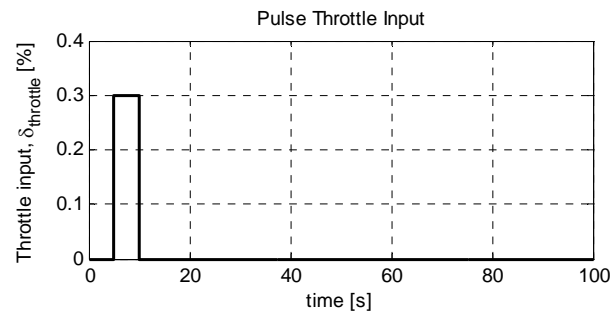
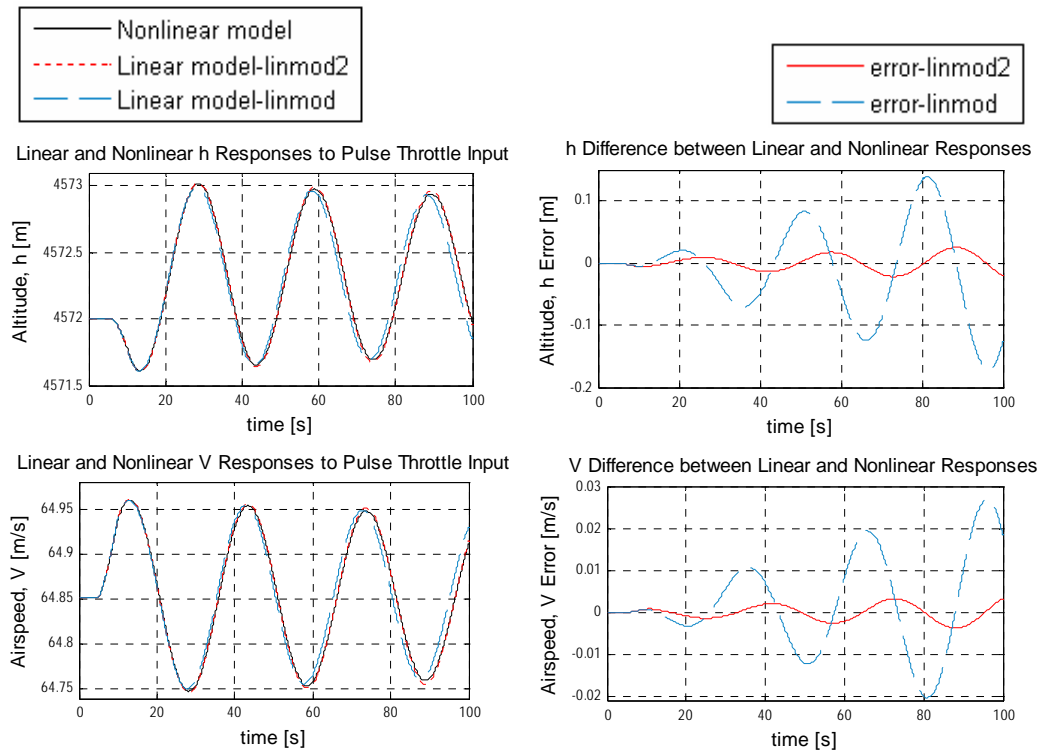


Figure 3.3 Pulse throttle input



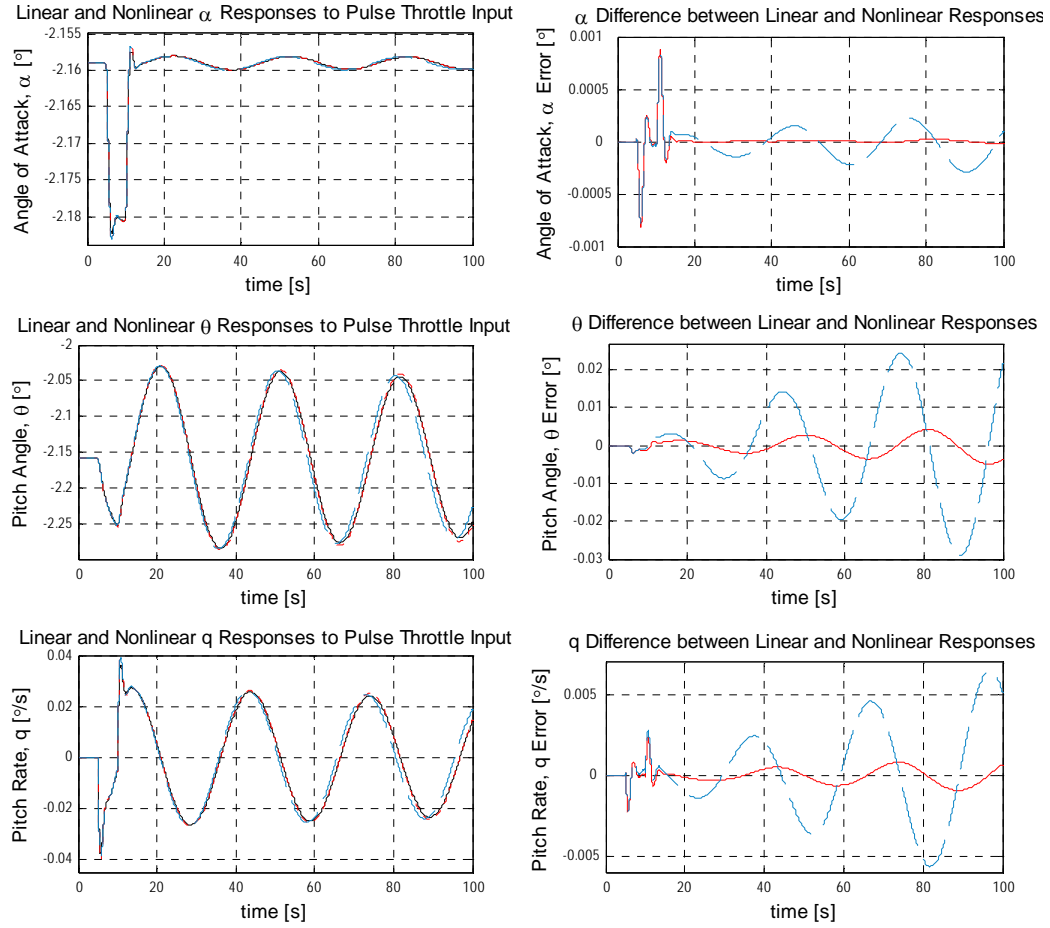


Figure 3.4 Linear and nonlinear responses to pulse throttle input

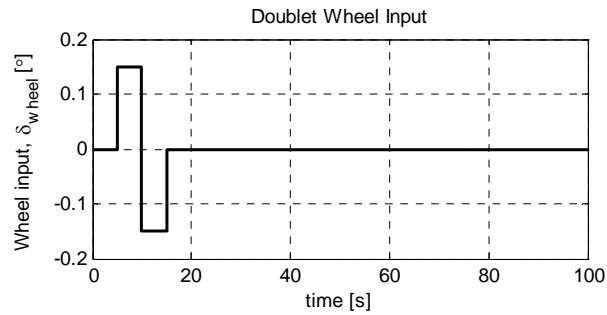
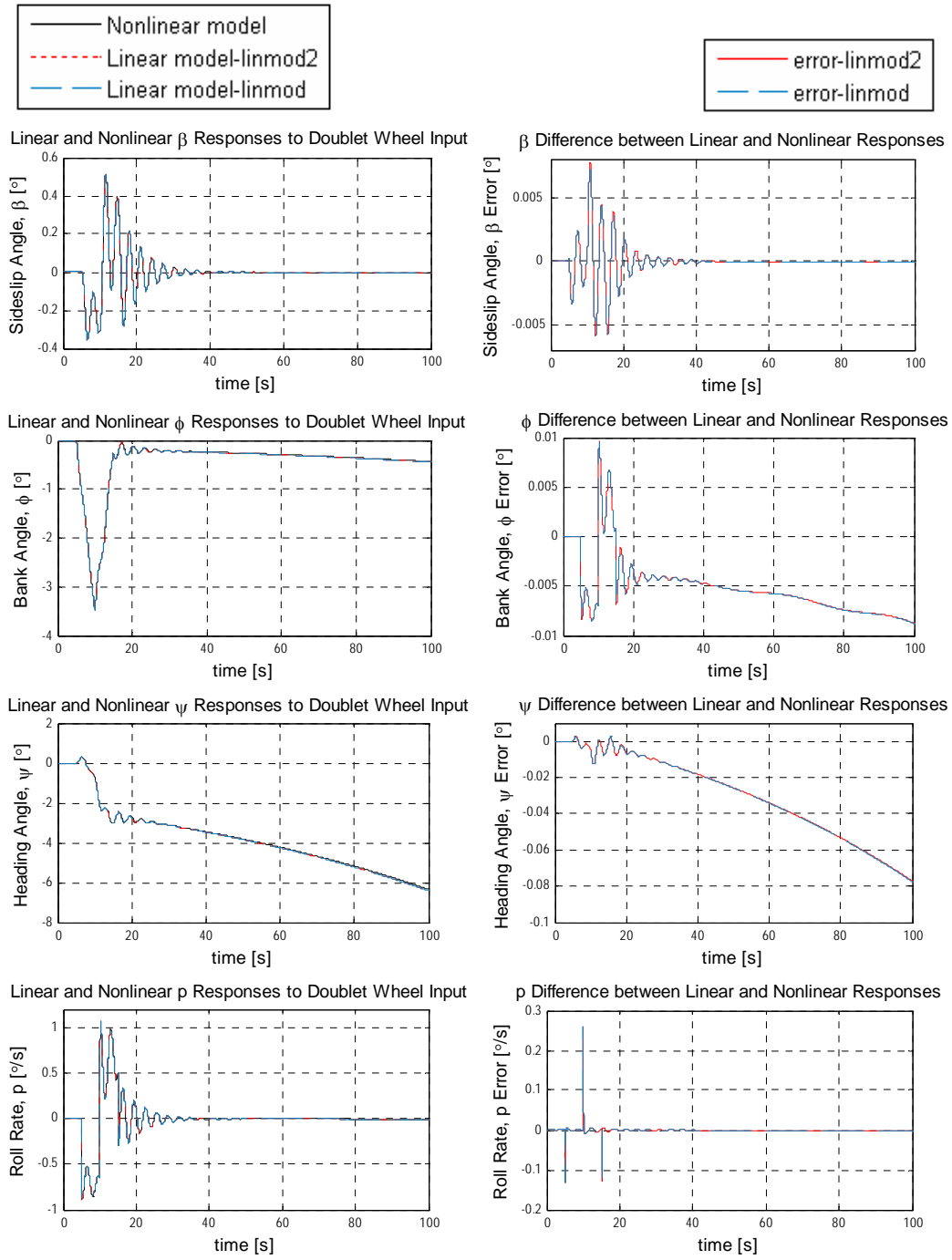


Figure 3.5 Doublet wheel input



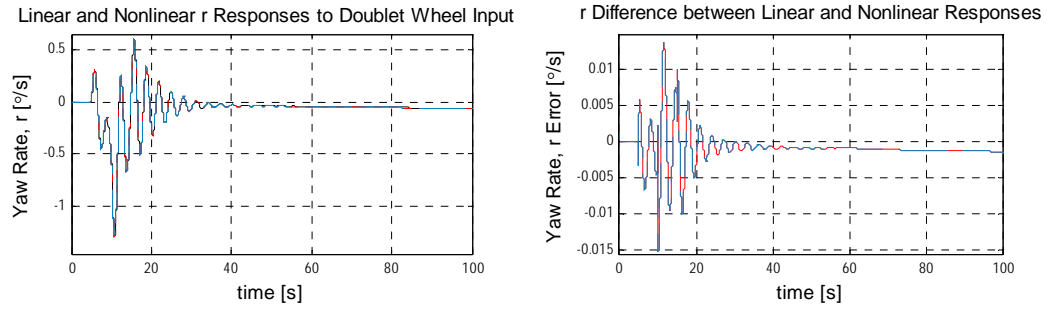


Figure 3.6 Linear and nonlinear responses to doublet wheel input

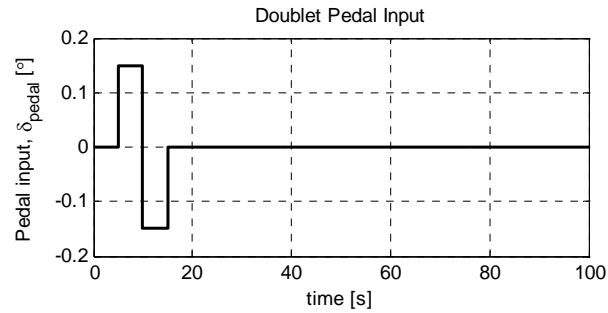
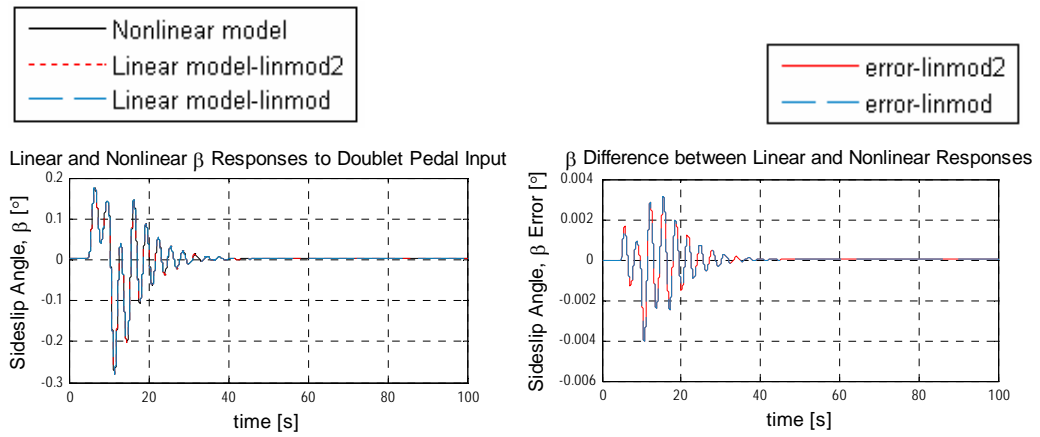


Figure 3.7 Doublet pedal input



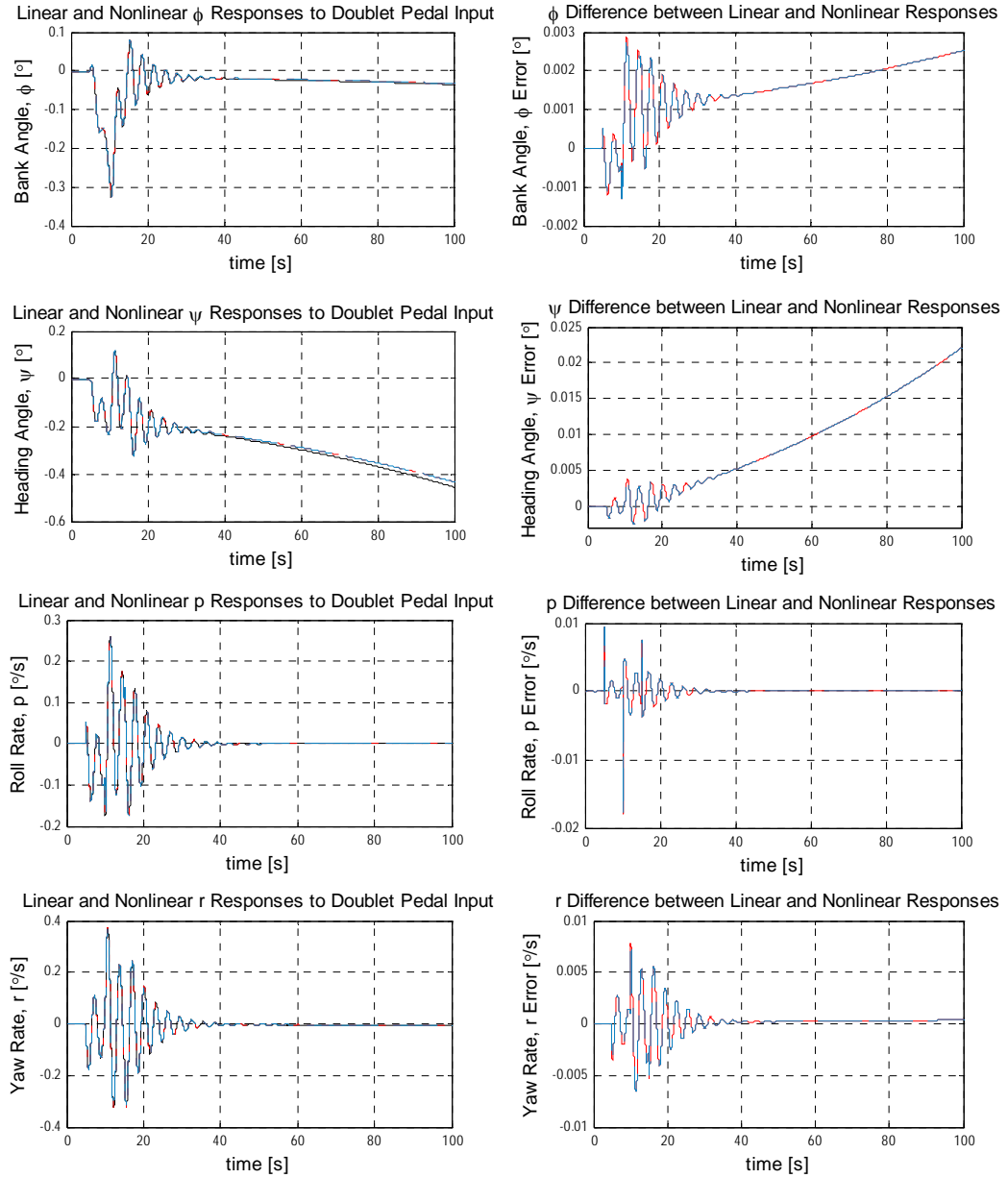


Figure 3.8 Linear and nonlinear responses to doublet pedal input

Figures 3.2, and 3.4, which stand for the motion variables about the longitudinal axis, express that, regardless of the input type applied, the difference between the linear

and nonlinear model responses increases through the ongoing time. It is obvious that the magnitude of this error increase is much greater for function `linmod` than for function `linmod2`. The source of this difference can be investigated from the linear application results including the respective system and control input matrices of the longitudinal linear models given by Equations (3.19) and (3.21), their eigenvalues given by Tables 3.1 and 3.2, and the respective modal matrices given by Equations (3.15) and (3.16). The eigenvalues show that different characteristics occur in phugoid and altitude modes, where phugoid mode is the dominant lightly damped oscillatory longitudinal mode, compatible with the simulation results. It has a higher frequency for longitudinal linear model dynamics of `linmod` with respect to the linear model dynamics of `linmod2`, causing a lag and thereby faster error increase with time with respect to the nonlinear model.

Figures 3.6 and 3.8 are the comparisons of the motion variables of lateral-directional axis. The results of the two linear methods applied are the same which can also be examined from the Equations (3.20) and (3.22), and the respective eigenvalues and the modal matrices. Regardless of the input types, the lateral-directional motion shows an oscillatory damped behavior compatible with the eigenvalues of the dominant Dutch roll mode. However for the heading and bank angle states, unstable spiral mode is also effective as can be investigated from the modal matrices of Equations (3.15) and (3.16), causing an additional aperiodic undamped motion. At the simulation time interval displayed by the graphs, the errors are small enough relative to the respective state amplitudes. Hence, it can be concluded that the matching degree is very well between linear and nonlinear responses.

Despite the same lateral-directional axis results of the two methods, the longitudinal axis dynamic behavior of the nonlinear model and the linear model output by `linmod2` are more alike than the dynamic behavior of the nonlinear model and the linear model output by `linmod`. Hence, it is decided to use the numerical-perturbation linearization method introduced by the function `linmod2` in this study

from now on. The repeated validation of these conclusions is to be carried out implicitly when the controllers designed using the obtained linear models are implemented to the nonlinear model and the simulations are performed. It should be noted that, the combination of the nonlinear model in Simulink[®], and the air vehicle trim and linearization routines makes it possible to do the whole linear and nonlinear implemented control system analyses in the same working environment. In this way, it is much easier to make the step from linear to nonlinear system analyses, encouraging the designer to do more experiments to analyze the systems, and at the same time reducing the risk of making errors.

CHAPTER 4

UAV MODEL VERIFICATION

4.1 Introduction

In this chapter, the verification of the nonlinear UAV model is to be carried out by the analyses done about the linear models obtained in the operational flight envelope, where they are proved to be the representatives of the nonlinear model in the previous chapter. In Section 4.2, the eigenvalues of the linear models of the whole operational envelope are to be shown on the MATLAB[®] pole-zero maps, displaying their locations on the figures with real and imaginary axes. Consequently, the figures give a sight about the dynamic characteristics of the longitudinal and lateral-directional standard flight modes of the subject UAV, by displaying the locations of the respective eigenvalues. In Section 4.3, the dynamic stability analyses throughout the operational flight envelope are to be carried out referring to some military standards in terms of dynamic stability level requirements specific to the subject UAV, and the results are to be compared with some known similar UAV data.

4.2 Pole-Zero Maps

The longitudinal and lateral-directional pole-zero maps covering the whole operational flight envelope are shown by Figures 4.1 through 4.4. Since it is aimed to display only the characteristic poles instead of zeros of the air vehicle, the MATLAB[®] function `pzmap` which outputs the pole-zero maps is given multi input-multi output (MIMO) linear systems as the inputs; thereby the zeros are not generated on the figures. These maps help previewing the characteristics of the air vehicle's standard dynamic flight modes by observing their locations with respect to real and imaginary axes. Each pole or eigenvalues represents the characteristic of a flight mode at a respective altitude and airspeed throughout the operational flight envelope. The airspeed interval is taken as 70 KEAS to 120 KEAS with 5 KEAS

increments, whereas the altitude interval is taken as 5,000 ft (1,524 m) to 30,000 ft (9,144 m) with 5,000 ft (1,524 m) increments. The relative locations of the eigenvalues given at Table 3.1 representing the dynamic characteristics of 100 KEAS and 15,000 ft (4,572 m) flight condition can also be investigated on these maps. The change of the flight mode characteristics with respect to airspeed and altitude is demonstrated and discussed in detail in Section 4.3 by figures of dynamic stability analyses. Hence, the purpose of the Figures 4.1 through 4.4 should be considered as examining the big picture of the standard air vehicle flight modes.

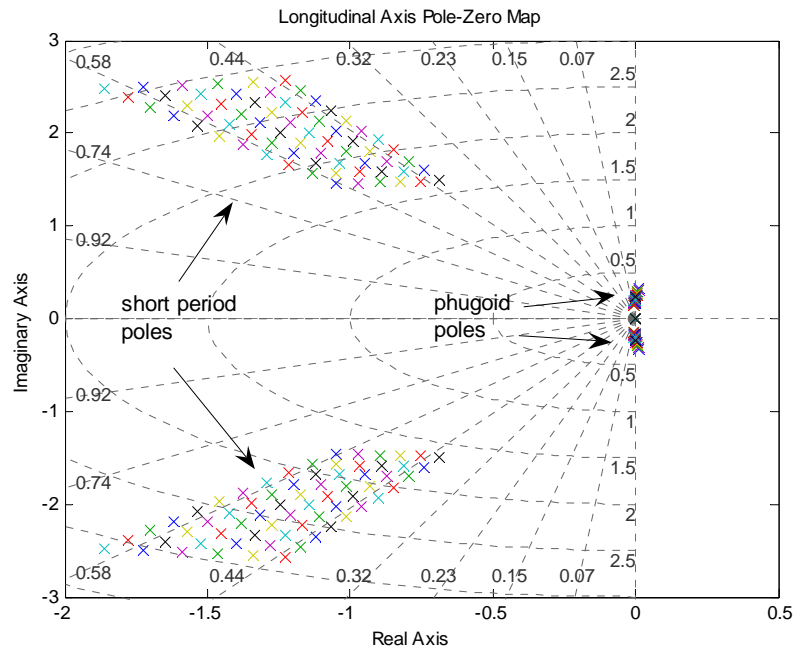


Figure 4.1 Longitudinal axis poles

In Figure 4.1, the poles of the longitudinal axis linear systems are displayed. The group of poles that lay out further from the imaginary axis represents the dynamics

of the short period flight mode of the air vehicle which is a heavily damped oscillation with a higher natural frequency with respect to the lightly damped oscillatory longitudinal flight mode, phugoid.

The poles that are around the origin on the real axis belong to the altitude mode. In order to have a closer view, Figure 4.1 is blown up and the Figure 4.2 is obtained in which the altitude mode around the origin and the oscillatory, lightly damped phugoid mode are focused on. It is observed from Figure 4.2 that, for some conditions of the operational flight envelope, the poles lay out on the positive side of the complex plane, expressing instability in the longitudinal axis regarding the dominating phugoid mode with its closer location to the origin and pairs of complex conjugate poles.

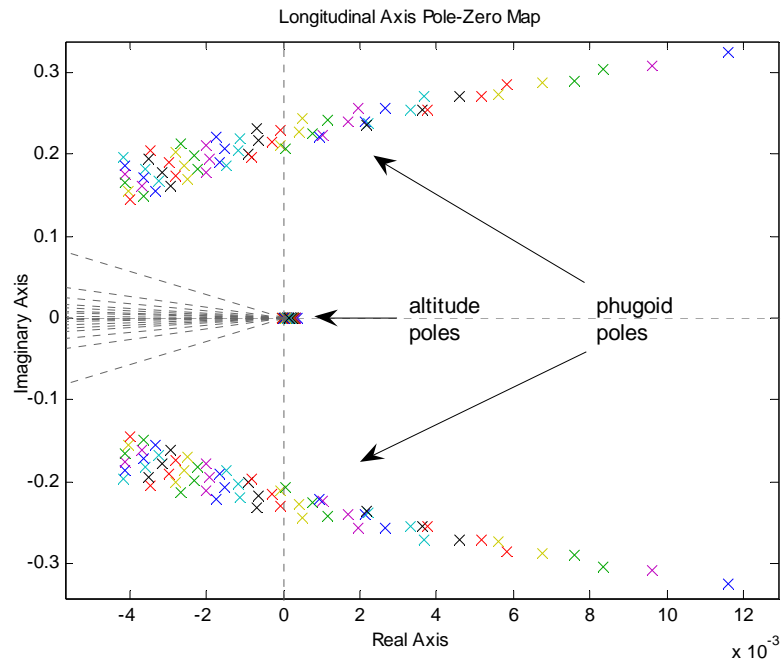


Figure 4.2 Blown up longitudinal axis poles around phugoid and altitude modes

In Figure 4.3, the poles of the lateral-directional axis linear systems are displayed. The group of poles that lay out on the real axis further from the origin represents the roll mode dynamics of the air vehicle which shows a heavily damped aperiodic motion; whereas the complex conjugate poles closer to the origin represent the dominating Dutch roll mode with a lightly damped periodic motion. Poles around the origin on the real axis belong to the spiral and heading modes. Blowing up Figure 4.3 and focusing on the flight modes around the imaginary axis the Figure 4.4 is obtained. It can be investigated by this figure that the spiral mode with positive poles on the real axis for the whole operational range shows a time to double (T_{2s}) aperiodic motion characteristic, whereas the heading mode is neutrally stable with the real poles on the origin.

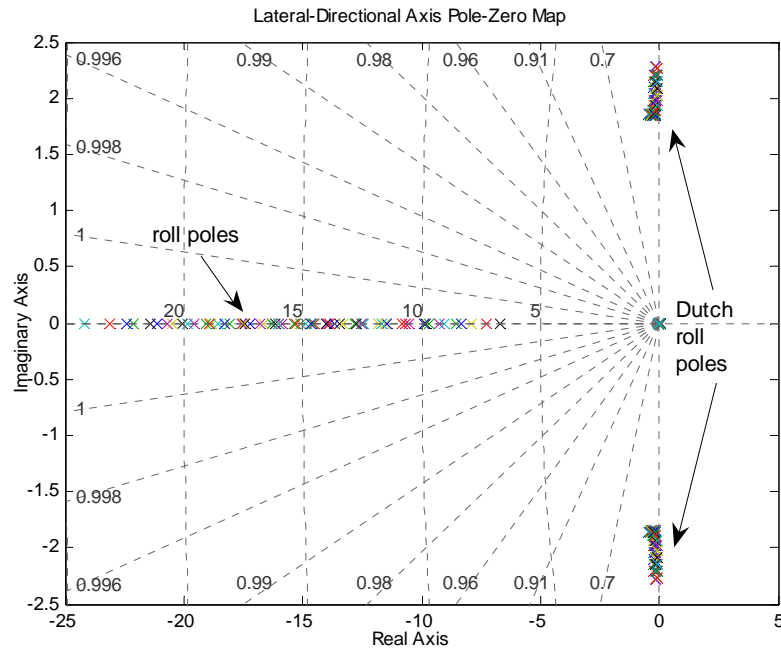


Figure 4.3 Lateral-directional axis poles

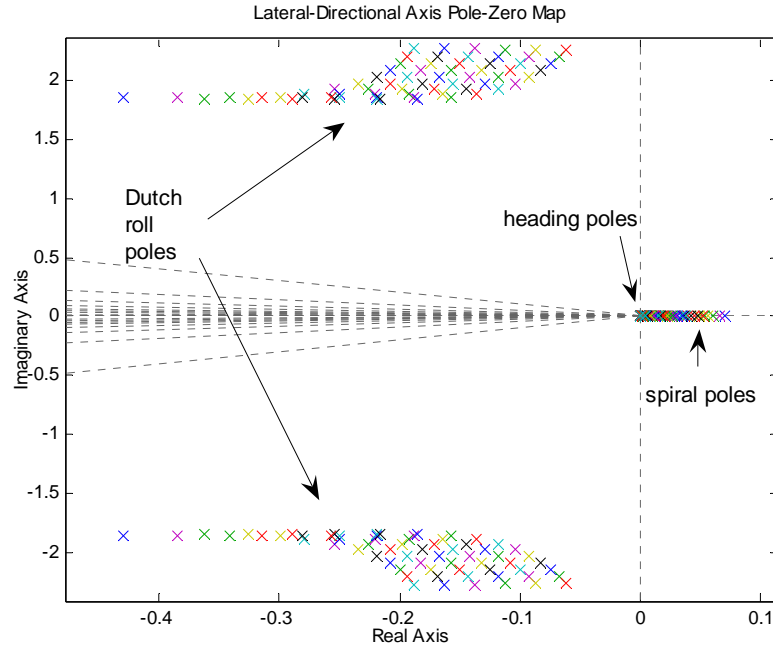


Figure 4.4 Blown up lateral-directional axis poles around Dutch roll, spiral, and heading modes

4.3 Dynamic Stability Requirements and Analyses Results

There are two extreme and opposite opinions about dynamic problems of UAVs [28]:

1. Sensors, actuators, on-board computers & fly-by-wire (FBW) systems “can do everything” – do not worry about dynamics and control,
2. There is no difference between dynamics of manned and unmanned aircraft.

Solve the problem using the same procedures.

The first opinion is valid for normal operations of the air vehicle, in which the autopilot is engaged without any problems. However, in case of failures, affecting the functioning of the autopilot and forcing the operator to override the control of the air vehicle, the handling and flying qualities of the air vehicle becomes the

determinative property in terms of work load of the operator to complete the mission and/or to safely recover the UAV. Therefore, the second opinion has to be taken into account, and dynamic stability properties of the unmanned aerial vehicles should also be investigated as it is the case in manned aircrafts. As a result of this investigation, if necessary, configuration of the air vehicle should be changed in order to enhance the inherent dynamic stability properties.

Dynamic stability is a very important field for the understanding of air vehicle flying qualities, since it is related to the dynamic, or transient part of the air vehicle response to the operator controlling the air vehicle remotely and disturbance inputs, in case the autopilot is not engaged. Therefore, although the steady state is the ultimate objective of an operator, the way an air vehicle behaves to reach that end, i.e. the transient response, may be more determinative for operators when assessing a certain configuration for accomplishing a specified task. Moreover, in certain tasks such as tracking, or combat flight, the operator continuously inputs commands, thereby rendering the steady state response less importance and increasing that of the dynamic response. This explains why dynamic stability is so important in the assessment of flying qualities and why the formal civil requirements are limited, since they make no explicit reference to dynamic stability parameters [29]. The formulation of flying qualities requirements draws upon the relevant requirements as stated in references [4, 30-31] that are the military documents RPV (Remotely Piloted Vehicles) Flying Qualities Design Criteria, MIL-F-8785C, and MIL-HDBK-1797, respectively. RPV Flying Qualities Design Criteria is the document that is adapted from MIL-F-8785C and MIL-HDBK-1797 to remotely piloted air vehicles in terms of flying qualities, and is the major document that is based on in this study both in terms of dynamic stability and flight control requirements.

As it is mentioned in Section 1.1, the subject UAV belongs to low maneuverability RPV's Class II with its 1,280 kg mass, which is heavier than 300 lbs (136 kg) and with the maximum load factor value of 2.5g it sustains which is smaller than 4g. The

major missions appointed by this class are surveillance/reconnaissance, electronic warfare, and relay command/control/communications. For the subject UAV, these missions are to be carried out at the flight phases of climb, cruise, loiter, and descent requiring gradual maneuvers without precision tracking, corresponding to Category B; the flight phases of go-around, take-off and landing which are the launch/recovery flight phases requiring rapid maneuvering, precision tracking or precise flight-path control, corresponding to Category C; and flight phase of approach which is also a launch/recovery flight phase that is normally accomplished using gradual maneuvers and without precision tracking, although accurate flight-path control may be required, corresponding to Category D [4]. In the scope of this study, the analyses and controller design are to be done only at Category B flight phases.

Before the results of dynamic stability analyses, the levels of the UAV flying qualities should also be defined [4, 30-31] as

- Level 1 (Normal system operation): UAV flying qualities are clearly adequate to accomplish the mission flight phase. The performance of the air vehicle should be at least this level in the operational flight envelope, if the autopilot is engaged.
- Level 2 (Degraded mission): UAV flying qualities remain adequate to perform mission flight phase with moderate degradation of mission effectiveness, a moderate increase in operator workload, or both.
- Level 3 (Recoverability): Degraded UAV flying qualities remain adequate to recover the air vehicle. Workload permits Categories B, C and D flight phases to be completed sufficiently to recover the air vehicle.

In summary, Level 1 is satisfactory, Level 2 is acceptable, and Level 3 is controllable.

4.3.1 Longitudinal Dynamic Stability Requirements and Analyses Results

The short period mode undamped natural frequency, ω_{nsp} and damping ratio, ζ_{sp} values are obtained by the MATLAB[®] function `damp` with the linear longitudinal

system matrix, \mathbf{A}_{long} , given as the input. In order to have an insight about the variable affecting this flight mode, short period approximations for ω_{nsp} in [rad/s] and ζ_{sp} are given by Equations (4.1) and (4.2) as [14]

$$\omega_{\text{nsp}} \approx \sqrt{\frac{Z_{\alpha} M_q}{V} - M_{\alpha}} \quad (4.1)$$

$$\zeta_{\text{sp}} \approx \frac{-\left(M_q + \frac{Z_{\alpha}}{V} + M_{\dot{\alpha}}\right)}{2\omega_{\text{nsp}}} \quad (4.2)$$

where $Z_{\alpha} = \frac{-\bar{q}S(C_{L_{\alpha}} + C_D)}{m}$: Vertical acceleration per unit angle of attack,

$M_q = \frac{\bar{q}S\bar{c}^2 C_{m_q}}{2I_{yy} V}$: Pitch angular acceleration per unit pitch rate,

$M_{\alpha} = \frac{\bar{q}S\bar{c} C_{m_{\alpha}}}{I_{yy}}$: Pitch angular acceleration per unit angle of attack,

$M_{\dot{\alpha}} = \frac{\bar{q}S\bar{c}^2 C_{m_{\dot{\alpha}}}}{2I_{yy} V}$: Pitch angular acceleration per unit change of angle of

attack.

The short period undamped natural frequency, ω_{nsp} , shall be within the limits shown in the Figure 4.5 for Category B flight phases [4, 30-32].

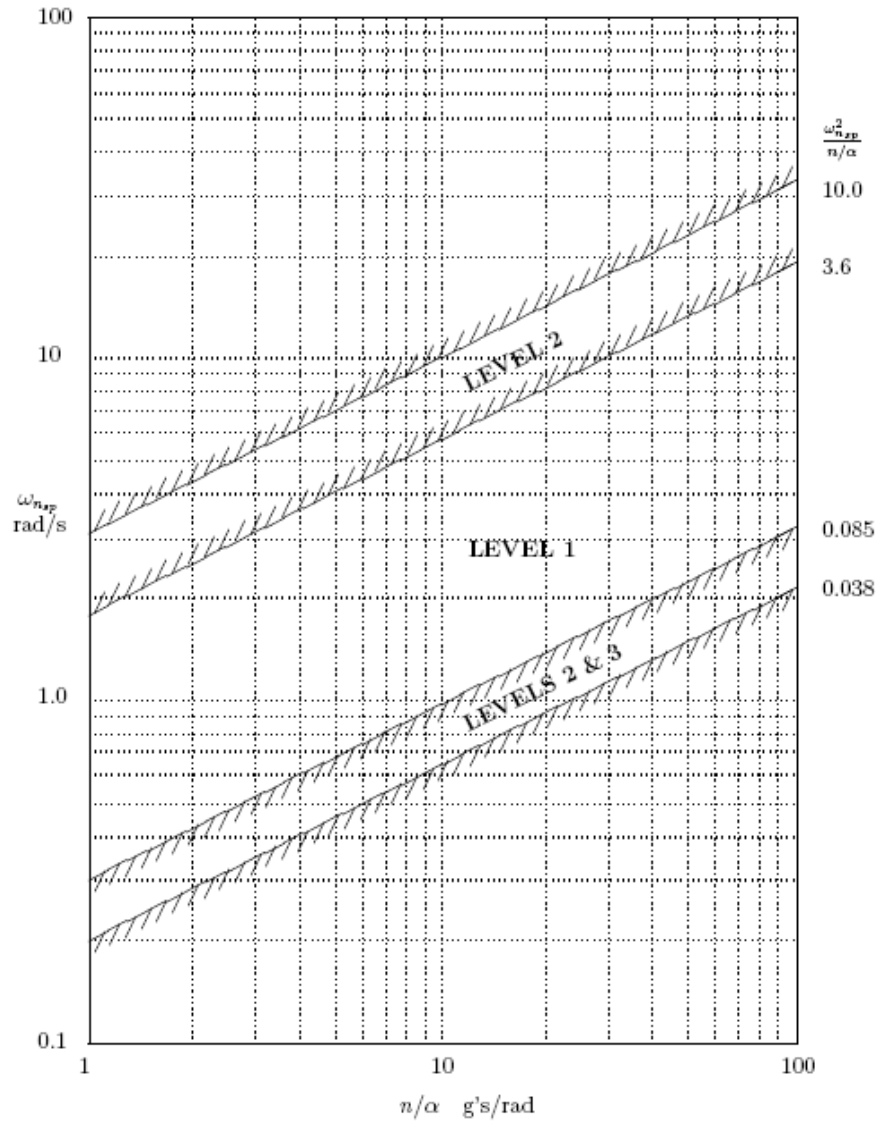


Figure 4.5 Short period mode undamped natural frequency, ω_{nsp} requirements – Category B Flight Phases [4, 30-32]

The n/α in [g/rad] is defined as the steady-state normal acceleration change per unit change in angle of attack for an incremental pitch control deflection at constant speed

(airspeed and Mach number); or is the acceleration sensitivity of the air vehicle. n/α is calculated as,

$$\frac{n}{\alpha} = \frac{CL_{\alpha} \bar{q} S}{mg} \quad (4.3)$$

where n : normal load factor,

CL_{α} : air vehicle lift-curve slope, $\partial CL / \partial \alpha$ [1/rad].

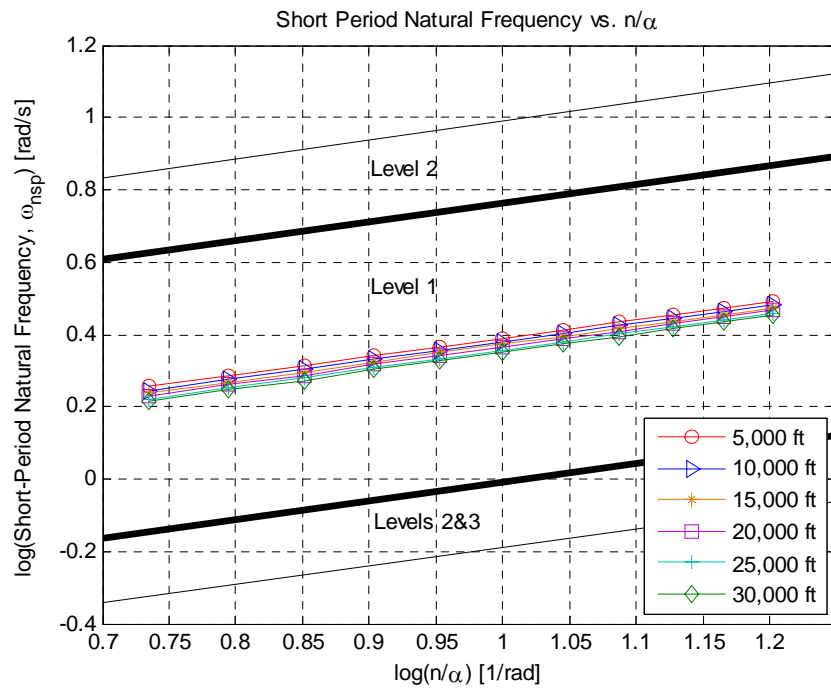


Figure 4.6 Short period mode undamped natural frequency, ω_{nsp}

The results of the dynamic stability analyses for short period natural frequency are displayed in Figure 4.6 in logarithmic scale. It can be seen from the figure that, the natural frequency values in the operational flight envelope provide the related requirement very well and remain in the region corresponding to flying qualities of Level 1, without even being close to the limits.

The short period mode damping ratio, ζ_{sp} values shall be within the limits given in Table 4.1 [4, 30-32]. The results of the dynamic stability analyses for short period mode damping ratio values with respect to airspeed and altitude in the operational flight envelope are displayed in Figure 4.7. The damping ratio values also remain in the region of Level 1 flying qualities.

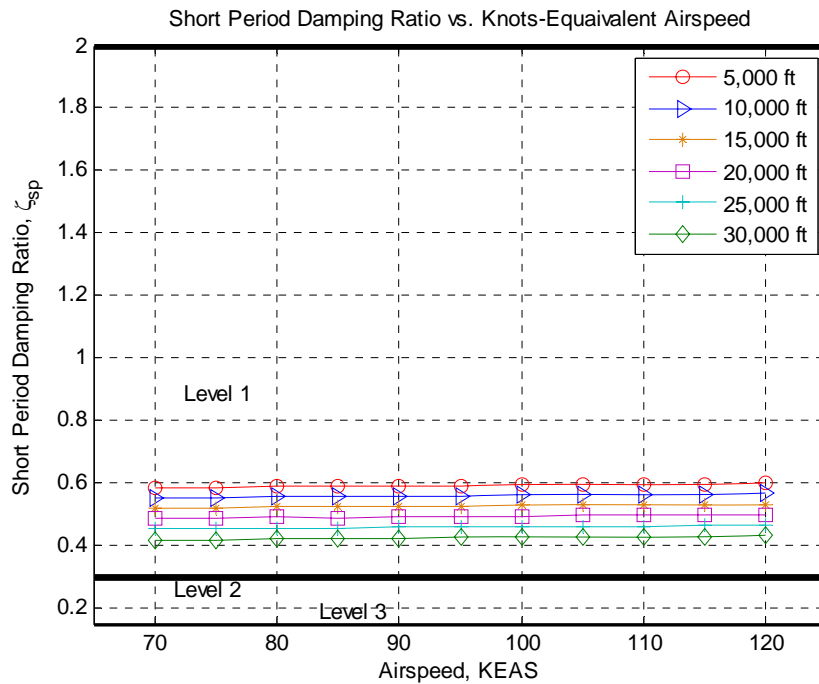


Figure 4.7 Short period mode damping ratio, ζ_{sp}

Table 4.1 Short period mode damping ratio, ζ_{sp} requirements – Category B Flight Phases

Levels	Category B Flight Phases	
	Minimum	Maximum
Level 1	0.3	2
Level 2	0.2	2
Level 3	0.15*	-

* May be reduced above 20,000 ft (6,096 m), if approved by the procuring activity.

The phugoid (long period) undamped natural frequency, ω_{nph} and damping ratio, ζ_{ph} values are also obtained by the MATLAB[®] function `damp` again with the linear longitudinal system matrix, \mathbf{A}_{long} , given as the input. In order to have an insight about the variables affecting this flight mode, phugoid approximations of ω_{nph} in [rad/s] and ζ_{ph} are given by Equations (4.4) and (4.5), whereas for low subsonic speed range, the further simplifying approximations are given by Equations (4.6) and (4.7) as [14]

$$\omega_{nph} \approx \sqrt{\frac{-gZ_u}{V}} \quad (4.4)$$

$$\zeta_{ph} \approx \frac{-X_u}{2\omega_{nph}} \quad (4.5)$$

where $Z_u = \frac{-\bar{q}S(CL_u + 2CL)}{mV}$: Vertical acceleration per unit change in speed,

$X_u = \frac{-\bar{q}S(CD_u + 2CD)}{mV}$: Forward acceleration per unit change in speed.

$$\omega_{\text{nph}} \approx \frac{g}{V} \sqrt{2} \quad (4.6)$$

$$\zeta_{\text{ph}} \approx \frac{\sqrt{2}}{2(\text{CL} / \text{CD})} \quad (4.7)$$

Equation (4.7) indicates that the phugoid damping ratio is inversely proportional to lift-to-drag ratio. This means that as the lift to drag ratio for an airplane is improved, the phugoid damping ratio is degraded. Typically, the lift-to-drag ratio is far more critical to an airplane's performance than the phugoid damping. However, in the case that the damping must be increased, Equations (4.5) and (4.7) clearly show that the only way to accomplish is to increase the air vehicle drag and therefore decrease the lift to drag ratio, which is very undesirable especially for a MALE type UAV which should have a long endurance. But, low phugoid damping can be a problem for precision landing maneuvers, so consideration should be given to ensure that the damping ratio is above the specified limit.

The phugoid (long period) mode oscillations that occur when the air vehicle seeks a stabilized airspeed following a disturbance shall meet the requirements of damping ratio, ζ_{ph} , to be $\zeta_{\text{ph}} \geq 0.04$ for Level 1, $\zeta_{\text{ph}} \geq 0.0$ for Level 2, and in case of negative damping ratio the requirement of “time to double amplitude”, $T_{2\text{ph}}$ to be $T_{2\text{ph}} \geq 55$ s for Level 3 [4, 30-32]. $T_{2\text{ph}}$ is obtained from the relationship given by Equation (4.8) as [13]

$$T_{2\text{ph}} = \frac{\ln 2}{|\zeta_{\text{ph}}| \omega_{\text{nph}}} = \frac{0.693}{|\zeta_{\text{ph}}| \omega_{\text{nph}}} \quad (4.8)$$

The results of the dynamic stability analyses for phugoid mode damping ratio values with respect to airspeed and altitude in the operational flight envelope are displayed in Figure 4.8. Phugoid mode seems to be critical for a considerable range of

relatively low airspeed values at which the phugoid damping ratio values remain in the flying qualities region of Level 3. The T_{2ph} values for this region are also shown on the right below corner of Figure 4.8. The damping ratio values increase with the increasing airspeed, which can also be concluded from Equations (4.4) and (4.5).

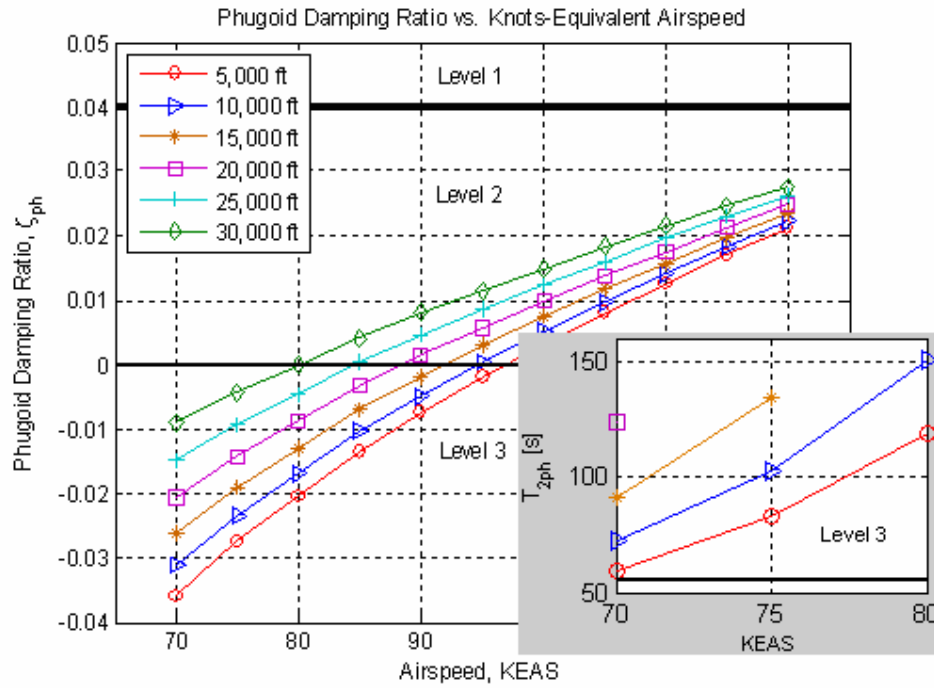


Figure 4.8 Phugoid mode damping ratio, ζ_{ph}

4.3.2 Lateral-Directional Dynamic Stability Requirements and Analyses Results

Again the MATLAB[®] function `damp` is used with the linear lateral-directional system matrix, $A_{lat-dir}$, given as the input to obtain the Dutch roll mode undamped natural frequency, ω_{ndr} and damping ratio, ζ_{dr} values. In order to have an insight

about the variables affecting this flight mode, Dutch roll approximations of ω_{ndr} in [rad/s] and ζ_{dr} are given by Equations (4.9) and (4.10) as [14]

$$\omega_{\text{ndr}} \approx \sqrt{N_{\beta} + \frac{1}{V} (Y_{\beta} N_r - N_{\beta} Y_r)} \quad (4.9)$$

$$\zeta_{\text{dr}} \approx \frac{-\left(N_r + \frac{Y_{\beta}}{V}\right)}{2\omega_{\text{ndr}}} \quad (4.10)$$

where, $N_{\beta} = \frac{\bar{q}SbCN_{\beta}}{I_{zz}}$: Yaw angular acceleration per unit sideslip angle,

$Y_{\beta} = \frac{\bar{q}SCY_{\beta}}{m}$: Lateral acceleration per unit sideslip angle,

$N_r = \frac{\bar{q}Sb^2CN_r}{2I_{zz}V}$: Yaw angular acceleration per unit yaw rate,

$Y_r = \frac{\bar{q}SbCY_r}{2mV}$: Lateral acceleration per unit yaw rate.

Table 4.2 Dutch roll mode damping ratio, ζ_{dr} , natural frequency, ω_{ndr} requirements – Category B Flight Phases / Class II

Levels	Category B Flight Phases / Class II		
	Minimum ζ_{dr}	Minimum ω_{ndr} [rad/s]	Minimum $\zeta_{\text{dr}}\omega_{\text{ndr}}$ [rad/s]
Level 1	0.08	0.4	0.15
Level 2	0.02	0.4	0.05
Level 3	0.02	0.4	-

The minimum Dutch roll mode damping ratio, ζ_{dr} , natural frequency, ω_{ndr} , and $\zeta_{\text{dr}}\omega_{\text{ndr}}$ values shall be within the limits given in Table 4.2, for Category B flight phases and Class II [4, 30-32]. The results of the dynamic stability analyses for

Dutch roll mode damping ratio, and natural frequency values with respect to airspeed and altitude in the operational flight envelope are displayed in Figure 4.9.

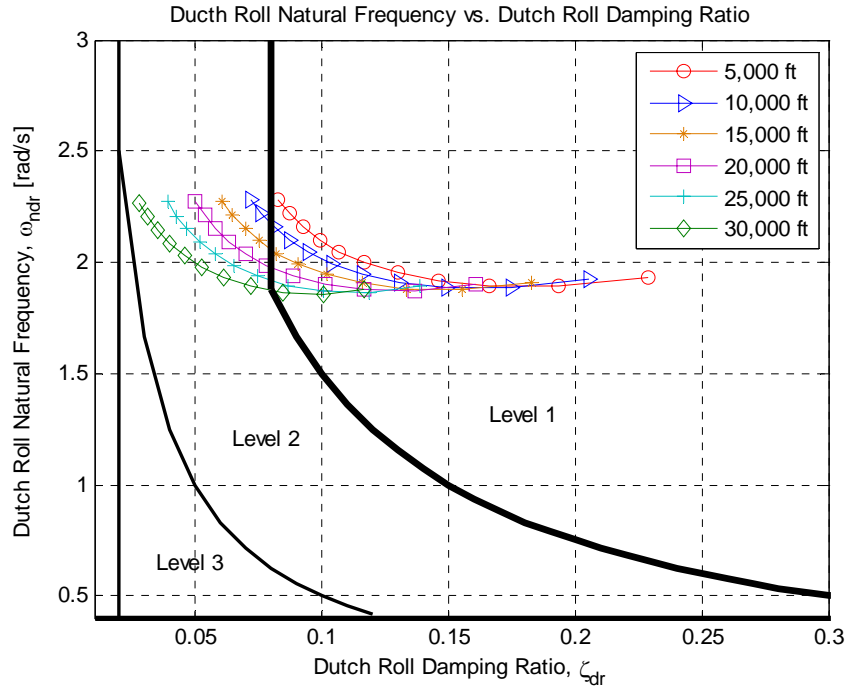


Figure 4.9 Dutch roll mode damping ratio, ζ_{dr} and natural frequency, ω_{ndr}

It is obvious from Figure 4.9 that, the worst region that Dutch roll mode dynamic characteristics in terms of damping ratio values fall in is Level 2 for the subject UAV, corresponding to higher airspeed and higher altitude conditions.

The MATLAB[®] function `damp` is also used with the linear lateral-directional system matrix, $\mathbf{A}_{lat-dir}$, given as the input to obtain the roll mode pole, s_{roll} values. The roll mode approximation of s_{roll} in [rad/s] is given by Equation (4.11) as [14]

$$s_{\text{roll}} \approx \frac{\bar{q} S b^2 C R_p}{2 I_{xx} V} \quad (4.11)$$

For Category B flight phases and Class II, the roll mode time constant, τ_r shall satisfy $\tau_r \leq 1.4$ s for Level 1, $\tau_r \leq 3$ s for Level 2, and $\tau_r \leq 10$ s for Level 3 [4, 30-32]. τ_r is the negative of the reciprocal of the s_{roll} . The results of the dynamic stability analyses for roll mode time constant values with respect to airspeed and altitude in the operational flight envelope are displayed in Figure 4.10. The roll mode characteristics satisfy the requirements very well in terms of time constant values.

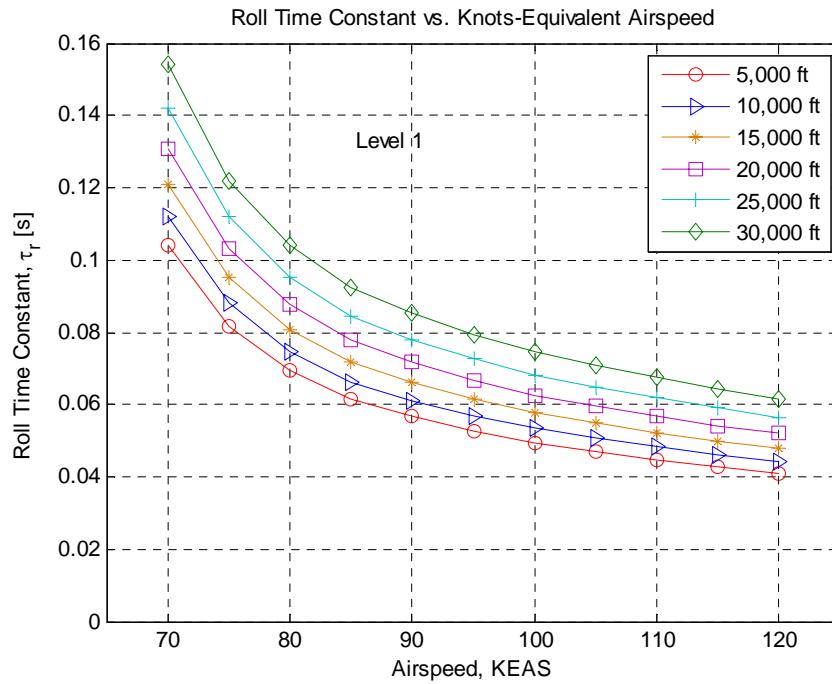


Figure 4.10 Roll mode time constant, τ_r

The MATLAB[®] function `damp` is also used with the linear lateral-directional system matrix, $\mathbf{A}_{\text{lat-dir}}$, given as the input to obtain the spiral mode pole, s_{spiral} values. The spiral mode approximation of s_{spiral} in [rad/s] is given by Equation (4.12) as [24].

$$s_{\text{spiral}} \approx -\frac{g}{V} \frac{CR_{\beta} CN_r - CN_{\beta} CR_r}{CR_{\beta} CN_p - CN_{\beta} CR_p - 2gI_{zz} CR_{\beta} / b^2 \bar{q} S} \quad (4.12)$$

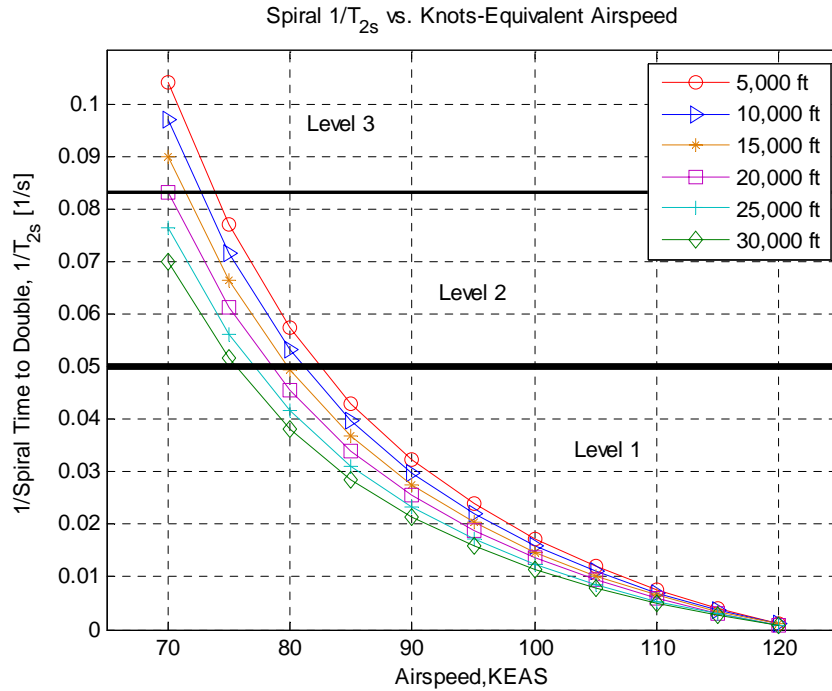


Figure 4.11 Spiral mode 1/Time to Double, 1/T_{2s}

For Category B flight phases and Class II, the spiral mode time to double, T_{2s} amplitude shall satisfy $T_{2s} \geq 20$ s for Level 1, $T_{2s} \geq 12$ s for Level 2, and $T_{2s} \geq 4$ s for

Level 3 [4]. The time to double amplitude values are obtained in the same way put forth by Equation (4.8), this time by considering the damping ratio as equal to -1 , and frequency as equal to the value of s_{spiral} .

In Figure 4.11, the results of the dynamic stability analyses for spiral mode characteristics are displayed in terms of 1/time to double amplitude values with respect to airspeed and altitude in the operational flight envelope. The spiral mode time to double amplitudes correspond to the Level 1 value range for most of the airspeed values, except for the airspeeds that are the lowest in the considered operational flight envelope.

Figures 4.6 through 4.11 show the change of dynamic characteristics of the major flight modes in both axes with respect to altitude and equivalent airspeed with figure forms regarding the flying quality requirements given in many references such as [4, 30-32]. It can be concluded that, any of the flight modes do not fall below flying qualities Level 3 for the uncontrolled UAV, in the considered range of altitude and airspeed values.

4.3.3 Validation of the Results

The graphs of the Figure 4.13 demonstrate the comparison of dynamic stability characteristics of the major flight modes between the subject UAV and Predator RQ-1, for which the three plan view is given in Figure 4.12.

This study is carried out in order to validate the model developed in this thesis. The resultant figures for dynamic stability analyses of Predator RQ-1 are obtained from [28]. Since the form of the figures can not be changed for Predator RQ-1 results, the figures of the subject UAV are adapted in order to have a better comparison. It is important to indicate that, in the reference [28], the graphs of the dynamic stability analyses were obtained using the parameters; “damping coefficient”, and “frequency”, which are defined as the real and imaginary parts of the corresponding eigenvalues, respectively. Hence, while obtaining the graphs of the subject UAV

shown on the left hand column of Figure 4.13, these parameters are calculated and plotted, and the x and y axes of the graphs are scaled similarly with the graphs of the Predator RQ-1 where possible. In addition, the airspeed values in the figures are the true airspeed values different from the former dynamic stability Figures 4.6 through 4.11.

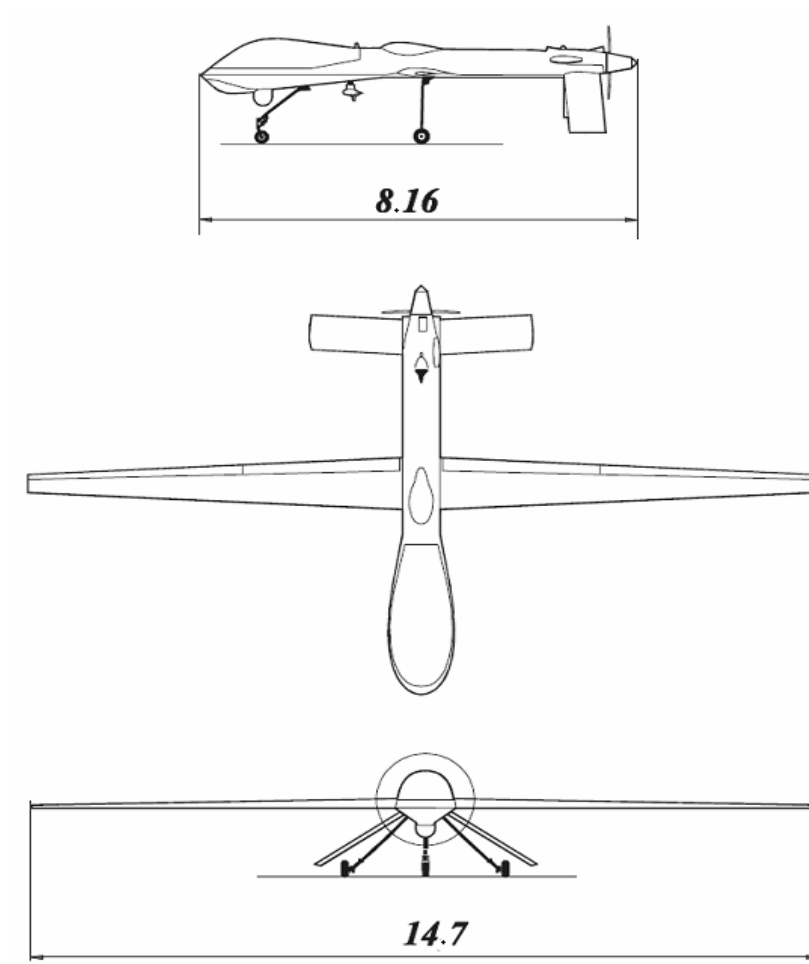
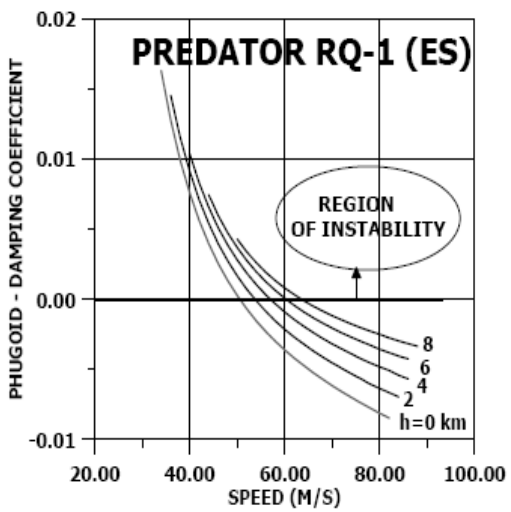
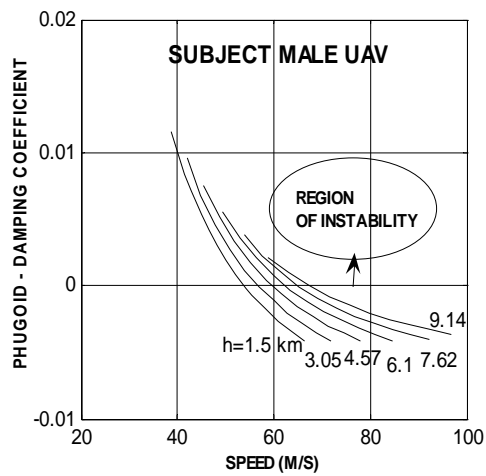
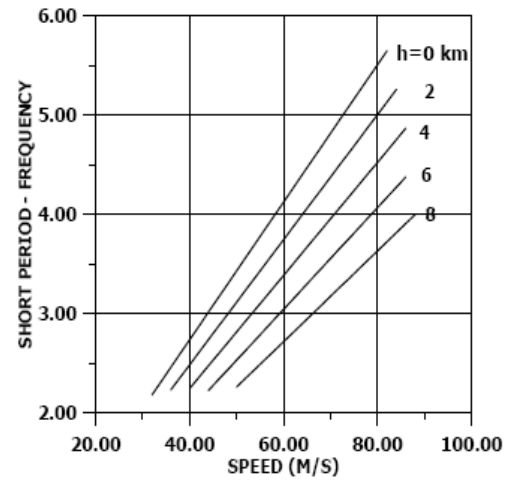
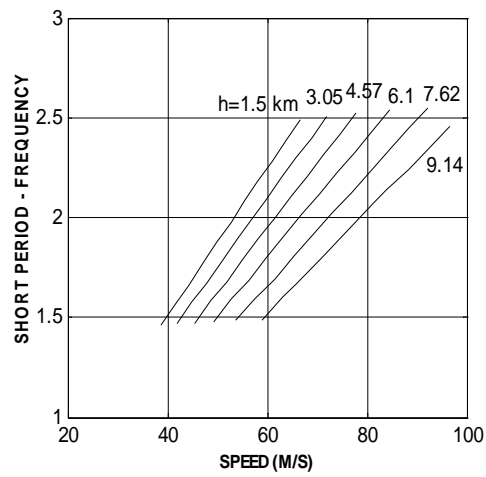
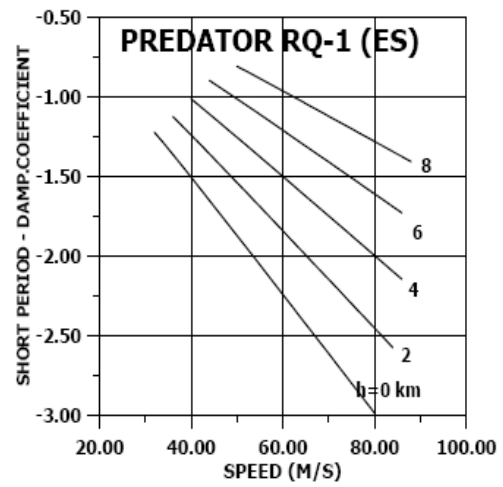
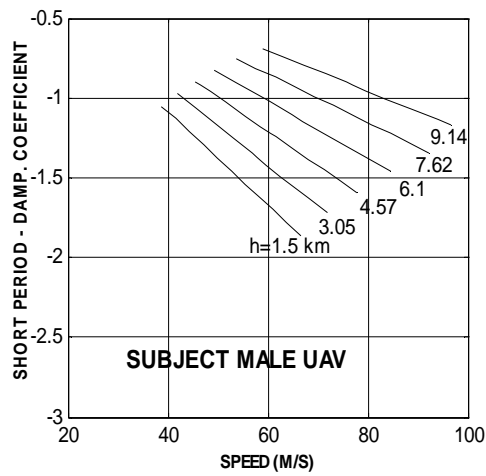
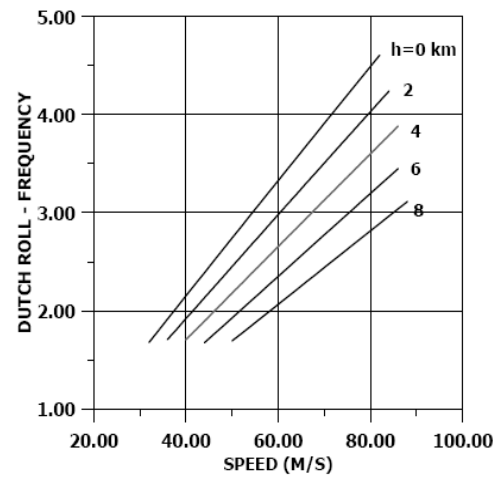
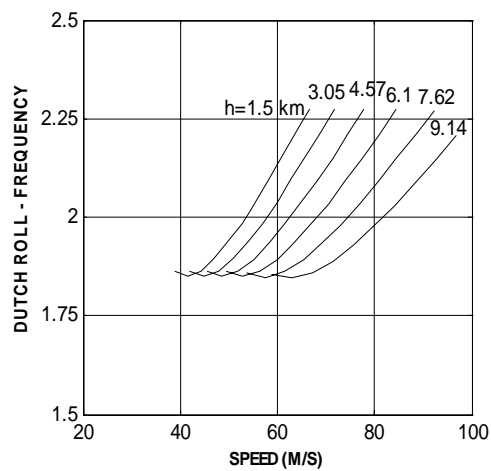
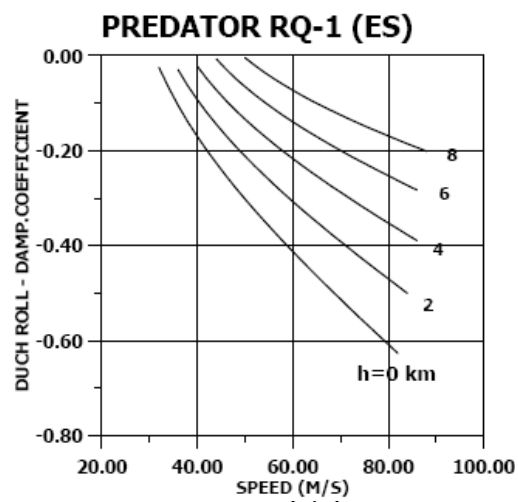
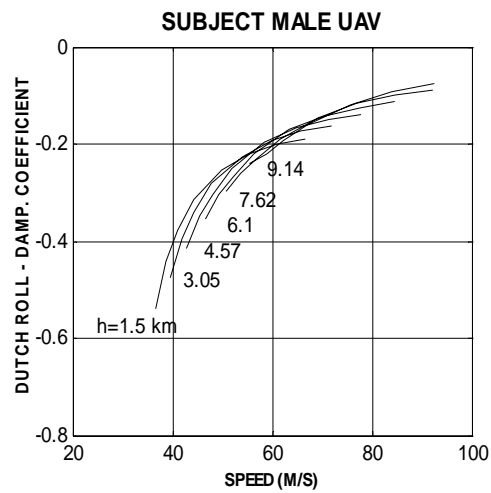
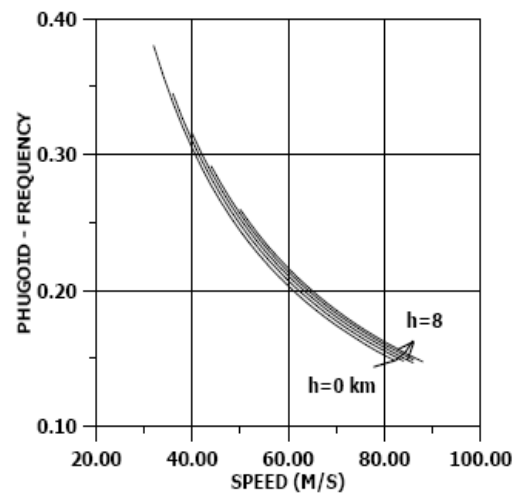
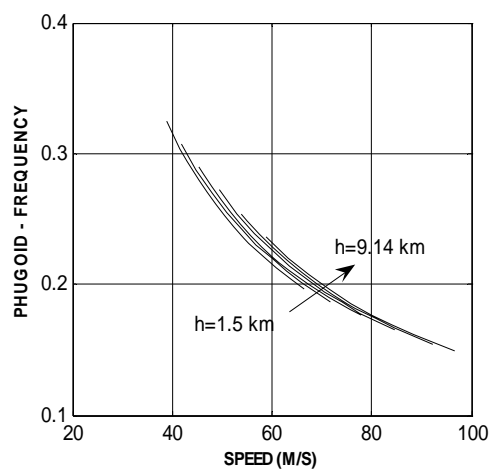


Figure 4.12 Three plan view of Predator RQ [28]





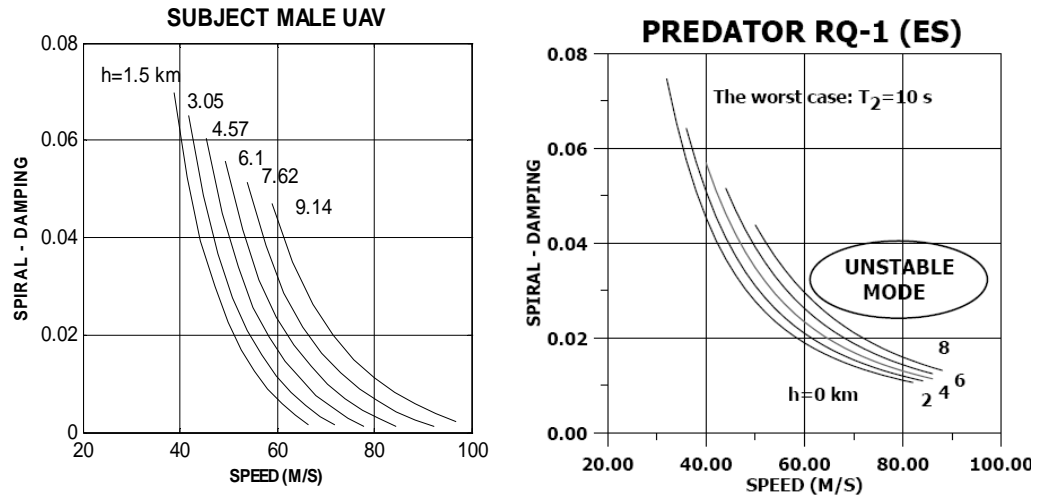


Figure 4.13 Results of dynamic stability comparisons between the subject UAV and Predator RQ-1 [28]

The graphs of Figure 4.13 show that, the trends of the dynamic stability characteristics of the major flight modes for the two UAVs of similar configurations are very close to each other. Especially for phugoid damping coefficient and frequency, spiral damping, and short period damping coefficient curves, the matching level of dynamic characteristics is of high degree between the two UAVs. The only important difference observed is in the Dutch roll mode damping coefficient curves. It is considered that the reason for the difference is the different tail configurations, since for the subject UAV, V-tail configuration is used, whereas for Predator RQ-1, an inverted V-tail is used, which causes a proverse yaw, in contrast to the normal V-tail characteristics. If the proverse yaw effect is evident, the damping of the Dutch roll motion is augmented by the spiral mode stabilization [32], as in the case of Predator RQ-1 dynamic characteristics.

One would also comment on the change of flight mode characteristics with respect to speed and altitude investigating the approximate formulas given by Equations (4.1) and (4.2) for short period mode, Equations (4.4) through (4.7) for phugoid mode,

Equations (4.9) and (4.10) for Dutch roll mode, Equation (4.11) for roll mode, and Equation (4.12) for spiral mode. However, it should be noted that, the approximate formulas for Dutch roll and spiral modes are only rough estimates causing poor agreement between the approximate and exact solutions. The reason is the Dutch roll motion being truly a three degree of freedom motion with strong coupling between the equations [27].

CHAPTER 5

FLIGHT CONTROL SYSTEM DESIGN

5.1 Introduction

The functions of an autopilot or “flight control system” can be divided in two areas: “guidance” and “control”, which can be defined as [12]:

- Guidance: The action of determining the course and speed, relative to some reference system, to be followed by the vehicle.
- Control: The development and application of appropriate forces and moments to the vehicle, which, establish some equilibrium state of vehicle motion, and restore a disturbed vehicle to its equilibrium state (operating point) and/or regulate, within desired limits, its departure from operation point conditions.

The control function of an autopilot constitutes a low-level control among the hierarchical levels of control that can be identified in a UAV autopilot system, including the stability and control (S&C) loops. This control function provides the air vehicle with improved dynamic stability, regulation of flight parameters, as well as tracking of basic autopilot commands. Specifically, since, the flying qualities of Dutch roll mode at some flight conditions remains in Level 2 region as displayed in Figure 4.9 of the previous chapter, the design and use of a yaw damper becomes unavoidable in this study. Also, it can be observed from Figure 4.8 that, the phugoid mode is very critical with Level 3 correspondence of related flying qualities for a large interval of flight conditions. This requires the design of a well performed autopilot for pitch attitude and airspeed which shall always be engaged during the flight. This requirement is extracted from Equation (3.15), where the dominating states for the phugoid mode are primarily the pitch angle and secondarily the forward airspeed. This fact is also indicated by the following statement [33], *“The airspeed loop benefits strongly from some derivative gain. This is one of the terms that will*

damp the long period (phugoid) mode. If you see the vehicle oscillating slowly, exchanging altitude for airspeed and vice versa, then add more derivative gain, or alternately add pitch angle feedback.”

Within the flight control requirements obtained from the military specifications; the control of four basic flight parameters is essential in the air vehicle maneuvering tasks; namely, attitude (pitch and roll), heading, altitude, and airspeed.

This chapter deals with the design of two flight control systems obtained by using the classical and optimal control approaches, separately. In the classical flight controller design, SRO tool of MATLAB[®]/Simulink[®] is implemented in order to obtain the PID gains of the controller structures. In the optimal flight controller design, an LQ controller methodology is applied as the core part of the complete controller (both for longitudinal and lateral-directional axes), whereas for the longitudinal controller, a synthesized use of optimal control with the SRO is carried out.

5.2 Assumptions

In addition to the assumptions related to modeling phase of the current study, given in Section 2.3, the following assumptions are used in the controller design phase:

1. Sensors provide information about the complete states of the air vehicle for all practical purposes available for feedback, which is the case in most of today's airplanes,
2. The task is to extract the information required from the real sensors to meet the control objectives; but in this study, no sensor characteristics are contributed into the design of the controller, as if all the states are measured perfectly,
3. It is assumed that no additional disturbances due to sensors nor any sensor noise exist,
4. Possible time delays that may result from the computations in the digital flight control system are not involved in the nonlinear model, hence in the controller design phase.

5.3 Flight Control Requirements

The flight control system requirements are based on the following military documents [4, 34-35]; RPV (Remotely Piloted Vehicles) Flying Qualities Design Criteria, MIL-F-9490D, and MIL-C-18244A. The section on the flight control system requirements of RPV Flying Qualities Design Criteria is essentially taken and adapted from MIL-F-9490D and MIL-C-18244A for remotely piloted air vehicles. These requirements apply to air vehicles regardless of the vehicle class or the flight phase category contrary to the dynamic stability requirements described in Section 4.3.

5.3.1 Attitude (Pitch & Roll) Control Requirements

5.3.1.1 Attitude Hold

Attitudes shall be maintained in smooth air with a static accuracy of $\pm 0.5^\circ$ in pitch attitude (with wings level) and $\pm 1.0^\circ$ in roll attitude with respect to the reference. These accuracies shall apply to automatic attitude hold functions which either maintain the vehicle attitude, or return the vehicle to a wings-level attitude at the time manual control maneuver inputs are removed [4, 34-35].

5.3.1.1.1 Pitch Transient Response

The short period pitch response shall be smooth and rapid. When the automatic flight control attitude hold function is intended to return the vehicle to a reference attitude after manual overrides which change the pitch attitude by at least $\pm 5^\circ$, the vehicle shall return to the reference attitude within one overshoot which shall not exceed 20% of the initial deviation. The period of overpowering shall be short enough to hold the airspeed change to within 5% of the trim airspeed [4, 34-35].

5.3.1.1.2 Roll Transient Response

The short period roll response shall be smooth and rapid. When the automatic flight control attitude hold function is intended to return the vehicle to a reference attitude after manual overrides which reach a bank angle of approximately 20° , the vehicle

shall return to the initial roll attitude within one overshoot which shall not exceed 20% of the initial deviation [4, 34-35].

5.3.2 Heading Control Requirements

5.3.2.1 Heading Hold

In smooth air, when the heading hold is engaged, the automatic flight control system shall maintain the vehicle at its existing heading within a static accuracy of $\pm 0.5^\circ$ with respect to the gyro accuracy [4, 34-35].

5.3.2.2 Heading Select

When an automatic heading selection system is used, the automatic flight control system shall automatically turn the vehicle through the smallest angle (left or right) to a selected heading and maintain that heading as in the heading hold mode. The heading selects shall have 360° of control. The bank angle while turning to the selected heading shall provide satisfactory turn rates and preclude impending stall. If used as an assist mode in manual control the operator shall be able to select bank angle by control inputs and then remove the command. The air vehicle shall not roll in a direction other than the direction required for the vehicle to assume its proper bank angle. In addition, the roll-in and roll-out shall be accomplished smoothly with no disturbing variation in roll rate [4, 34-35].

5.3.2.2.1 Transient Heading Response

Entry into and termination of the turn shall be smooth and rapid and the aircraft shall not overshoot the selected headings by more than 1.5° [4, 34-35].

5.3.2.2.2 Altitude Coordinated Turns

It shall be possible to maintain altitude within the accuracies specified in Table 5.1 during coordinated turns in either direction, for the maximum pitch, roll, yaw maneuvering attitudes [4, 34-35].

5.3.3 Altitude Control Requirements

Engagement of the altitude hold function at rates of climb or descent less than 2,000 fpm (10.16 m/s), shall select the existing indicated (sensed) altitude and control the vehicle to this altitude as a reference. For engagement at rates above 2,000 fpm (10.16 m/s), the automatic flight control system shall not cause any unsafe vehicle maneuvers. Within the vehicle thrust-drag capability and at steady bank angles, this function shall provide control accuracies shown in Table 5.1 [4, 34-35].

Table 5.1 Minimum Acceptable Control Accuracy

BankAngle [°] Altitude [ft]	0-1	1-30	30-60
0 to 30,000	± 30 ft (± 9.1 m)	± 60 ft (± 18.3 m) or $\pm 0.3\%$ whichever is larger	± 90 ft (± 27.4 m) or $\pm 0.4\%$ whichever is larger

5.3.4 Airspeed Control Requirements

The airspeed existing at the engagement of airspeed hold shall be the reference. Indicated airspeed shall be maintained within ± 5 knots (2.57 m/s) or $\pm 2\%$, whichever is greater, of the reference airspeed [4, 34-35].

5.4 Classical Controller Design

5.4.1 Controller Loops Generation

The first low-level flight control system is based on the classical inner-outer loop methodology. At this stage, the linearized models of the subject UAV are used at various conditions in the operational flight envelope. Hence, the states, inputs, and outputs of the linear controller structures are the respective perturbed states, inputs and outputs. In order to obtain the classic PID gains of these controllers, the MATLAB®/Simulink® Simulink Response Optimization (SRO) tool is utilized. Normally, the gains obtained around the linearized models are treated as the initial

gains of the controller that are to be fine tuned by implementing the same tool in the nonlinear model. For this study, it is anticipated that this fine tuning procedure is not necessary at all, because of the high matching level of the linear and nonlinear model responses to the same inputs, which is validated in Section 3.3.3.

In general, the procedure consists of adjusting control loop gains using the SRO tool in order to achieve the desired response given by the requirements of Section 5.3, in each loop with step commands. The details of the structures of the controllers are described under heading, altitude, and airspeed control loops generation, respectively.

5.4.1.1 Building Heading Controller

The heading controller is responsible for controlling the yaw rate, roll attitude, and heading. This is accomplished with four inner servo loops; bank angle, roll rate, turn coordination, and yaw rate controllers, and one outer loop, heading controller. The inner loops produce efforts that drive the aileron and ruddervator, which are driven by the respective operator controls wheel and pedal, as described in Actuators Model, Section 2.7. The outer loop produces commanded values for the inner loops.

The four inner lateral loops are as follows:

1. “Wheel from Roll” control loop generates an aileron deflection from the roll error. This loop is responsible for holding the roll attitude of the air vehicle under the requirements stated in Section 5.3.1. The controller structure is shown in Figure 5.1. This structure for roll attitude control is also stated in [32, 37]. A PI compensator is used for better tracking of bank angle commands, ϕ_c since the transfer function from wheel control input in $[\circ]$ to bank angle state in $[\circ]$, indicates that the single input-single output (SISO) system is of Type 0, without any free integrals in its denominator. This transfer function is as

$$\frac{\phi}{\delta_{\text{wheel}}} = \frac{-105.84(s^2 + 0.3454s + 3.113)}{(s + 17.32)(s - 0.01025)(s^2 + 0.3349s + 4.166)} \quad (5.1)$$

It should be noted that, the following procedure is applied in order to obtain this transfer function using MATLAB[®]: The output matrices of the function `linmod2` are given as inputs to the function `ss` to define the multi input-multi output (MIMO) system. Using the command `set`, names are attained to the inputs, outputs, and states of this MIMO system, based on their known orders. Again from this MIMO system, the name of the desired input-output pair is picked up to define a new SISO system. By inputting this SISO system into the function `zpk`, the transfer function is obtained.

2. “Wheel from Roll Rate” control loop generates an aileron deflection from the roll rate, p with a feedback gain [15, 32, 37]. It is responsible for damping the roll rate of the air vehicle by decreasing the roll mode time constant, τ_r and named as “roll damper”. The control effort for this loop is summed with the effort from the “Wheel from Roll” control loop and sent to the aileron servo actuator. The loop is shown in Figure 5.1.

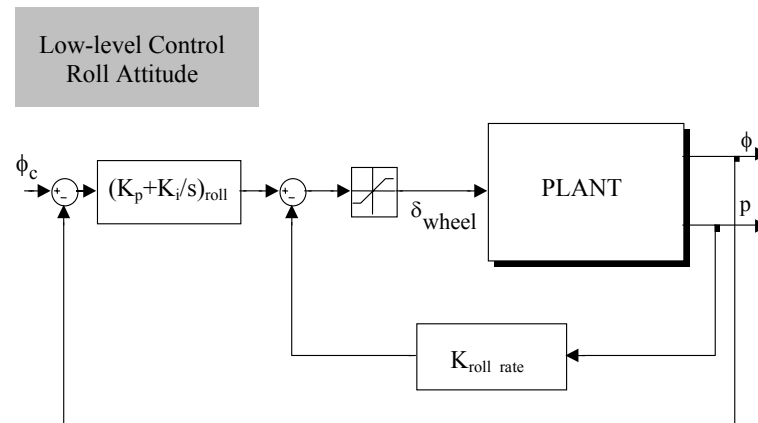


Figure 5.1 Inner roll attitude and roll rate control loops

It can be observed from Figure 5.1 that the control input saturation block is also included in the controller structure. The purpose is to have control on magnitude of the obtained gains. It is to be accomplished tuning the gains by confirming if an unavoidable saturation occurs for a reasonable, i.e. large enough reference command input or if possible by avoiding the occurrence of the saturation of the control input.

3. “Pedal from velocity in y-axis” control loop generates a ruddervator deflection from the velocity in y-axis or alternatively the sideslip velocity, v with a feedback gain [24, 32]. It is responsible for accomplishing a coordinated turn by eliminating a sideslip motion under the requirements stated in Section 5.3.2.2.2 when a constant roll command is input. The loop is displayed in Figure 5.2.
4. “Pedal from Yaw Rate” control loop controls the yaw rate, r of the air vehicle by driving the ruddervator actuator servo. It is responsible for damping the yaw rate of the air vehicle by increasing the Dutch roll mode damping ratio, ζ_{dr} and named as “yaw damper”. The control effort for this loop is summed with the effort from the “Pedal from velocity in y-axis” control loop and sent to the ruddervator servo actuator. This summed up controller structure is called as “sideslip suppression system” [32]. A washout filter is to be used with the yaw rate feedback gain, since there is another factor that has to be taken into account next to damping the yaw rate all the time. During a steady turn, the value of r is not zero and if a ruddervator angle is commanded by the yaw damper because of sensing a nonzero r , the angle would no doubt not be the right one needed for a coordinated turn. Therefore, this characteristic of the yaw damper is undesirable and necessitates the use of a washout filter, which is a high pass filter with zero gain at the steady state and unity gain at

high frequency [13]. The transfer function of the washout filter used is given in Equation 5.2 and the related control is displayed in Figure 5.2.

$$WO = \frac{s}{s + 0.25} \quad (5.2)$$

where 4 seconds is chosen as the washout filter time constant, τ_{wo} , which is a reasonable value when the yaw rate time response of the UAV is considered.

The saturation block is again included in the controller structure as shown in the figure, with the same reasons explained in roll attitude control structure generation.

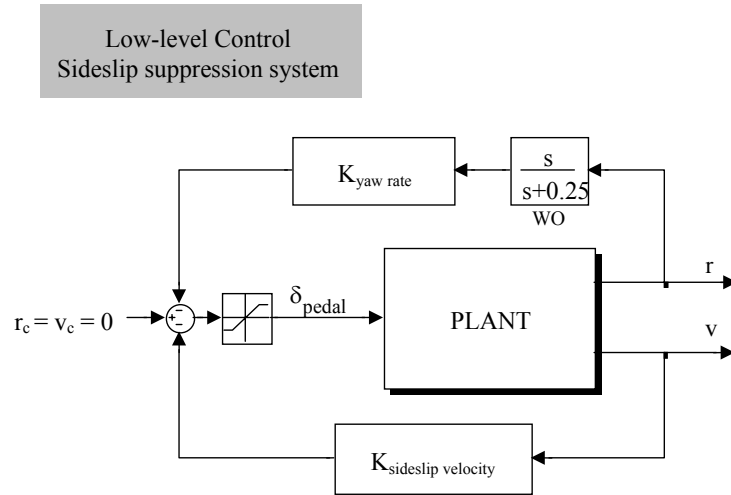


Figure 5.2 Inner yaw rate control loop with washout filter and coordinated turn control loop

The outer lateral loop is as follows:

1. “Roll from Heading” control loop generates a bank angle reference command, ϕ_c , from the heading error with a proportional compensator. This bank angle serves as the commanded roll attitude for the “Aileron from Roll” control loop. This loop is responsible for controlling the heading, ψ of the air vehicle under the requirements stated in Section 5.3.2. The controller structure for the outer loop heading control is as given in [15, 32].

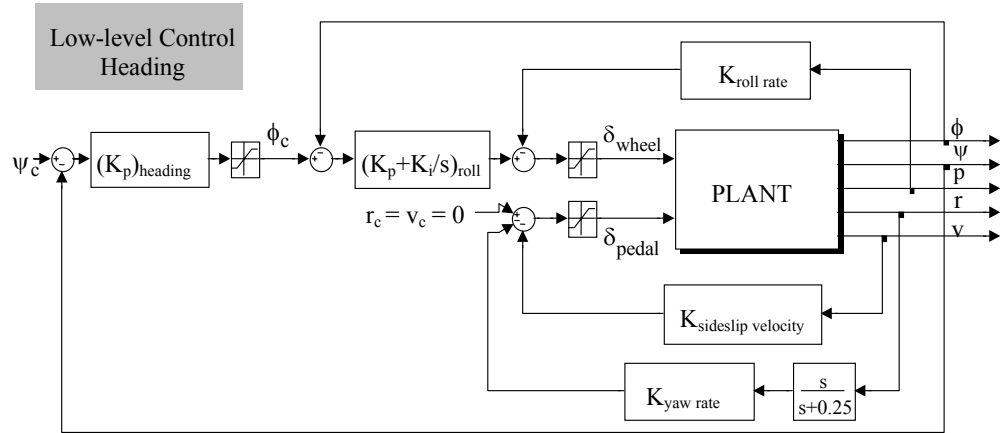


Figure 5.3 Heading controller structure

The complete lateral controller structure with inner and outer loops described so far is shown in Figure 5.3. An additional saturation block regarding the maximum and minimum values of the inner loop reference roll attitude command is also included. This prevents commanding high heading reference inputs to the inner loop controllers, which are to be designed considering only the reference roll attitude limits.

5.4.1.2 Building Altitude Controller

The altitude controller is responsible for controlling the pitch attitude and altitude. This is accomplished by two inner servo loops; namely, the pitch rate and pitch angle controllers, and by an altitude controller as an outer loop. The inner loops produce efforts that drive the ruddervator, which is driven symmetrically by respective operator control column, as described in Actuators Model, Section 2.7. The outer loop produces commanded values for the inner loops.

The two inner altitude loops are as follows:

1. “Column from Pitch” control loop generates a ruddervator deflection from the pitch error. This loop is responsible for holding the pitch attitude of the air vehicle under the requirements stated in Section 5.3.1. It increases the phugoid mode damping ratio, ζ_{ph} , whereas it somehow decreases the short period damping ratio and therefore should be compensated with a pitch rate feedback [12]. This controller structure is shown in Figure 5.4. This structure for the pitch attitude control is as stated in [32, 37]. A PI compensator is used for a better tracking of pitch angle commands, θ_c , since the transfer function given by Equation (5.3) from column control input in $[\circ]$ to pitch angle state in $[\circ]$, indicates that the single input-single output (SISO) system is of Type 0, without any free integrals in its denominator. The procedure to obtain this transfer function is in the similar manner as described in roll attitude control structure generation part of Section 5.4.1.1.

$$\frac{\theta}{\delta_{\text{column}}} = \frac{-5.4343(s + 1.702)(s + 0.03575)(s - 0.0001545)}{(s - 0.0002)(s^2 + 0.00308s + 0.04283)(s^2 + 2.627s + 6.162)} \quad (5.3)$$

2. “Column from Pitch Rate” control loop generates a ruddervator deflection from the pitch rate, q with a feedback gain [15, 32, 37]. It is responsible for damping the pitch rate of the air vehicle by increasing the short period mode damping ratio, ζ_{sp} and named as “pitch damper”. The control effort of this

loop is summed with the effort from “Column from Pitch” control loop and sent to the ruddervator servo actuator. The loop is shown in Figure 5.4.

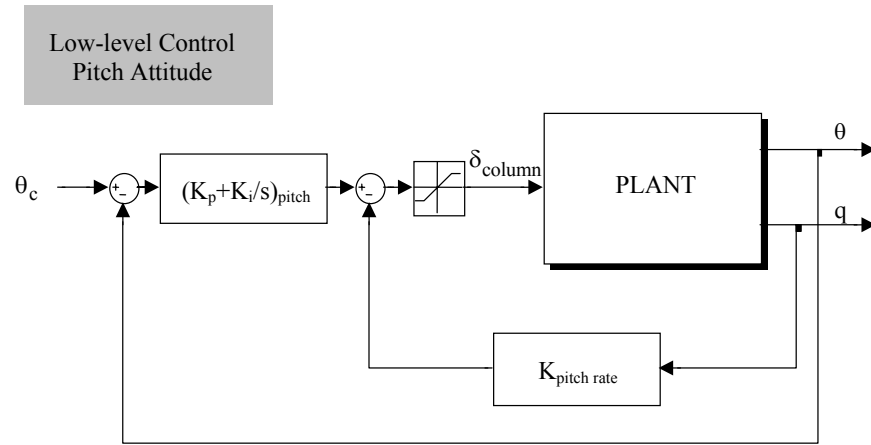


Figure 5.4 Inner pitch attitude and pitch rate control loops

The outer altitude loop is as follows:

1. “Pitch from Altitude” control loop generates a pitch angle reference command, θ_c , from the altitude error. This pitch angle serves as the commanded pitch attitude for the “Column from Pitch” control loop. This loop is responsible for controlling the altitude of the air vehicle under the requirements stated in Section 5.3.3. The controller structure is shown in Figure 5.5. A rate damper is designed in the feedback path, in order to improve the transient response of altitude rate and smooth the ruddervator deflections [15]. A PI compensator is also needed to be used in order to eliminate the steady state altitude errors.

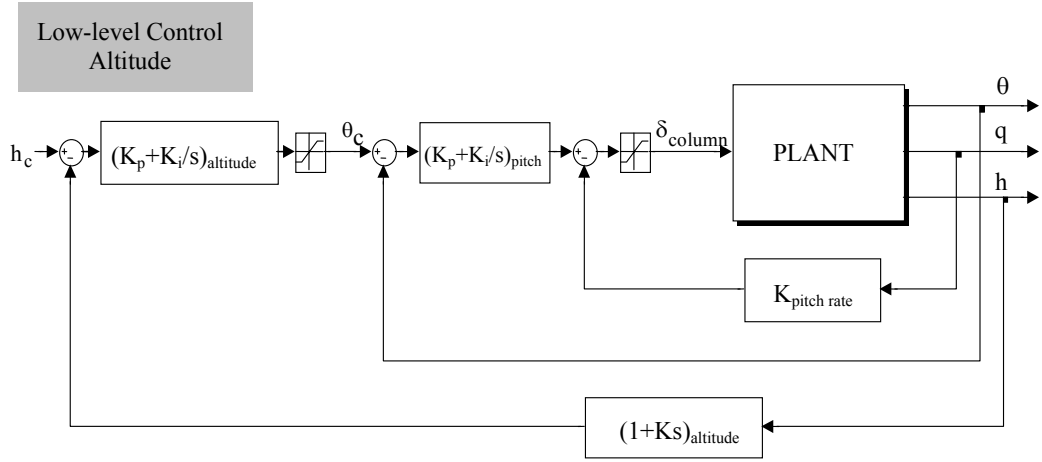


Figure 5.5 Altitude controller structure

In order to limit the reference altitude commands that generate the inner loop reference pitch attitude commands via the PI compensator, again an additional saturation block is included in the controller structure shown in Figure 5.5.

5.4.1.3 Building Airspeed Controller

“Throttle from Airspeed” control loop serves to control the UAV’s airspeed, V by adjusting the throttle. This loop is responsible for controlling the airspeed of the air vehicle under the requirements stated in Section 5.3.4. The controller structure is as shown in Figure 5.6.

In the controller structure, similar to the altitude controller, a rate damper in the feedback path is used in order to improve the transient response of the acceleration and PI compensator is designed for better tracking of airspeed commands, since the transfer function from throttle input in [%] to airspeed state in [m/s], indicates that the single input-single output (SISO) system is of Type 0, without any free integrals

in its denominator [15]. The transfer function is obtained in the similar manner as described in roll attitude control structure generation part of Section 5.4.1.1, which is given as

$$\frac{V}{\delta_{\text{throttle}}} = \frac{0.0356(s + 0.4358)(s + 0.00223)(s^2 + 2.034s + 5.674)}{(s - 0.0002)(s^2 + 0.00308s + 0.04283)(s^2 + 2.627s + 6.162)} \quad (5.4)$$

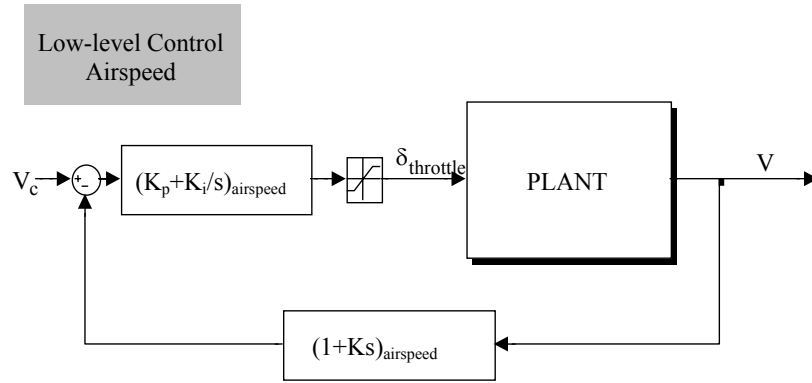


Figure 5.6 Airspeed controller structure

5.4.1.4 Simulink Response Optimization (SRO) Application

The SRO is implemented to the controller structures developed in Sections 5.4.1.1 through 5.4.1.3 with the desired response characteristics mainly selected by considering the respective military flight control requirements. Additionally, while determining the desired response characteristics, for each controller structure, the results of the response optimization processes carried out until a satisfactory response could be reached are also taken into account.

As also mentioned in the previous controller structures build up sections, the control input saturation blocks are included in the structures while determining the gains using the SRO tool. The purpose is to determine the gains of reasonable magnitudes

not causing undesirably strong saturations when the highest possible reference inputs are commanded. However, it should be noted that, this implementation is especially effective in the lateral-directional controller structures for which the highest control variables can be commanded at a flight condition apart from the longitudinal altitude and airspeed controllers. Since, the steady wings-level flight trim condition characteristics change with respect to the altitude and airspeed in this study at each flight condition, the longitudinal linear models by having different trim control input and state values necessitates changing the control input saturation limits and the magnitude of the reference input commands at every respective condition. Consequently, in SRO applications, the reference step command inputs in the desired response characteristics of the longitudinal altitude and airspeed controller structures are left as the default value 1, not to deal with the saturations of the controller inputs.

The response optimization processes at the very beginning are initialized by randomly picked up gains. Once the desired response and the corresponding gains are obtained for the initial flight condition at the beginning, the remaining controller gains of the linear models; namely the flight conditions, are obtained in a predetermined order. This procedure is to be explained in detail in Gain Scheduling section. The desired response characteristics and the response optimization results of the each controlled parameter are displayed representatively for the nominal flight condition of 100 KEAS and 15,000 ft (4,572 m) altitude.

5.4.1.4.1 Roll Attitude Response Characteristics

Table 5.2 displays the roll attitude desired response characteristics, in which 60° bank angle, i.e. the maximum predetermined bank angle value for the subject UAV is selected as the maximum step reference input value with a percent settling value of 1.5% corresponding to $\pm 0.9^\circ$. The military $\pm 1.0^\circ$ static accuracy requirement that shall be satisfied for the whole range of bank angle commands is depended on this selection.

Table 5.2 Roll attitude desired response characteristics

Step response characteristics	Value
Initial value [°]	0
Final value [°]	60
Step time [s]	0
Rise time [s]	10
Rise [%]	95
Settling time [s]	40
Settling [%]	1.5
Overshoot [%]	15
Undershoot [%]	2

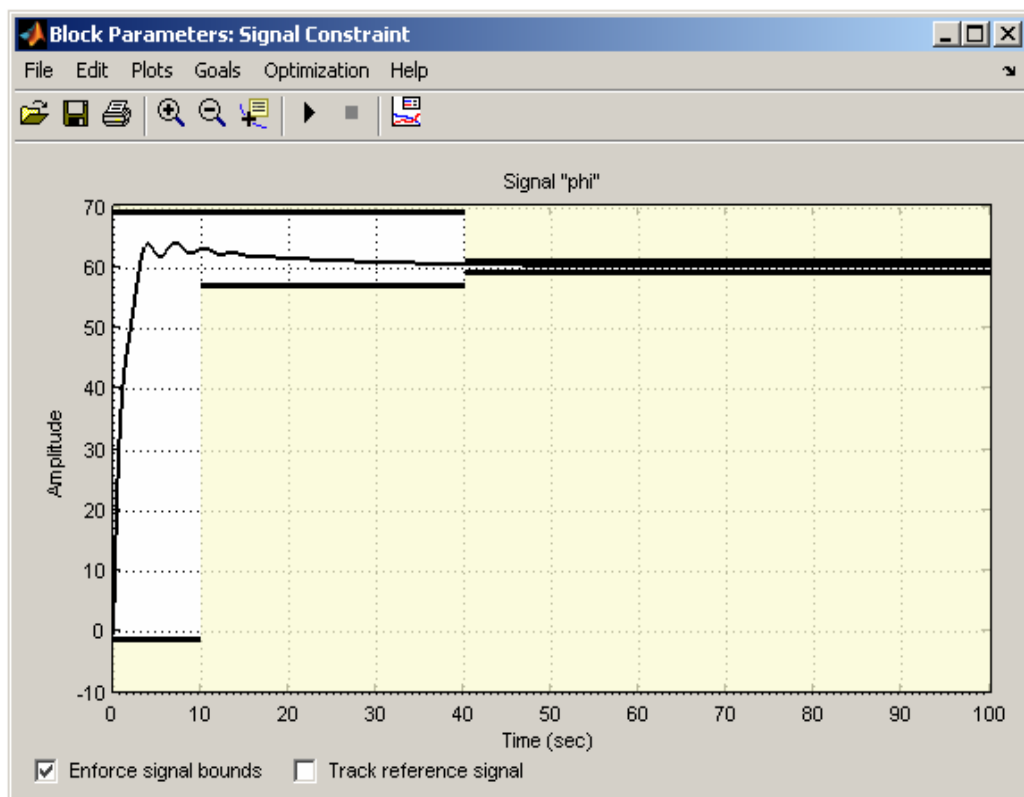


Figure 5.7 Roll attitude final response to 60° step input

The controller structure in which the SRO block is connected to the bank angle signal is given in Figure 5.1. The tuned parameters are the roll attitude PI gains and roll rate feedback gain, together. The resultant roll attitude response optimization to 60° bank angle step input at the end of several iterations is given in Figure 5.7. It should be noted that, the constraint lines demonstrated in the figure are all determined by the desired roll attitude response characteristics given by Table 5.2.

5.4.1.4.2 Turn Coordination Response Characteristics

The main criteria in determining the desired response characteristics for turn coordination is that for a roll attitude command input, the sideslip velocity shall be zero with a constant yaw rate, despite the yaw rate feedback effect. The yaw rate feedback opposition to turn coordination is solved by using a washout filter with a proper time constant, as explained in detail in fourth item of Section 5.4.1.1, where the related sideslip suppression system structure is shown in Figure 5.2. Hence, in order to provide turn coordination gains under dominating effects, the response optimization is performed by involving sideslip suppression and roll attitude control structures in a single Simulink® model. A 60° roll attitude command is given while the Response Optimization Block is connected to the sideslip velocity signal with the selected desired response characteristics displayed in Table 5.3.

Table 5.3 Turn coordination desired response characteristics

Step response characteristics	Value
Initial value [m/s]	8
Final value [m/s]	0
Step time [s]	0
Rise time [s]	4
Rise [%]	85

Table 5.3 Turn coordination desired response characteristics (continued)

Settling time [s]	20
Settling [%]	0.25
Overshoot [%]	15
Undershoot [%]	2

The picked tuned parameters are the sideslip velocity and yaw rate feedback gains together, while holding the roll attitude and roll rate control gains constant that are obtained formerly. The resultant linear model response at the end of several iterations is given by Figure 5.8.

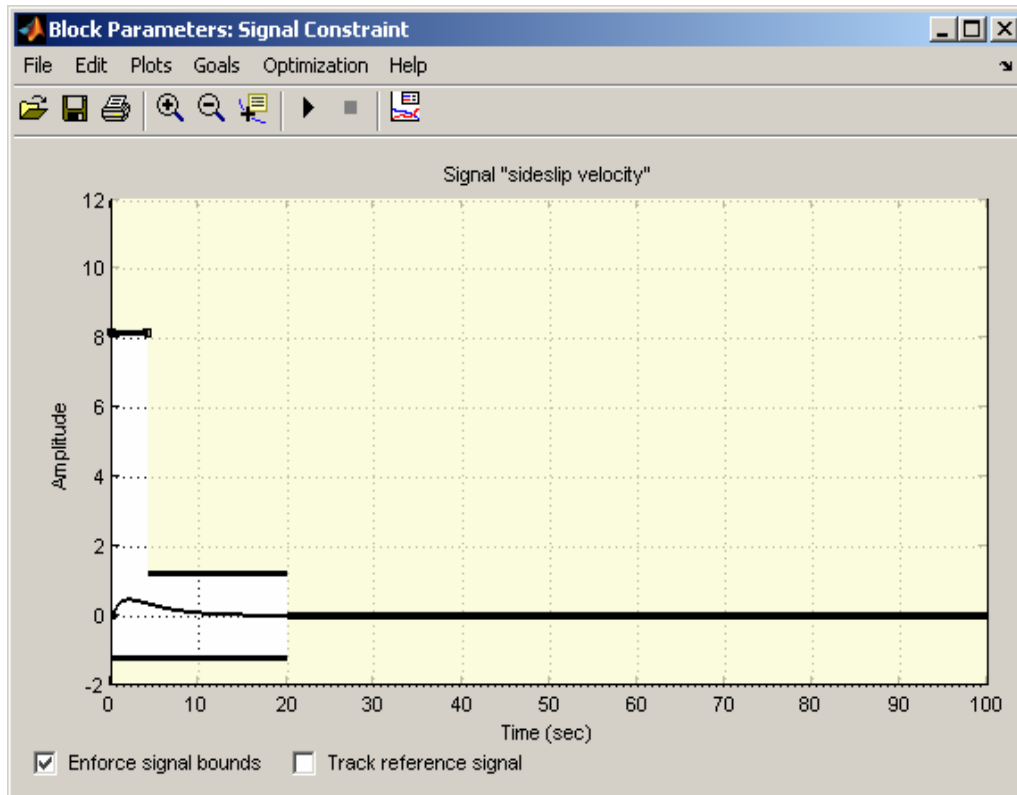
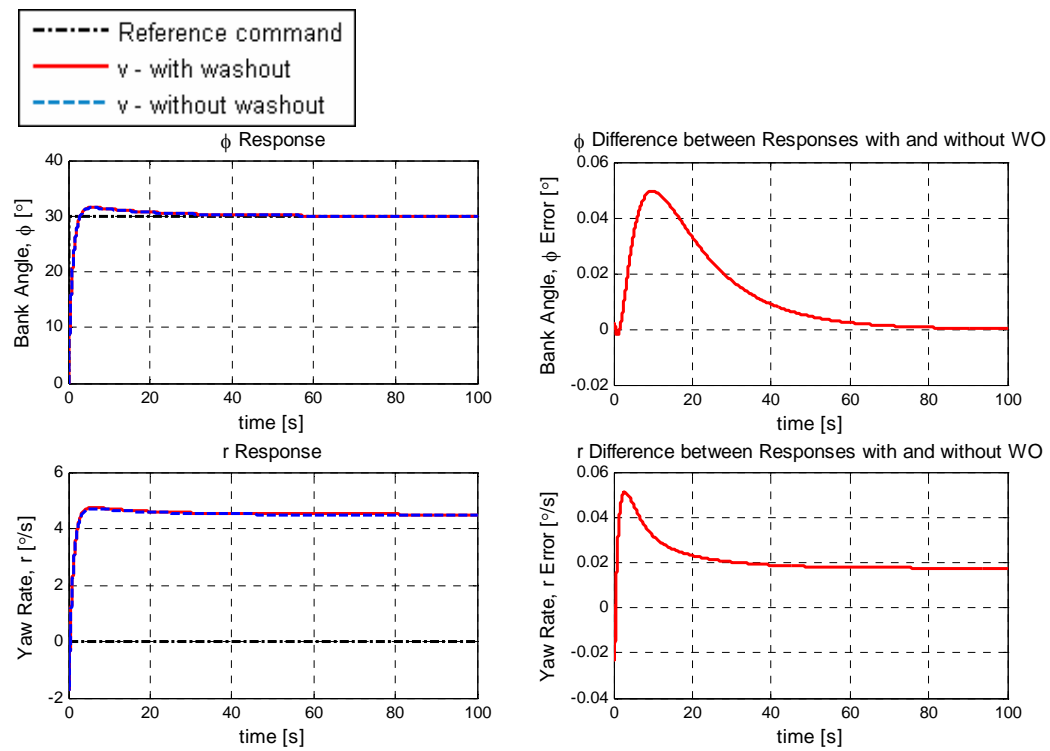


Figure 5.8 Sideslip velocity final response

In order to visualize the washout filter effects, the graphs of Figure 5.9 are plotted, demonstrating the linear model sideslip velocity responses to 30° reference step bank angle command with and without washout filter. The effect of the small yaw rate response change caused by the removal of the washout filter on sideslip velocity can be seen clearly from the graphs. It should be mentioned that, the turn coordination related military requirement mentioned in Section 5.3.2.2.2 can only be checked when all the controller structures including the altitude controller are implemented into the nonlinear model.



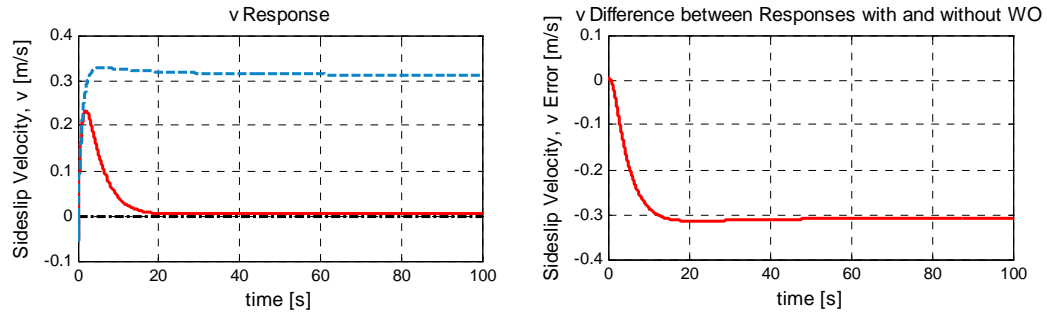


Figure 5.9 Linear model responses to +30° reference ϕ command with and without washout filter

5.4.1.4.3 Heading Response Characteristics

Table 5.4 Heading desired response characteristics

Step response characteristics	Value
Initial value [°]	0
Final value [°]	90
Step time [s]	0
Rise time [s]	25
Rise [%]	90
Settling time [s]	75
Settling [%]	0.25
Overshoot [%]	2
Undershoot [%]	2

Similar to the case in roll attitude desired response selection, the percent settling (percent steady-state error) value is selected as 0.25%, where for 180° – the maximum possible heading value, it corresponds to $\pm 0.45^\circ$ static accuracy, compatible with the respective military $\pm 0.5^\circ$ static accuracy requirement which shall be satisfied for the whole range of heading commands. The maximum step reference input value selected is 90° as it can also be observed in heading desired response characteristics given in Table 5.4. While obtaining the resultant response, the only picked tuned parameter is the proportional heading gain. The remaining inner loop

gains that are formerly determined are held constant. The controller structure is displayed in Figure 5.3. The resultant heading response optimization to 90° heading angle step input at the end of several iterations is given in Figure 5.10.

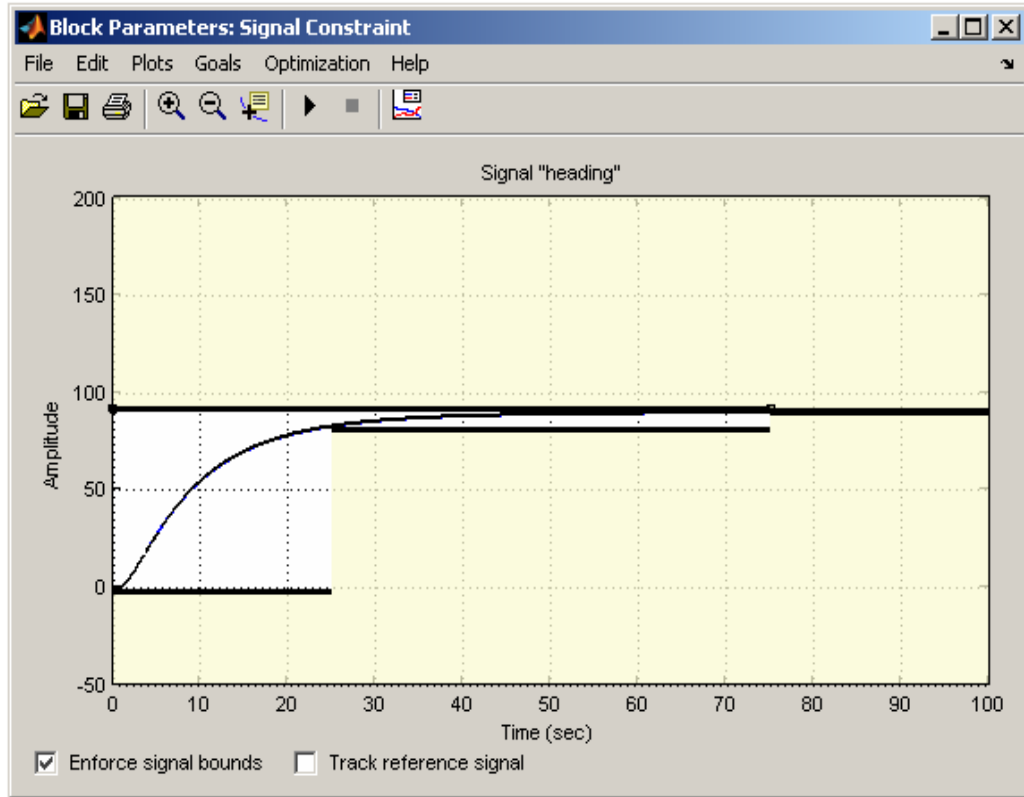


Figure 5.10 Heading final response to 90° step input

5.4.1.4.4 Pitch Attitude Response Characteristics

The percent settling (percent steady-state error) value of the pitch attitude is selected as 0.1%, as it can be observed from Table 5.5. This value corresponds to a $\pm 0.01^\circ$ static accuracy for a 10° maximum possible pitch angle value, whereas the respective

military requirement requires a $\pm 0.5^\circ$ static accuracy that shall be satisfied for the whole range of pitch attitude commands. Hence, it is obvious that, the current percent settling value is too small with respect to the related requirement. However, since pitch attitude control is the inner loop of the altitude controller structure which has the tendency of experiencing steady state errors due to the possible large altitude commands, it is required for this value to be as small as possible. Therefore, in this case it is reasonable to select the possible smallest value for the pitch attitude percent settling value.

Table 5.5 Pitch attitude desired response characteristics

Step response characteristics	Value
Initial value [$^\circ$]	0
Final value [$^\circ$]	1
Step time [s]	0
Rise time [s]	5
Rise [%]	95
Settling time [s]	20
Settling [%]	0.1
Overshoot [%]	5
Undershoot [%]	2

The controller structure in which the SRO block is connected to the pitch angle signal is given in Figure 5.4. 1° is selected as the maximum step reference input value for the response optimization process. While obtaining the resultant response, the tuned parameters that are picked are the gains related to pitch attitude and pitch rate. The resultant pitch angle response optimization to 1° pitch angle step input at the end of several iterations is given by Figure 5.11.

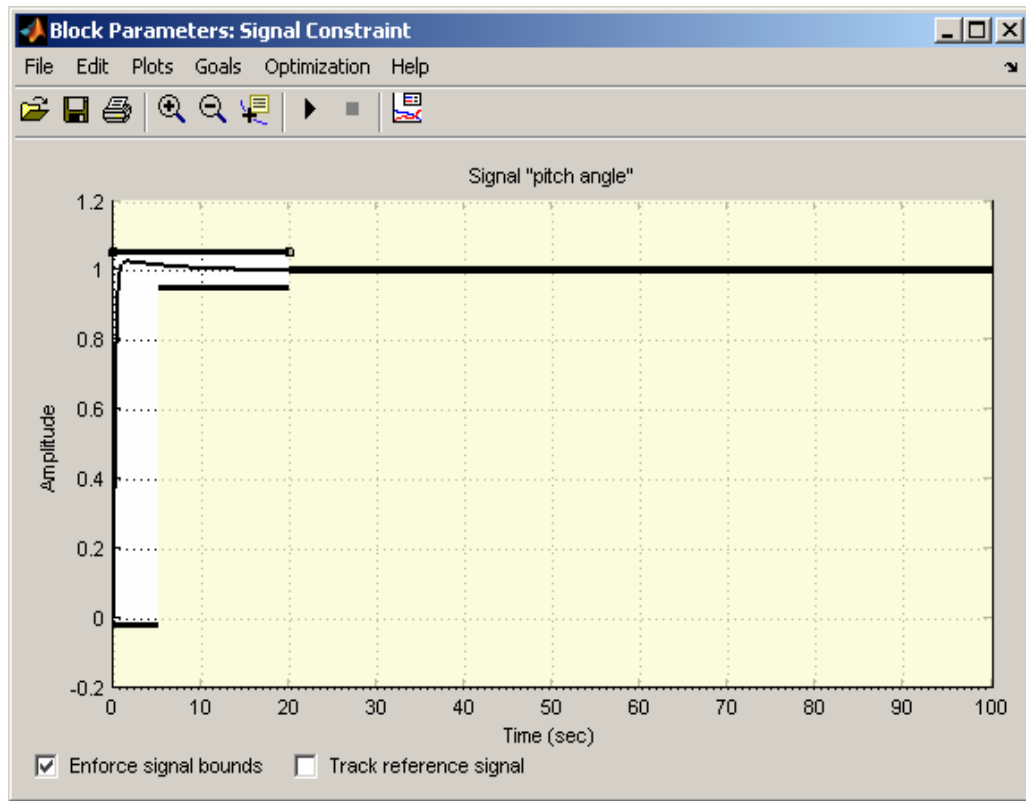


Figure 5.11 Pitch angle final response to 10° step input

5.4.1.4.5 Altitude Response Characteristics

As it can be observed from Table 5.6, the percent settling (percent steady-state error) value is selected as 0.1%. This value is selected based on the respective military ± 30 ft (± 9.144 m) static accuracy requirement, that shall be satisfied for the whole altitude range of 0-30,000 ft (0-9,144 m), where for the maximum possible altitude command of 9,144 m, it corresponds to a $\pm 0.1\%$ settling value. Therefore, it can be concluded from the linear model response optimization results that, the highly probable steady state error in controlling altitude could be eliminated, but still it should be checked from the nonlinear model results when complete controller is implemented.

Table 5.6 Altitude desired response characteristics

Step response characteristics	Value
Initial value [m]	0
Final value [m]	1
Step time [s]	0
Rise time [s]	15
Rise [%]	90
Settling time [s]	30
Settling [%]	0.1
Overshoot [%]	5
Undershoot [%]	2

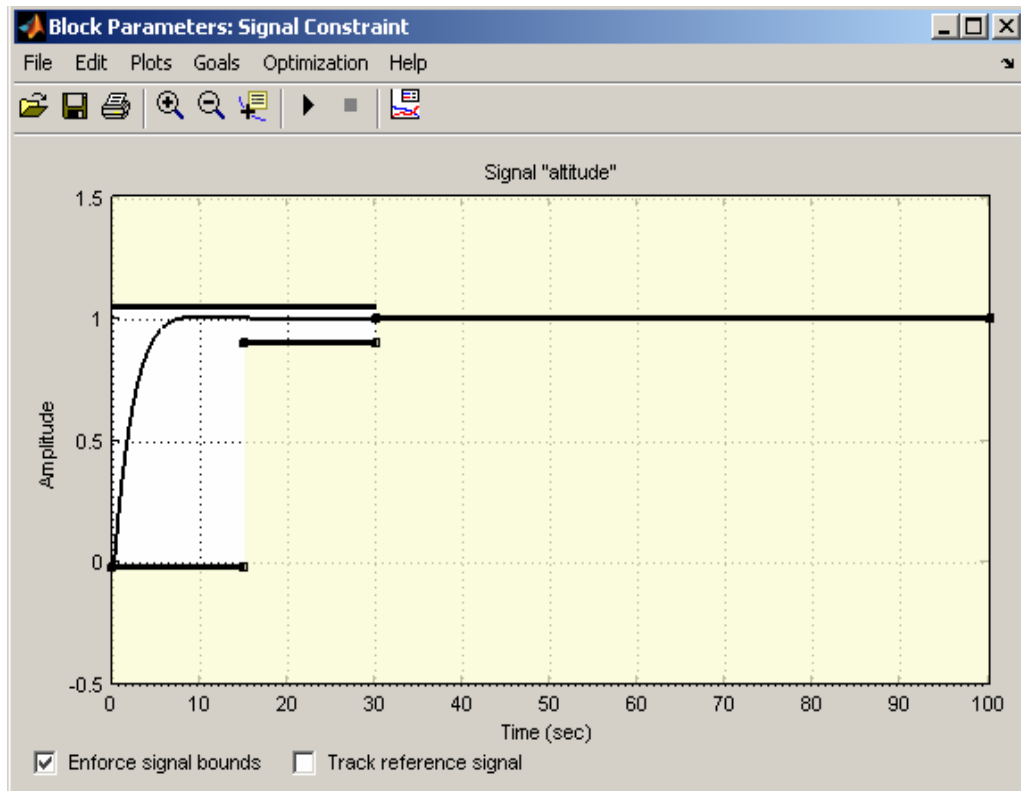


Figure 5.12 Altitude final response to 1 m step input

The controller structure in which the SRO block is connected to the altitude signal is given in Figure 5.5. 1 m is selected as the maximum step reference input value of response optimization process. While obtaining the resultant altitude response, the tuned parameters that are picked are the gains related to altitude only, where the inner pitch attitude and pitch rate control loop gains which were determined at pitch attitude response optimization are held constant. The resultant altitude response optimization to 1 m altitude step input at the end of several iterations is given by Figure 5.12.

5.4.1.4.6 *Airspeed Response Characteristics*

As it can be observed from Table 5.7, the airspeed percent settling (percent steady-state error) value is selected as 0.2%, which is in fact a stricter constraint than the respective military requirement dictates, since it gives the relaxation of choosing ± 5 knots or $\pm 2\%$, whichever is greater for the airspeed.

Table 5.7 Airspeed desired response characteristics

Step response characteristics	Value
Initial value [m/s]	0
Final value [m/s]	1
Step time [s]	0
Rise time [s]	10
Rise [%]	90
Settling time [s]	25
Settling [%]	0.2
Overshoot [%]	5
Undershoot [%]	2

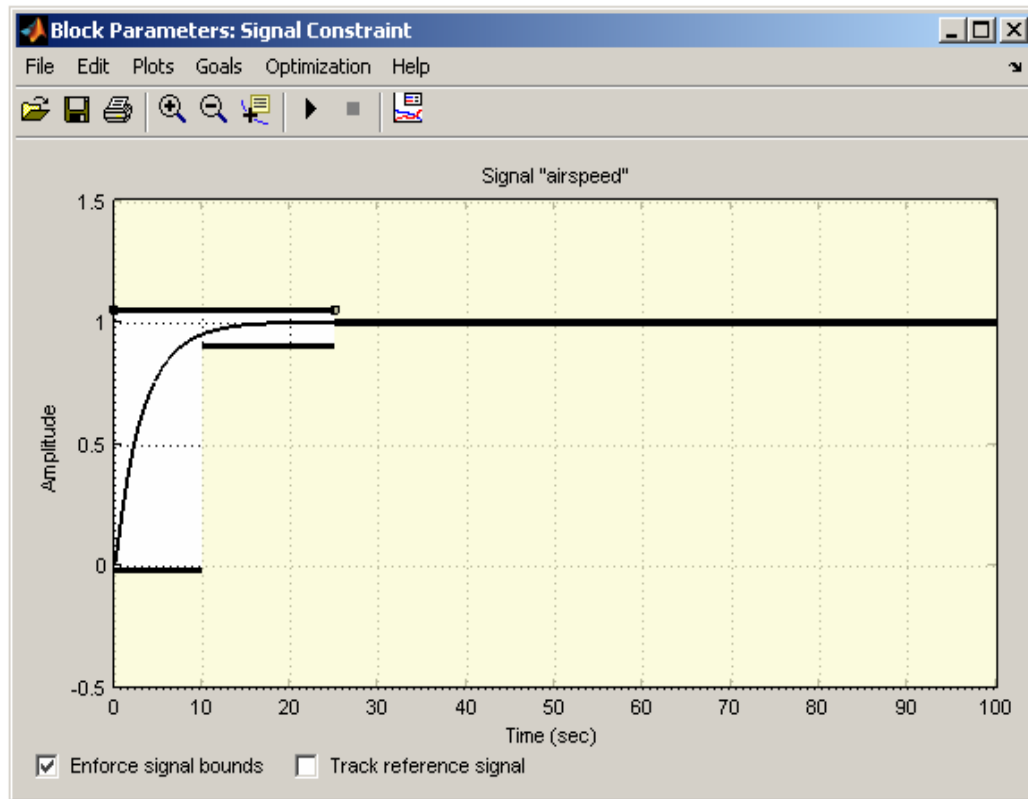


Figure 5.13 Airspeed final response to 1 m/s step input

The controller structure in which the SRO block is connected to the airspeed signal is given in Figure 5.6. 1 m/s is selected as the maximum step reference input value in response optimization process. The resultant airspeed response optimization to 1 m/s airspeed step input at the end of several iterations is given in Figure 5.13.

5.4.1.5 Closed Loop Poles

5.4.1.5.1 Lateral-Directional Controller – Closed Loop Poles

Obtaining the whole lateral-directional controller structure with respective gains of heading, roll attitude, roll rate, yaw rate and sideslip velocity controllers, the closed loop lateral-directional axis eigenvalues can be provided and compared with the open

loop eigenvalues of the corresponding flight condition, which are also shown in Table 3.1 of Section 3.3. The open loop and closed loop lateral-directional eigenvalues are together displayed in Table 5.8.

Table 5.8 Eigenvalues of the nominal open loop and closed loop linear models in lateral-directional axis

	Eigenvalues	Damping Ratio, ζ	Natural Frequency, ω_n [rad/s]
Open loop linear model / lateral-directional axis	0.0103	-	-
	0.0	-	-
	$-0.167 + 2.03i$	0.0821	2.04
	$-0.167 - 2.03i$		
	-17.3	-	-
Closed loop linear model / lateral-directional axis	-0.0535	-	-
	-0.124	-	-
	-0.254	-	-
	-0.789	-	-
	$-9.63 + 13i$	0.596	16.2
	$-9.63 - 13i$		
	-31.9	-	-

It can be concluded from the closed loop linear model dynamics results that the oscillatory lateral-directional Dutch roll mode is satisfying the Level 1 requirements in terms of dynamic stability at a region considerably beyond Level 2, for which the respective open loop dynamic stability characteristics are given in Figure 4.9 of Section 4.3.2. Additionally, the undamped spiral and heading modes of the open loop system are damped now.

5.4.1.5.2 Longitudinal Controller – Closed Loop Poles

Obtaining the whole longitudinal controller structure with respective gains of airspeed, altitude, pitch attitude and pitch rate controllers, the closed loop longitudinal axis eigenvalues can be provided and compared with the open loop

eigenvalues of the corresponding flight condition, which are also shown in Table 3.1 of Section 3.3. The open loop and closed loop longitudinal eigenvalues are together displayed in Table 5.9.

Table 5.9 Eigenvalues of the nominal open loop and closed loop linear models in longitudinal axis

	Eigenvalues	Damping Ratio, ζ	Natural Frequency, ω_n [rad/s]
Open loop linear model / longitudinal axis	0.000188	-	-
	$-0.00154 + 0.207i$	0.00744	0.207
	$-0.00154 - 0.207i$		
	$-1.31 + 2.11i$	0.529	2.48
	$-1.31 - 2.11i$		
Closed loop linear model / longitudinal axis	-0.143	-	-
	-0.667	-	-
	$-0.0640 + 1.37i$	0.0466	1.37
	$-0.0640 - 1.37i$		
	$-0.359 + 1.55i$	0.227	1.59
	$-0.359 - 1.55i$		
	-5.57	-	-
	-72.5	-	-

It can be concluded for the closed loop system that the lightly damped oscillatory longitudinal phugoid mode now satisfies the Level 1 requirements in terms of dynamic stability at the limit with a damping ratio value of 0.0466, for which the respective open loop damping ratio value is 0.00744 remaining in the Level 2 region as given in Figure 4.8 of Section 4.3.1. The other oscillatory mode with high frequency, short period, has its natural frequency still in Level 1 region but the damping ratio value corresponds to Level 2 region now, since pitch attitude feedback decreases the damping of short period, while being compensated by the use of pitch rate feedback. However the resultant decrease in short period damping can not be

avoided. Additionally, all the real axis poles of the longitudinal dynamics are damped in the closed loop system including the altitude mode.

5.4.2 Complete Controller – Implementing in Nonlinear Model

In the scope of implementation of the generated linear controller structures into the nonlinear UAV plant; gain scheduling, controller input linearization and anti integral wind-up scheme are carried out. Gain scheduling is to be accomplished for the purpose of having similar controller performance at all flight trim conditions with the linear model controller at one condition. Controller input linearization is accomplished by implementing perturbation controller inputs, $\tilde{\mathbf{u}}$ into an air vehicle that only understands real control variables, \mathbf{u} . Additionally, an anti integral wind-up scheme is implemented, in order to deal with the possible integral wind-up which occurs when large step inputs are commanded and cause one or more actuators to saturate.

5.4.2.1 Gain Scheduling

Since air vehicles are nonlinear dynamic systems that must operate over a wide range of flight conditions, a set of design gains are to be determined, using multiple linear models. This is caused by the fact that a controller designed using a linear model, is only valid in the neighborhood of the single trim point that linear model is obtained at. Hence, to cover whole operational flight envelope can be accomplished by using gain scheduling to produce a set of controller gains. Using standard classical techniques, it is not realistic to determine design gains for every conceivable flight condition. Each linear model, which corresponds to a single trim point, is representative of a range of flight conditions selected by the controller designer. The design gains obtained at these flight conditions are programmed in tabular, table look up form and then linearly interpolated according to the current value of the scheduling signals of the independent parameters [15, 38]. Gain scheduling is accomplished with respect to one or more independent variables, where in this study, knots-equivalent airspeed, KEAS, and altitude, h are taken as the two independent parameters that cover the physical effects of the flight envelope. The case in this

study is to perform the design task over the two-dimensional envelope since the subject UAV is of low maneuverable type, and additionally the nonlinear aerodynamic effects are not included in the database. However, it should be denoted that in reality, the angle of attack, i.e. the third gain scheduling dimension, should additionally be taken into account in order to cover the effects of aerodynamic nonlinearities. Next to this, if the subject UAV was a highly maneuverable type air vehicle with relatively faster responses to disturbances such as gust, wind-turbulence, etc., than the angle of attack parameter would have to be considered even within the linear region, in order to handle the distinct changes in the flight parameters. In addition, the effects of changes in mass, inertia and centre of mass need to be considered when a more detailed air vehicle nonlinear model and controller design is the case [39].

In order to perform gain scheduling, in the design of classical controller by using SRO, the linear controller design procedure described in Section 5.4.1 for one flight condition are repeated and respective controller gains are obtained for the linear models at the airspeeds ranging between 70 KEAS and 110 KEAS by 10 KEAS increments and at 5,000 ft (1,524 m), 15,000 (4,572 m), 20,000 (6,096 m), 25,000 ft (7,620 m), and 30,000 ft (9,144 m) altitudes. Therefore, 25 total trim points for gain scheduling are picked up. The gain scheduling breakpoint values for airspeed and altitude values are given in Table 5.10.

While obtaining the gains, the order of flight conditions is given importance, i.e. the two dimensional controller gain sets are obtained beginning with the flight condition having the smallest airspeed, KEAS and the altitude, h . For the next higher KEAS value, again the procedure is continued with the smallest h value to highest until the next KEAS and so on. The desired response characteristics of one controlled parameter for one flight condition are accomplished with several possible gains. Hence, it is considered that this queued approach helps the gains to follow a reasonable increasing or decreasing trend, which is essential, since an interpolation

procedure with look up tables is to be applied to the controller gains. As the result of this procedure, it is seen that some of the controller gains are constant throughout the flight envelope and the remaining depends on the two scheduling variables, KEAS and h .

Table 5.10 Gain scheduling breakpoint values of airspeed and altitude

h-breakpoint # KEAS-breakpoint #	1	2	3	4	5
1	70 KEAS, 5,000 ft	70 KEAS, 15,000 ft	70 KEAS, 20,000 ft	70 KEAS, 25,000 ft	70 KEAS, 30,000 ft
2	80 KEAS, 5,000 ft	80 KEAS, 15,000 ft	80 KEAS, 20,000 ft	80 KEAS, 25,000 ft	80 KEAS, 30,000 ft
3	90 KEAS, 5,000 ft	90 KEAS, 15,000 ft	90 KEAS, 20,000 ft	90 KEAS, 25,000 ft	90 KEAS, 30,000 ft
4	100 KEAS, 5,000 ft	100 KEAS, 15,000 ft	100 KEAS, 20,000 ft	100 KEAS, 25,000 ft	100 KEAS, 30,000 ft
5	110 KEAS, 5,000 ft	110 KEAS, 15,000 ft	110 KEAS, 20,000 ft	110 KEAS, 25,000 ft	110 KEAS, 30,000 ft

The values of the controller gains are given in Table 5.11 for the constant gains and in graphs of Figure 5.14 for the varying ones. In the two-dimensional graphs of Figure 5.14, the x and y axes are displayed as the altitude and KEAS breakpoint numbers respectively, for which the corresponding breakpoint values are given in Table 5.10.

Table 5.11 Dependency condition of the controller gains and values of constant ones

Gains	Dependent variables	Value
Roll rate feedback gain	constant	−0.1515
Roll proportional gain	constant	−0.3463
Roll integral gain	constant	−0.0201
Sideslip velocity feedback gain	constant	87.7484
Yaw rate feedback gain	constant	−6.1119
Heading proportional gain	KEAS, h	See Figure 5.14

Table 5.11 Dependency condition of the controller gains and values of constant ones (continued)

Pitch rate feedback gain	constant	−14.12
Pitch proportional gain	constant	−69.98
Pitch integral gain	constant	−10.0055
Altitude proportional gain	constant	1.2179
Altitude integral gain	constant	0.6371
Altitude rate feedback gain	constant	2.0561
Airspeed proportional gain	constant	9.087
Airspeed integral gain	constant	74.3
Airspeed rate feedback gain	KEAS, h	See Figure 5.14

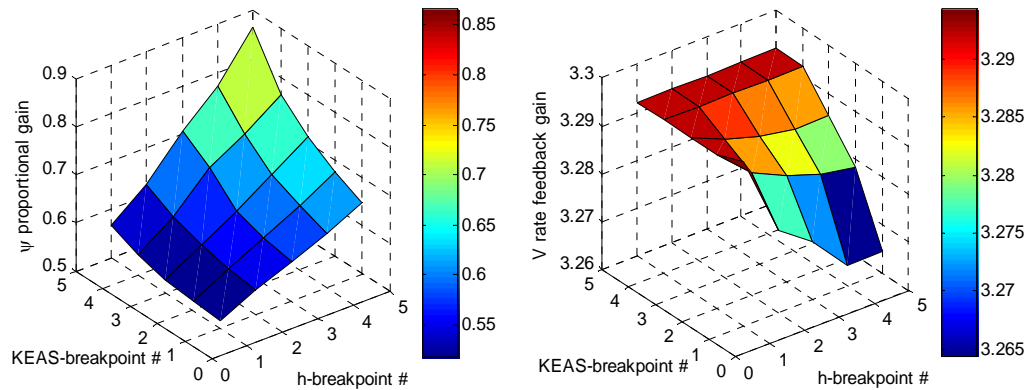


Figure 5.14 Graphs of the varying controller gains with respect to the dependent parameter(s)

5.4.2.2 Controller Input Linearization

All controllers developed in this study are based on the linear perturbed model of the air vehicle. The states represented by $\tilde{\mathbf{x}} = \mathbf{x} - \mathbf{x}_n$, inputs by $\tilde{\mathbf{u}} = \mathbf{u} - \mathbf{u}_n$ and outputs by $\tilde{\mathbf{y}} = \mathbf{y} - \mathbf{y}_n$ vectors of the linear model are the perturbed states, inputs and outputs, respectively, which are also defined in Linearization Methods, Section 3.3.1. This

implies that the controller inputs and outputs, i.e. the linear model outputs and inputs respectively, are also the perturbed values of the corresponding nonlinear plant variables from their nominal or trim amplitudes [15, 36]. The implementation of perturbation controller input $\tilde{\mathbf{u}}$, into a nonlinear air vehicle model that only understands total control variables \mathbf{u} , is shown in Figure 5.15. It is to be applied to the inner-outer loops of each controller structure defined in Sections 5.4.1.1 through 5.4.1.3.

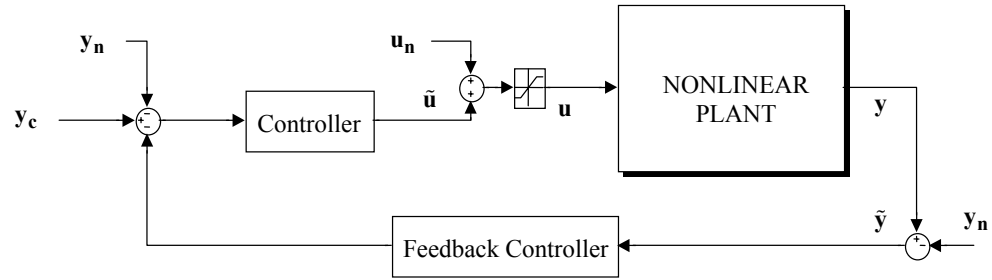


Figure 5.15 Implementation of perturbation controller into nonlinear model

5.4.2.3 Anti Integral Wind-up Scheme

One of the major implementation issues is the actuator saturation. Since, in flight controls, the plant inputs are limited, in order to describe the actual case in an air vehicle control system, nonlinear saturation functions are forced to be included in the control channels as shown in Figure 5.16, where \mathbf{d} is the demanded plant input and \mathbf{u} is the actual plant input. In addition, defining the \mathbf{u}_{\max} and \mathbf{u}_{\min} as the maximum and minimum allowable control effort limits, respectively, the integral wind-up process is described as follows: Consider the case where the controller including an integral has the input \mathbf{e} and output \mathbf{d} . All is well as long as \mathbf{d} is between \mathbf{u}_{\max} and \mathbf{u}_{\min} , for in this region air vehicle input \mathbf{u} equals \mathbf{d} . However, if \mathbf{d} exceeds \mathbf{u}_{\max} , then \mathbf{u} is limited to

its maximum value u_{\max} . This in itself may not be a problem, but the problem arises if e remains positive, for then the integral continues to integrate and d may increase well beyond u_{\max} . Then e becomes negative, it may take considerable time for d to decrease below u_{\max} . In the meantime, u is held at u_{\max} , giving an incorrect control input to the plant. This effect of integral saturation is called as “wind-up”. In order to correct the integral wind-up, it is necessary to limit the state of the controller so that it is consistent with the saturation effects being experienced by the plant input u [24].

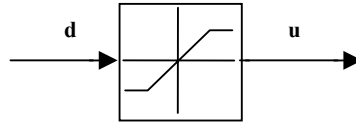


Figure 5.16 Actuator saturation function

In this study, the state of the controller is limited by a conditional anti integral wind-up scheme, named as “integrator clamping”, which is shown by Figure 5.17. The method is found to be the best in [40-41].

Engine throttle is one of the controls that can experience command saturation, which is also the case in this study. Hence, the indicated conditional anti integral wind-up scheme is implemented to the integrals of altitude, airspeed, and pitch attitude controllers where each has effect on throttle input. Referring to Figure 5.17, when both e multiplied with d is positive and an inequality occurs between d and u , representing the saturation case, the condition is satisfied causing the integrals of the altitude and pitch attitude controllers to be disabled and reset their outputs, and the integral of airspeed controller to be disabled and differently held its output to prevent limit cycle occurrence.

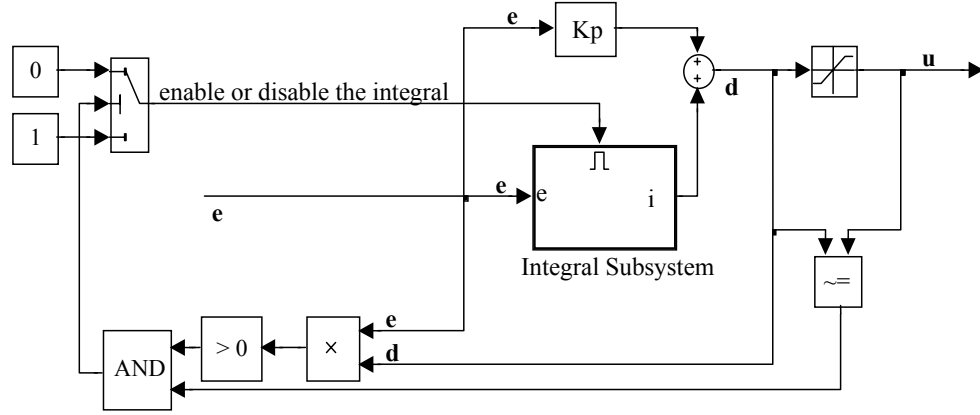


Figure 5.17 Integrator clamping ($e \cdot d > 0$)

In addition to the anti integral wind-up scheme, another important application to avoid adverse wind-up affects is the proper parameter limiting. Since the limited pitch angle, θ is commanded by the altitude controller including commands coming through high desired altitude values in the operational flight envelope, it is important to have reasonable limits for θ values throughout the flight envelope not to deal with a contrasting condition with the anti integral wind-up. This leads utilizing a dynamic limiting function in Simulink[®] complete controlled nonlinear model, next to the anti integral wind-up scheme. The upper θ limits are determined by trimming the nonlinear model by fixing the throttle to the maximum value and floating the flight path angle, γ , whereas in a similar process, the lower θ limits are determined by trimming for the minimum throttle value. These trims are carried out at the flight conditions corresponding to the breakpoint values of KEAS and h given in Table 5.10 of Section 5.4.2.1, and implemented into the two dimensional look up tables to interpolate and extrapolate the values. Since, the output of these lookup tables are the total θ values of the air vehicle, in order to comply with the perturbation controller

structure as defined in Section 5.4.2.2, the trim θ values are subtracted from the lookup table outputs to generate the upper and lower bounds of the dynamic saturation function feeding into the perturbed pitch attitude controller. By this way, depending on KEAS and h , the lower and upper limits are changed during the simulation process, not to have an unnecessarily high or low pitch attitude commands.

The graphs displaying the lower and upper total air vehicle θ values and their dependency on airspeed and altitude are given in Figure 5.18.

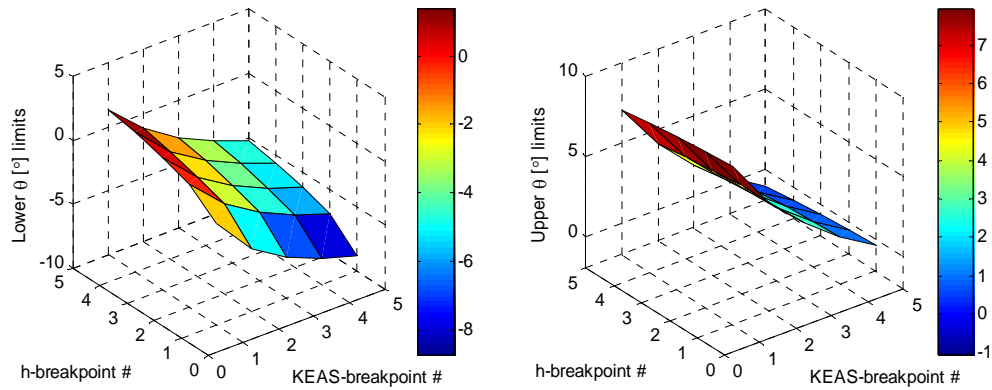
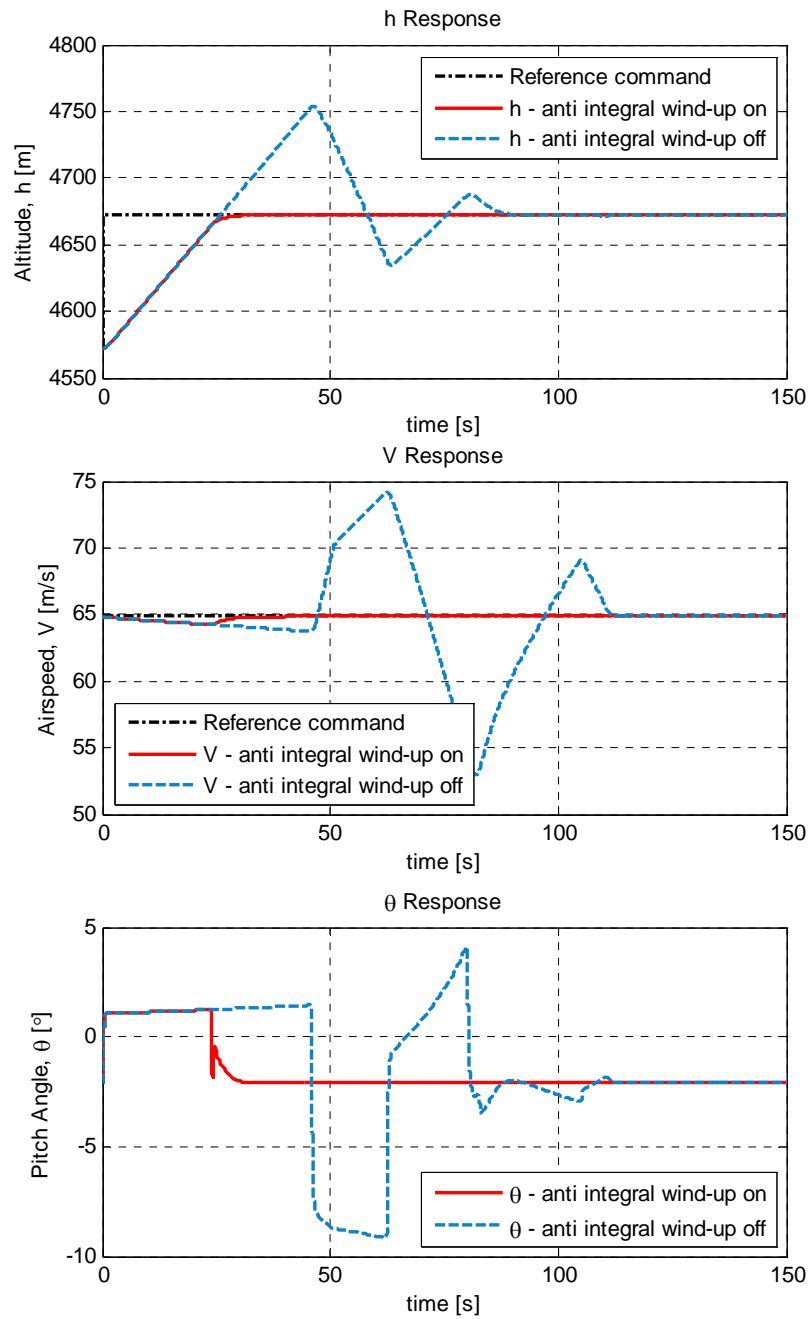


Figure 5.18 Lower and upper θ limits throughout the operational flight envelope

The effects of the anti integral wind-up scheme together with the dynamic θ limiting implementations are displayed by graphs of Figure 5.19 and 5.20 for h , θ , V , and demanded throttle input parameters. The graphs are obtained by comparing the results of the complete controlled nonlinear model with and without the anti integral wind-up engagement.



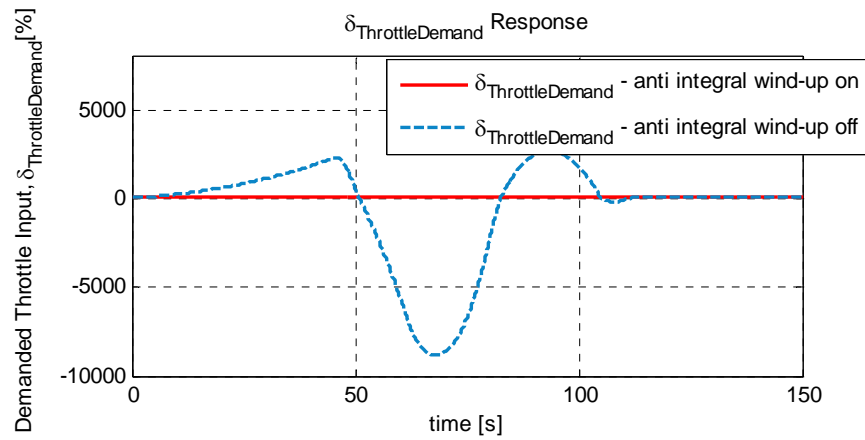
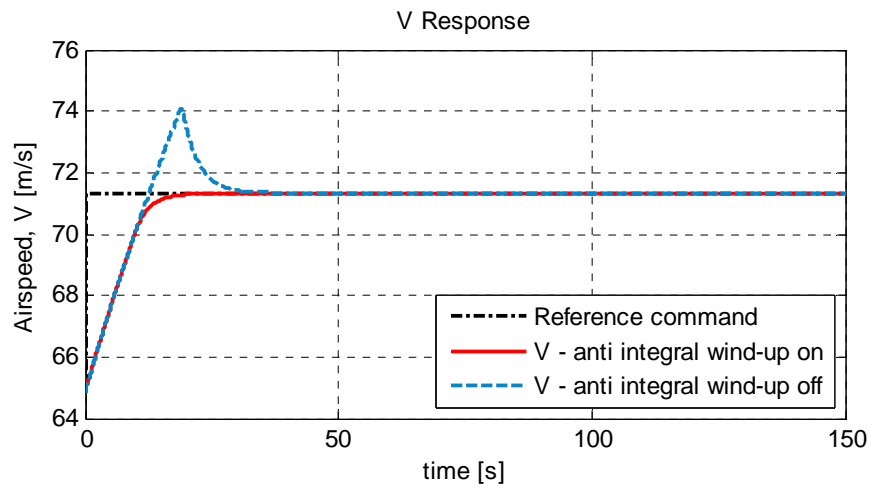


Figure 5.19 Responses to 100 m reference altitude increase command with and without anti-integral wind up



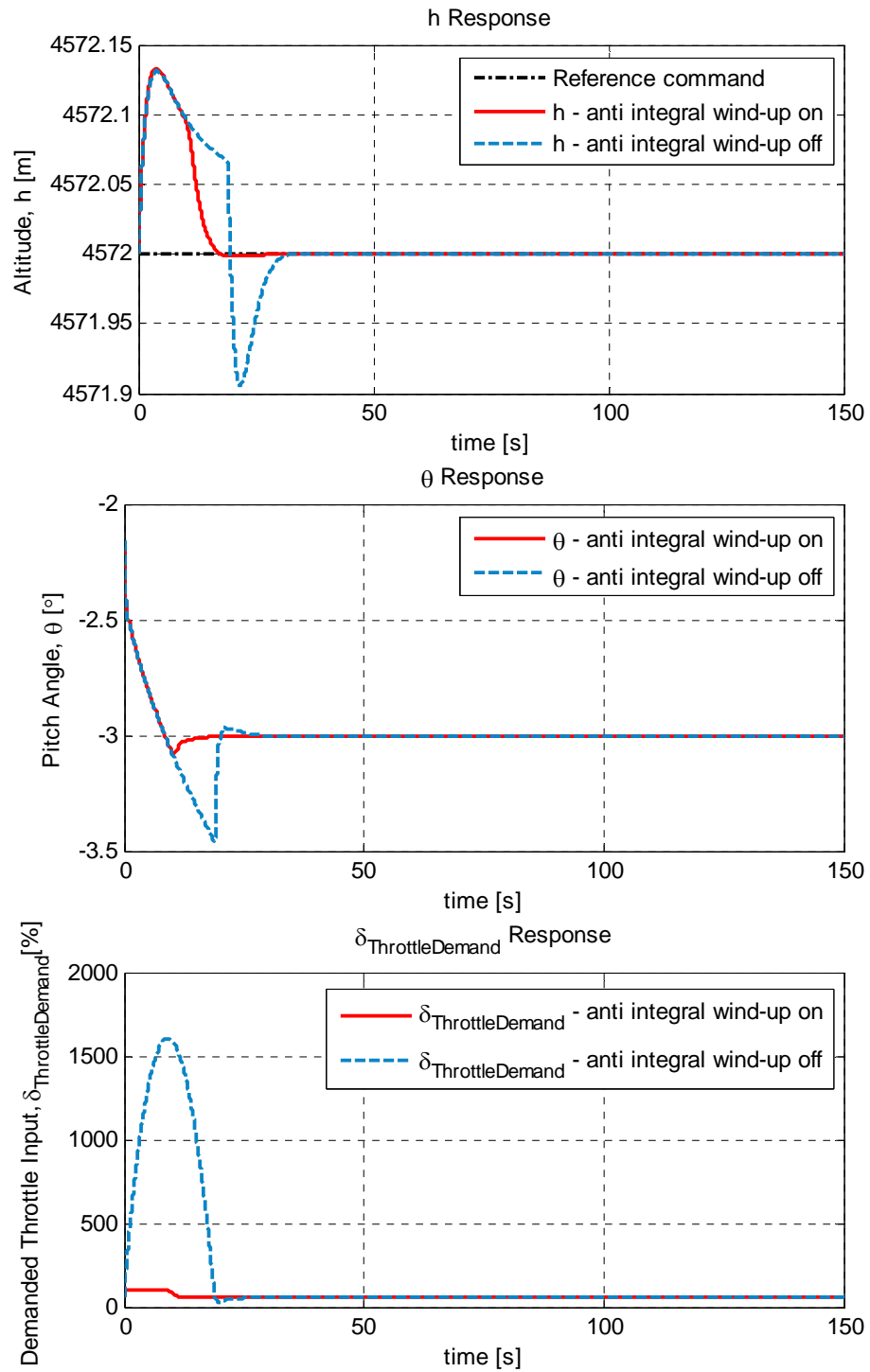


Figure 5.20 Responses to 10 knots reference KEAS increase command with and without anti-integral wind up

Figure 5.19 displays the responses to a +100 m reference altitude increase command and Figure 5.20 displays the responses to a +10 knots reference airspeed increase command starting from an initial condition of 100 KEAS and 15,000 ft (4,572 m) altitude. These figures show the importance of anti integral wind-up implementation in the classical controller, by implying how high the errors between the actual and commanded values of the regulated parameters may reach to, if the related integration processes of the controller are not eliminated when the throttle actuator saturates.

5.5 Optimal Controller Design

The second low-level flight control system is designed based on linear quadratic (LQ) controller approach. The main purpose of the controller is to increase the inherent stability characteristics in terms of damping ratio and undamped natural frequency values of the open loop system and to provide a good performance of tracking a reference control command in both lateral-directional and longitudinal axes.

Similar to the classical controller design of the previous section, the general design procedure involves designing a flight control system satisfying the flight control requirements given in Section 5.3 for a nominal linear model, and based on the controller structure of this linear model, obtaining the controller gains for the remaining predetermined trim conditions of the operational flight envelope – namely the gain scheduling is carried out. It is to serve compensating with the nonlinearities of the UAV model and physical changes in the environment; since the controller is designed around the linear models that are provided by numerical perturbation of nonlinear models therefore is valid for respective narrow flight condition intervals. Obtaining the gain sets, the linear perturbation controller is implemented into the

nonlinear model by controller input linearization, and anti integral wind-up scheme is built up against for throttle control saturation adverse effects.

Since the coupling effects between dynamics of the lateral-directional and longitudinal axes of the subject UAV are considerably small as concluded in modal matrix analysis in Section 3.3, the controllers are designed separately for both axes as if they are ideally decoupled. Total Energy Control System (TECS) is the method used for the longitudinal flight control system development based on the LQ controller design. TECS involves developing an integrated autothrottle/autopilot controller design; apart from classical separate single objective control systems in which autopilot controls flight path, whereas autothrottle controls speed. The work on the NASA B737-100 Transport System Research Vehicle (TSRV), in improving the operation of the Automatic Flight Control System (AFCS), has led to the development of TECS method [42]. The lateral-directional flight control system is designed by feeding all lateral-directional states back into the controller in the conventional multivariable approach, again based on LQ controller design. For both axes, for better tracking purposes and to eliminate the steady state errors, integrators are also embedded for the control of the commanded variables, for which the design approach is also named as “integral LQ”.

5.5.1 Linear Quadratic (LQ) Controller Approach

For both longitudinal and lateral-directional control systems, integral LQ design is developed using the linear system models, since it is a useful design procedure which as mentioned in [43];

1. Produces required feedback gains simultaneously for all feedback variables,
2. Has a root locus that stays in the left half plane for all gain values,
3. Stability margins are inherently good,
4. Provides direct design of multivariable control systems, i.e. applications with two or more controls and two or more regulated variables.

The perturbation linear model in standard state space form is represented again as,

$$\dot{\tilde{\mathbf{x}}} = \mathbf{A}\tilde{\mathbf{x}} + \mathbf{B}\tilde{\mathbf{u}} \quad (5.5)$$

$$\tilde{\mathbf{y}} = \mathbf{C}\tilde{\mathbf{x}} + \mathbf{D}\tilde{\mathbf{u}} \quad (5.6)$$

where $\tilde{\mathbf{x}} = \mathbf{x} - \mathbf{x}_n$, $\tilde{\mathbf{u}} = \mathbf{u} - \mathbf{u}_n$, and $\tilde{\mathbf{y}} = \mathbf{y} - \mathbf{y}_n$ are the perturbed states, inputs and outputs around the trim states, \mathbf{x}_n , inputs, \mathbf{u}_n , and outputs, \mathbf{y}_n , respectively. In terms of control, $\tilde{\mathbf{x}}$ and $\tilde{\mathbf{u}}$ can be defined as the errors between the actual state and control values, and the state and control values at the commanded trim point. Hence, the objective is to drive $\tilde{\mathbf{x}}$ and $\tilde{\mathbf{u}}$ to zero [15]. It is required to determine the optimal gain matrix, \mathbf{K}_{lqr} with the state feedback law such as,

$$\tilde{\mathbf{u}} = -\mathbf{K}_{lqr}\tilde{\mathbf{x}} \quad (5.7)$$

which by driving the errors to zero minimizes the performance index (quadratic cost function) given as,

$$\mathbf{J} = \int_0^{\infty} (\tilde{\mathbf{x}}^T \mathbf{Q} \tilde{\mathbf{x}} + \tilde{\mathbf{u}}^T \mathbf{R} \tilde{\mathbf{u}}) dt \quad (5.8)$$

subject to the system dynamics represented by Equation (5.5), where \mathbf{Q} is a positive semi-definite symmetric weighting matrix, $\mathbf{Q} \geq 0$; and \mathbf{R} is a positive definite symmetric weighting matrix, $\mathbf{R} > 0$. The value of \mathbf{R} affects the amount of perturbation control used, $\tilde{\mathbf{u}}(t)$ and the values of the elements of \mathbf{Q} affect the perturbation system response, $\tilde{\mathbf{x}}(t)$. \mathbf{K}_{lqr} is obtained as

$$\mathbf{K}_{lqr} = \mathbf{R}^{-1} \mathbf{B}^T \mathbf{S} \quad (5.9)$$

where \mathbf{S} is computed by solving the reduced matrix Riccati equation given in Equation (5.10) for \mathbf{Q} and \mathbf{R} weighting matrices.

$$\mathbf{A}^T \mathbf{S} + \mathbf{S} \mathbf{A} - \mathbf{S} \mathbf{B} \mathbf{R}^{-1} \mathbf{B}^T \mathbf{S} + \mathbf{Q} = 0 \quad (5.10)$$

MATLAB[®] functions `lqr` and `lqry` are to be used in order to determine the \mathbf{K}_{lqr} gain matrix. The general flow of LQ controller design phase is displayed by Figure 5.21. The two blocks at the beginning of the flowchart, i.e. constructing the synthesis model and then linearizing, are accomplished for the purpose of having the accurate linear model to be input to the MATLAB[®] `lqr` and `lqry` functions, including the states contributed from integrators, filters, etc., existing in the controller structure. In other words, this process helps including the possible additional controller states other than the open loop plant inherent states in the controller structure. The obtained linear model has now the augmented state space system, control, and output matrices, represented by \mathbf{A}' , \mathbf{B}' , and \mathbf{C}' . The synthesis model construction approach differs for longitudinal and lateral-directional control systems design applications, which is to be defined in detail in the respective sections. After obtaining the accurate linear model to be input to the MATLAB[®] `lqr` and `lqry` functions, in order to start iteration with some feasible values for diagonal weighting matrices, \mathbf{Q} and \mathbf{R} , Bryson inverse square method is applied as represented in (5.11). This method helps normalizing the magnitudes and eliminating the effects of different units of different states and control inputs [10, 24].

$$\mathbf{Q} : \left\{ \mathbf{q}_{ii} = \frac{1}{\mathbf{q}_i(\max)^2} \right\}_{i=1}^{q'}, \mathbf{R} : \left\{ \mathbf{r}_{ii} = \frac{1}{\mathbf{r}_i(\max)^2} \right\}_{i=1}^p \quad (5.11)$$

where based on the LQ controller design approach in this study, q' is the number of rows of \mathbf{C}' matrix, i.e. the number of outputs of synthesis models, whereas p is the number of columns of \mathbf{B}' matrix. Consequently, $\mathbf{q}_i(\max)$ stands for the maximum

value the i^{th} output parameter may take and likely $r_i(\text{max})$ stands for the maximum value the i^{th} control input may take.

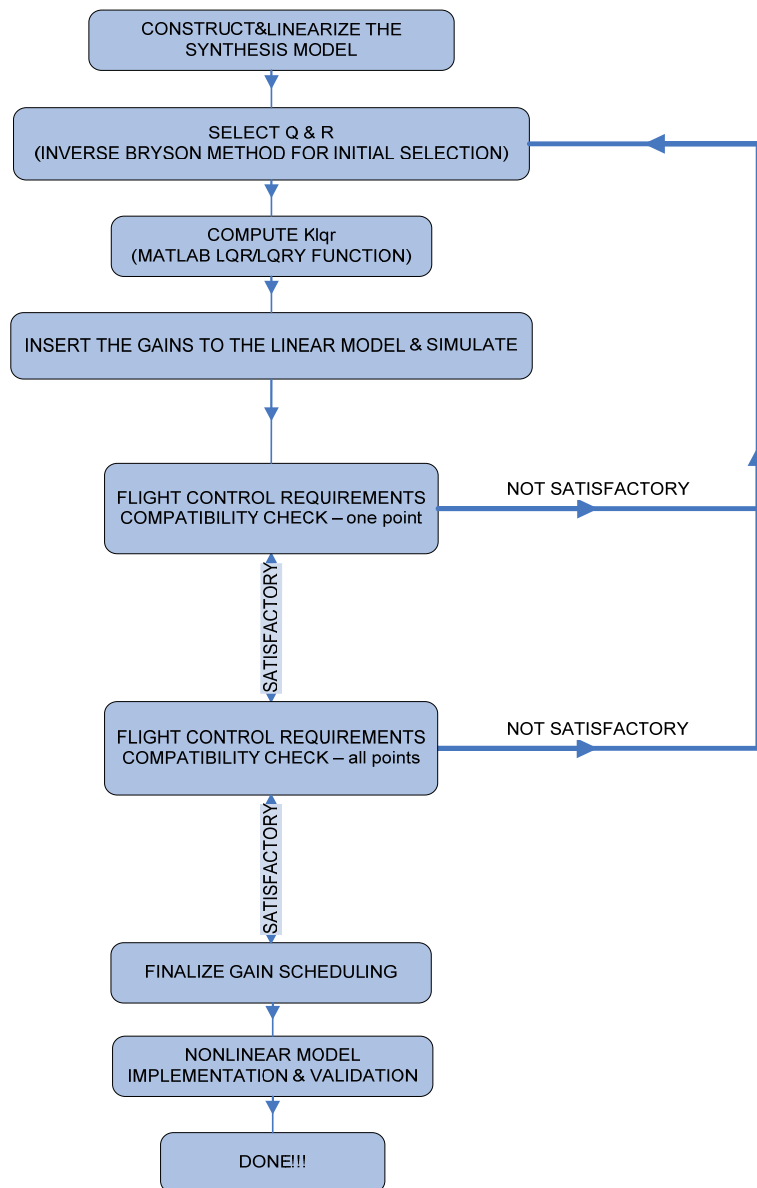


Figure 5.21 LQ controller design flowchart

5.5.2 Building Longitudinal Controller (TECS)

Total Energy Control System (TECS) method is used for the longitudinal flight control system design in order to provide coordinated use of throttle and ruddervator controls – namely the use of integrated autothrottle/autopilot. Specifically, the design method, as mentioned in [42] is applied to;

1. Direct synthesis of a multivariable inner-loop feedback control system based on total energy control principles,
2. Synthesis of speed and altitude hold designs as outer-loop feedback control systems around the inner-loop.

The work of developing an integrated autopilot/autothrottle was originally initiated to solve the problems identified with conventional uncoupled autopilots and autothrottles as defined in [44];

1. Since, the responses to elevator (or ruddervator) and throttle are coupled in speed and altitude, pilots have learned through training to decouple flight path angle (FPA), γ and speed control. General automatic control modes fail to account for this control coupling, by distinct appointment of throttle control to airspeed and elevator (or ruddervator) control to flight path upcoming from the single input-single output (SISO) nature of the control design. It can be said that TECS approach is used to achieve a pilot-like quality in automatic control, by taking into account these coupling effects,
2. Autopilot, autothrottle, and flight management system (FMS) control laws have developed over a long period of time that has led to duplication of function in the autopilot and FMS computer.

These problems led to a general design philosophy for TECS;

1. Design the system as a multi input-multi output (MIMO) system,

2. Design with a generalized inner loop structure and design the outer loop functions to interface with the common inner loop, thus minimizing software duplication,
3. Provide under-speed and over-speed protection for all modes.

By this philosophy, the conventional pitch and speed control functions are integrated into a single control system, and the replacement of the autopilot and autothrottle found in current airplanes by a single auto-flight line replaceable unit (LRU) is facilitated.

The approach of TECS is given as follows [44-45];

1. The basic concept of TECS is to control the total energy of the airplane. The total energy of the system can be expressed as the sum of the potential and kinetic energy as,

$$E = Wh + \frac{1}{2} \frac{W}{g} V^2 \quad (5.12)$$

where, W is the air vehicle weight in [N], h is the altitude in [m], g is the acceleration due to gravity in [m/s^2], and V is the airspeed in [m/s].

2. By differentiating the total energy, E given by Equation (5.12), the total energy rate, \dot{E} is found as,

$$\dot{E} \approx WV \left(\frac{\dot{V}}{g} + \gamma \right) \quad (5.13)$$

where, γ is the Flight Path Angle (FPA) in [rad], which is assumed to be small, thus approximating from $\sin \gamma$ to γ .

3. From the flight dynamics relationship along the flight path, the thrust required to maneuver is;

$$\text{Thrust}_{\text{REQ}} = W \left(\gamma + \frac{\dot{V}}{g} \right) + \text{Drag} \quad (5.14)$$

4. Assuming that drag variation with time is slow, it is observed that the engine thrust required to maneuver i.e. the first right hand side term of Equation (5.14), is proportional to the total energy rate given by Equation (5.13). Hence, normalizing the total energy rate, \dot{E} by velocity gives $\Delta \text{Thrust}_{\text{REQ}}$. This implies that the total energy of the air vehicle can be regulated directly by throttle control input. In response to speed derivative or flight path changes then, a control law can be developed that uses the throttles to drive the total energy rate error to zero as,

$$\delta_{\text{throttle}} = \left(K_{\text{TP}} + \frac{K_{\text{TI}}}{s} \right) \frac{\dot{E}_e}{V} = \left(K_{\text{TP}} + \frac{K_{\text{TI}}}{s} \right) \left(\frac{\dot{V}_e}{g} + \gamma_e \right) \quad (5.15)$$

where \dot{E}_e , \dot{V}_e and γ_e are the total energy rate, air vehicle acceleration, and flight path angle errors, respectively between the corresponding real and commanded values. K_{TP} and K_{TI} are the proportional-integral throttle gains. As mentioned before, integral compensator is utilized in order to reduce the steady state errors.

5. Besides controlling the total energy rate, there is one more parameter that still exists and has to be regulated, which is the energy rate distribution error, since for example too high a γ_e value and too low a \dot{V}_e value may occur, without any regulation applied. Hence, to distribute the total energy rate between γ_e and \dot{V}_e as desired, elevator (or ruddervator) control is to be used. In this study the ruddervator control is driven by operator control column, which is also defined in Actuators Model, Section 2.7. Consequently, the longitudinal linear models are obtained for the control inputs column and

throttle. Therefore, the control strategy used for regulating the rate distribution error is as,

$$\delta_{\text{column}} = \left(\mathbf{K}_{\text{CP}} + \frac{\mathbf{K}_{\text{Cl}}}{s} \right) \left(\frac{\dot{\mathbf{V}}_{\text{e}}}{\mathbf{g}} - \gamma_{\text{e}} \right) \quad (5.16)$$

where K_{CP} and K_{CI} are the proportional-integral column gains. The general inner loop TECS structure defined up to here is demonstrated by Figure 5.22.

6. The outer loops generate the altitude and airspeed command loops through the proportional gains, K_h , and K_v , giving commands to FPA and acceleration respectively. The outer loop TECS structure is demonstrated by Figures 5.23.

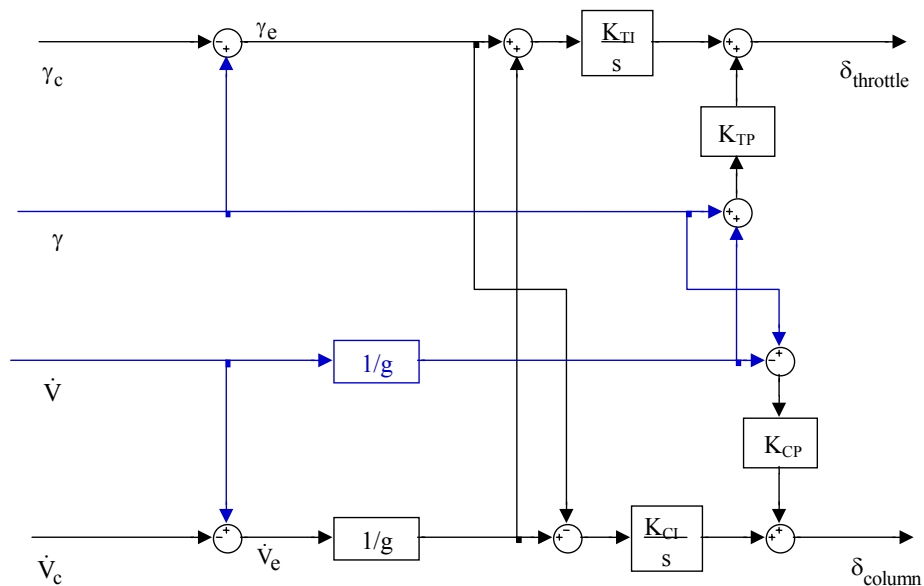


Figure 5.22 General Inner loop TECS structure – γ and \dot{V} controller

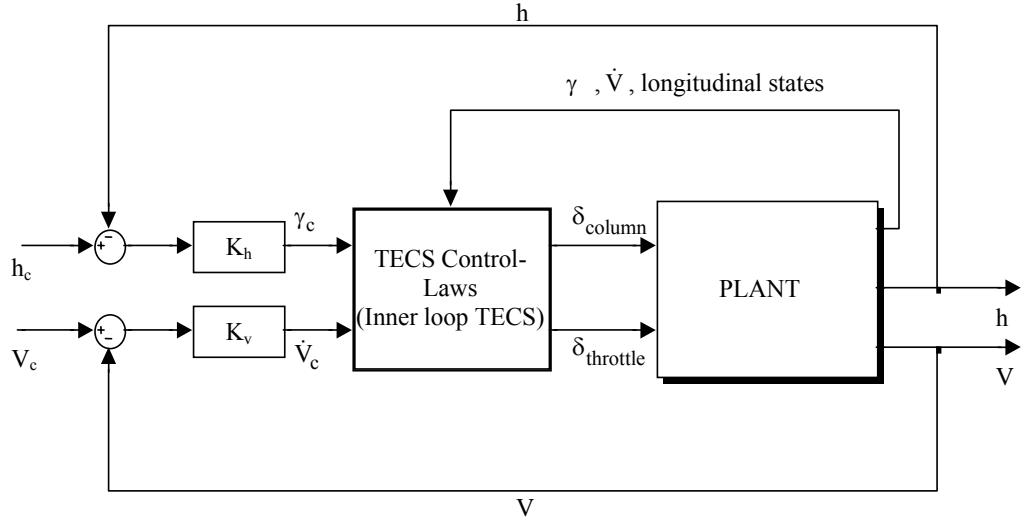


Figure 5.23 Outer loop TECS structure – h and V controller

5.5.2.1 Building up Inner Loop TECS

This section describes building up the inner loop TECS, where its general structure is displayed by Figure 5.22. The inner loop build up procedure is based on the general flow of the LQ controller design given by Figure 5.21.

5.5.2.1.1 *Synthesis Model*

The synthesis model of the inner loops is formed, as given in Figure 5.24. The linearized synthesis model is to be used as an input to the MATLAB[®] `lqry` function by which the full state feedback gains are solved. The synthesis model is built using the open loop model as its core [46]. Criterion outputs, \mathbf{Z} are formed for output weighting with the `lqry` function, where they are selected among the parameters to be regulated. Free integrators are placed on the outputs or combination of outputs to be controlled. The integrators thus produce infinite cost at zero frequency in cost function. It should be noted that the number of output variables to be controlled must not exceed the number of independent control effectors [47]. This places a limit on

number of free integrators. For the longitudinal controller, TECS design, these variables to be controlled are selected as the $\left(\frac{\dot{V}_e}{g} + \gamma_e\right)$ and $\left(\frac{\dot{V}_e}{g} - \gamma_e\right)$.

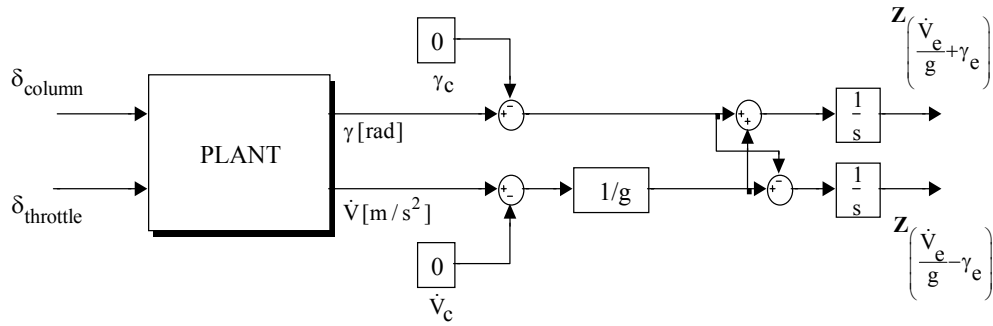


Figure 5.24 Longitudinal synthesis model

Following the construction of the synthesis model, linearizing should be accomplished in order to obtain the new state space model including the integral states. The linearized synthesis model system matrix, $\mathbf{A}'_{\text{long}}$, control input matrix, $\mathbf{B}'_{\text{long}}$, and output matrix, $\mathbf{C}'_{\text{long}}$, at a nominal flight condition, 100 KEAS and 15,000 ft (4,572 m) altitude are given by Equations 5.17, 5.18, and 5.19 respectively.

$$\mathbf{A}'_{\text{long.}} = \begin{bmatrix} 0 & 0 & -0.0018 & -0.0042 & 0.0045 & 0 & 0 \\ 0 & 0 & -0.0007 & 0.0266 & -1.9955 & 0 & 0 \\ 0 & 0 & -0.0255 & 0.0421 & -9.7613 & 2.3992 & -0.0001 \\ 0 & 0 & -0.3475 & -1.8019 & 0.2947 & 63.6411 & -0.0009 \\ 0 & 0 & 0 & 0 & 0 & 1 & 0 \\ 0 & 0 & 0.0004 & -0.0736 & 0 & -0.802 & 0 \\ 0 & 0 & 0.0377 & 0.9993 & -64.8501 & 0 & 0 \end{bmatrix} \quad (5.17)$$

with states, $\text{Integrator}\left(\frac{\dot{V}_e + \gamma_e}{g}\right)$, $\text{Integrator}\left(\frac{\dot{V}_e - \gamma_e}{g}\right)$, u , w , θ , q , and z , respectively.

$$\mathbf{B}'_{\text{long.}} = \begin{bmatrix} 0 & 0.0036 \\ 0 & 0.0036 \\ -0.0047 & 0.0338 \\ -0.1153 & -0.0467 \\ 0 & 0 \\ -0.0948 & -0.0069 \\ 0 & 0 \end{bmatrix} \quad (5.18)$$

with control inputs, δ_{column} , and δ_{throttle} , respectively for the first and second columns.

$$\mathbf{C}'_{\text{long.}} = \begin{bmatrix} 1 & 0 & 0 & 0 & 0 & 0 & 0 \\ 0 & 1 & 0 & 0 & 0 & 0 & 0 \end{bmatrix} \quad (5.19)$$

5.5.2.1.2 Weighting Matrices Selection – Obtaining \mathbf{K}_{lqr}

The next task is to determine the feedback gains by choosing the cost function weights, \mathbf{Q} and \mathbf{R} and solving the Riccati equation by using MATLAB[®] `lqrry` function to specify the gains. The initial values are obtained by Bryson inverse square method, as defined in Section 5.5.1, and represented by Equation (5.11). The resulting diagonal matrices have values 100, 120 for \mathbf{Q} matrix and 0.0012, 0.0003 for \mathbf{R} matrix as their diagonal elements. The optimal \mathbf{K}_{lqr} gain matrix given by Equation

(5.20), which satisfy the desired stability and track performance, is obtained by utilizing MATLAB[®] `lqr` function.

$$\mathbf{K}_{lqr} = \begin{bmatrix} -196.6733 & 231.4812 & -0.4447 & 3.8829 & -419.313 & -55.4185 & -0.002 \\ 422.6249 & 430.8896 & -0.4502 & 1.8223 & -213.2046 & -15.5899 & -0.0027 \end{bmatrix} \quad (5.20)$$

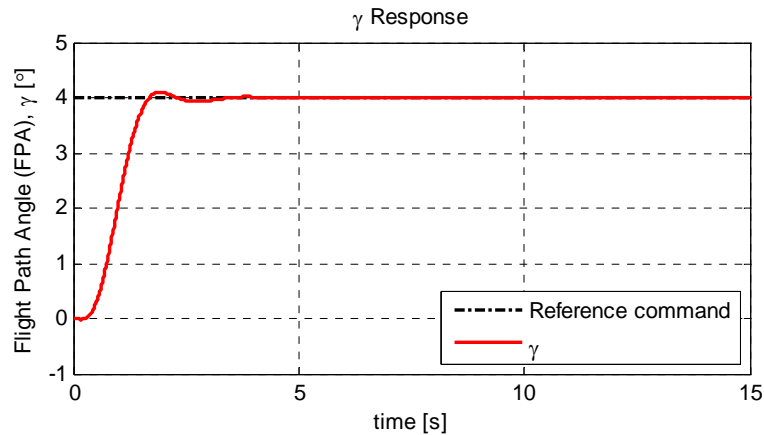
where, the columns correspond to the gains of the respective states of the enhanced system matrix, \mathbf{A}'_{long} given by Equation (5.17) with the command tracking error integrator states, $\text{Integrator}\left(\frac{\dot{V}_e}{g} + \gamma_e\right)$, $\text{Integrator}\left(\frac{\dot{V}_e}{g} - \gamma_e\right)$ at the first two columns; and the rows correspond to the gains of the respective control inputs of the enhanced control input matrix \mathbf{B}'_{long} , given by Equation (5.18). It is obvious that the current control design method gives the advantage of obtaining cooperating control loops by the proper selection of the weights given to the diagonals of the \mathbf{Q} and \mathbf{R} matrices by the designer for the tracking command control and regulation of the respective states, apart from the SISO control systems. Inserting the obtained gains in the longitudinal linear controller model is in a matrix multiplication form based on Equation (5.7) as,

$$\begin{bmatrix} \mathbf{u}(1) \\ \mathbf{u}(2) \end{bmatrix} = - \begin{bmatrix} \mathbf{K}_{lqr}(1,1) & \mathbf{K}_{lqr}(1,2) & \mathbf{K}_{lqr}(1,3) & \mathbf{K}_{lqr}(1,4) & \mathbf{K}_{lqr}(1,5) & \mathbf{K}_{lqr}(1,6) & \mathbf{K}_{lqr}(1,7) \\ \mathbf{K}_{lqr}(2,1) & \mathbf{K}_{lqr}(2,2) & \mathbf{K}_{lqr}(2,3) & \mathbf{K}_{lqr}(2,4) & \mathbf{K}_{lqr}(2,5) & \mathbf{K}_{lqr}(2,6) & \mathbf{K}_{lqr}(2,7) \end{bmatrix} \cdot \begin{bmatrix} \mathbf{x}(1) \\ \mathbf{x}(2) \\ \mathbf{x}(3) \\ \mathbf{x}(4) \\ \mathbf{x}(5) \\ \mathbf{x}(6) \\ \mathbf{x}(7) \end{bmatrix} \quad (5.21)$$

It should be noted that, apart from the demonstration of the general inner loop TECS structure by Figure 5.22, the multiplication of the LQ controller integrator gains with

the error integrator states is in the form of a gain matrix multiplication with integrator states vector, based on the multivariable optimal controller approach.

The longitudinal linear model with inner loop TECS is simulated to check if the commanded reference inputs, γ_c , and \dot{V}_c are tracked accurately with no steady state errors and with proper control input change magnitudes. The linear model time simulation responses to $+4^\circ$ reference FPA command and a simultaneous $+0.1 \text{ m/s}^2$ reference acceleration command for the nominal trim condition of 100 KEAS and 15,000 ft (4,572 m) altitude are given in Figure 5.25. It can be concluded from the graphs that the inner loop TECS controller is accomplished to give satisfying results. It should not be forgotten that, since during the build up of inner loop TECS by using LQ controller approach, the longitudinal model state feedback gains together with the error integrator state gains are obtained simultaneously, the proportional gains K_{TP} , and K_{CP} , which are demonstrated in Figure 5.22 are not provided. But, it is obvious from the time simulation response results that, they do not need to be obtained additionally.



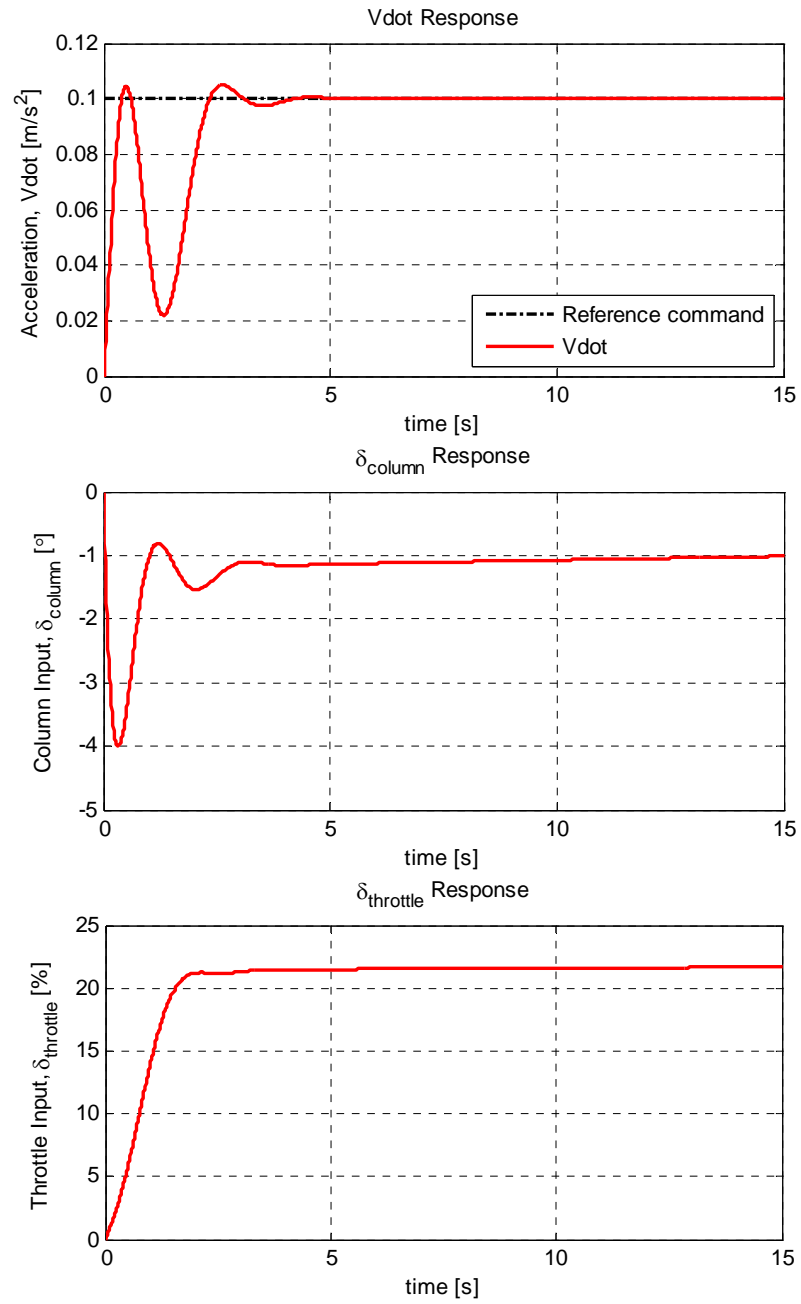


Figure 5.25 Inner loop TECS – Linear model time simulation responses to simultaneous +4° FPA and 0.1 m/s² acceleration reference commands

Concluding that the time simulation results are satisfactory for all trim points in the flight envelope, the longitudinal axis \mathbf{Q} and \mathbf{R} weighting matrices are frozen, and the gain sets are obtained utilizing the determined \mathbf{Q} and \mathbf{R} matrices for all linear models of different conditions in flight envelope. These sets are to be implemented into the nonlinear model, in the scope of gain scheduling.

5.5.2.2 Building up Outer Loop TECS

Outer loop TECS is built up based on the structure given by Figure 5.23, where the inner loop TECS with its \mathbf{K}_{lqr} gains is designed in the Section 5.5.2.1.

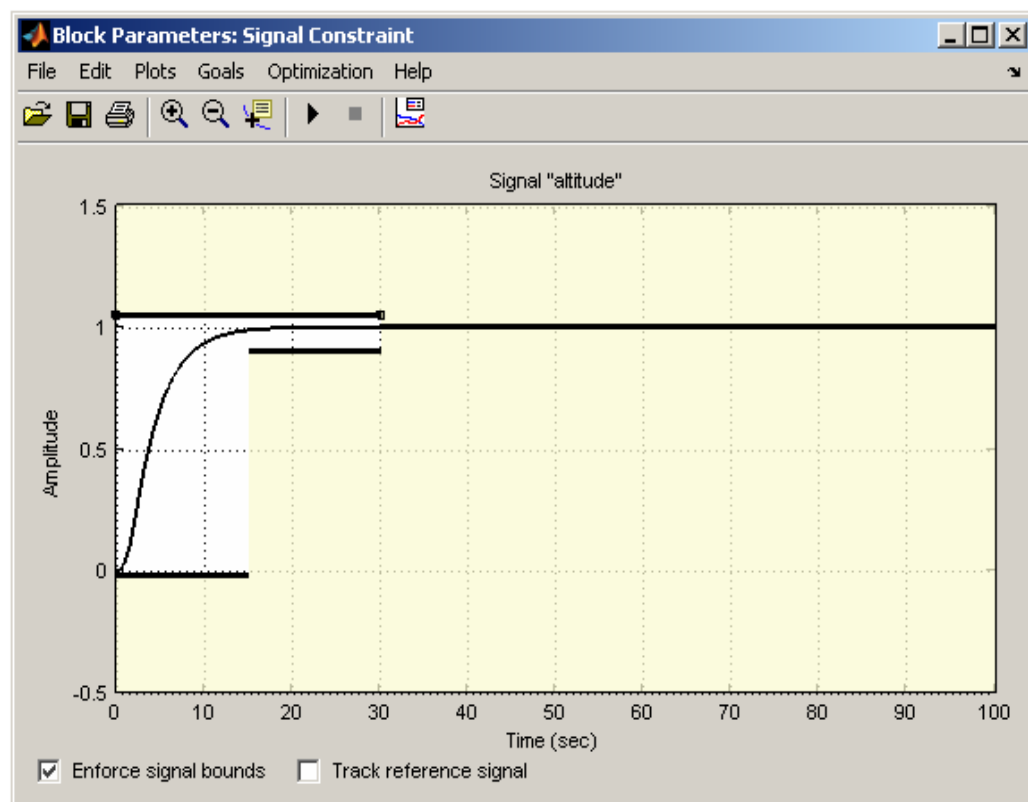


Figure 5.26 Altitude final response to 1 m step input

In order to obtain the outer loop TECS gains, K_h and K_v , SRO tool is utilized. Two response optimization blocks are embedded in the linear Simulink® model, by connecting to the altitude, h and airspeed, V output signals.

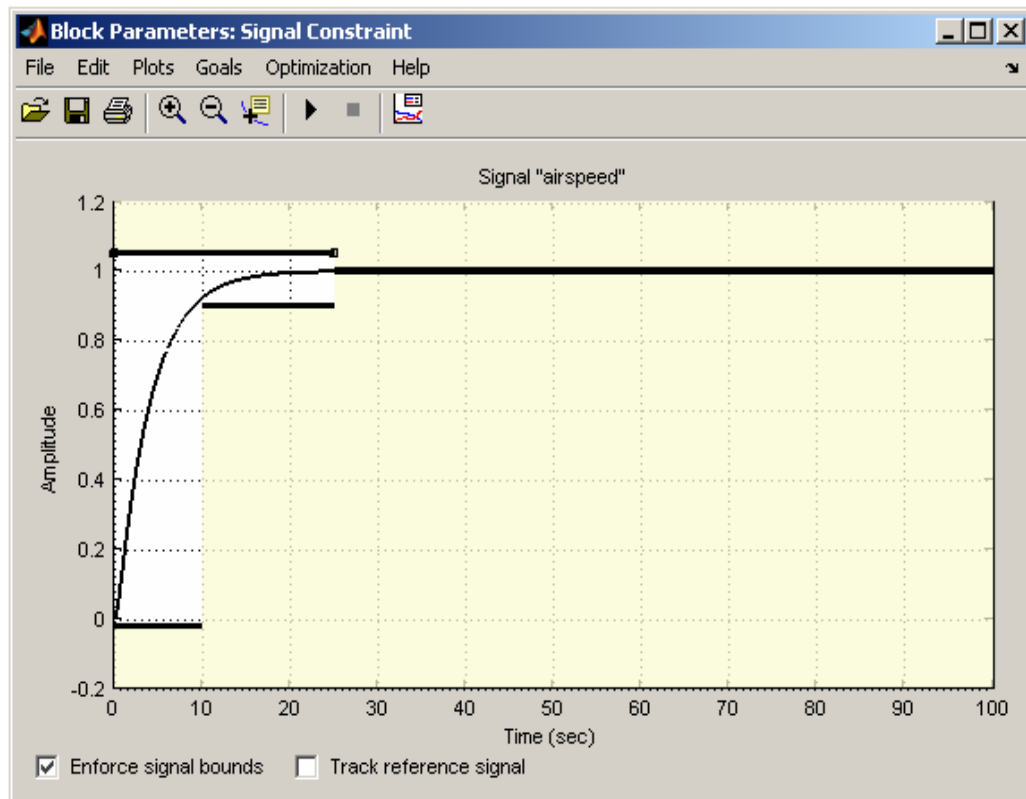


Figure 5.27 Airspeed final response to 1 m/s step input

The same desired response characteristics are selected as the classical controller altitude and airspeed controllers', demonstrated in Section 5.4.1.4.5 by Table 5.6 and Section 5.4.1.4.6 by Table 5.7, respectively. The only tuned parameters that are picked up are K_h and K_v , while holding inner loop K_{lqr} gains constant. The K_h is

found to be 0.0034, whereas K_v is 0.2418, which are to be constant for all the trim points of whole operational flight envelope. The resultant altitude and airspeed responses obtained at 100 KEAS and 15,000 ft (4,572 m) altitude condition are given by Figures 5.26 and 5.27, respectively.

5.5.3 Building Lateral-Directional Controller

The main purpose of the lateral-directional controller build up is to control bank angle at the inner loop, and heading at the outer loop, for which the structures are displayed by Figures 5.34 and Figure 5.35, respectively. The analyses and simulation results shown throughout this section are for the trim condition of 100 KEAS and 15,000 ft (4,572 m) altitude.

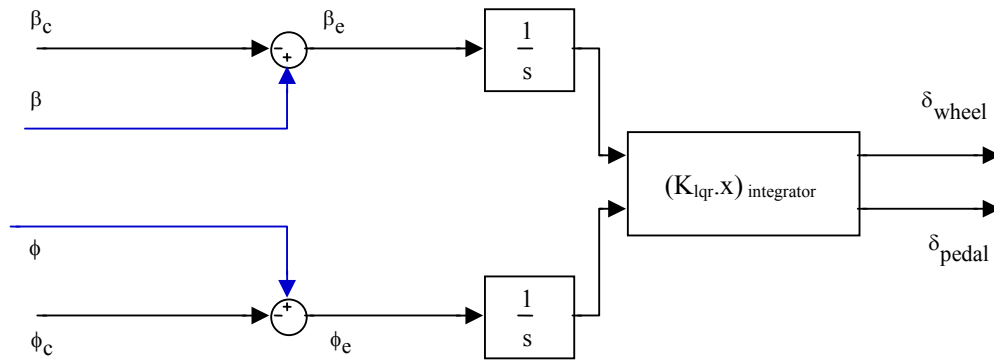


Figure 5.28 Inner loop lateral-directional LQ controller structure – β and ϕ controller

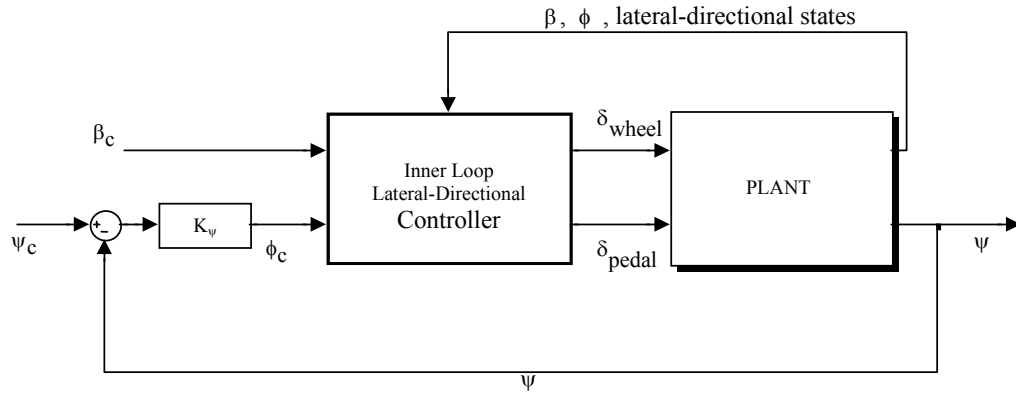


Figure 5.29 Outer loop lateral-directional controller structure – ψ controller

5.5.3.1 Building up Inner Loop Lateral-Directional Controller

The design phase of the inner loop lateral-directional controller is based on the tasks given by the LQ controller design flowchart demonstrated by Figure 5.21. The inner loop design includes bank angle, ϕ and sideslip angle, β control.

5.5.3.1.1 Synthesis Model

The synthesis model is formed, as given in Figure 5.30. The linearized synthesis model is to be used as an input to the MATLAB[®] `lqr` function, by which the full state feedback gains are solved. In synthesis model construction, again criterion outputs, \mathbf{Z} are formed, for the selected lateral-directional parameters to be controlled. Since, accomplishment of roll attitude control and turn coordination are essential in the concept of lateral-directional autopilot in this study, sideslip angle, β and bank angle, ϕ are selected as the output variables to be controlled with zero steady state errors. Apart from the longitudinal TECS synthesis model, the lateral-directional synthesis model allows setting “target zeros” in addition to attaching integrators to drive steady state errors to zero, where criterion outputs \mathbf{Z}_{β_e} and \mathbf{Z}_{ϕ_e} are to be formed independently. Free integrators and target zeros are attached to these two parameters in order to have tracking control, compatible with the number of control

inputs. Target zeros are the designer determined transmission zeros, in addition to the inherent plant transmission zeros. An important feature of this design technique is the asymptotic tendency of the closed loop eigenvalues to migrate toward the transmission zeros [43, 46-47]. Target zeros are determined in a manner that set the desired dynamics of the flight modes affected by the parameters to be controlled. In this case, a complex pair of zeros is added to the sideslip angle error, β_e (alternative to the sideslip velocity error, v_e) criterion output to attract the Dutch roll mode poles, whereas a real zero is added to bank angle error, ϕ_e criterion output to affect spiral mode dynamics. The effectiveness of these parameters on the respective flight modes can also be observed from the modal matrix formed in Section 3.3. In setting complex target zeros at $[\zeta, \omega_n]$, as observed from Figure 5.30, the generation of \mathbf{Z}_{β_e} is in the form of,

$$G(s) = \frac{s^2 + K_p s + K_i}{s} \quad (5.22)$$

where proportional gain $K_p = 2\zeta\omega_n$, integral gain $K_i = \omega_n^2$, and derivative gain $K_d = 1$. In creating a real target zero at $[-\lambda]$, as observed from Figure 5.30, the generation of \mathbf{Z}_{ϕ_e} is in the form of,

$$G(s) = \frac{s + \lambda}{s} \quad (5.23)$$

where proportional gain $K_p = 1$, integral gain $K_i = \lambda$, and derivative gain $K_d = 0$ [43].

The plant itself has transmission zeros over which the designer has no control (other than choosing different inputs and outputs). The plant's inherent and additional transmission zeros, can be computed by constructing the synthesis model in square form, i.e. making the number of control inputs equal to the number of regulated outputs as in this case. The obtained transmission zeros are given in Table 5.12.

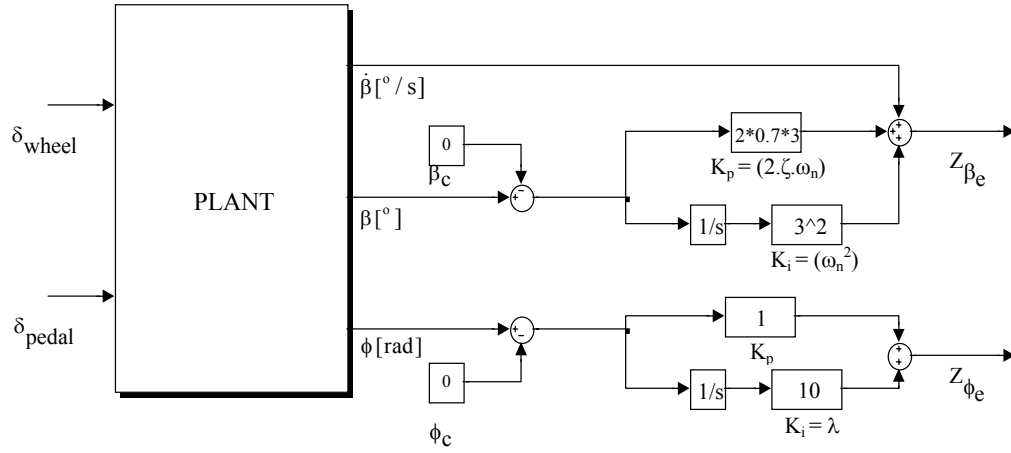


Figure 5.30 Lateral-directional synthesis model

Table 5.12 Transmission zeros of lateral-directional synthesis model

Transmission zeros	Eigenvalue	Damping, ζ	Frequency, ω_n [rad/s]
Plant's inherent	-40.33	-	-
Attached to Z_{ϕ_e}	-10.0	-	-
Attached to Z_{β_e}	$-2.1 + 2.14i$	0.7	3.0
	$-2.1 - 2.14i$		

When selecting zero locations one must keep in mind the constraints of control effectors and physics of the problem at hand. Hence, the zeros should be placed in the desired closed-loop pole locations that are consistent with the physics of the air vehicle. It was shown that by creating frequency weighted criterion variables, the designer can incorporate into the construction of synthesis model the design requirements and physical insight of the problem [47].

Following the construction of the synthesis model, linearizing should be accomplished in order to obtain the new state space model to be input to the

MATLAB[®] `lqr` function. The linearized synthesis model system matrix, $\mathbf{A}'_{\text{lat-dir.}}$, control input matrix, $\mathbf{B}'_{\text{lat-dir.}}$, and additionally the output matrix $\mathbf{C}'_{\text{lat-dir.}}$ are given by Equations (5.24), (5.25), and (5.26) respectively.

$$\mathbf{A}'_{\text{lat-dir.}} = \begin{bmatrix} -0.1425 & 9.7591 & -2.6881 & -64.5518 & 0 & 0 & 0 \\ 0 & 0 & 1 & -0.0377 & 0 & 0 & 0 \\ -0.3033 & 0 & -17.4441 & 3.5477 & 0 & 0 & 0 \\ 0.0377 & 0 & -1.3019 & -0.0604 & 0 & 0 & 0 \\ 0 & 0 & 0 & 1.0007 & 0 & 0 & 0 \\ 0.8835 & 0 & 0 & 0 & 0 & 0 & 0 \\ 0 & 1 & 0 & 0 & 0 & 0 & 0 \end{bmatrix} \quad (5.24)$$

with states, v , ϕ , p , r , ψ , $\text{Integrator}(\beta_e)$, and $\text{Integrator}(\phi_e)$, respectively.

$$\mathbf{B}'_{\text{lat-dir.}} = \begin{bmatrix} -0.008 & 0.0659 \\ 0 & 0 \\ -1.8496 & 0.1347 \\ -0.0605 & -0.0361 \\ 0 & 0 \\ 0 & 0 \\ 0 & 0 \end{bmatrix} \quad (5.25)$$

with control inputs, δ_{wheel} , and δ_{pedal} , respectively for the first and second columns.

$$\mathbf{C}'_{\text{lat-dir.}} = \begin{bmatrix} 3.5848 & 8.6221 & -2.3749 & -57.0313 & 0 & 9 & 0 \\ 0 & 1 & 0 & 0 & 0 & 0 & 10 \end{bmatrix} \quad (5.26)$$

with criterion outputs \mathbf{Z}_{β_e} and \mathbf{Z}_{ϕ_e} , respectively for the first and second rows.

5.5.3.1.2 Weighting Matrices Selection – Obtaining K_{lqr}

The next task is to determine the feedback gains by choosing the cost function weights, \mathbf{Q} and \mathbf{R} and solving the Riccati equation using MATLAB[®] `lqr` function to specify the gains. The initial values of weights are obtained by Bryson inverse square method, as defined in Section 5.5.1, and represented by Equation (5.11). The resulting \mathbf{Q} matrix diagonal elements have values of 20, 2, whereas \mathbf{R} matrix diagonal elements have values 0.4, 0.3. This point is where the target zero implementation brings advantage. If zeros are selected properly, it will require relatively small gains to move the poles near the zeros. It should be denoted that by selecting the criterion output with target zeros, the designer effectively takes care of any need for off diagonal terms in \mathbf{Q} and \mathbf{R} matrices to achieve the performance characteristics. The ambiguity of selecting proper \mathbf{Q} and \mathbf{R} weightings is alleviated and the LQ controller design approach becomes a straightforward technique well suited for use by practical control engineers [47]. The quadratic cost function of LQ approach given by Equation (5.8) is solved in the form of [43],

$$\mathbf{J} = \int_0^{\infty} (\tilde{\mathbf{x}}^T (\mathbf{C}^T \mathbf{Q} \mathbf{C}) \tilde{\mathbf{x}} + \tilde{\mathbf{u}}^T \mathbf{R} \tilde{\mathbf{u}}) dt \quad (5.27)$$

in order to involve the selected target zeros into the new \mathbf{Q} matrix, $(\mathbf{C}^T \mathbf{Q} \mathbf{C})$. The new \mathbf{Q} is given as,

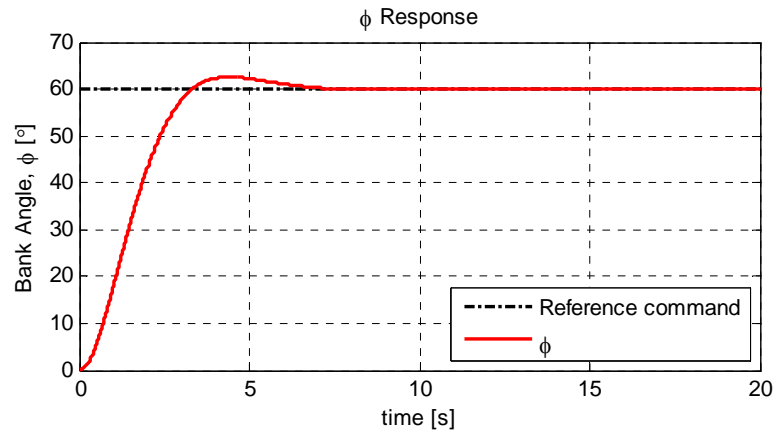
$$(\mathbf{C}^T \mathbf{Q} \mathbf{C}) = \begin{bmatrix} 257.01 & 618.17 & -170.27 & -4088.87 & 0 & 645.26 & 0 \\ 618.17 & 1488.82 & -409.54 & -9834.63 & 0 & 1551.98 & 20 \\ -170.27 & -409.54 & 112.81 & 2708.904 & 0 & -427.487 & 0 \\ -4088.87 & -9834.63 & 2708.904 & 65051.35 & 0 & -10265.6 & 0 \\ 0 & 0 & 0 & 0 & 0 & 0 & 0 \\ 645.26 & 1551.98 & -427.487 & -10265.6 & 0 & 1620 & 0 \\ 0 & 20 & 0 & 0 & 0 & 0 & 200 \end{bmatrix} \quad (5.28)$$

Utilizing MATLAB[®] `lqr` function, the optimal \mathbf{K}_{lqr} gains that satisfy the desired stability and track performance, are obtained as,

$$\mathbf{K}_{lqr} = \begin{bmatrix} 11.9831 & -1.1685 & -14.8791 & -174.1499 & 0.0 & 31.8022 & -19.3685 \\ 27.4093 & 96.4444 & 12.7923 & -506.6139 & 0.0 & 63.6514 & 12.9028 \end{bmatrix} \quad (5.29)$$

where, the columns correspond to the gains of the respective states of the enhanced system matrix, $\mathbf{A}'_{lat-dir.}$ given by Equation (5.24); and the rows correspond to the gains of the respective control inputs of the enhanced control input matrix $\mathbf{B}'_{lat-dir.}$, given by Equation (5.25). The obtained gains are inserted into the lateral-directional linear controller model in the same manner as given by Equations (5.7) and (5.21).

The lateral-directional linear model with inner loop controller is simulated to check if the roll attitude control with coordinated turn is accomplished well, in terms of related flight control requirements, given in Section 5.3. The linear model time simulation responses to 60° reference ϕ command around the mentioned trim condition are displayed by the graphs of Figure 5.31.



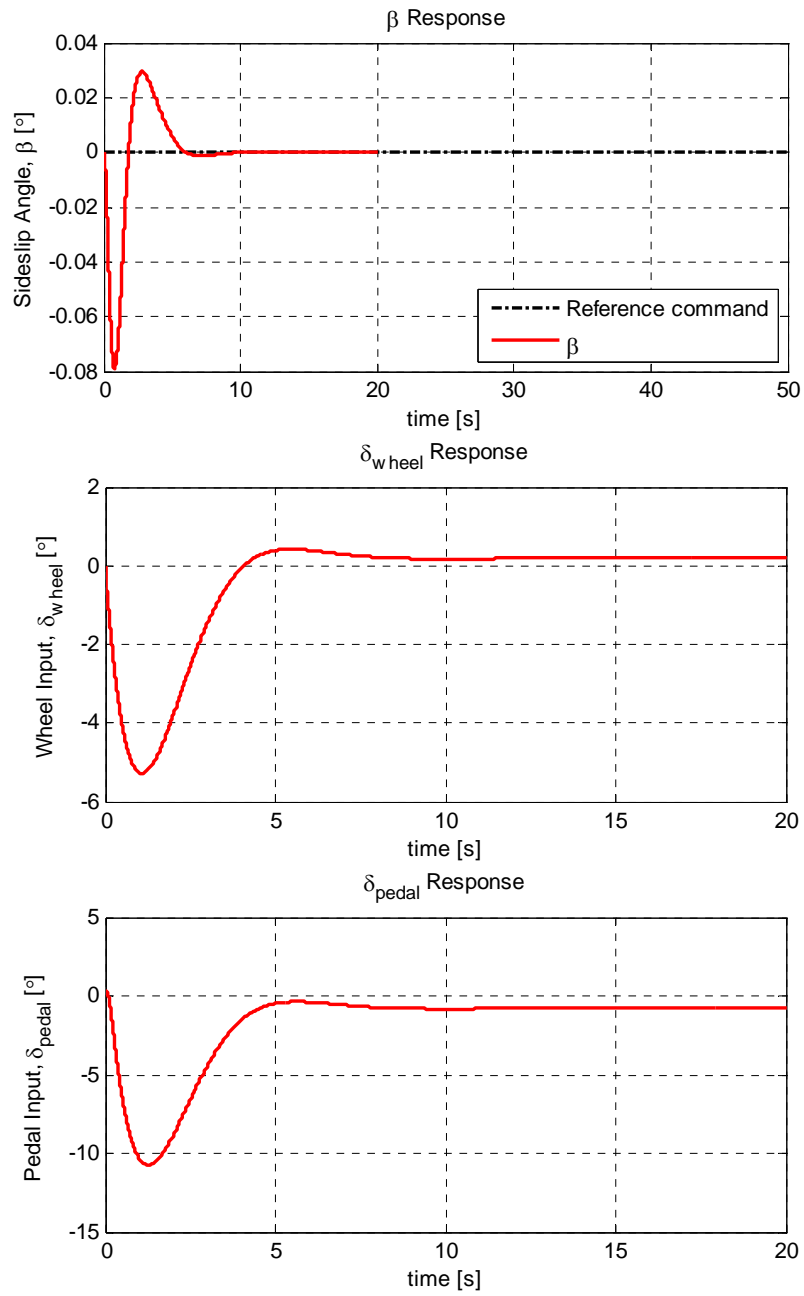


Figure 5.31 Inner loop lateral-directional controller – Linear model time simulation responses to +60° bank angle command

It can be concluded from the results that the inner loop lateral-directional controller is accomplished to give satisfying results. It is obvious that, the required $\pm 1.0^\circ$ static accuracy in roll attitude with respect to the reference given in Section 5.3.1.1 is provided with a high margin. Zero sideslip obtained after minimal changes in β parameter shows that turn coordination is well performed also. Different from the classical controller sideslip suppression system including a washout filter, in LQ controller approach, the usage of filter is not needed. This is a result of the simultaneous establishment of all the gains by optimizing, while both the sideslip regulation and bank angle control are constructed in the same synthesis model. Despite the maximum desired bank angle reference input, the changes in control inputs seem to be in moderate magnitudes, especially for δ_{wheel} . This may be an indication of too much excess control left for ailerons, since it is given a control input range of -25° to $+25^\circ$. But, it should not be forgotten that this excess control is necessary, since the possible deflection of the highly flexible long aspect ratio wings decreases the effectiveness of the ailerons located at the wing tips in real life.

Concluding that the time simulation results are satisfactory for all trim points in the flight envelope, the lateral-directional axis **Q** and **R** weighting matrices are frozen, and the gain sets are obtained utilizing the determined **Q** and **R** matrices for all linear models of different conditions in flight envelope. These sets are to be implemented into the nonlinear model, which is to be mentioned in detail in gain scheduling part.

5.5.3.2 Building up Outer Loop Lateral-Directional Controller

The outer loop lateral-directional controller structure is similar to the structure defined in respective classical controller section, 5.4.1, where the heading error acts like the reference bank angle command through a proportional gain. In outer loop heading design of the current section, the initially checked results for unity proportional heading gain, K_ψ is observed to be sufficient for a heading control with a good performance, for all flight conditions in the envelope. The time simulation heading and bank angle responses to 180° heading angle reference command of the

lateral-directional linear model with heading controller are given by the graphs of Figure 5.32. It should be noted that the inner loop bank angle command is limited to $\pm 45^\circ$. It can be concluded that, the responses are satisfying the requirements of static heading accuracy of $\pm 0.5^\circ$ of Section 5.3.2.1, and overshoot less than 1.5° , of Section 5.3.2.2.1.

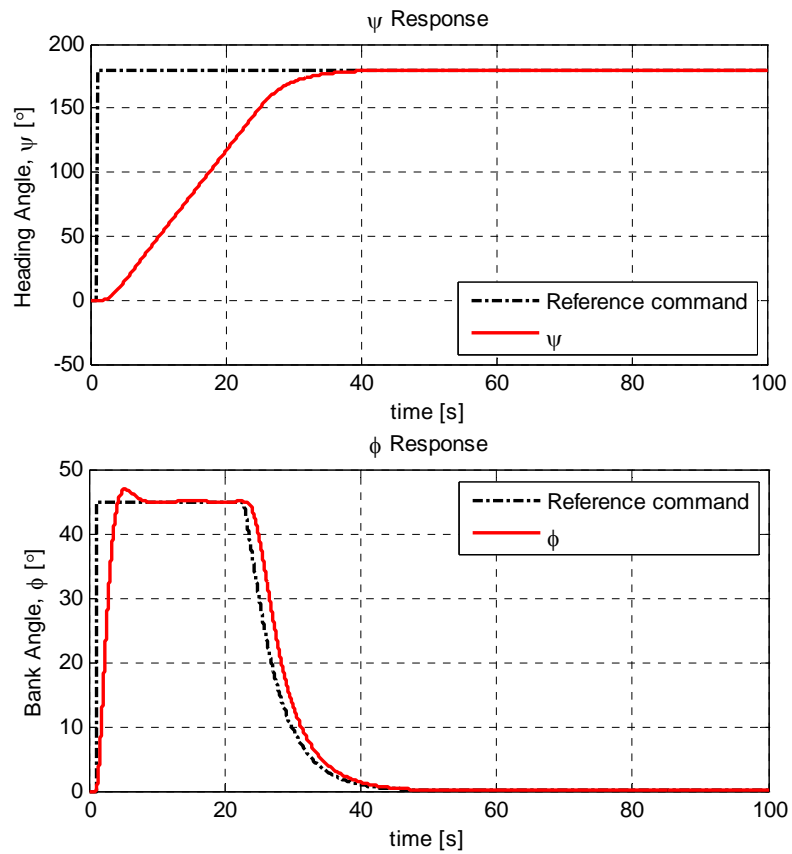


Figure 5.32 Lateral-directional linear model with heading controller simulation responses to $+180^\circ$ bank angle command

5.5.4 Closed Loop Poles

5.5.4.1 Longitudinal Controller – Closed Loop Poles

Obtaining the whole longitudinal controller structure with inner and outer loop TECS design based on LQ controller approach, the closed loop longitudinal eigenvalues can be provided and compared with the closed loop eigenvalues of the linear dynamics controlled with classical controller and open loop eigenvalues of the corresponding flight condition, which are also shown in Table 3.1 of Section 3.3. The open loop and two sets of closed loop longitudinal eigenvalues are together displayed in Table 5.13.

It is obvious from Table 5.13 that, for the LQ controlled closed loop dynamics; the lightly damped oscillatory longitudinal phugoid mode satisfies the Level 1 requirements in terms of dynamic stability with a damping ratio value of 0.969, as it is also the case for the classical controlled linear model damping ratio value, 0.0466, but with a considerable difference in values. The respective open loop damping ratio value is 0.00744 remaining in the Level 2 region as also given in Figure 4.8 of Section 4.3.1. The other oscillatory mode with high frequency, short period, is still in Level 1 region. Again, a decrease in the damping of the short period occurs, with the pitch attitude feedback to increase the phugoid mode, which is compensated by the use of pitch rate feedback to a limited level. It is obvious that, in LQ controlled dynamics, the decrease in short period damping is lower relative to the classical controlled linear model dynamics. All the real axis poles of the longitudinal dynamics are damped in the closed loop system including the altitude mode for both controllers.

Table 5.13 Eigenvalues of the nominal open loop and two closed loop linear models in longitudinal axis

	Eigenvalues	Damping Ratio, ζ	Natural Frequency, ω_n [rad/s]
Open loop linear model / longitudinal axis	0.000188	-	-
	$-0.00154 + 0.207i$	0.00744	0.207
	$-0.00154 - 0.207i$		
	$-1.31 + 2.11i$	0.529	2.48
	$-1.31 - 2.11i$		
Closed loop linear model (classical control) / longitudinal axis	-0.143	-	-
	-0.667	-	-
	$-0.0640 + 1.37i$	0.0466	1.37
	$-0.0640 - 1.37i$		
	$-0.359 + 1.55i$	0.227	1.59
	$-0.359 - 1.55i$		
	-5.57	-	-
	-72.5	-	-
Closed loop linear model (LQ control) / longitudinal axis	-0.264	-	-
	-0.298	-	-
	$-2.73 + 0.699i$	0.969	2.82
	$-2.73 - 0.699i$		
	$-1.41 + 3.03i$	0.422	3.34
	$-1.41 - 3.03i$		
	-1.69	-	-

5.5.4.2 Lateral-Directional Controller – Closed Loop Poles

Obtaining the whole lateral-directional controller structure with inner and outer loop controller design based on LQ controller approach, the closed loop lateral-directional axis eigenvalues can be provided and compared with the closed loop eigenvalues of the linear dynamics controlled with classical controller and open loop eigenvalues of the corresponding flight condition, which are also shown in Table 3.1 of Section 3.3. The open loop and two set of closed loop longitudinal eigenvalues are together displayed in Table 5.14.

Table 5.14 Eigenvalues of the nominal open loop and two closed loop linear models in lateral-directional axis

	Eigenvalues	Damping Ratio, ζ	Natural Frequency, ω_n [rad/s]
Open loop linear model / lateral-directional axis	0.0103	-	-
	0.0	-	-
	$-0.167 + 2.03i$	0.0821	2.04
	$-0.167 - 2.03i$		
	-17.3	-	-
Closed loop linear model (classical control) / lateral-directional axis	-0.0535	-	-
	-0.124	-	-
	-0.254	-	-
	-0.789	-	-
	$-9.63 + 13i$	0.596	16.2
	$-9.63 - 13i$		
	-31.9	-	-
Closed loop linear model (LQ control) / lateral-directional axis	-0.226	-	-
	$-0.606 + 0.561i$	0.734	0.826
	$-0.606 - 0.561i$		
	$-2.07 + 2.14i$	0.695	2.98
	$-2.07 - 2.14i$		
	-13.3	-	-
	-58.5	-	-

It can be concluded from Table 5.14 that, the closed loop oscillatory Dutch roll mode satisfies the Level 1 requirements with both of the controllers, in terms of dynamic stability at a region considerably beyond Level 2, for which the respective open loop dynamic stability characteristics are given in Figure 4.9 of Section 4.3.2. A damping ratio of 0.596 and a natural frequency of 16.2 rad/s is the result for classical controlled linear model, whereas a damping ratio of 0.695 and a natural frequency of 2.98 rad/s is the result for LQ controlled linear model. It should be reminded that the damping ratio and natural frequency values are designer selected values in LQ controller approach by implementation of target zeros. Additionally, the undamped

spiral and heading modes of the open loop system are damped with both controllers implementation, where in LQ controlled linear model, the real axis spiral mode is transferred to complex poles, with a damping ratio of 0.734 and natural frequency of 0.826 rad/s. It is known that target zero implementation in criterion output ϕ_e is effective for this mode. In both controlled linear models, the spiral mode has the time to half characteristic, instead of open loop time to double trend, which is also demonstrated in Figure 4.11 of Section 4.3.2.

5.5.5 Complete Controller – Implementing in Nonlinear Model

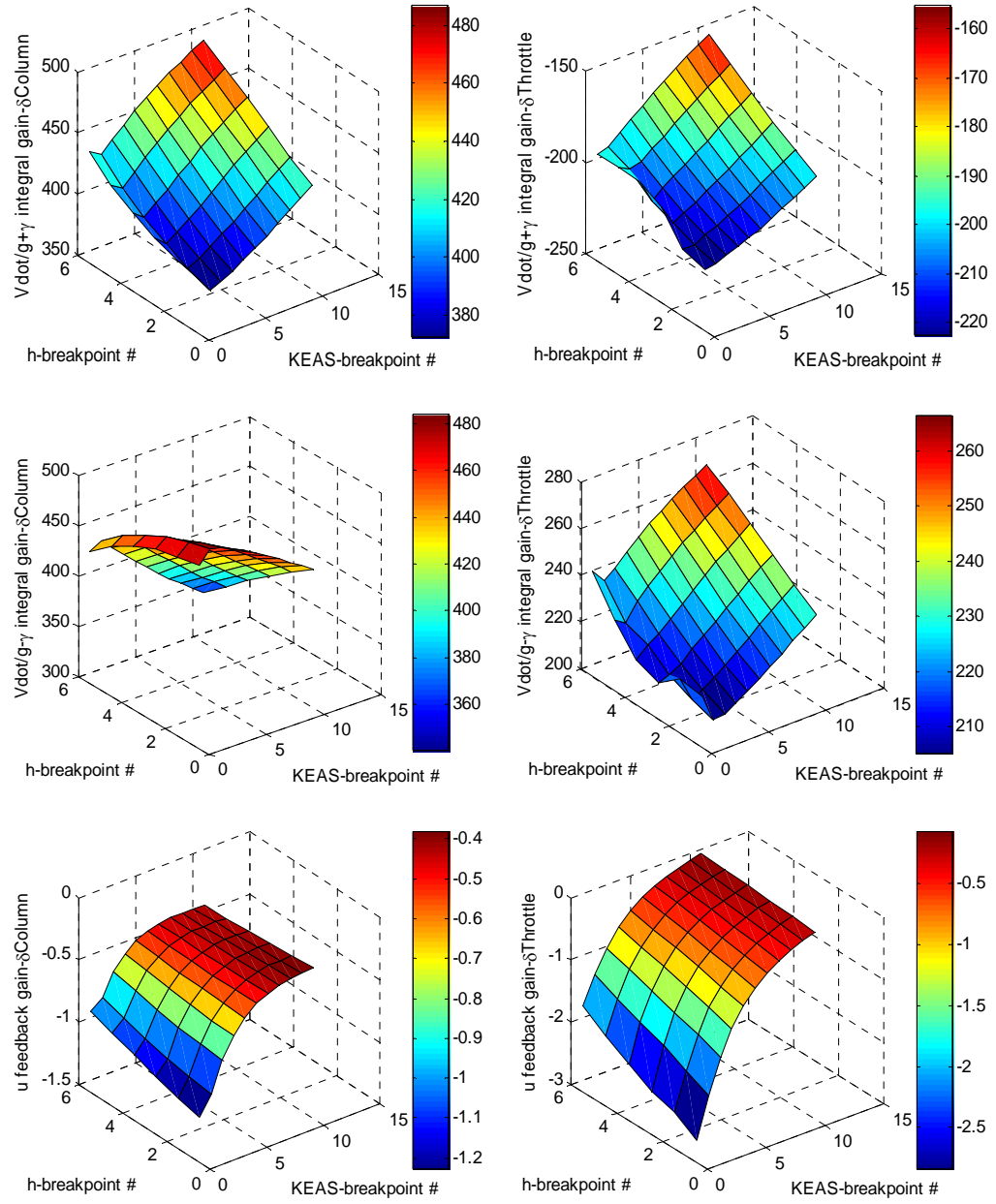
5.5.5.1 Gain Scheduling

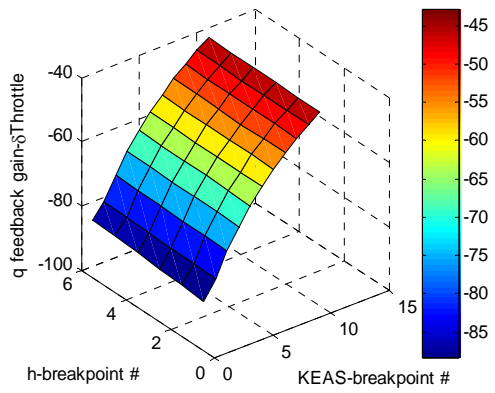
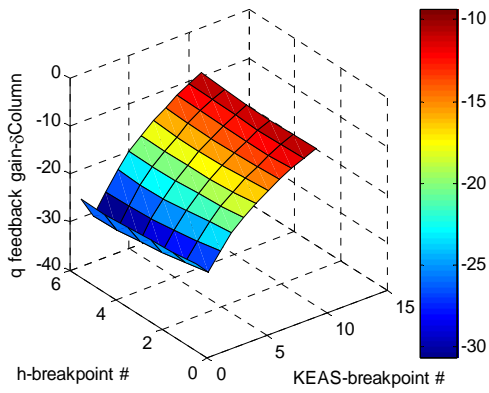
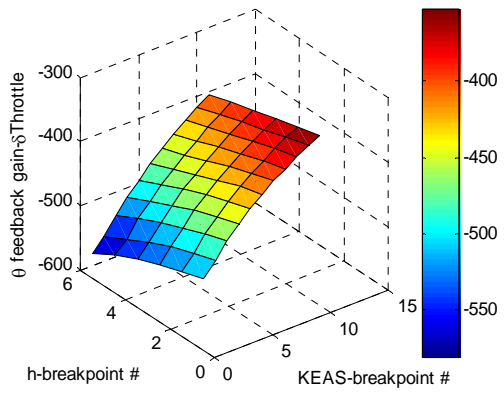
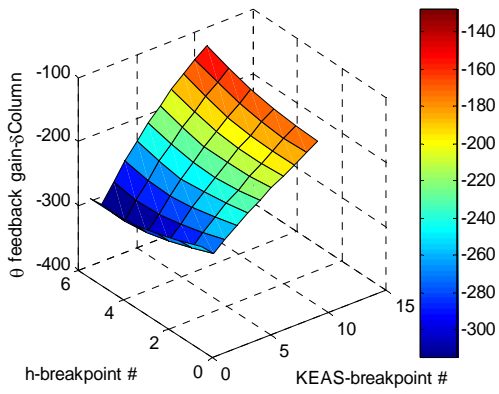
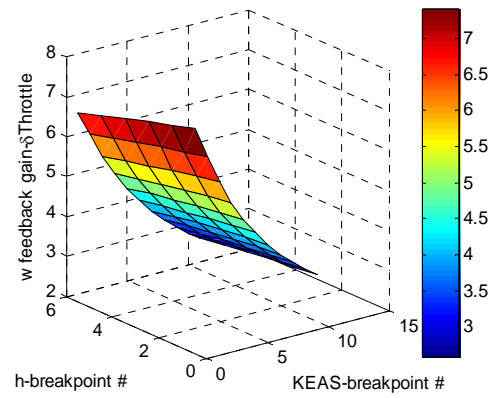
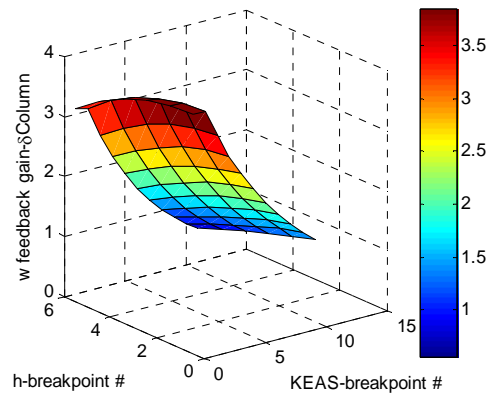
General gain scheduling definition is overviewed in detail in Section 5.4.2.1, where it also involves the procedure applied in classical controller design. The gain scheduling application procedure differs in some points for LQ controller approach. Although it is not realistic to determine design gains for every conceivable flight condition using standard classical techniques; the LQ related MATLAB[®] functions give opportunity of automating the design phase and thus increasing the gain scheduling design points in the operational flight envelope. Increasing the number of trim points is desirable for controller designs to be much more effective and realistic over the whole envelope, since they are linearly interpolated. Once frozen, the **Q** and **R** weighting matrices are to be used for all predetermined trim points to obtain the gains with respect to KEAS and altitude. Similar to the classical controller gain scheduling approach, the design gains obtained at the flight trim conditions are programmed in tabular, table look up form, and then linearly interpolated with respect to the current value of the scheduling signals of the independent parameters [15, 38]. In order to perform gain scheduling, respective controller gains are obtained for the linear models at the airspeeds ranging between 70 KEAS and 120 KEAS by 5 KEAS increments, and between 5,000 ft (1,524 m) and 30,000 ft (9,144 m) altitudes by 5,000 ft (1,524 m) increments. Therefore, apart from the classical controller gain scheduling points, 66 total trim points for gain scheduling are picked up. The breakpoint values for KEAS and altitude are given in Table 5.15.

Table 5.15 Breakpoint values of airspeed and altitude

h-breakpoint # KEAS-breakpoint #	1	2	3	4	5	6
1	70 KEAS, 5,000 ft	70 KEAS, 10,000 ft	70 KEAS, 15,000 ft	70 KEAS, 20,000 ft	70 KEAS, 25,000 ft	70 KEAS, 30,000 ft
2	75 KEAS, 5,000 ft	75 KEAS, 10,000 ft	75 KEAS, 15,000 ft	75 KEAS, 20,000 ft	75 KEAS, 25,000 ft	75 KEAS, 30,000 ft
3	80 KEAS, 5,000 ft	80 KEAS, 10,000 ft	80 KEAS, 15,000 ft	80 KEAS, 20,000 ft	80 KEAS, 25,000 ft	80 KEAS, 30,000 ft
4	85 KEAS, 5,000 ft	85 KEAS, 10,000 ft	85 KEAS, 15,000 ft	85 KEAS, 20,000 ft	85 KEAS, 25,000 ft	85 KEAS, 30,000 ft
5	90 KEAS, 5,000 ft	90 KEAS, 10,000 ft	90 KEAS, 15,000 ft	90 KEAS, 20,000 ft	90 KEAS, 25,000 ft	90 KEAS, 30,000 ft
6	95 KEAS, 5,000 ft	95 KEAS, 10,000 ft	95 KEAS, 15,000 ft	95 KEAS, 20,000 ft	95 KEAS, 25,000 ft	95 KEAS, 30,000 ft
7	100 KEAS, 5,000 ft	100 KEAS, 10,000 ft	100 KEAS, 15,000 ft	100 KEAS, 20,000 ft	100 KEAS, 25,000 ft	100 KEAS, 30,000 ft
8	105 KEAS, 5,000 ft	105 KEAS, 10,000 ft	105 KEAS, 15,000 ft	105 KEAS, 20,000 ft	105 KEAS, 25,000 ft	105 KEAS, 30,000 ft
9	110 KEAS, 5,000 ft	110 KEAS, 10,000 ft	110 KEAS, 15,000 ft	110 KEAS, 20,000 ft	110 KEAS, 25,000 ft	110 KEAS, 30,000 ft
10	115 KEAS, 5,000 ft	115 KEAS, 10,000 ft	115 KEAS, 15,000 ft	115 KEAS, 20,000 ft	115 KEAS, 25,000 ft	115 KEAS, 30,000 ft
11	120 KEAS, 5,000 ft	120 KEAS, 10,000 ft	120 KEAS, 15,000 ft	120 KEAS, 20,000 ft	120 KEAS, 25,000 ft	120 KEAS, 30,000 ft

The inner loop longitudinal and lateral-directional LQ controller gain values depending on KEAS and h are plotted and given by graphs of Figures 5.33 and 5.34, respectively. In these two-dimensional graphs, the x and y axes are displayed as the altitude and KEAS breakpoint numbers respectively, for which the corresponding breakpoint values are given in Table 5.15. It can be concluded from the graphs that, among longitudinal gain sets, altitude feedback gain values can be approximated to zero and be ignored, whereas among lateral-directional gain sets, heading feedback gains can be ignored in the same manner. Two longitudinal outer loop proportional gains; $K_h = 0.0034$, and $K_v = 0.2418$, and one lateral-directional outer loop proportional gain, $K_\psi = 1$, are constant throughout the envelope.





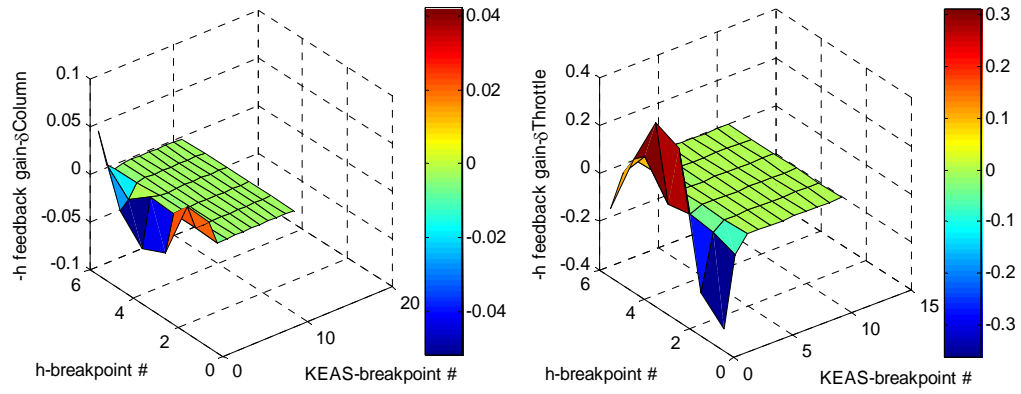
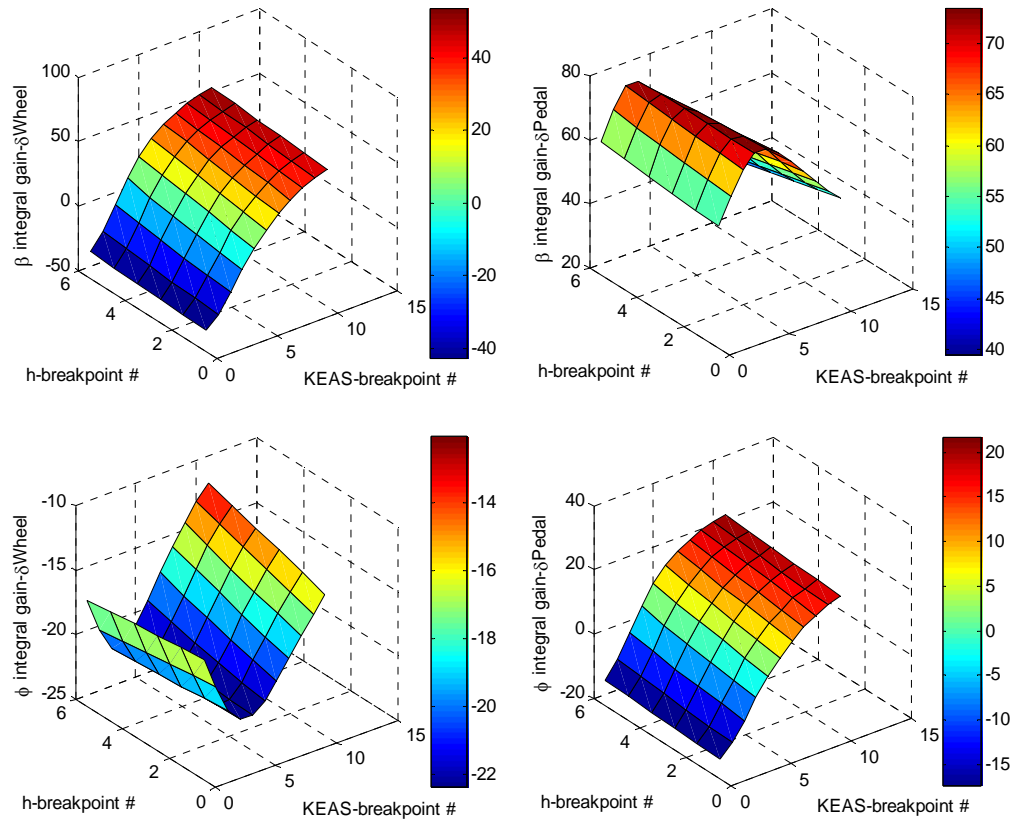
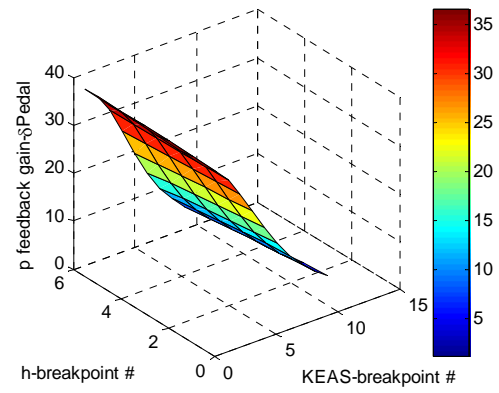
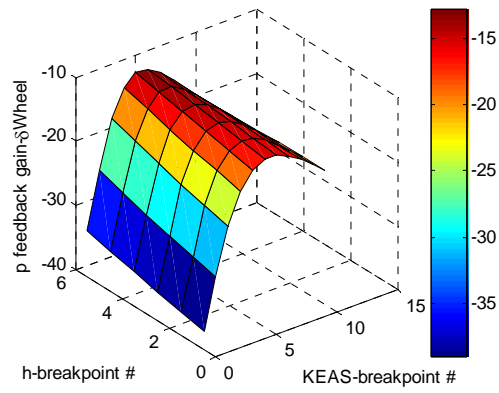
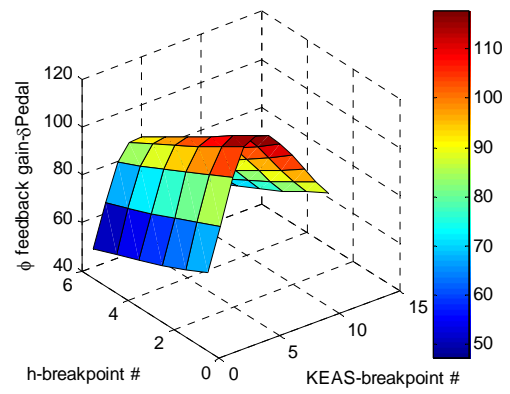
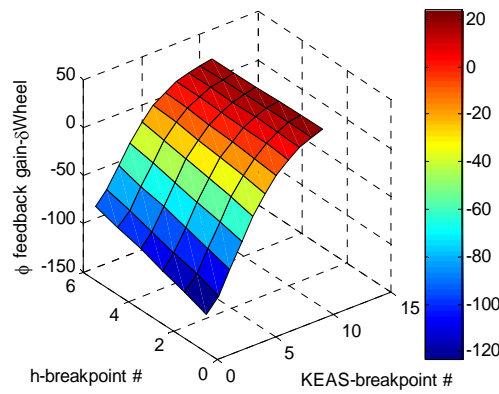
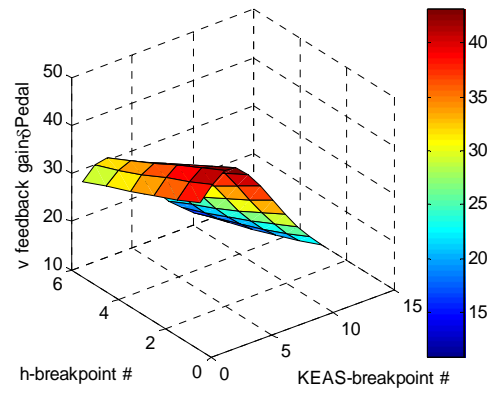
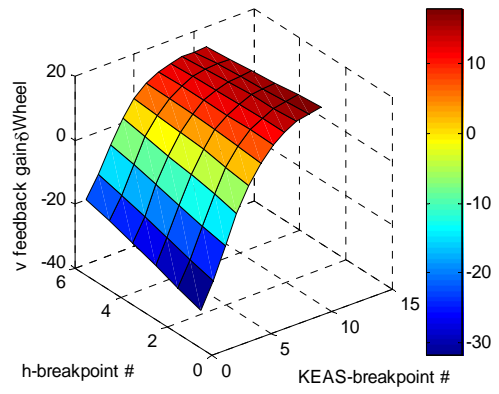


Figure 5.33 Graphs of the longitudinal LQ controller gains with respect to the dependent parameters





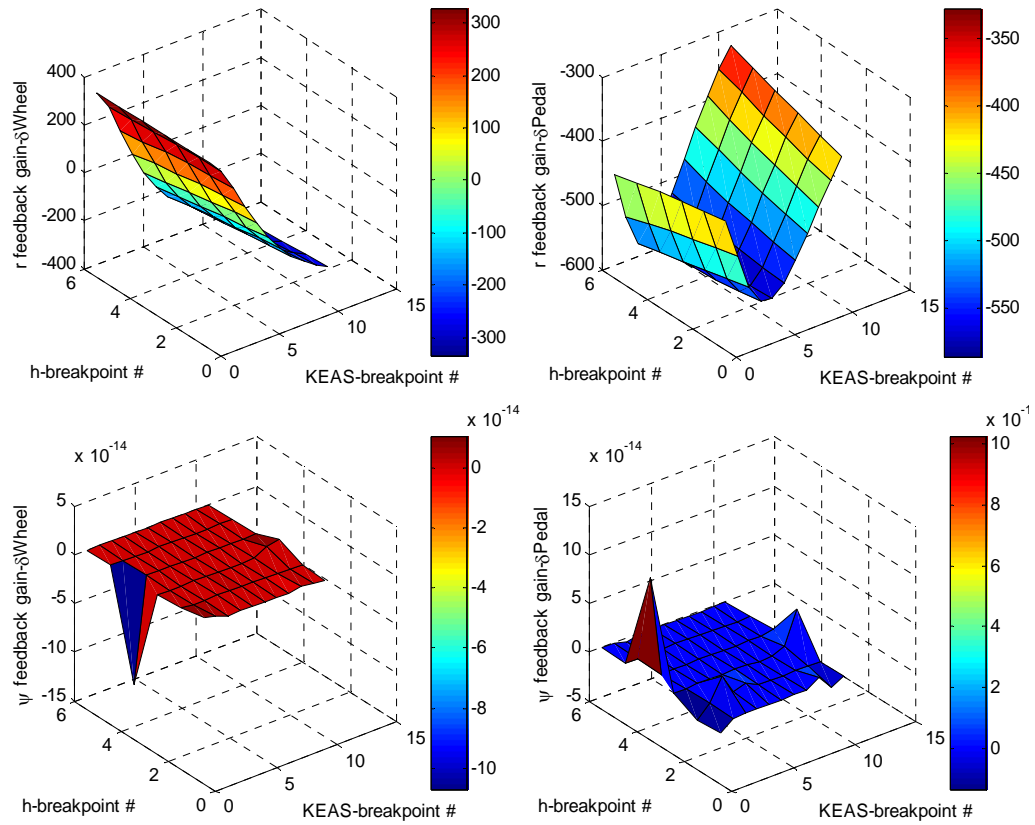


Figure 5.34 Graphs of the lateral-directional LQ controller gains with respect to the dependent parameters

5.5.5.2 Controller Input Linearization

The procedure is defined in Section 5.4.2.2, in detail. Figure 5.15 is again given in this section by Figure 5.35, in order to demonstrate the procedure, which is also applied for all inner and outer loop longitudinal and lateral-directional LQ controller structures.

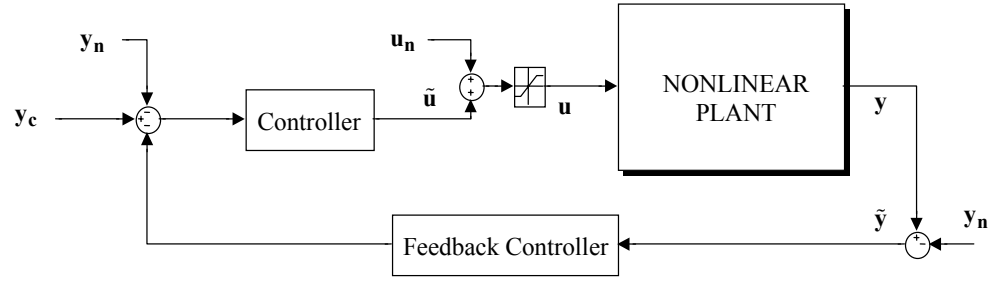


Figure 5.35 Implementation of perturbation controller into nonlinear model

5.5.5.3 Anti Integral Wind-up Scheme

The anti integral wind-up scheme constructing method, “integrator clamping” applied in this study is defined in detail in Section 5.4.2.3 of classical controller nonlinear implementation. The anti integral related figures demonstrating the construction scheme, shown by Figures 5.16 and 5.17 formerly are again displayed in this section by Figures 5.36 and 5.37, in order to remind the approach.

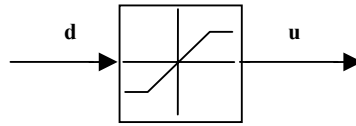


Figure 5.36 Actuator saturation function

Similar to the classical controller, in LQ controller nonlinear implementation, the engine throttle is the control on which the anti integral scheme is to be applied, since it is one of the controls that can experience command saturation. Hence, the defined

conditional anti integral wind-up scheme is implemented to the integrals of inner loop TECS, i.e. the Integrator $\left(\frac{\dot{V}_e}{g} + \gamma_e\right)$ and Integrator $\left(\frac{\dot{V}_e}{g} - \gamma_e\right)$, by disabling and holding their outputs when both \mathbf{e} multiplied with \mathbf{d} is positive and an inequality occurs between \mathbf{d} and \mathbf{u} , as shown in Figure 5.37.

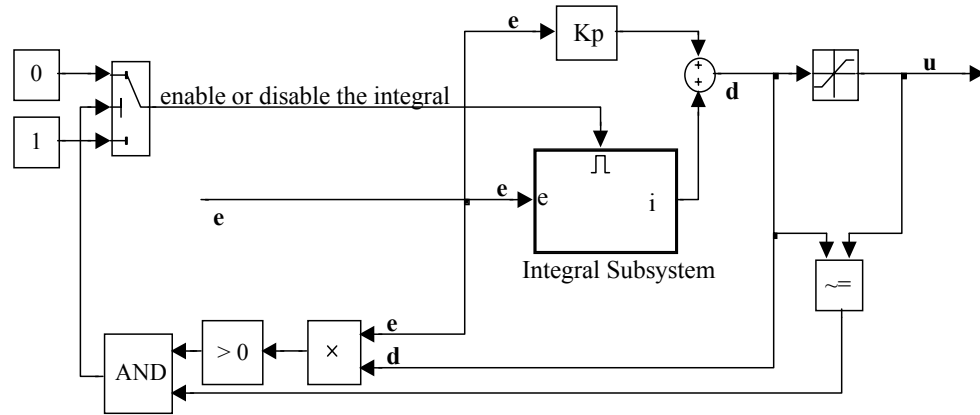


Figure 5.37 Integrator clamping ($\mathbf{e} \cdot \mathbf{d} > 0$)

Since, this time FPA, γ is commanded by the longitudinal TECS including commands coming through high desired altitude and airspeed values in the operational flight envelope, it is important to have reasonable limits for γ values throughout the flight envelope in LQ controller structure. In a similar case, a dynamic limiting function in Simulink[®] complete controlled nonlinear model is utilizing, besides the anti integral wind-up scheme. The upper γ limits are determined by trimming the nonlinear model by fixing the throttle to the maximum value and floating the FPA, whereas the lower γ limits are determined by trimming for the minimum throttle value and floating the FPA. These trims are carried out at the flight conditions corresponding to the LQ controller gain scheduling breakpoint values of

KEAS and h given in Table 5.15 and implemented into the two dimensional look up tables to interpolate and extrapolate the values. Since, the output of these lookup tables are the total γ values of the air vehicle, in order to comply with the perturbation controller structure, the trim γ values are subtracted from the lookup table outputs to generate the upper and lower bounds of the dynamic saturation function feeding into the perturbed inner loop TECS. By this way, depending on KEAS and h , the lower and upper limits are changed during the simulation process, not to have an unnecessarily high or low FPA commands. The graphs displaying the lower and upper total air vehicle γ values and their dependency on airspeed and altitude are given by Figure 5.38.

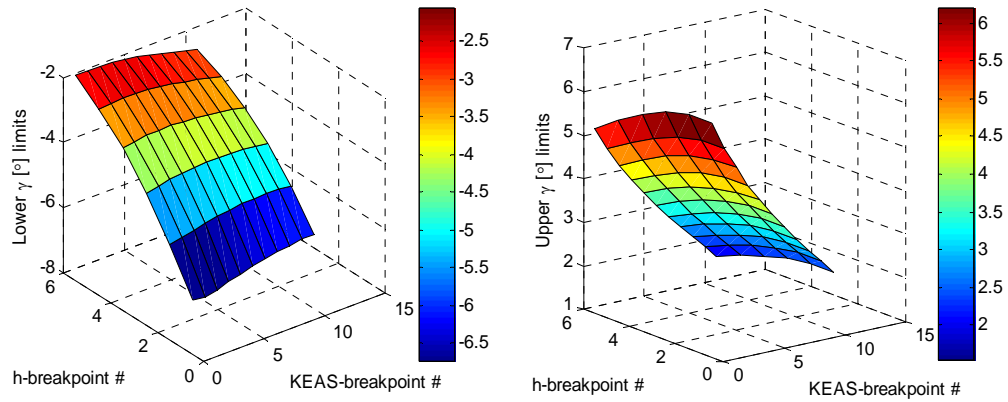
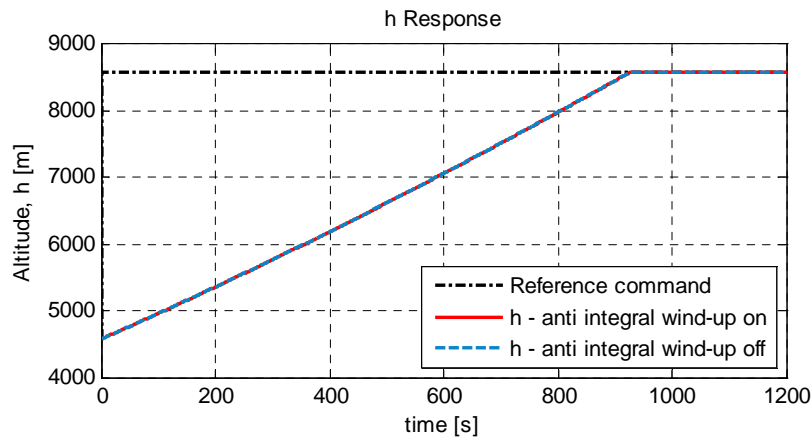


Figure 5.38 Lower and upper γ limits throughout the operational flight envelope

The effects of the anti integral wind-up scheme together with the dynamic γ limiting implementations are displayed by graphs of Figure 5.39 and 5.40 for h , FPA, V , throttle input and demanded throttle input parameters. The graphs are obtained by comparing the results of the complete controlled nonlinear model with and without

the indicated implementations. Figure 5.39 shows the responses to a +4,000 m reference altitude increase command, and Figure 5.40 shows the responses to a +35 knots reference airspeed increase command starting from an initial condition of 100 KEAS and 15,000 ft (4,572 m) altitude. It can be seen from the Figure 5.39 that how the structure of the TECS design decreases the dependency on anti integral wind up implementation apart from the classical longitudinal controller. The small proportional altitude gain, K_h , between desired altitude input and FPA limiter without any beforehand integrator pass is of primary importance in this case. Thus, the altitude errors do not reach undesirably high values causing the aft coming integrators; Integrator $\left(\frac{\dot{V}_e}{g} + \gamma_e\right)$ and Integrator $\left(\frac{\dot{V}_e}{g} - \gamma_e\right)$ to wind up. The effect of the anti integrator wind-up is only sensed when a high airspeed command is given, as seen from Figure 5.40. However, it is a fact that the existence of such a scheme is important, against the model uncertainties and possible computed higher than real air vehicle limits of FPA, γ .



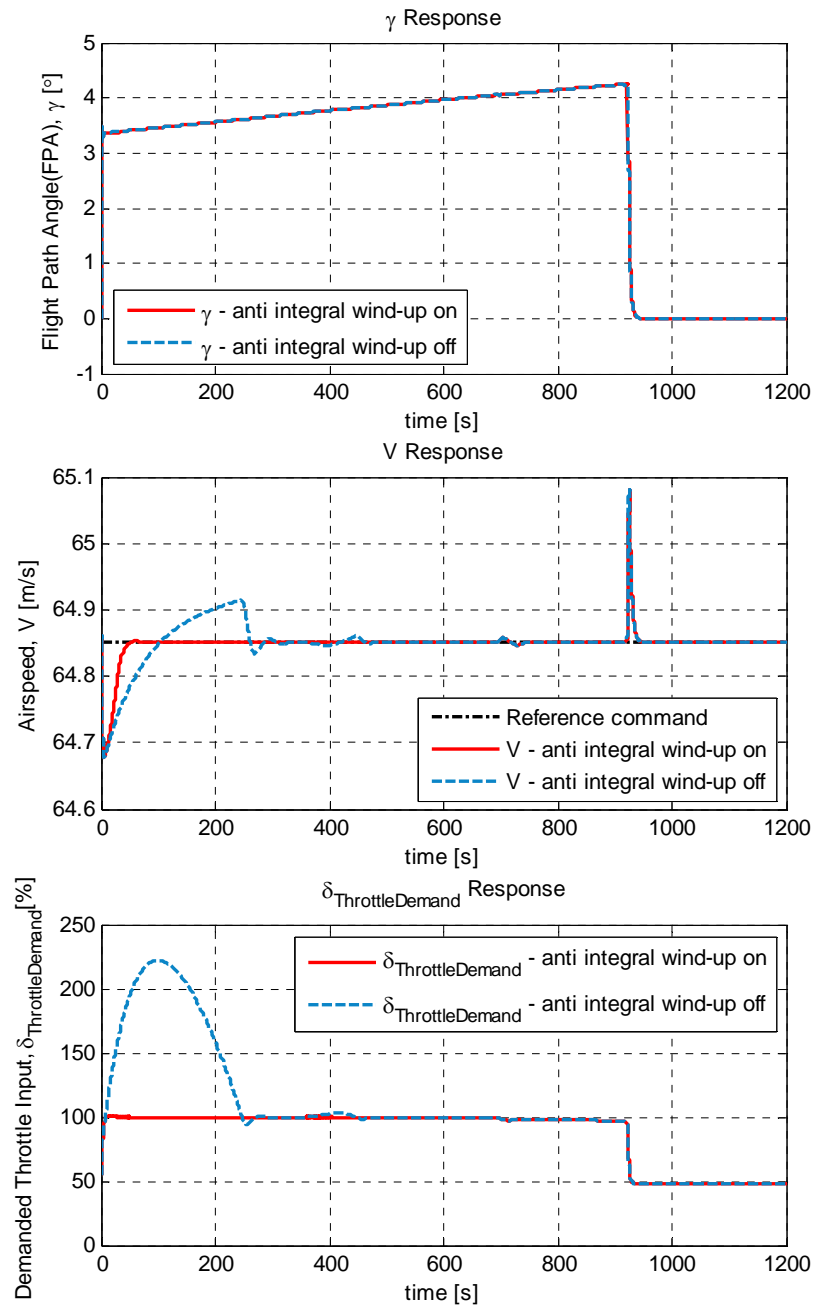
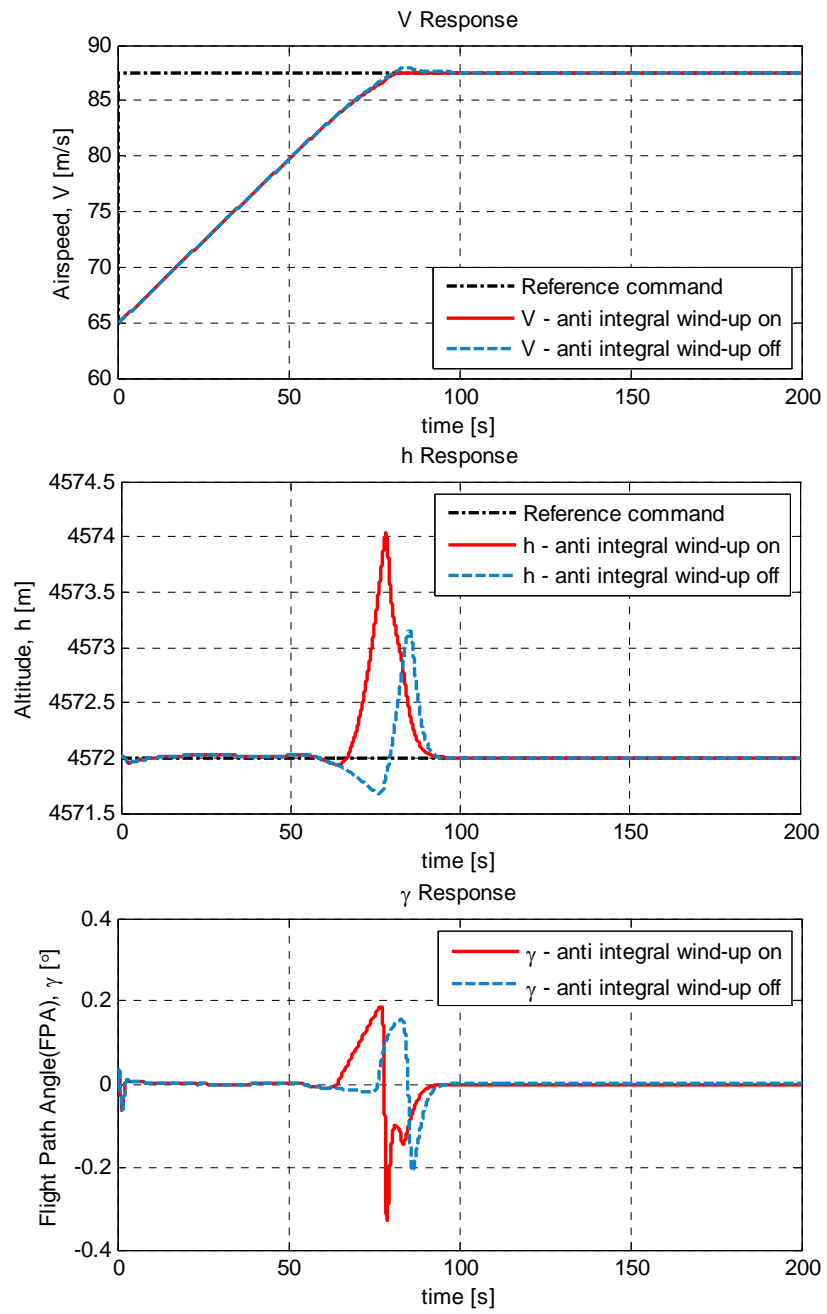


Figure 5.39 Responses to 4,000 m reference altitude increase command with and without anti-integral wind up



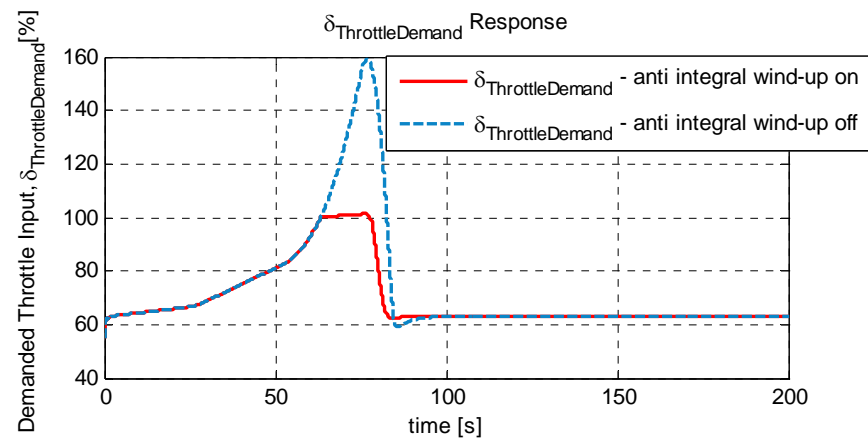


Figure 5.40 Responses to 35 knots reference KEAS increase command with and without anti-integral wind up

CHAPTER 6

CASE STUDIES – CLOSED LOOP NONLINEAR MODEL SIMULATIONS & COMPARISON

6.1 Introduction

This chapter focuses on the time simulation results of the nonlinear model with two different embedded controllers designed throughout the previous chapter with classical and LQ control approaches. The time simulation responses are to be compared in terms of the flight control requirements of Section 5.3.

It should be noted that all the analyses are done starting from the trim condition 100 KEAS 15,000 ft (4,572 m), and the anti integral wind-up scheme is engaged all the time.

6.2 Comparison Results – Flight Control Requirements

CASE I: *Pitch attitude hold flight control requirement; Refer to flight control requirements Section 5.3.1.1 requiring a static accuracy of $\pm 0.5^\circ$ in pitch attitude (assumed to be applicable to flight path angle, γ control regarding the LQ controller also).*

CASE I(a): Responses to $+3^\circ$ pitch attitude, θ increase reference step command for closed loop nonlinear model with classical controller are shown by graphs of Figure 6.1.

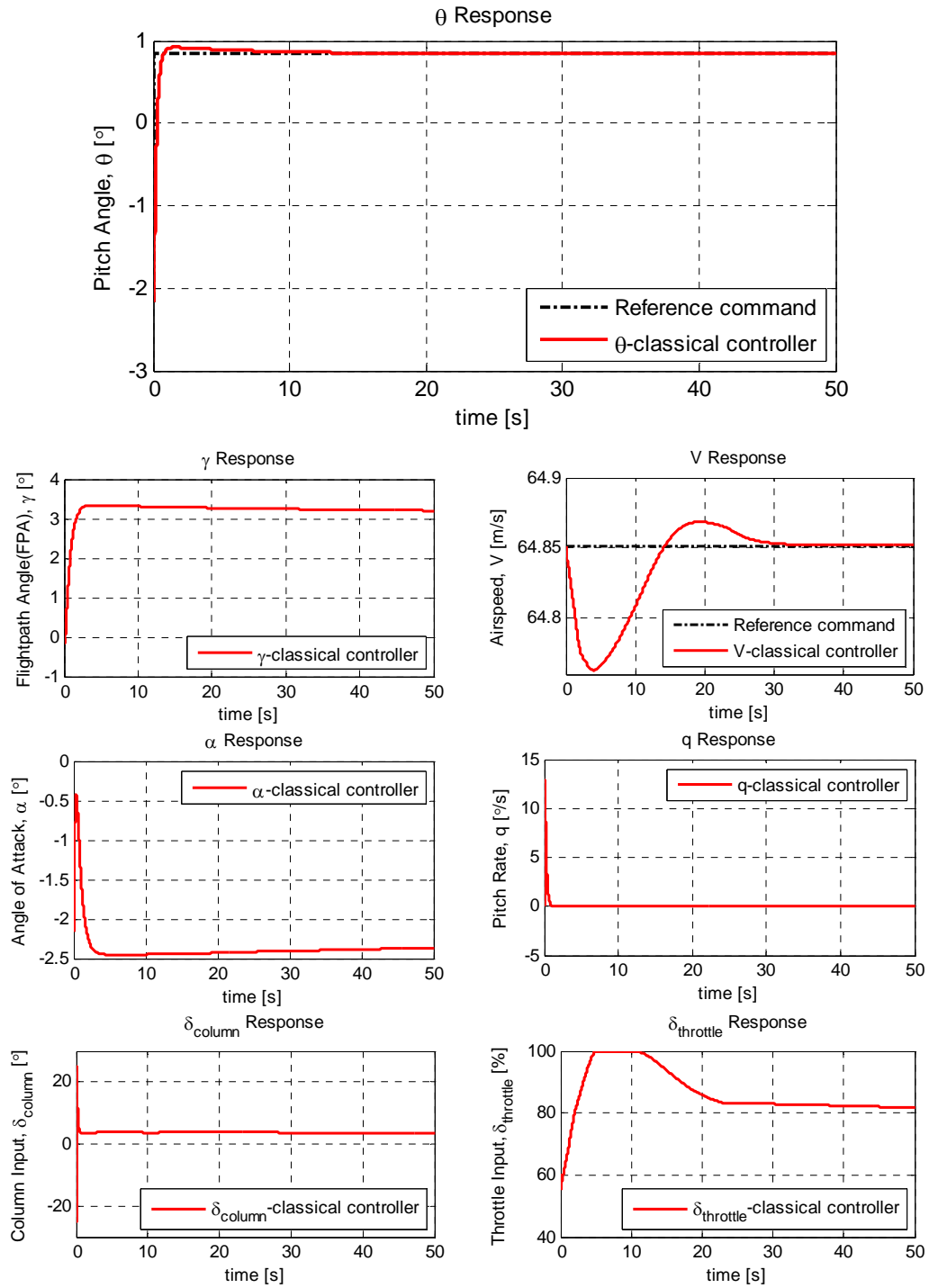


Figure 6.1 Classical controlled nonlinear model responses to +3° θ increase reference step command

In this case, a $+3^\circ$ θ increase reference command is given with respect to the reference attitude, -2.16° pitch angle. Around the current flight condition, it is a high value demand regarding the maximum throttle response, 100%, as seen in the throttle response graph. The compatibility with the respective flight control requirement is investigated by the first graph of Figure 6.1, for which the minimum accuracy in the graph's time range is $+0.001^\circ$, well satisfying the requirement.

CASE I(b): Responses to $+3.35^\circ$ flight path angle, γ increase reference step command for closed loop nonlinear model with LQ controller are shown by graphs of Figure 6.2.

In this case, a $+3.35^\circ$ γ increase reference command is given with respect to the reference attitude, 0° flight path angle. Around the current flight condition, it is a high value demand regarding the maximum throttle response, 100%, as seen in the throttle response graph. The compatibility with the respective flight control requirement is investigated by the first graph of Figure 6.2, for which the static accuracy is peak-to-peak $+0.0002^\circ$ and -0.0004° , well satisfying the requirement.

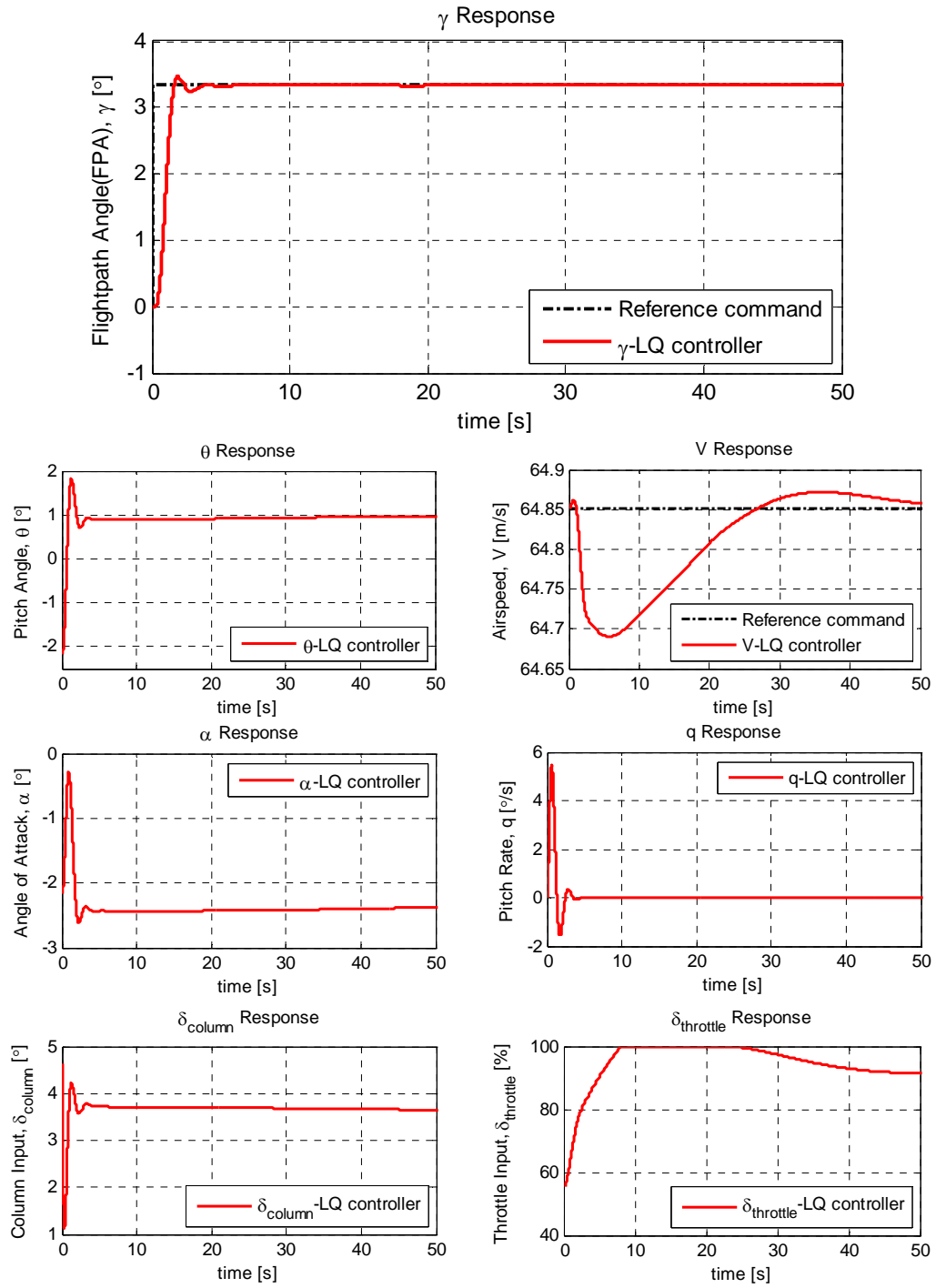


Figure 6.2 LQ controlled nonlinear model responses to +3.35° γ increase reference step command

The equivalent commands for pitch attitude and FPA are tried to be given for classical and LQ controlled models, respectively. Therefore, comparing Figures 6.1 and 6.2, leads to the conclusion that, the rise time of the classical pitch attitude controller is lower than the rise time of the LQ flight path angle controller, which seems advantageous, especially in terms of faster airspeed deviation termination. However, the classical controlled model has the responses showing considerably high peak pitch rate and column control input magnitudes with respect to the LQ controlled responses, which is not very desirable.

CASE II: *Pitch transient response flight control requirement; Refer to flight control requirements Section 5.3.1.1.1 (assumed to be applicable to flight path angle, γ control regarding the LQ controller also).*

CASE II(a): Responses of Figure 6.3 are obtained by giving a negative continuous column input that create pitch attitude disturbance causing $+4.4^\circ$ ($+6.56^\circ$ increase with respect to reference attitude, -2.16°) at 1.35 seconds which exceeds at least $\pm 5^\circ$ pitch angle change condition of the requirement.

It can be concluded from the first graph of Figure 6.3 that, the pitch attitude is returned to its initial condition with no overshoot, which is a desirable behavior put forward by the requirement. The other requirement for the pitch transient response, allowing change of airspeed within 5% of the trim airspeed is well satisfied with a 2.24% maximum change in airspeed.

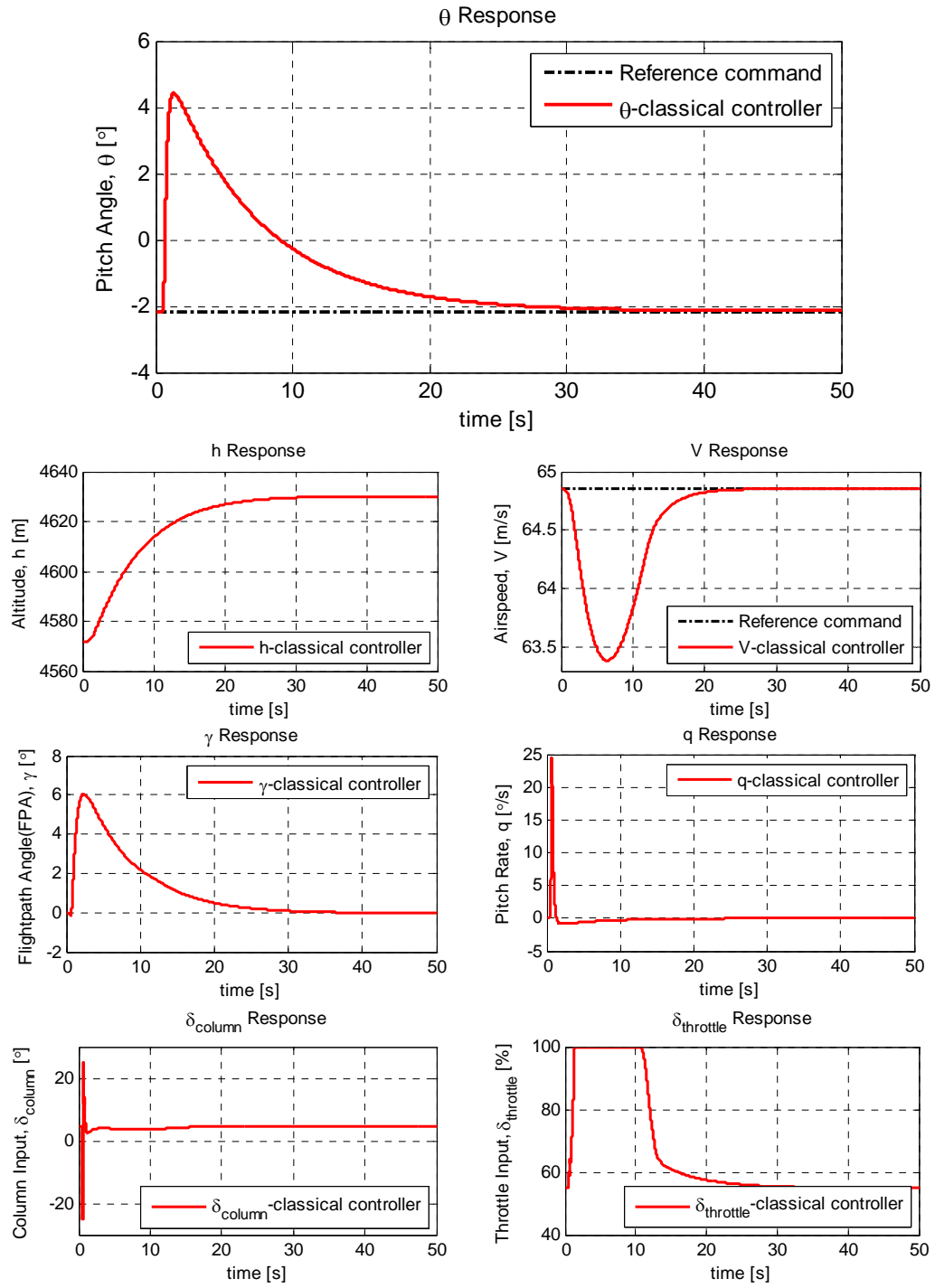
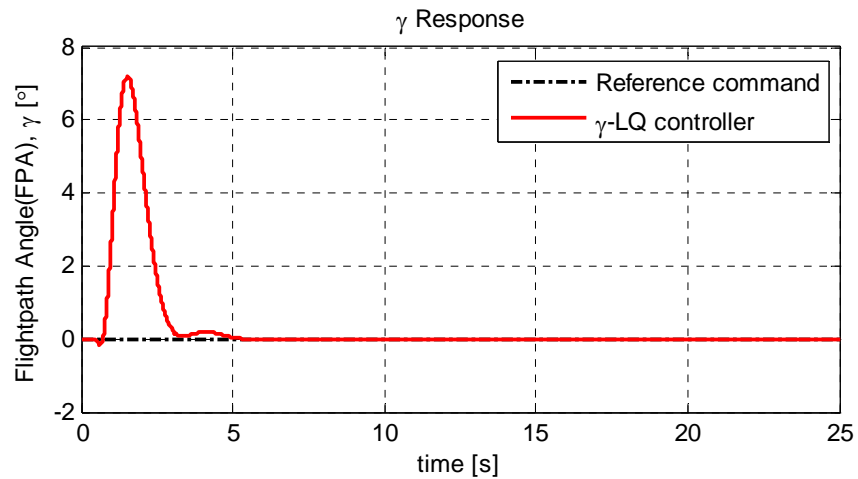


Figure 6.3 Classical controlled nonlinear model responses to continuous column input generating +6.56° change in pitch attitude

CASE II(b): Responses of Figure 6.4 are obtained by again giving a continuous negative column input that create flight path angle disturbance causing a $+7.2^\circ$ increase with respect to 0° reference FPA at 1.53 seconds time, which exceeds $\pm 5^\circ$ FPA change regarding the requirement.

It can be concluded from the first graph of Figure 6.4 that, the FPA is returned to its initial condition after the disturbance with undershoot which is 2.58% of the respective deviation, for which it can be concluded that the requirement is satisfied since no overshoot occurs. The other requirement for the pitch transient response, allowing change of airspeed within 5% of the trim airspeed is well satisfied with an 0.98% maximum change in airspeed.



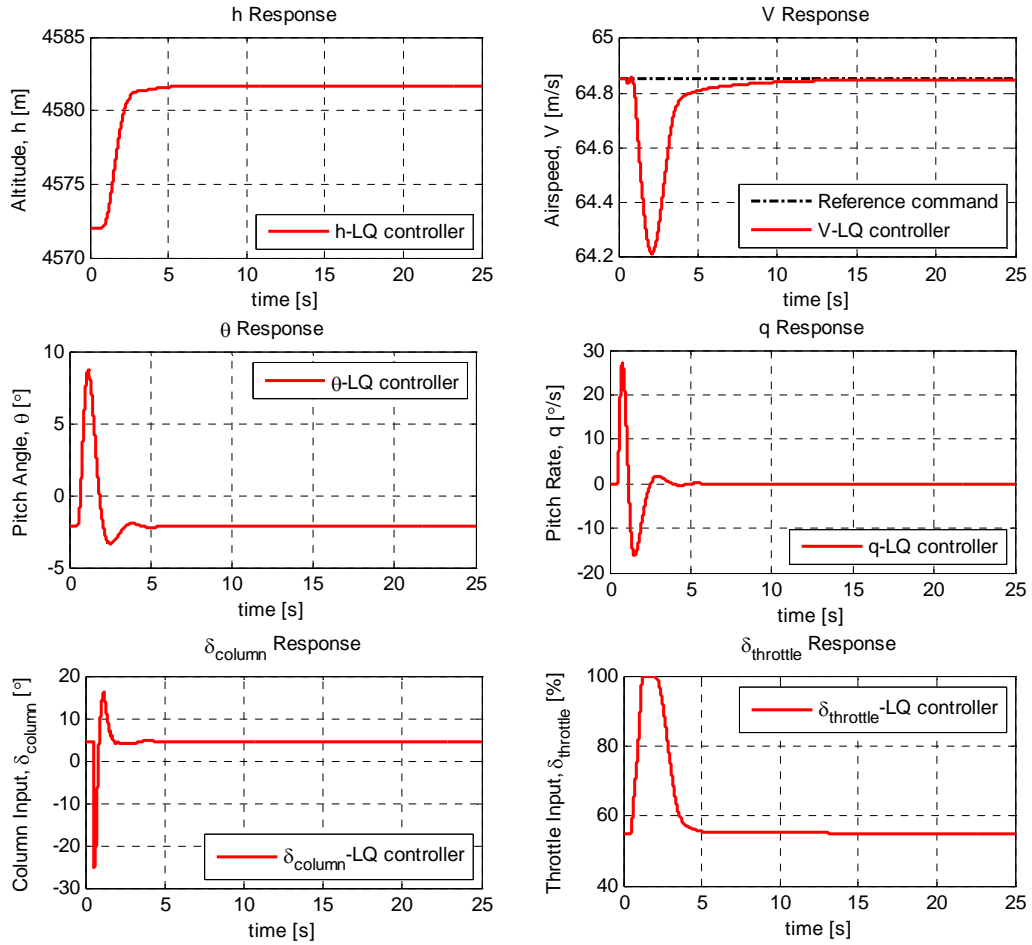


Figure 6.4 LQ controlled nonlinear model responses to column pulse input generating +7.2° change in FPA

Again as a result of a rough comparison between Case II(a) and (b), it can be concluded that, the transient responses to reject disturbances are faster for LQ controlled model than classical controlled one, which also causes the overpowering period to become shorter and airspeed related requirement to be satisfied better. However this causes oscillatory characteristics for the LQ controlled model at the time the vehicle is returned to its initial attitude, whereas for the classical controlled model the return characteristic is very smooth.

CASE III: *Roll attitude hold flight control requirement; Refer to flight control requirements Section 5.3.1.1 requiring a static accuracy of $\pm 1.0^\circ$ in roll attitude / Altitude coordinated turn flight control requirement; Refer to flight control requirements Section 5.3.2.2.2.*

Responses to $+45^\circ$ roll attitude, ϕ increase reference step command for closed loop nonlinear models with classical and LQ controllers together are shown by graphs of Figure 6.5.

In this case, a $+45^\circ$ ϕ increase reference command is given with respect to the reference attitude, 0° roll angle. It is a high value demand since it is selected to be the limit value to be commanded. The compatibility with the respective flight control requirement is investigated by the first graph of Figure 6.5, for which the minimum static accuracy is $+0.165^\circ$ for classical controlled response for the displayed time range, whereas for LQ controlled response the static accuracy has a constant value of zero, well satisfying the related requirement.

Another important difference can also be observed from the first graph that settling time for classical controlled response is about 40 s whereas it is approximately 8 s for LQ controlled response. Also, the peak magnitudes of roll rate, wheel and pedal control input responses are high for classical controlled model, for which the excess is not desirable by being close to saturation points.

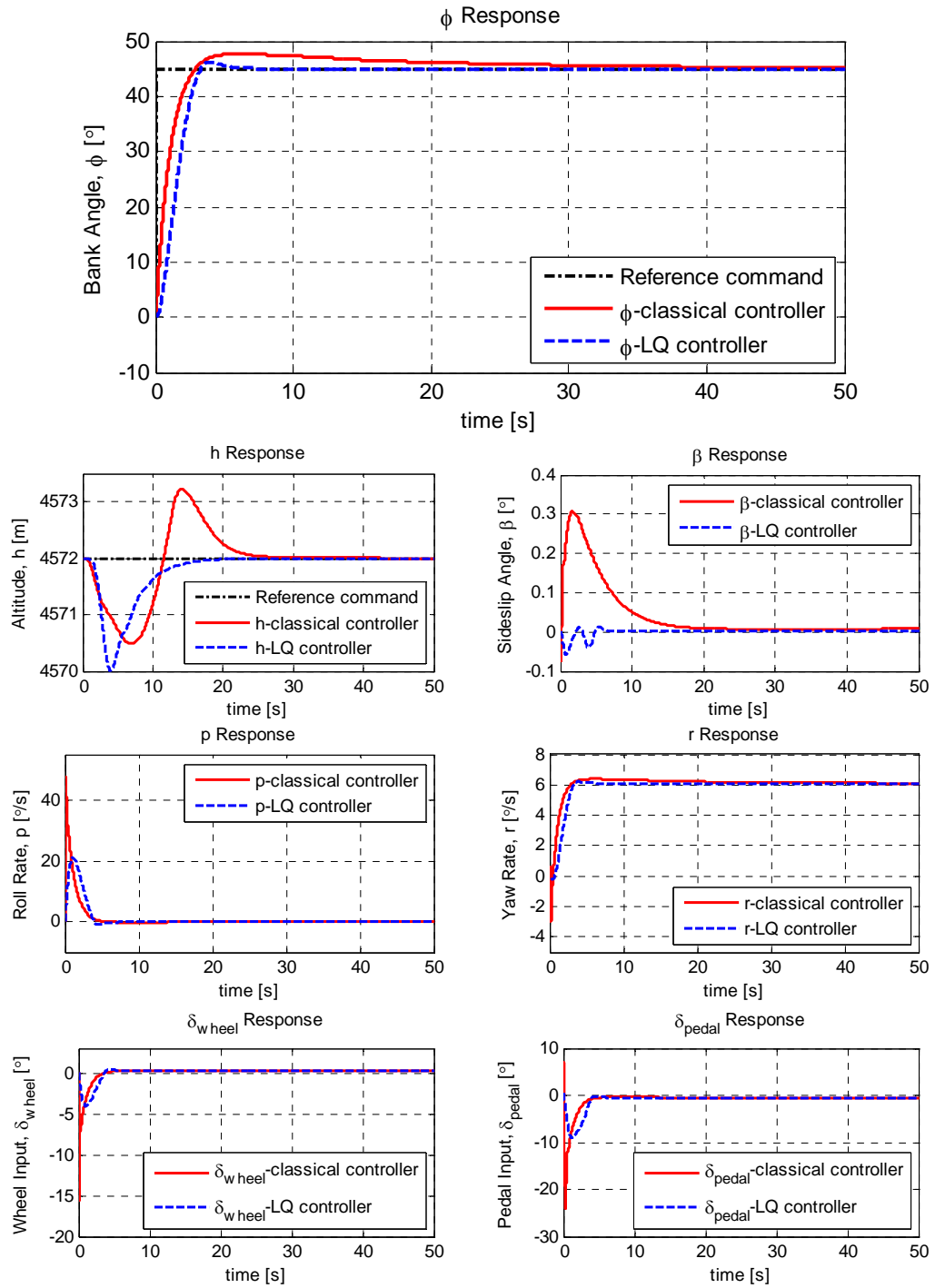


Figure 6.5 Classical and LQ controlled nonlinear model responses to +45° ϕ increase reference step command

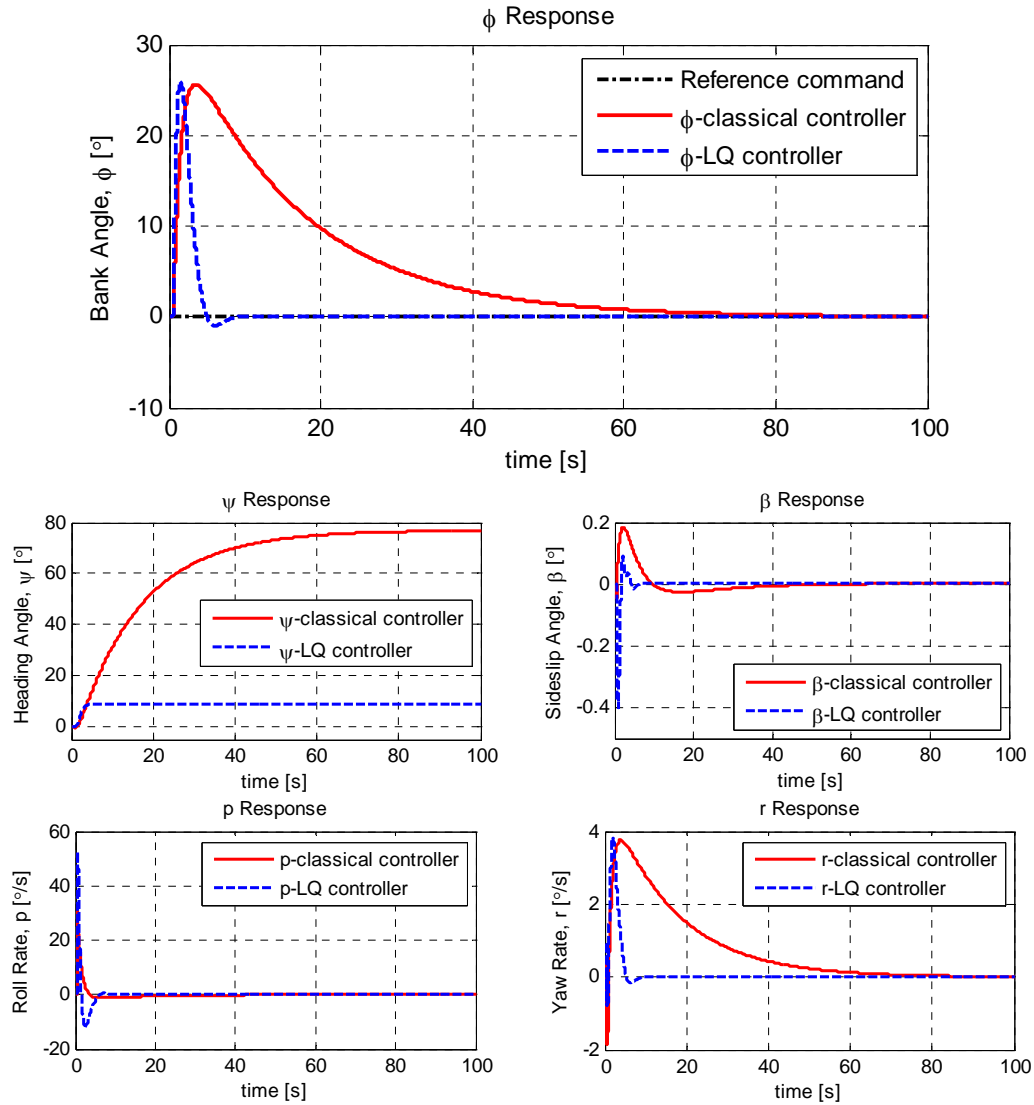
The sideslip angle, and altitude graphs demonstrate the turn coordination performance of the controllers according to the military requirement given by Section 5.3.2.2.2 for a high roll maneuvering attitude. It can be observed that the altitude coordinated turn performance is achieved with both controllers under the high roll maneuvering attitude with altitude static accuracy of minimum +0.0015 m for classical controlled model and -0.0001 m for LQ controlled model. The maximum altitude deviation during bank maneuver from the reference altitude is approximately -1.5122 m for classical controlled model, and -2 m for LQ controlled model from the reference altitude.

CASE IV: *Roll transient response flight control requirement; Refer to flight control requirements Section 5.3.1.1.2.*

Responses of Figure 6.6 are obtained by giving negative continuous wheel inputs of different magnitudes starting at the same time, which create similar peak bank angle disturbances for each controlled nonlinear model with respect to 0° reference bank angle. For classical controlled model, at 3.6 seconds time $+25.631^\circ$ bank angle increase, whereas for LQ controlled model, at 1.5 seconds time $+26^\circ$ bank angle increase is obtained, which are around 20° as the condition of the requirement.

It can be concluded from the first graph of Figure 6.6 that, the bank angle is returned to its initial condition with no overshoot after the disturbance for the classical controlled model, whereas for LQ controlled model one overshoot is observed, which is the 3.85% of the respective deviation, not exceeding the maximum 20% allowance given by the requirement.

The roll transient response characteristics are similar as the pitch (or FPA) transient response characteristics for both controllers, where for the classical controlled model, settling time to return to initial condition is much higher than the LQ controlled model, but with a smoother trend causing no overshoot.



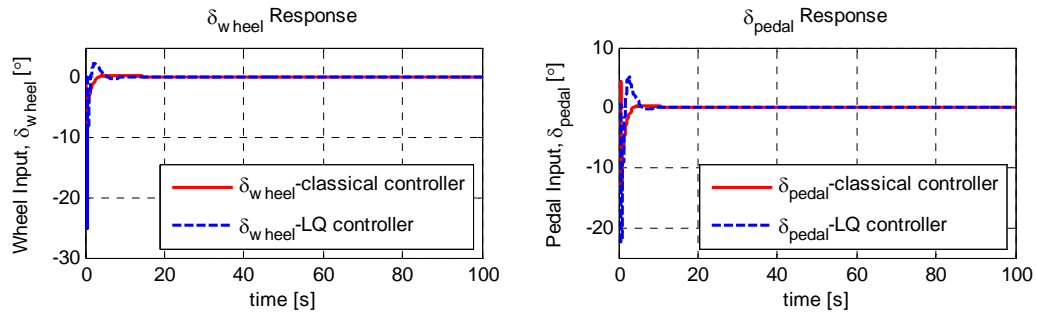
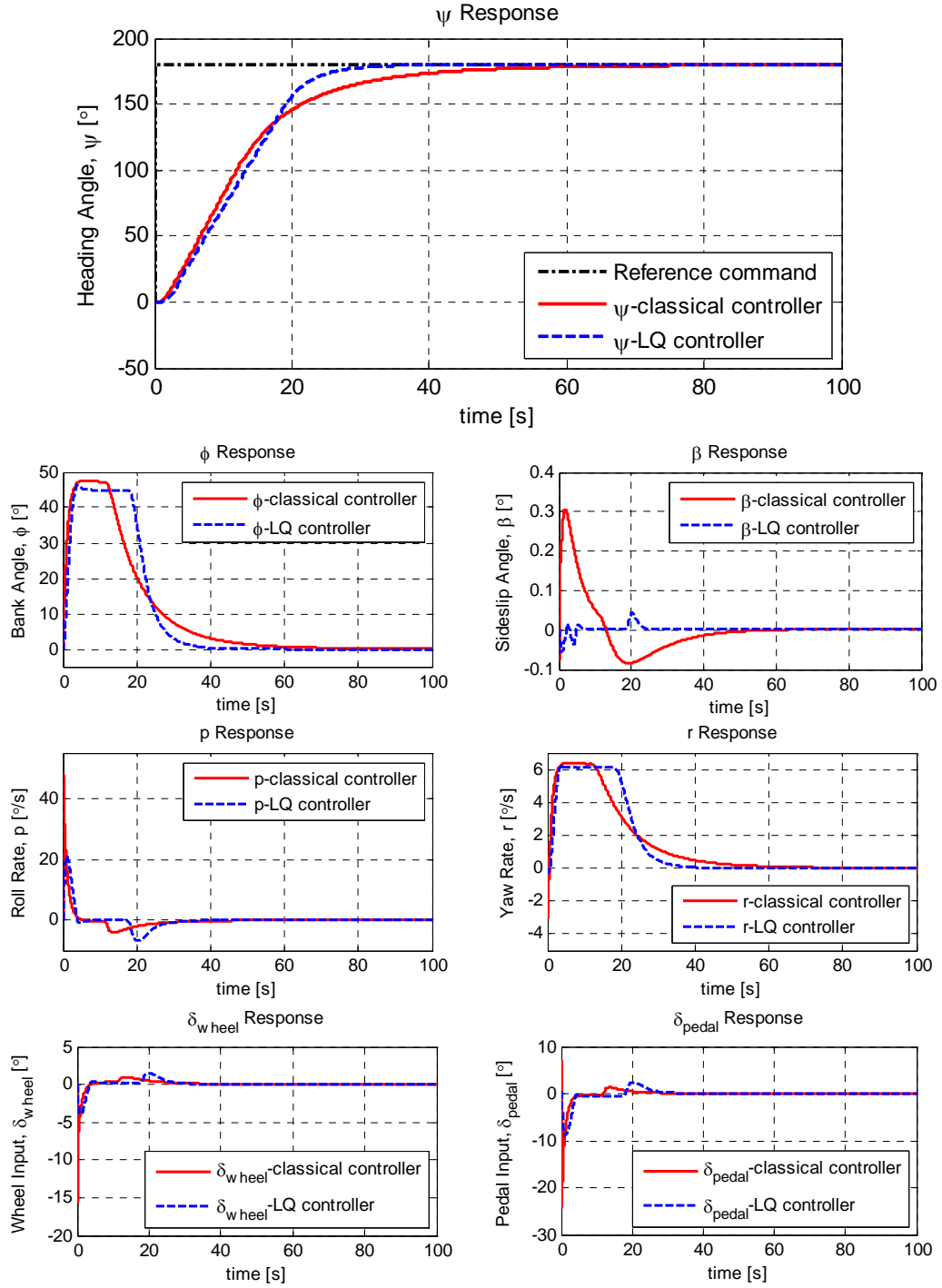


Figure 6.6 Classical and LQ controlled nonlinear model responses to negative continuous wheel inputs

CASE V: *Heading hold flight control requirement; Refer to flight control requirements Section 5.3.2.1 requiring a static accuracy of $\pm 0.5^\circ$ in heading angle / Heading select with transient heading response flight control requirement; Refer to flight control requirements Sections 5.3.2.2, 5.3.2.2.1 / Altitude coordinated turn flight control requirement; Refer to flight control requirements Section 5.3.2.2.2.*

Responses to $+180^\circ$ heading attitude, ψ increase reference step command for closed loop nonlinear models with classical and LQ controllers together are shown by graphs of Figure 6.7.

In this case, a $+180^\circ$ ψ increase reference command is given with respect to the reference heading of 0° . It is the maximum heading value demand. The compatibility with the respective heading hold flight control requirement is investigated by the first graph of Figure 6.7, for which the minimum static accuracy is -0.19° for classical controlled response for the displayed time range, whereas for LQ controlled response the static accuracy has a constant value of 0° . It can be concluded that both controllers well satisfy the related requirement.



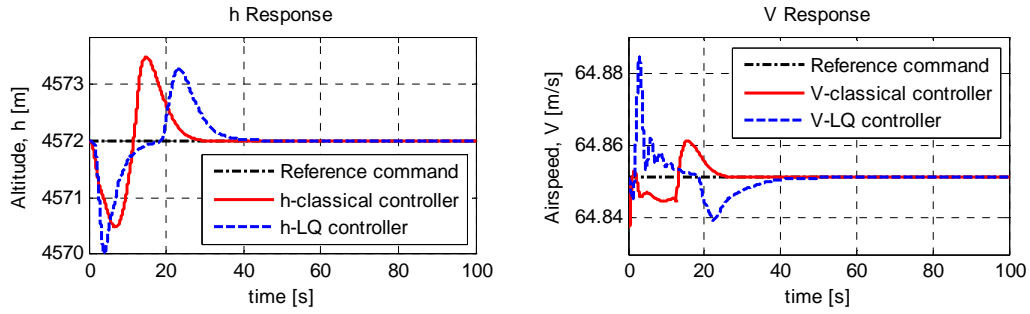


Figure 6.7 Classical and LQ controlled nonlinear model responses to $+180^\circ \psi$ increase reference step command

As heading select requirement puts forward, both controllers shall provide satisfactory turning rates, which can be concluded to be provided for both controllers from yaw rate, r response graph. The other heading select requirement which requires smoothly roll-in roll-out accomplishment with no disturbing variation in roll rate, p is better provided with LQ controlled model with the maximum roll rate, p value reached that is considerably smaller than the classical controlled model maximum roll rate response at the time roll-in is initiated.

The transient heading response requirement is provided by both controllers with no overshoots generated, but it is obvious that the more rapid entry into and termination of the turn is generated by the LQ controller.

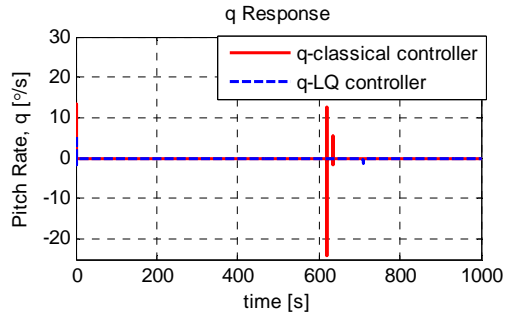
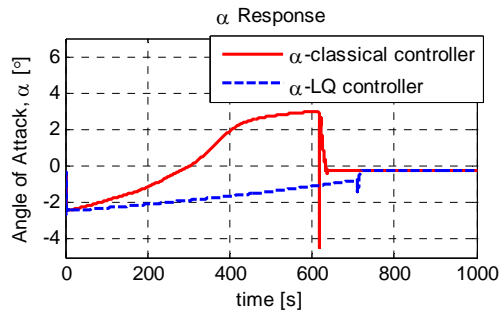
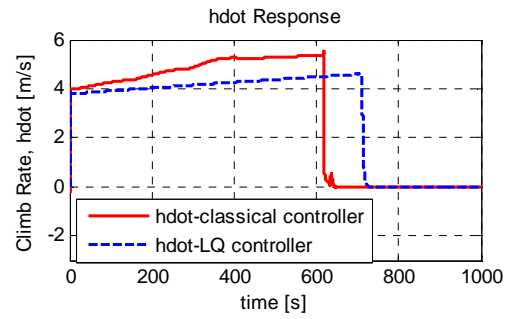
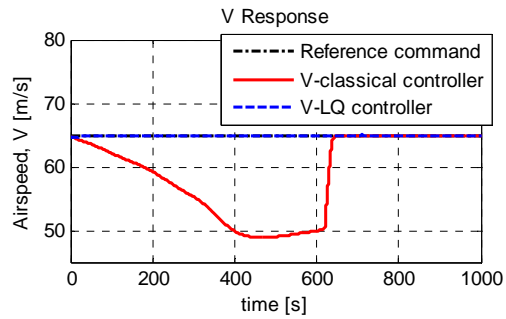
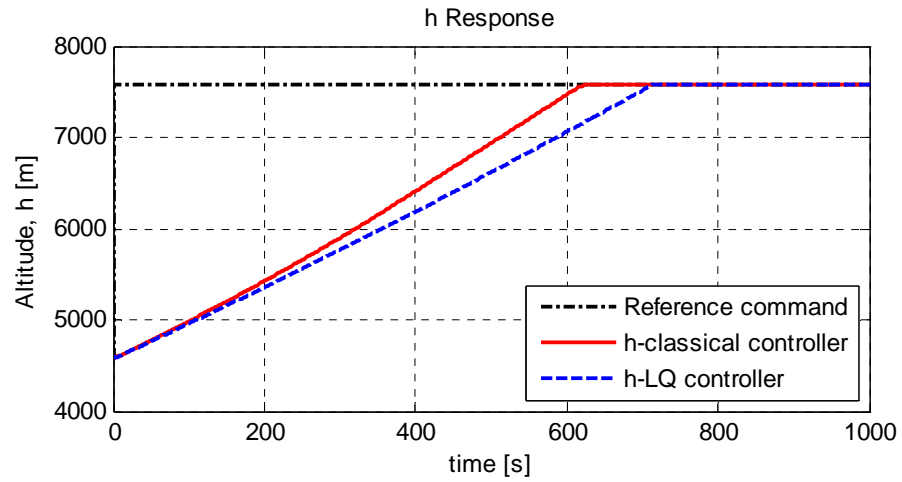
The sideslip angle, and altitude graphs demonstrate the turn coordination performance of the controllers for a heading maneuvering of a high value demand. It can be observed that the altitude coordinated turn performance is achieved with both controllers with altitude static accuracy of minimum 0 m for both controlled models, whereas the maximum altitude deviation during turn from the reference altitude is approximately -1.51 m for classical controlled model, and -2 m for LQ controlled model.

CASE VI: *Altitude hold flight control requirement; Refer to flight control requirements Section 5.3.3.*

Responses to +3,000 m altitude, h increase reference step command for closed loop nonlinear models with classical and LQ controllers together are shown by graphs of Figure 6.8.

In this case, a +3,000 m h increase reference command is given with respect to the reference altitude, 4,572 m. It is a very high altitude increase demand, but by the help of anti integral wind-up scheme and pitch angle and FPA limiters for classical and LQ controllers, respectively, no overshoot occurred even for this high altitude command for both controlled models. The effect of anti integral wind-up and limiters can also be observed from Figures 5.19 and 5.39 of Sections 5.4.2.3 and 5.5.5.3, respectively which also show that, without anti integral wind-up, classical controlled model experiences serious overshoots. This is because of the structure of the classical controller, where it has to involve an altitude integrator in the forward path before commanding to pitch attitude, in order to decrease the steady state error occurrences, since the related military requirement focuses on the static accuracy. In LQ controlled model, the steady state error elimination could be achieved without a pre-integrator necessity in forward path, thus wind-up in altitude control do not cause large overshoots, even with disengagement of anti-integral wind-up scheme. It only has a small proportional gain multiplied by the altitude error, before the FPA limiter entry in its structure.

It is investigated from the climb rate, \dot{h} graph that, the value does not exceed 10.16 m/s for both controlled models as the requirement mentions that is relatively safe. The compatibility with the respective flight control requirement is investigated by the first graph of Figure 6.8, for which the static accuracy is 0 m for both controllers, very well satisfying the requirement.



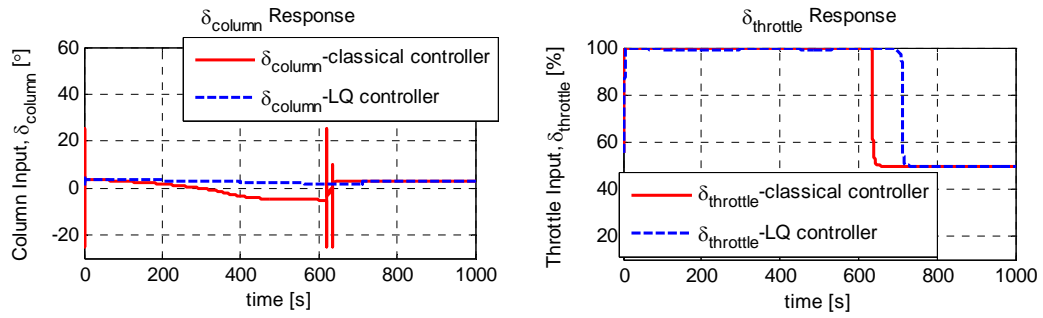


Figure 6.8 Classical and LQ controlled nonlinear model responses to +3,000 m h increase reference step command

There are pros and cons for both controller performances, such as for the classical controlled model altitude response rise time is about 100 seconds smaller than LQ controlled model response as an advantage, however the corresponding decrease in velocity is considerably higher as a disadvantage, which may lead to entrance into stall regions unexpectedly. This is the point where the TECS design comes out with its advantage of coordinated and effective usage of column and throttle controls together, compatible with the flight dynamics. In addition, in classical controlled model, the high peaks occurring in column input response at the initial time and at the time the desired altitude is reached are also not desirable.

CASE VII: *Airspeed hold flight control requirement; Refer to flight control requirements Section 5.3.4.*

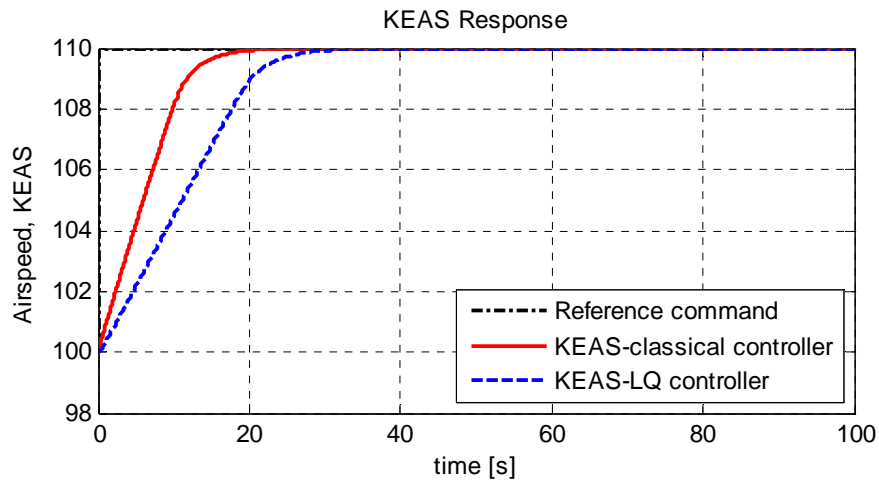
Responses to +10 knots airspeed, KEAS increase reference step command for closed loop nonlinear models with classical and LQ controllers together are shown by graphs of Figure 6.9.

In this case, a +10 knots KEAS increase reference command is given with respect to the reference KEAS, 100 knots. The compatibility with the respective flight control

requirement is investigated by the first graph of Figure 6.9, for which the static accuracy is approximately 0 knots for both controlled models, very well satisfying the requirement.

It is obvious from the first graph that, the classical controlled model response settling time is again smaller about 7 s, than the LQ controlled model response, in a similar manner to altitude responses. However, the correspondent disadvantage of this case is the considerably higher usage of throttle by classical controlled model with respect to the LQ controlled model.

The advantage of optimal control and TECS, making use of control inputs in a well coordinated way can also be observed from the airspeed control responses, next to altitude control responses.



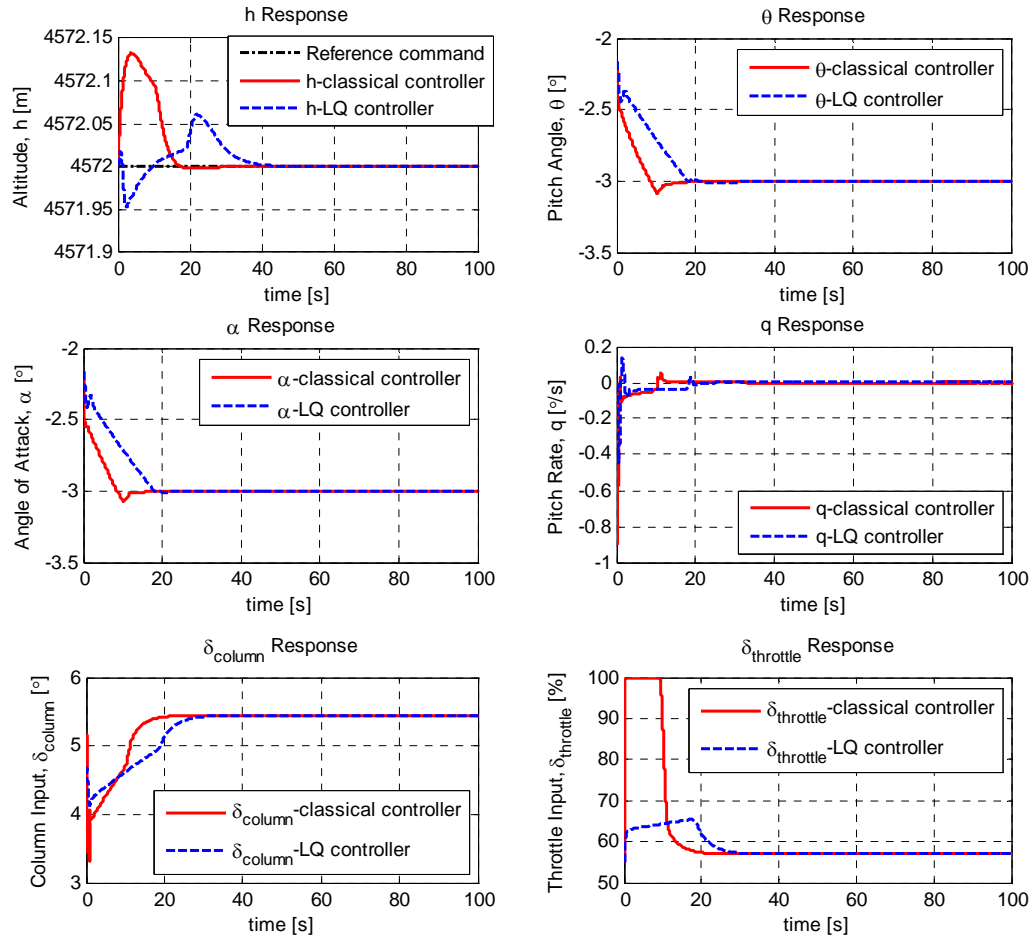


Figure 6.9 Classical and LQ controlled nonlinear model responses to +10 KEAS increase reference step command

CHAPTER 7

SUMMARY, CONCLUSIONS AND RECOMMENDATIONS

7.1 Summary

The tasks accomplished throughout the whole thesis include the nonlinear modeling of an unmanned aerial vehicle, trim and linearization processes of the developed nonlinear model, design of two frequently used controllers in industry using the obtained linear models; using the classical, and optimal approaches respectively. Many analyses are also carried out correspondingly for verification purposes and in order to have reasonable comments on the results obtained.

The nonlinear modeling part constitutes the baseline of this thesis, where all the latter tasks are accomplished based on this developed nonlinear model in MATLAB®/Simulink® environment. The major air vehicle and environmental components are included in the nonlinear model, such as actuators, gravity, engine, atmosphere, wind-turbulence models, as well as the aerodynamics components in the 6 DOF equations of motion. This developed nonlinear model is trimmed using MATLAB® `trim` function with a pre-tailoring process to flight dynamics. The obtained trim states, inputs, and outputs are used in order to linearize the nonlinear model by using the two MATLAB® functions, `linmod` and `linmod2`. The modal matrices are obtained for the purpose of validating the decoupling condition between the two major axes; namely the longitudinal and lateral-directional. With these modal matrices, the dominant states on the main air vehicle flight modes are also demonstrated. The linearization methods are verified, too by comparing the linear model simulation responses with the nonlinear model simulation responses to the same control inputs and investigating the matching degree. It is concluded that the numerical perturbation linearization method `linmod2` gives better results; thereby the linear models for the latter tasks of the study are obtained using this method.

Since the accuracy of the nonlinear model is important, the analyses for the open loop dynamic stability are carried out for examining the flight modes in terms of flying quality levels. Additionally, a validation task is introduced by comparing the dynamic stability results with respect to airspeed and altitude throughout the envelope with the correspondent dynamic stability results of a known UAV which has a very a similar configuration.

In the scope of classical controller design, the Simulink Response Optimization (SRO) tool of MATLAB[®]/Simulink[®] is utilized, and PID gains are provided on the built up inner-outer loop classical controller structures. The controllers designed using this approach that are responsible for the low-level control functions are the roll attitude, turn coordination, heading, pitch attitude, altitude, and airspeed controllers. Once they are designed for one flight trim condition satisfying the flight control requirements introduced by military specifications, the same procedure is repeated with respect to different altitude and airspeed values, in order to have gain scheduling. Additional tasks are carried out for the nonlinear implementation, such as controller input linearization to introduce the perturbed linear controller states and inputs to nonlinear model having the total states and control input variables, and anti integral wind-up scheme implementation to avoid the possible wind-up of integrators in the controllers in case the throttle saturates.

The second controller using optimal approach is designed using linear quadratic (LQ) method. The decoupled longitudinal and lateral-directional axes are based on in the design procedure. In longitudinal axis, the controller is designed using the total energy control system (TECS) principle, which provides an effective control approach by controlling the total energy of the air vehicle. The controller structure is composed of flight path angle and total acceleration control in the inner loop, and altitude and airspeed control at the outer loop. In lateral-directional control, “target zeros” are set in the synthesis model, to obtain the LQ controller gains by carrying the eigenvalues to the desired zeros. The nonlinear implementations of gain

scheduling, control input linearization, and anti integral wind-up scheme are also carried out in a similar manner as the classical controller.

The two developed controllers are compared based on the military flight control requirements.

7.2 Conclusions

The major accomplishments throughout the whole thesis are to implement air vehicle modeling and two different controller designs around this model with transient analyses between those, such as the linear model open loop dynamic stability analyses, investigation of modal matrix, eigenvalues & pole-zero maps, etc. These are carried out in order to build up correlations between the flight dynamics and mathematics introduced by controller design phases.

The structure of the simulation model on the whole is very effective. The nonlinear model is very detailed, and is well-integrated with detailed atmospheric and gravity models. In addition, the methods and respective implementations carried out to trim and linearize the nonlinear model are well defined and the results are highly satisfying which can also be observed from the linear and nonlinear models comparison graphs given by Figures 3.1 through 3.8. The effectiveness of trim and linearization can also be investigated from the direct implementation of the linear controllers into nonlinear model without any need for tuning the provided gains of both controllers.

It can be concluded from the overall results of the controlled model responses that the present controllers designed have several advantages and disadvantages with respect to each other. However, it should be denoted that, the design considerations of the two controllers in fact are not completely identical, since they are designed independently from each other's results depending only on the common target requirements, i.e. the military flight requirements. Therefore the conclusions reached reflect the comparisons of methodologies used in a sense. An approach for a better

comparison of the time response results would be to obtain the LQ controller simulation responses initially to be the baseline for the SRO desired response characteristics. But this approach is out of the scope of this study, since the independency between controller designs except for the same targeted military requirements is important similar to the real design phases. The main conclusions reached by comparing the time responses of the classical controlled and LQ controlled nonlinear model under these considerations are as follows:

1. LQ controller performed better in terms of optimized and smaller control input responses, which is very important by being far away from the saturation level for most of the commands. This is not only because of the optimal control approach making use of both control inputs based on its MIMO nature, but also because of the utilization of TECS approach in the controller structure, which takes into account the longitudinal dynamics of the air vehicle and controls its total energy by using both control inputs in a very effective way. TECS methodology and implementation is explained in detail in Section 5.5.2.
2. It is obvious from the case studies done in the previous chapter that longitudinal classical controlled responses are faster in terms of rise time, but the settling time for disturbance rejections are slower than the LQ controlled responses, which may be dangerous under frequently occurring disturbances.
3. Based on its longitudinal controller structure, the classical controlled nonlinear model is highly dependant on the anti integral wind-up scheme and limiters, different from the LQ controlled model which is also discussed in the previous chapter.
4. An important advantage of classical controller is the very little need in gain scheduling look up tables, since almost every gain of the controller with two exceptions are constant. However, every LQ controller gains have to be interpolated/extrapolated throughout the whole flight envelope by look up tables, increasing the complexity of the controller. Because of the uncertainties that always exist in the nonlinear models, mostly based on the

aerodynamic database, troubleshooting and tuning of the gains are to be needed during latter design phases such as flight tests, etc. Consequently, these tasks become hard to achieve with the gain look tables.

5. The classical controller designs are much more time consuming than LQ controller designs, because of their gradually build up controller loop structures not allowing highly automating design tools. This is another important consideration in practical design phases necessitating too many design loops.
6. Despite the time consuming feature of the classical controller structure, generally the classical controller design is easier and more straightforward to implement and to get deeper knowledge about the effects of each parameter and control loops.

Hence, the results of this thesis are of considerable importance; since mainly they show the major pros and cons of both controllers designed around the same nonlinear model, and based on the necessities of the designer, give an idea about the controller design approach to choose.

The assumptions done for the modeling phase listed in Section 2.3 affect on the designed controllers besides modeling, since the lack of aerodynamic nonlinearities and aeroelastic effects in the model causes less inquiries to become necessary during the controller design phases. The additional assumptions that have direct effect on controllers given in Section 5.2 are also not to be forgotten with assumptions of perfect state measurements, and no time delays existence, which generate additional relaxation in terms of the tasks to be done. All of these deficiencies in this study idealize the model and controllers apart from the real life. Hence, it is recommended that they should be considered in a practical design phase. But it is definite that the tasks accomplished in this study form the basis of implementation of such a controller design phase that a designer can not pass by.

To conclude: this thesis has developed a considerable body of work towards the design and control of the subject air vehicle. This work constitutes a solid foundation for possible future work on this air vehicle design, and with the tools implemented and other conclusions reached, acts as a guide for any air vehicle design. It forms an important baseline for more realistic air vehicle systems design, by applying all the major air vehicle modeling and control phases.

7.3 Recommendations for Future Work

For the two controllers designed, the analyses for robustness should be carried out additionally, in order to compare the controllers in this scope, which is also very important. Next to this, accomplishing comparisons of the results of the two controllers under strong wind-turbulence effects are recommended, which are included in the nonlinear model, but the effects are not investigated. Additionally, carrying out the real time applications by first discretizing the controller developed in this study, which are continuous, may be considered as a possible future work.

REFERENCES

- [1] Newcome, Laurence R., *Unmanned Aviation: A Brief History of Unmanned Aerial Vehicles*, 1st Edition, AIAA, Inc. Reston, Virginia, 2004.
- [2] Goraj Z., Frydrychewicz A., Świtkiewicz R., Hernik B., Gadomski J., Goetzendorf-Grabowski T., Figat M., Suchodolski St. and Chajec W., *High Altitude Long Endurance Unmanned Aerial Vehicle of a New Generation – A Design Challenge For a Low Cost, Reliable and High Performance Aircraft*, Bulletin of the Polish Academy of Sciences Technical Sciences, Vol. 52, No. 3., 2004.
- [3] Anonymous, *MALE UAV Configurations*, Capecon - WP5, Meeting n°13, Eilat, Israel, May 2005, URL: <http://www.uavnet.com> (last accessed on 30.03.2007).
- [4] Rockwell International Corporation Missile Systems Division, *RPV Flying Qualities Design Criteria*, Technical Report AFFDL-TR-76-125, Ohio, December 1976.
- [5] Altenkirch, D., Schmitt, D.-R., *Inflight Simulation of UAV Flight Guidance Concepts*, UAVNET Meeting No. 3, Warsaw, 2002, URL: <http://www.uavnet.com> (last accessed on 30.03.2007).
- [6] Defense Update, International Online Defense Magazine: *MQ-9 Reaper-Predator B UAV*, Issue 2, 2005, URL: <http://www.defense-update.com/products/p/predatorB.htm> (last accessed on 25.08.2007).
- [7] Balas, G.J., *Flight Control Law Design: An Industry Perspective*, European Control Conference, 2003.
- [8] Lim, B.-A., *Design and Rapid Prototyping of Flight Control and Navigation System for an Unmanned Aerial Vehicle*, Naval Postgraduate School, Monterey, California, MSc Thesis, March 2002.
- [9] Liang, F., *Rapid Development Of UAV Autopilot Using MATLAB®/Simulink®*, AIAA 2002-4976, AIAA Modeling and Simulation Technologies Conference and Exhibit, Monterey, California, 5-8 August 2002.

- [10] Ross, A., *Modeling and Control of the SimiCon UAV*, University of Glasgow, Department of Electronics and Electrical Engineering, MSc Thesis, January 2003.
- [11] Rauw, M.O., *A SIMULINK[®] Environment for Flight Dynamics and Control Analysis – application to the DHC-2 “Beaver”, Part I. Implementation of a model library in SIMULINK[®]*, Delft University of Technology, Faculty of Aerospace Engineering, Disciplinary Group for Stability and Control, MSc Thesis, July 1993, URL: <http://www.dutchroll.com> (last accessed on 21.10.2006).
- [12] Rauw, M.O., *A SIMULINK[®] Environment for Flight Dynamics and Control Analysis – application to the DHC-2 “Beaver”, Part II. Nonlinear analysis of the “Beaver” autopilot*, Delft University of Technology, Faculty of Aerospace Engineering, Disciplinary Group for Stability and Control, MSc Thesis, July 1993, URL: <http://www.dutchroll.com> (last accessed on 21.10.2006).
- [13] Etkin B., Reid L. D., *Dynamics of Flight, Stability and Control*, 3rd Edition, John Wiley&Sons, Inc., 1996.
- [14] Roskam J., *Airplane Flight Dynamics and Automatic Flight Controls, Part I*, DARcorporation, 2001.
- [15] Downing D. R., Valasek J., *Digital Flight Control Systems: Analysis and Design*, The University of Kansas Continuing Education, San Diego, CA., 2006.
- [16] McDonnell Douglas Astronautics Company – St. Louis Division: *The USAF Stability and Control Digital DATCOM Volume I, Users Manual*, Technical Report AFFDL-TR-79-3032, Vol. I, Missouri, April 1979.
- [17] The MathWorks: *Aerospace Blockset User’s Guide, For Use with Simulink[®]*, Version I, The MathWorks, Inc., July 2002.
- [18] Duke, E.L., Antoniewicz, R.F., Krambeer, K.D., *Derivation and Definition of a Linear Aircraft Model*, NASA Reference Publication 1207, August 1988.

- [19] Eick, R.S., *A Reconfiguration Scheme for Flight Control Adaptation to Fixed-Position Actuator Failures*, The University of Florida, MSc Thesis, 2003.
- [20] The MathWorks: *Optimization Toolbox User's Guide, For Use with MATLAB*, Version 3, The MathWorks, Inc., June 2004.
- [21] Unmanned Dynamics: *AeroSim Aeronautical Simulation Blockset User's Guide*, Version 1.2, Unmanned Dynamics, LLC, URL: <http://www.udynamics.com> (last accessed on 21.07.2007).
- [22] Wolfram Research: *Control System Professional Documentation / Local Linearization of Nonlinear Systems*, Wolfram Research, Inc., 2007, URL: <http://documents.wolfram.com/applications/control/NonlinearControlSystems/11.1.html> (last accessed on 21.07.2007).
- [23] The MathWorks: *Simulink® Control Design / Block-by-Block Analytic Linearization*, The MathWorks, Inc., 2007, URL: <http://www.mathworks.com/access/helpdesk/help/toolbox/slcontrol/>
- [24] Stevens, B.L., Lewis, F.L., *Aircraft Control and Simulation*, 2nd Edition, Wiley, October 2003.
- [25] Stengel, R. F., *Flight Dynamics*, Princeton University Press, 2004.
- [26] Wazsak, M. R., Schmidt, D. S., *Analysis of Flexible Aircraft Longitudinal Dynamics and Handling Qualities*, NASA Contractor Report 177943, Volume I, Purdue University, Indiana, June 1985.
- [27] Nelson, R. C., *Flight Stability and Automatic Control*, McGraw-Hill Book Company, 1989.
- [28] Goraj, Z., *Dynamic Characteristics of Different UAV Configurations*, UAV-NET Meeting, Italy, February 2002.
- [29] Castro, H.V., *Flying and Handling Qualities of a Fly-by-Wire Blended-Wing-Body Civil Transport Aircraft*, Cranfield University, School of Engineering, PhD Thesis, December 2003.
- [30] Department of Defense, *Flying Qualities of Piloted Airplanes*, Military Specification, MIL-F-8785C, USA, November 1980.

- [31] Department of Defense, *Flying Qualities of Piloted Aircraft*, Military Standard, MIL-HDBK-1797, Washington D.C., USA, December 1997.
- [32] McLean, D., *Automatic Flight Control Systems*, Prentice-Hall, 1990.
- [33] Vaglianti, B., *Initial Flight Test Cards*, Cloud Cap Technology, Inc., August 2006.
- [34] Department of Defense, *Flight Control Systems – Design, Installation and Test of Piloted Aircraft, General Specification for*, Military Specification, MIL-F-9490D, USA, June 1975.
- [35] Department of Navy, *Control and Stabilization Systems: Automatic, Piloted Aircraft, General Specification for*, Military Specification, MIL-C-18244A(WEP), USA, December 1962.
- [36] AlSwailem, S.I., *Application of Robust Control in Unmanned Vehicle Flight Control System Design*, Cranfield University, College of Aeronautics, PhD Thesis, March 2004.
- [37] Christiansen, R.S., *Design of an Autopilot for Small Unmanned Aerial Vehicles*, Brigham Young University, Department of Electrical and Computer Engineering, MSc Thesis, August 2004.
- [38] Rademakers, N.G.M., *Control of a Tailless Fighter using Gain-Scheduling*, Eindhoven University of Technology, Department Mechanical Engineering Dynamics and Control Group, Traineeship Report, Eindhoven, January 2004.
- [39] Fielding, C., *The Design of Fly-by-Wire Flight Control Systems*, BAE Systems, Aerodynamics (W427D).
- [40] Visioli, A., *Modified Anti-Windup Scheme for PID Controllers*, IEE Control Theory and Applications, 150(1):49-54, January 2003.
- [41] Vrančić, D., *Design of Anti-Windup and Bumpless Transfer Protection*, University of Ljubljana, PhD Thesis, Slovenia, 1997.
- [42] Ly, U.-L., Voth, C., Sanjay, S., *Robust Integrated Autopilot/Autothrottle Design Using Constrained Parameter Optimization*, Department of Aeronautics and Astronautics University of Washington, Seattle, 1988.
- [43] Gangsaas, D., Blight, J.D., *Linear Quadratic Design*, May 2005.

- [44] Bruce, K.R., *NASA B737 Flight Test Results of the Total Energy Control System*, Boeing Commercial Airplane Company, Seattle, Washington, January 1987.
- [45] Lambregts, A.A., *Engine Controls Integration Flight Control / Propulsion Control Function Integration*, Advanced Controls Chicago DER Recurrent Seminar; August 2004.
- [46] Kaminer, I., Benson, R.A., Coleman, E.E., Ebrahimi, Y.S., *Design of Integrated Pitch Axis for Autopilot/Autothrottle and Integrated Lateral Axis for Autopilot/Yaw Damper for NASA TSRV Airplane Using Integral LQG Methodology*, NASA Contractor Report 4268, January 1990.
- [47] Kaminer, I., *On Use of Frequency Weightings in LQR Design of Transport Aircraft Control Systems*, Boeing Commercial Airplanes; Seattle, Washington.

APPENDIX A

DERIVATION OF 6 DOF EQUATIONS OF MOTION

In this appendix, the derivation of 6 DOF equations of motion is focused on. The derivation procedure is defined starting with application of Newton's second law to the airplane of Figure A.1 [14-15].

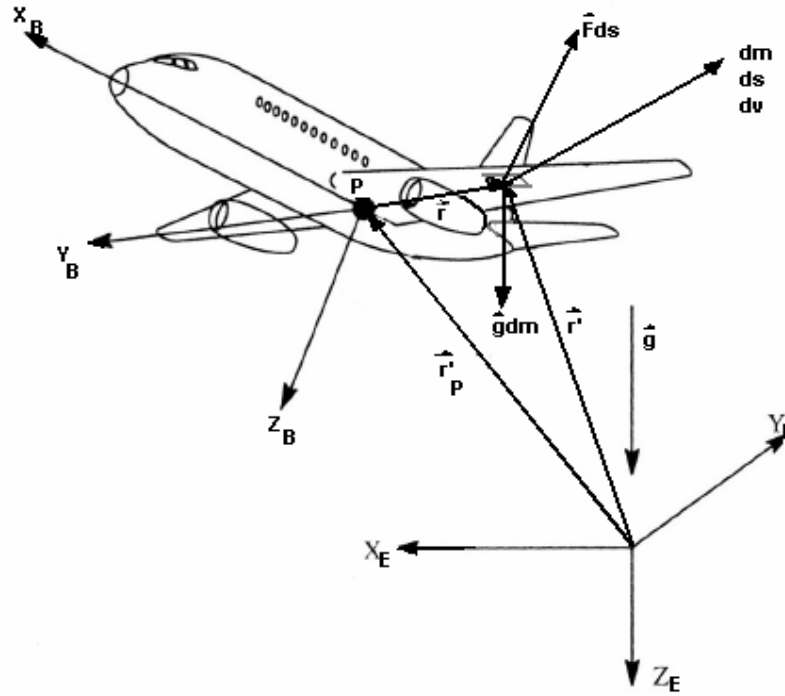


Figure A.1 Earth-Fixed and Body-Fixed Coordinate Systems [14-15]

In the figure, P is taken as the vehicle center of mass. The airplane is assumed to consist of a continuum of mass elements, dm . Those mass elements located at the surface of the airplane are subjected to a combined aerodynamic and thrust force per unit area, \vec{F} and to the acceleration of gravity, \vec{g} . $X_B Y_B Z_B$ denotes a body-fixed (rotating) axes system and $X_E Y_E Z_E$ denotes an Earth-fixed (non-rotating) axes system, where arrows indicate the positive directions.

Newton's law of linear motion is given as

$$\frac{d}{dt} \left[\int_V \frac{d\vec{r}'}{dt} dm \right] = \int_V \vec{g} dm + \int_S \vec{F} ds \quad (A.1)$$

where LHS corresponds to the time derivative of linear momentum and RHS corresponds to the applied forces. Euler's law of angular motion is given as

$$\frac{d}{dt} \left[\int_V \vec{r} \times \frac{d\vec{r}'}{dt} dm \right] = \int_V \vec{r} \times \vec{g} dm + \int_S \vec{r} \times \vec{F} ds \quad (A.2)$$

where LHS corresponds to the “time derivative of angular momentum” and RHS corresponds to the “applied moments”. The integrals \int_V and \int_S represent volume and surface integrals for the entire airplane.

Rotational equations of motion: In order to obtain rotational equations of motion, the following steps are applied

1. Eliminating \vec{r}' using $\vec{r}' = \vec{r}_p' + \vec{r}$; and substituting into Equation (A.2) starting from left hand side (LHS)

$$\text{LHS} = \frac{d}{dt} \left[\int_V (\vec{r}_p' + \vec{r}) \times \frac{d}{dt} (\vec{r}_p' + \vec{r}) dm \right] \quad (\text{A.3})$$

$$\text{LHS} = \frac{d}{dt} \left[\int_V \vec{r}_p' \times \frac{d\vec{r}_p'}{dt} dm + \int_V \vec{r}_p' \times \frac{d\vec{r}}{dt} dm + \int_V \vec{r} \times \frac{d\vec{r}_p'}{dt} dm + \int_V \vec{r} \times \frac{d\vec{r}}{dt} dm \right] \quad (\text{A.4})$$

2. If point P is the vehicle center of mass, the relation $\int_V \vec{r} dm = 0$ must be satisfied. Also \vec{r}_p' is constant over vehicle volume. Since mass is a constant, the relation $\frac{dm}{dt} = 0$ must be satisfied, also. Continuing from equation (A.4)

$$\text{LHS} = \frac{d}{dt} \left[\vec{r}_p' \times \int_V \frac{d\vec{r}_p'}{dt} dm + \vec{r}_p' \times \underbrace{\frac{d}{dt} \int_V \vec{r} dm}_0 + \underbrace{\int_V \vec{r} dm}_0 \times \frac{d\vec{r}_p'}{dt} + \int_V \vec{r} \times \frac{d\vec{r}}{dt} dm \right] \quad (\text{A.5})$$

$$\text{LHS} = \frac{d}{dt} \left[\vec{r}_p' \times \int_V \frac{d\vec{r}_p'}{dt} dm + \int_V \vec{r} \times \frac{d\vec{r}}{dt} dm \right] \quad (\text{A.6})$$

$$\text{LHS} = \underbrace{\frac{d\vec{r}_p'}{dt} \times \frac{d\vec{r}_p'}{dt}}_0 \int_V dm + \vec{r}_p' \times \frac{d^2 \vec{r}_p'}{dt^2} \int_V dm + \frac{d}{dt} \left[\int_V \vec{r} \times \frac{d\vec{r}}{dt} dm \right] \quad (\text{A.7})$$

$$\text{LHS} = \vec{r}_p' \times \frac{d^2 \vec{r}_p'}{dt^2} \int_V dm + \frac{d}{dt} \left[\int_V \vec{r} \times \frac{d\vec{r}}{dt} dm \right] \quad (\text{A.8})$$

where, the last relationship obtained can be related to Equation (A.9), i.e. to Newton's law of linear motion as follows

$$\vec{r}_p \times \left[\frac{d}{dt} \left(\int_V \frac{d\vec{r}'}{dt} dm \right) - \int_V \vec{g} dm - \int_S \vec{F} ds \right] = 0 \quad (\text{A.9})$$

$$\vec{r}_p \times \left[\frac{d^2}{dt^2} \left(\int_V \vec{r}' dm \right) - \int_V \vec{g} dm - \int_S \vec{F} ds \right] = 0 \quad (\text{A.10})$$

$$\vec{r}_p \times \left[\frac{d^2}{dt^2} \left(\int_V (\vec{r}_p' + \underbrace{\vec{r}}_0) dm \right) - \int_V \vec{g} dm - \int_S \vec{F} ds \right] = 0 \quad (\text{A.11})$$

$$\vec{r}_p \times \frac{d^2 \vec{r}_p'}{dt^2} \int_V dm - \vec{r}_p \times \int_V \vec{g} dm - \vec{r}_p \times \int_S \vec{F} ds = 0 \quad (\text{A.12})$$

Returning back to the LHS and substituting Equation (A.12) gives

$$\text{LHS} = \vec{r}_p \times \int_V \vec{g} dm + \vec{r}_p \times \int_S \vec{F} ds + \frac{d}{dt} \left[\int_V \vec{r} \times \frac{d\vec{r}}{dt} dm \right] \quad (\text{A.13})$$

3. Now looking at the RHS of Equation (A.2)

$$\text{RHS} = \int_V [(\vec{r}_p' + \vec{r}) \times \vec{g}] dm + \int_S [(\vec{r}_p' + \vec{r}) \times \vec{F}] ds \quad (\text{A.14})$$

$$\text{RHS} = \vec{r}_p \times \int_V \vec{g} dm + \int_V \vec{r} \times \vec{g} dm + \vec{r}_p \times \int_S \vec{F} ds + \int_S \vec{r} \times \vec{F} ds \quad (\text{A.15})$$

4. Since \vec{g} is constant over vehicle volume, the relation, $\int_V \vec{r} \times \vec{g} dm = 0$ must be satisfied, so

$$\text{RHS} = \vec{r}_p \times \int_V \vec{g} dm + \vec{r}_p \times \int_S \vec{F} ds + \int_S \vec{r} \times \vec{F} ds \quad (\text{A.16})$$

5. Equating relationships (A.13) and (A.16) gives

$$\vec{r}_p \times \int_V \vec{g} dm + \vec{r}_p \times \int_S \vec{F} ds + \frac{d}{dt} \left[\int_V \vec{r} \times \frac{d\vec{r}}{dt} dm \right] = \vec{r}_p \times \int_V \vec{g} dm + \vec{r}_p \times \int_S \vec{F} ds + \int_S \vec{r} \times \vec{F} ds \quad (\text{A.17})$$

where the first two terms of both sides omit and finally the Equation (A.2) i.e. Euler's law of angular motion becomes

$$\frac{d}{dt} \left[\int_V \vec{r} \times \frac{d\vec{r}}{dt} dm \right] = \int_S \vec{r} \times \vec{F} ds \quad (\text{A.18})$$

Expanding Equation (A.18)

$$\left[\int_V \underbrace{\frac{d\vec{r}}{dt} \times \frac{d\vec{r}}{dt}}_0 + \vec{r} \times \frac{d^2\vec{r}}{dt^2} dm \right] = \int_S \vec{r} \times \vec{F} ds, \quad \text{and} \quad \text{introducing } \int_S \vec{r} \times \vec{F} ds = \vec{M}_A + \vec{M}_T$$

give

$$\left[\int_V \vec{r} \times \frac{d^2\vec{r}}{dt^2} dm \right] = \vec{M}_A + \vec{M}_T \quad (\text{A.19})$$

Equation (A.19) is the governing equation of angular motion.

The observed rate of change of a vector will depend on the coordinate frame in which the observer resides. So, the rate of change of \vec{r} in (A.19), as seen by an observer in the fixed coordinate frame $X_E Y_E Z_E$ is as Equations (A.20) and (A.21);

$$\frac{d\vec{r}}{dt} = \frac{\delta\vec{r}}{\delta t} + \vec{\omega} \times \vec{r} \quad (\text{A.20})$$

$$\frac{d^2\vec{r}}{dt^2} = \frac{\delta^2\vec{r}}{\delta t^2} + \vec{\omega} \times \frac{\delta\vec{r}}{\delta t} + \dot{\vec{\omega}} \times \vec{r} + \vec{\omega} \times \vec{\omega} \times \vec{r} \quad (\text{A.21})$$

where $\vec{\omega}$ is the angular rate of the body-fixed rotating coordinate frame $X_B Y_B Z_B$. Substituting these relationships about rate of change of a vector into Equation (A.19) gives the general angular equations of motion for a rigid aircraft, for which $\frac{\delta^2\vec{r}}{\delta t^2} = \frac{\delta\vec{r}}{\delta t} = 0$;

$$\boxed{\int_V \vec{r} \times (\dot{\vec{\omega}} \times \vec{r} + \vec{\omega} \times \vec{\omega} \times \vec{r}) dm} = \vec{M}_A + \vec{M}_T \quad (\text{A.22})$$

Translational equations of motion: In order to obtain translational equations of motion, the following steps are applied:

1. Eliminating \vec{r}' using $\vec{r}' = \vec{r}_p' + \vec{r}$; and substituting into Equation (A.1)

$$\frac{d}{dt} \left[\int_V \frac{d}{dt} (\vec{r}_p' + \vec{r}) dm \right] = \int_V \vec{g} dm + \int_S \vec{F} ds \quad (\text{A.23})$$

2. Since $\int_V \vec{r} dm = 0$ and \vec{g} is constant over vehicle volume, Equation (A.23) becomes

$$\frac{d}{dt} \left[\int_V \frac{d\vec{r}_p'}{dt} dm \right] + \frac{d^2}{dt^2} \underbrace{\left[\int_V \vec{r} dm \right]}_0 = \vec{g}m + \int_S \vec{F} ds \quad (\text{A.24})$$

3. Introducing $\int_S \vec{F} ds = \vec{F}_T + \vec{F}_A$, $\vec{V}_P = \frac{d\vec{r}_P}{dt}$, $\dot{\vec{V}}_P = \frac{\delta^2 \vec{r}_P}{\delta t^2}$, and substituting these variables into Equation (A.24) gives

$$\frac{d}{dt} \left[\int_V \vec{V}_P dm \right] = m\vec{g} + \vec{F}_A + \vec{F}_T \quad (\text{A.25})$$

4. Denoting that, $\dot{\vec{V}}_P, \vec{V}_P, \vec{\omega}$ are constant over vehicle volume and substituting into Equation (A.25) give the general linear equations of motion of the center of mass of the airframe as

$$\boxed{m[\dot{\vec{V}}_P + \vec{\omega} \times \vec{V}_P] = m\vec{g} + \vec{F}_A + \vec{F}_T} \quad (\text{A.26})$$

APPENDIX B

DERIVATION OF THE FLIGHT PARAMETERS; $\dot{V}, \dot{\alpha}, \dot{\beta}$

In this appendix, the derivation of the wind-axes translational acceleration parameters; \dot{V} , $\dot{\alpha}$ & $\dot{\beta}$ is focused on referring to [18].

Derivation of \dot{V} : Beginning with definition of V in terms of u , v , and w , also given by Equation (2.25a) with wind velocity terms

$$V = \sqrt{u^2 + v^2 + w^2} \quad (B.1)$$

By taking the derivative and expanding Equation (B.1), the \dot{V} equation becomes

$$\dot{V} = \frac{d}{dt} V = \frac{1}{V} (u\dot{u} + v\dot{v} + w\dot{w}) \quad (B.2)$$

where the definitions of u , v and w are $u = V \cos \alpha \cos \beta$, $v = V \sin \beta$, and $w = V \sin \alpha \cos \beta$, respectively. Substituting these definitions and canceling V terms, Equation (B.2) yields

$$\dot{V} = \dot{u} \cos \alpha \cos \beta + \dot{v} \sin \beta + \dot{w} \sin \alpha \cos \beta \quad (B.3)$$

The definitions for \dot{u} , \dot{v} , and \dot{w} , which are also given by Equations (2.6)

$$\dot{u} = \frac{1}{m} (X_G + X_A + X_T) + vr - wq \quad (B.4a)$$

$$\dot{v} = \frac{1}{m}(Y_G + Y_A + Y_T) - ur + wp \quad (B.4b)$$

$$\dot{w} = \frac{1}{m}(Z_G + Z_A + Z_T) + uq - vp \quad (B.4c)$$

are used with Equation (B.3) to give

$$\begin{aligned} \dot{V} = & \frac{\cos \alpha \cos \beta}{m}(X_G + X_A + X_T) + \cos \alpha \cos \beta(vr - wq) + \frac{\sin \beta}{m}(Y_G + Y_A + Y_T) \dots \\ & + \sin \beta(-ur + wp) + \frac{\sin \alpha \cos \beta}{m}(Z_G + Z_A + Z_T) + \sin \alpha \cos \beta(uq - vp) \end{aligned} \quad (B.5)$$

Since, $\vec{F} = \begin{bmatrix} X \\ Y \\ Z \end{bmatrix} = \begin{bmatrix} (X_G + X_A + X_T) \\ (Y_G + Y_A + Y_T) \\ (Z_G + Z_A + Z_T) \end{bmatrix}$, from Equations (2.4) and (2.10a), Equation

(B.5) becomes

$$\begin{aligned} \dot{V} = & \frac{1}{m}(X \cos \alpha \cos \beta + Y \sin \beta + Z \sin \alpha \cos \beta) + vr \cos \alpha \cos \beta \dots \\ & - wq \cos \alpha \cos \beta - ur \sin \beta + wp \sin \beta + uq \sin \alpha \cos \beta - vp \sin \alpha \cos \beta \end{aligned} \quad (B.6)$$

Equation (B.6) can be simplified by recognizing that the terms involving the vehicle rotational rates are identically zero, which becomes obvious after substituting for u , v , and w in these terms. Hence, the final equation becomes

$$\boxed{\dot{V} = \frac{1}{m}(X \cos \alpha \cos \beta + Y \sin \beta + Z \sin \alpha \cos \beta)} \quad (B.7)$$

Derivation of $\dot{\alpha}$: The equation for $\dot{\alpha}$ can be derived from the definition of α , which is also given by Equation (2.25b) with wind velocity terms,

$$\alpha = a \tan\left(\frac{w}{u}\right) \quad (\text{B.8})$$

Taking the derivative and expanding Equation (B.8) yields

$$\dot{\alpha} = \frac{d}{dt} a \tan\left(\frac{w}{u}\right) = \frac{1}{u^2 + w^2} (u\dot{w} - \dot{u}w) \quad (\text{B.9})$$

where the definitions of u and w are $u = V \cos \alpha \cos \beta$, and $w = V \sin \alpha \cos \beta$, respectively. Substituting these definitions into Equation (B.9) gives

$$\dot{\alpha} = \frac{\dot{w} \cos \alpha - \dot{u} \sin \alpha}{V \cos \beta} \quad (\text{B.10})$$

Using Equations (B.4a) and (B.4c) to substitute for \dot{u} and \dot{w} , and again using definitions, $u = V \cos \alpha \cos \beta$ and $w = V \sin \alpha \cos \beta$ to substitute into (B.4a) and (B.4c), the Equation (B.10) becomes,

$$\dot{\alpha} = \frac{-(X_G + X_A + X_T) \sin \alpha + (Z_G + Z_A + Z_T) \cos \alpha}{mV \cos \beta} + q - \tan \beta (p \cos \alpha + r \sin \alpha) \quad (\text{B.11})$$

Again from the relation, $\vec{F} = \begin{bmatrix} X \\ Y \\ Z \end{bmatrix} = \begin{bmatrix} (X_G + X_A + X_T) \\ (Y_G + Y_A + Y_T) \\ (Z_G + Z_A + Z_T) \end{bmatrix}$, Equation (B.11) becomes,

$$\dot{\alpha} = \frac{-X \sin \alpha + Z \cos \alpha}{mV \cos \beta} + q - \tan \beta (p \cos \alpha + r \sin \alpha) \quad (\text{B.12})$$

Derivation of $\dot{\beta}$: The equation for $\dot{\beta}$ can be derived from the definition of β , which is also given by Equation (2.25c) with wind velocity term

$$\beta = a \sin \left(\frac{v}{V} \right) \quad (\text{B.13})$$

Taking the derivative of Equation (B.13), expanding, substituting for V and canceling yields

$$\dot{\beta} = \frac{d}{dt} a \sin \left(\frac{v}{V} \right) = \frac{1}{V} (-\dot{u} \cos \alpha \sin \beta + \dot{v} \cos \beta - \dot{w} \sin \alpha \sin \beta) \quad (\text{B.14})$$

Using Equations (B.4a) and (B.4b) to substitute for \dot{u} , \dot{v} , and \dot{w} , (B.14) becomes

$$\begin{aligned} \dot{\beta} = & \frac{1}{mV} [-(X_G + X_A + X_T) \cos \alpha \sin \beta + (Y_G + Y_A + Y_T) \cos \beta - \dots \\ & (Z_G + Z_A + Z_T) \sin \alpha \sin \beta] + \frac{1}{V} [(-vr + wq) \cos \alpha \sin \beta + (-ur + wp) \cos \beta + \dots \\ & (-uq + vp) \sin \alpha \sin \beta] \end{aligned} \quad (\text{B.15})$$

Substituting the definitions, $u = V \cos \alpha \cos \beta$, $v = V \sin \beta$ and $w = V \sin \alpha \cos \beta$,

and the relation, $\vec{F} = \begin{bmatrix} X \\ Y \\ Z \end{bmatrix} = \begin{bmatrix} (X_G + X_A + X_T) \\ (Y_G + Y_A + Y_T) \\ (Z_G + Z_A + Z_T) \end{bmatrix}$, and rearranging the terms, Equation

(B.15) becomes

$$\dot{\beta} = \frac{1}{mV} (-X \cos \alpha \sin \beta + Y \cos \beta - Z \sin \alpha \sin \beta) + (-r \cos \alpha + p \sin \alpha) \quad (\text{B.16})$$

APPENDIX C

NONLINEAR MODELING BLOCKS – MATLAB®/SIMULINK®

Figure C.1 demonstrates the main level open loop nonlinear model of the UAV in MATLAB®/Simulink®, where the air vehicle inputs and outputs can be observed. It is obvious from the Figures C.1 and C.2 that, the developed nonlinear model helps analyses to be carried out regarding the change in c.m. and wind velocities addition.

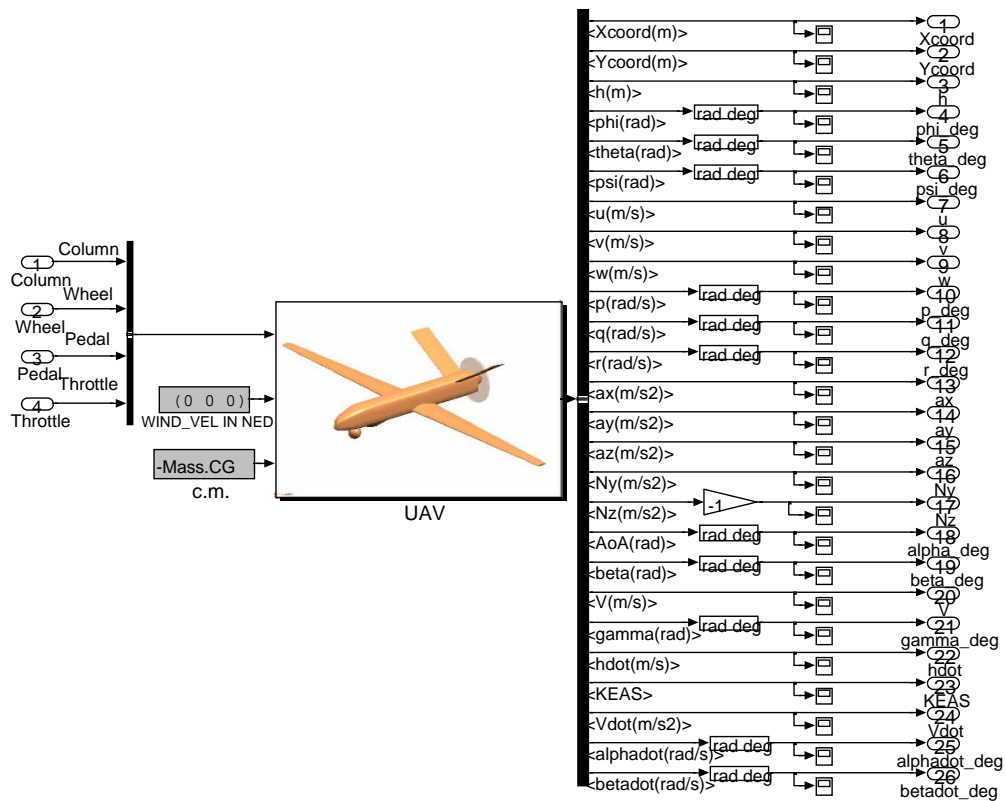


Figure C.1 Main level nonlinear model MATLAB®/Simulink® display

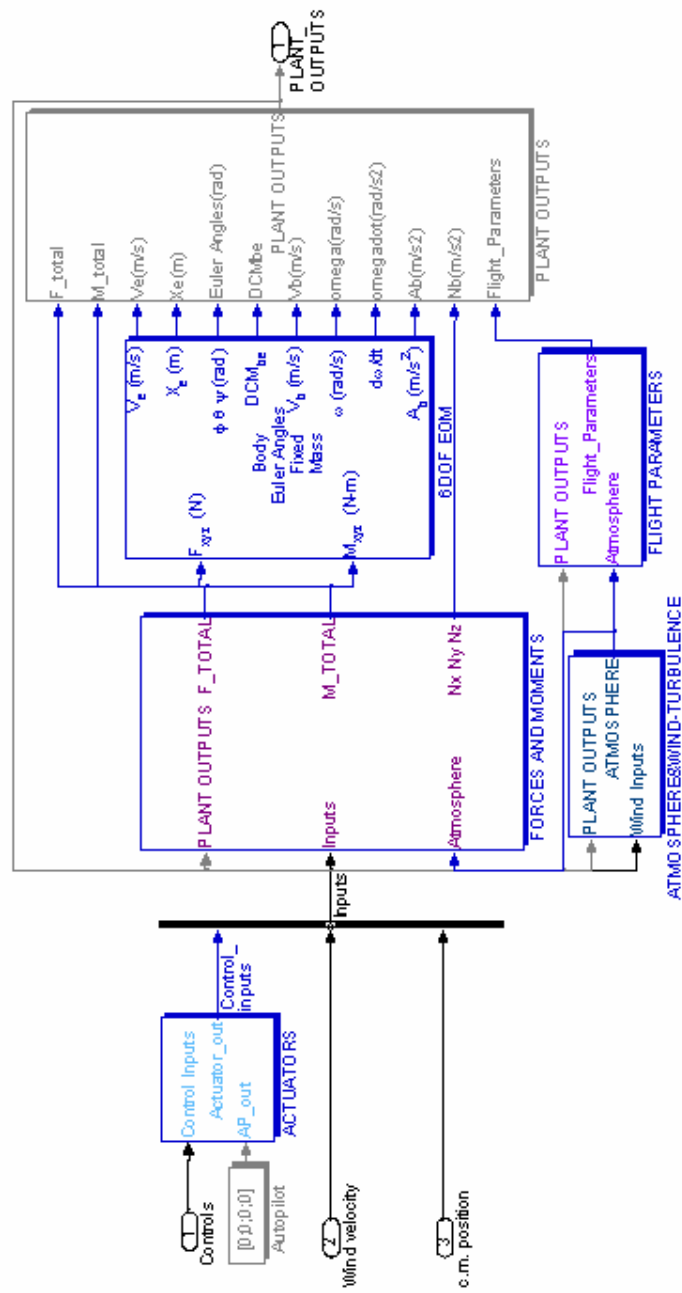


Figure C.2 Major nonlinear model build up blocks of the UAV subsystem

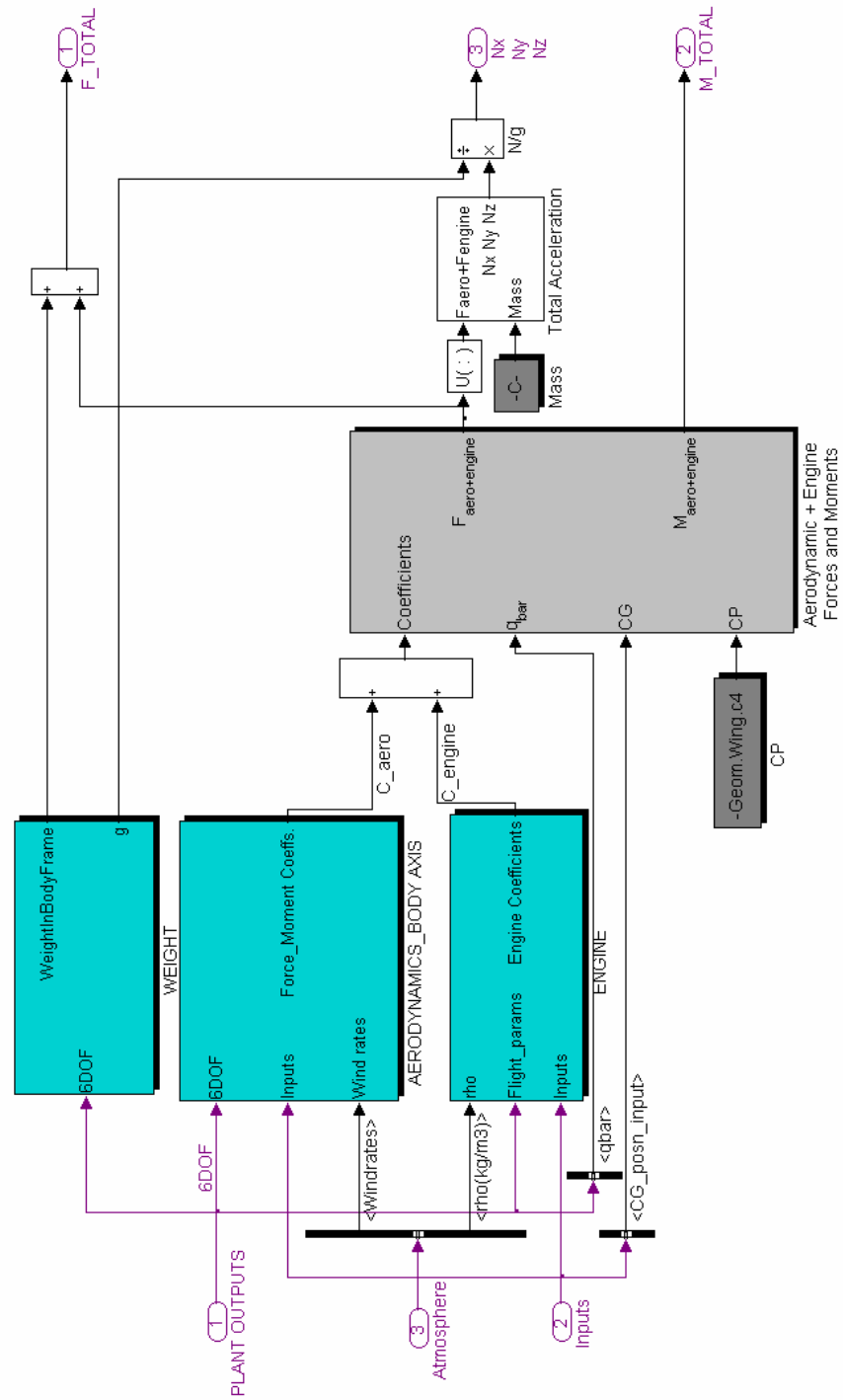


Figure C.3 FORCES AND MOMENTS subsystem

Figure C.2 displays the second level UAV subsystem, composed of the nonlinear model build up components explained throughout Chapter 2. The third level FORCES AND MOMENTS subsystem; including components of forces and moments and forming the core of the nonlinear model is displayed by Figure C.3. The input-output parameters seen on Figure C.1 are listed with their correspondent symbols and definitions in Table C.1.

Table C.1 List of parameter definitions and symbols used in main level Simulink[®] diagram input-outputs

List of input-output variables in the main level nonlinear model (in alphabetical order)	Correspondent symbol and/or definition
alpha_deg	angle of attack, α in $[\circ]$ at the output
alphadot_deg	derivative of α , $\dot{\alpha}$ in $[\circ/\text{s}]$ at the output
ax	acceleration in x-axis, a_x in $[\text{m}/\text{s}^2]$ at the output
ay	acceleration in y-axis, a_y in $[\text{m}/\text{s}^2]$ at the output
az	acceleration in z-axis, a_z in $[\text{m}/\text{s}^2]$ at the output
beta_deg	sideslip angle, β in $[\circ]$ at the output
betadot_deg	derivative of β , $\dot{\beta}$ in $[\circ/\text{s}]$ at the output
c.m.	user input c.m. location in [m]; default is initiated by <code>init_uav.m</code>
Column	column control input, δ_{column} in $[\circ]$
gamma_deg	flight path angle, γ in $[\circ]$ at the output
h	altitude, $-Z_E$ in [m] at the output
hdot	altitude rate, \dot{h} in $[\text{m}/\text{s}]$ at the output
KEAS	knots-equivalent airspeed at the output
Ny	acceleration as a sum of aerodynamic and propulsion forces in y-axis, n_y in $[\text{m}/\text{s}^2]$ at the output
Nz	acceleration as a sum of aerodynamic and propulsion forces in z-axis, n_z in $[\text{m}/\text{s}^2]$ at the output
p_deg	roll rate, p in $[\circ/\text{s}]$ at the output
Pedal	pedal control input δ_{pedal} in $[\circ]$

Table C.1 List of parameter definitions and symbols used in main level Simulink[®] diagram input-outputs (continued)

phi_deg	bank angle, ϕ in $[\text{°}]$ at the output
psi_deg	heading angle, ψ in $[\text{°}]$ at the output
q_deg	pitch rate, p in $[\text{°/s}]$ at the output
r_deg	yaw rate, p in $[\text{°/s}]$ at the output
theta_deg	pitch angle, θ in $[\text{°}]$ at the output
Throttle	throttle control input, δ_{throttle} in $[\text{°}]$
u	velocity in x-axis, u in $[\text{m/s}]$ at the output
v	velocity in y-axis, u in $[\text{m/s}]$ at the output
V	true airspeed, V in $[\text{m/s}]$ at the output
Vdot	derivative of V , \dot{V} in $[\text{m/s}^2]$ at the output
w	velocity in z-axis, u in $[\text{m/s}]$ at the output
Wheel	wheel control input, δ_{wheel} in $[\text{°}]$
WIND_VEL IN NED	User input wind velocity in north-east-down directions respectively in $[\text{m/s}]$; default is $[0, 0, 0]$
Xcoord	position in x-direction, X_E in $[\text{m}]$ at the output
Ycoord	position in y-direction, Y_E in $[\text{m}]$ at the output

APPENDIX D

TRIM-LINEARIZATION SCRIPT – “trimUAV.m”

```
% Trim UAV model.
% by Deniz Karakas 01.10.2006
format compact
%
% Define the trimmed flight condition and linearise the model
%-----
%-----
%-----
%% Step 1 : Initialization
fprintf('\nSetting initial trim parameters...');
%
% Simulink model name to trim
TrimParam.SimModel = 'trim_linearization';
fprintf('\nThe Simulink model %s.mdl will be trimmed.',
TrimParam.SimModel);
%
% Get the sim options structure
TrimParam.SimOptions = simget(TrimParam.SimModel);
%-----
%-----
KEAS_s = input('Trim equivalent airspeed [kts]: ');
Alt_s = input('Trim altitude [ft]: ');

for i_alt=1:size(Alt_s,2)
    for i_keas=1:size(KEAS_s,2)
        KEAS = KEAS_s(i_keas);
        Alt = Alt_s(i_alt);

%-----
%-----
Alt          = Alt*0.3048;    % in meters
%-----
%-----
% Define initial inputs
Column      = 0;
Wheel       = 0;
Pedal       = 0;
Throttle    = 55;
%
u0 = [Column; Wheel; Pedal; Throttle];
%
% Define initial states
```

```

%
xe          = 0;          % in m
ye          = 0;          % in m
ze          = -Alt;       % Trim Height [m]
%-----
[sqsig,sound,p_p0,Rho,mu,DhpDh,T_T0]=atmospheric_calc(abs(ze),
0.0);
%-----
phi         = 0;
% in rad
theta      = 0;
% in rad
psi        = 0;
% in rad
vb         = 0;
% in m/s
wb         = 0;
% in m/s
ub         = sqrt(((KEAS*0.5145)/sqsig)^2-vb^2-wb^2);
% tas in m/s
p          = 0;
% in rad/s
q          = 0;
% in rad/s
r          = 0;
% in rad/s
%
x0 = [xe; ye; ze; phi; theta; psi; ub; vb; wb; p; q; r];
%
% Define initial outputs
%
Xcoord     = xe;
Ycoord     = ye;
h          = -ze;
phi_deg    = phi*180/pi;
theta_deg  = theta*180/pi;
psi_deg    = psi*180/pi;
u          = ub;
v          = vb;
w          = wb;
p_deg      = p*180/pi;
q_deg      = q*180/pi;
r_deg      = r*180/pi;
ax         = 0;
ay         = 0;
az         = 0;
Ny         = 0;
Nz         = 1;
alpha_deg  = 0;
beta_deg   = 0;

```

```

Airspeed      = sqrt(ub^2+vb^2+wb^2); %
TAS
gamma_deg     = 0;
hdot          = 0;
KEAS          = KEAS;
%
y0 = [Xcoord; Ycoord; h; phi_deg; theta_deg; psi_deg; u; v;...
      w; p_deg; q_deg; r_deg; ax; ay; az; Ny; Nz; alpha_deg;
      beta_deg; Airspeed;...
      gamma_deg; hdot; KEAS];
%-----
%-----
%-----
% Step 2 : Find names and ordering of States, inputs, outputs
& improve the initial guesses in SIMULINK model
[state_names,input_names,out_names,nx,nxc] =
names(0,TrimParam.SimModel);
%-----
%-----
% The trim error threshold
MaxErrKEAS = 3;
MaxErrAlt = 5;
MaxErrBank = 0.1; %deg
%
% The control surface gains
KColumn = -0.1;
KWheel = 0.0125;
KThrottle = 0.00025;
%
fprintf('\nComputing the initial estimates for the trim
inputs...');
%
GoodGuess = 0; Niter = 1;
while (~GoodGuess)&(Niter<30)
% Run Simulink model for a short time (3 s)
[SimTime, SimStates, SimOutputs] = sim(TrimParam.SimModel, [0
3], TrimParam.SimOptions, [0 u0'; 3 u0']);
% Compute errors in trim
ErrKEAS = SimOutputs(end,23) - KEAS; % in KTS
ErrAlt = SimOutputs(end,3) - Alt; % in meters
ErrBank = SimOutputs(end,4) - phi*180/pi; % in degrees
fprintf('\nIteration #%2d, Airsp err = %6.2f kts, Alt err
= %8.2f m, phi err = %6.2f deg.', Niter, ErrKEAS, ErrAlt,
ErrBank);
%
% If all errors are within threshold

```

```

        if
            (abs(ErrKEAS)<MaxErrKEAS)&(abs(ErrAlt)<MaxErrAlt)&(abs(ErrBank)
            )<MaxErrBank)
                % We are done with the initial guess
                GoodGuess = 1;
            else
                % Adjust aircraft controls
                u0(1) = u0(1) + KColumn * ErrKEAS;
                u0(2) = u0(2) + KWheel * ErrBank;
                u0(4) = u0(4) + KThrottle * ErrAlt;
            end
            Niter = Niter + 1;
        end
        % Save initial guess
        ub = SimStates(end,7);
        vb = SimStates(end,8);
        wb = SimStates(end,9);
        phi = SimStates(end,4)*pi/180;
        theta = SimStates(end,5)*pi/180;
        psi = SimStates(end,6)*pi/180;

        xe = SimStates(end,1);
        ye = SimStates(end,2);
        ze = -SimStates(end,3);
        p = SimStates(end,10)*pi/180;
        q = SimStates(end,11)*pi/180;
        r = SimStates(end,12)*pi/180;
        %
        Column = u0(1);
        Wheel = u0(2);
        Pedal = u0(3);
        Throttle = u0(4);
        %-----
        -----
        %-----
        -----
        %% Step 3: Specify which states (fixed_states) are fixed and
        which state derivatives (fixed_derivatives) are to be trimmed
        % Steady wings-level gamma=0 conditions, default Throttle=55
        %
        fixed_states      = [{ 'phi' } { 'vb' } { 'p' } { 'q' } { 'r' }
        { 'ze' }];
        fixed_derivatives = [{ 'ub' } { 'vb' } { 'wb' } { 'phi' } { 'theta' }
        { 'psi' } { 'p' } { 'q' } { 'r' } { 'ze' } { 'ye' }];
        fixed_outputs     = [{ 'beta_deg' } { 'KEAS' } { 'phi_deg' }
        { 'gamma_deg' }];
        fixed_inputs      = [];
        %-----
        -----
        echo off
    
```

```

n_states=[];n_deriv=[];n_out=[];n_input=[];
for i = 1:length(fixed_states)
    n_states=[n_states
    find(strcmp(fixed_states{i},state_names))];
end
for i = 1:length(fixed_derivatives)
    n_deriv=[n_deriv
    find(strcmp(fixed_derivatives{i},state_names))];
end
for i = 1:length(fixed_outputs)
    n_out=[n_out find(strcmp(fixed_outputs{i},out_names))];
end
for i = 1:length(fixed_inputs)
    n_input=[n_input
    find(strcmp(fixed_inputs{i},input_names))];
end
%
%% Step 4 : Trim the Model & write the results in workspace in
trimRes structure
%
Options(1) = 1;          % show some output
Options(2) = 1e-6;       % tolerance in X
Options(3) = 1e-6;       % tolerance in F
Options(4) = 1e-6;
Options(10) = 10000;     % max iterations
%
[X_trim,U_trim,Y_trim,DX] =
trim(TrimParam.SimModel,x0,u0,y0,n_states,n_input,n_out,[],n_d
eriv,Options);
%
trimRes(i_alt,i_keas).xt = X_trim;
trimRes(i_alt,i_keas).ut = U_trim;
trimRes(i_alt,i_keas).yt = Y_trim;
trimRes(i_alt,i_keas).altitude = Alt/0.3048;    %in ft
trimRes(i_alt,i_keas).velocity = KEAS;
trimRes(i_alt,i_keas).dynp = 1/2*Rho*(Y_trim(20)^2);
%% Step 5 : Linearize Model & write the results in workspace
in trimRes structure
[A,B,C,D] =
linearization(TrimParam.SimModel,X_trim,U_trim,'all','linmod2'
,1.5e-2);
%
trimRes(i_alt,i_keas).sys.A=A;
trimRes(i_alt,i_keas).sys.B=B;
trimRes(i_alt,i_keas).sys.C=C;
trimRes(i_alt,i_keas).sys.D=D;
%
% longitudinal matrix is-->
Along = A((1:5),(1:5));
trimRes(i_alt,i_keas).syslong.A = Along;

```

```

%
Blong = B((1:5),(1:2));
trimRes(i_alt,i_keas).syslong.B = Blong;
%
Clong = C((1:8),(1:5));
trimRes(i_alt,i_keas).syslong.C = Clong;
%
Dlong = D((1:8),(1:2));
trimRes(i_alt,i_keas).syslong.D = Dlong;
%
%lateral-directional A matrix is-->
Alat = A((6:9),(6:9));
trimRes(i_alt,i_keas).syslat.A = Alat;
%
Blat = B((6:9),(3:4));
trimRes(i_alt,i_keas).syslat.B = Blat;
%
Clat = C((9:15),(6:10));
trimRes(i_alt,i_keas).syslat.C = Clat;
%
Dlat = D((9:15),(3:4));
trimRes(i_alt,i_keas).syslat.D = Dlat;
    end
end

```

An output display example of the script in the MATLAB[®] command window is given as follows;

```

Setting initial trim parameters...
The Simulink model trim_linearization.mdl will be
trimmed.Trim equivalent airspeed [kts]: 100
Trim altitude [ft]: 15000

Computing the initial estimates for the trim inputs...
Iteration # 1, Airsp err = -6.98 kts, Alt err = 25.40
m, phi err = -0.04 deg.
Iteration # 2, Airsp err = -6.04 kts, Alt err = 22.13
m, phi err = -0.02 deg.
Iteration # 3, Airsp err = -5.21 kts, Alt err = 19.23
m, phi err = -0.01 deg.
Iteration # 4, Airsp err = -4.49 kts, Alt err = 16.68

```



```

m, phi err = 0.00 deg.
Iteration # 5, Airsp err = -3.86 kts, Alt err = 14.46
m, phi err = 0.01 deg.
Iteration # 6, Airsp err = -3.33 kts, Alt err = 12.52
m, phi err = 0.01 deg.
Iteration # 7, Airsp err = -2.86 kts, Alt err = 10.84
m, phi err = 0.01 deg.
Iteration # 8, Airsp err = -2.47 kts, Alt err = 9.38
m, phi err = 0.01 deg.
Iteration # 9, Airsp err = -2.12 kts, Alt err = 8.11
m, phi err = 0.01 deg.
Iteration #10, Airsp err = -1.82 kts, Alt err = 7.02
m, phi err = 0.01 deg.
Iteration #11, Airsp err = -1.57 kts, Alt err = 6.07
m, phi err = 0.01 deg.
Iteration #12, Airsp err = -1.35 kts, Alt err = 5.26
m, phi err = 0.01 deg.
Iteration #13, Airsp err = -1.16 kts, Alt err = 4.55
m, phi err = 0.01 deg.f-COUNT      MAX{g}      STEP
Procedures
  18      4.33335      1
  36      2.21942      1
  54      0.0112845    1
  72      0.00307995    1  Hessian modified
  90      0.0030643     1  Hessian modified twice
 108      0.0030633     1  Hessian modified
 109      0.00306328    1  Hessian modified
Optimization Converged Successfully
Active Constraints:
  1
  2
  3
  4

```

5
6
7
8
9
10
11
13
29
30

The given trim-linearization algorithm calls four scripts, respectively; “atmospheric_calc.m”, function calculating necessary atmospheric variables at the given flight altitude, “names.m”, function helping recognizing the names of the states, inputs, and outputs of the Simulink® model to be trimmed and linearized, “trim.m”, the MATLAB® trim function; and “linearization.m”, function acting like an interface between MATLAB® linearization function `linmod2` and the nonlinear model again by calling `names.m`. It should be denoted that, the nonlinear UAV model that is trimmed and linearized by the `trimUAV.m` is a simpler version of the complete nonlinear model, where the extra states introduced by the “ACTUATORS” block, and unit delays introduced by the “Turbulence” block are not included. This simpler model is named as “trim_linearization.mdl”, including only the 12 air vehicle states given by Equations (3.3). The complete nonlinear model, named as “UAV.mdl” consists of the eliminated blocks in “trim_linearization.mdl” and is used for open-loop simulation and analyses purposes with proper initial state and control input values obtained from flight trimming of the trim model. In order to investigate the closed-loop time simulation results, starting with a desired trim condition, instead of UAV.mdl, the model “UAV_cl_controlled.mdl”, i.e. the classical controlled model, or the model “UAV_lqr_controlledtz2.mdl”, i.e. the LQ controlled model should be simulated without any additional task.